



734  
2019

# Berichte

zur Polar- und Meeresforschung

Reports on Polar and Marine Research

## Russian-German Cooperation: Expeditions to Siberia in 2018

Edited by

Stefan Kruse, Dmitry Bolshiyarov, Mikhail Grigoriev,  
Anne Morgenstern, Luidmila Pestryakova, Leonid Tsibizov,  
and Annegret Udke

with contributions of the participants

Die Berichte zur Polar- und Meeresforschung werden vom Alfred-Wegener-Institut, Helmholtz-Zentrum für Polar- und Meeresforschung (AWI) in Bremerhaven, Deutschland, in Fortsetzung der vormaligen Berichte zur Polarforschung herausgegeben. Sie erscheinen in unregelmäßiger Abfolge.

Die Berichte zur Polar- und Meeresforschung enthalten Darstellungen und Ergebnisse der vom AWI selbst oder mit seiner Unterstützung durchgeführten Forschungsarbeiten in den Polargebieten und in den Meeren.

Die Publikationen umfassen Expeditionsberichte der vom AWI betriebenen Schiffe, Flugzeuge und Stationen, Forschungsergebnisse (inkl. Dissertationen) des Instituts und des Archivs für deutsche Polarforschung, sowie Abstracts und Proceedings von nationalen und internationalen Tagungen und Workshops des AWI.

Die Beiträge geben nicht notwendigerweise die Auffassung des AWI wider.

Herausgeber

Dr. Horst Bornemann

Redaktionelle Bearbeitung und Layout

Birgit Reimann

Alfred-Wegener-Institut  
Helmholtz-Zentrum für Polar- und Meeresforschung  
Am Handelshafen 12  
27570 Bremerhaven  
Germany

[www.awi.de](http://www.awi.de)  
[www.awi.de/reports](http://www.awi.de/reports)

Der Erstautor bzw. herausgebende Autor eines Bandes der Berichte zur Polar- und Meeresforschung versichert, dass er über alle Rechte am Werk verfügt und überträgt sämtliche Rechte auch im Namen seiner Koautoren an das AWI. Ein einfaches Nutzungsrecht verbleibt, wenn nicht anders angegeben, beim Autor (bei den Autoren). Das AWI beansprucht die Publikation der eingereichten Manuskripte über sein Repository ePIC (electronic Publication Information Center, s. Innenseite am Rückdeckel) mit optionalem print-on-demand.

The Reports on Polar and Marine Research are issued by the Alfred Wegener Institute, Helmholtz Centre for Polar and Marine Research (AWI) in Bremerhaven, Germany, succeeding the former Reports on Polar Research. They are published at irregular intervals.

The Reports on Polar and Marine Research contain presentations and results of research activities in polar regions and in the seas either carried out by the AWI or with its support.

Publications comprise expedition reports of the ships, aircrafts, and stations operated by the AWI, research results (incl. dissertations) of the Institute and the Archiv für deutsche Polarforschung, as well as abstracts and proceedings of national and international conferences and workshops of the AWI.

The papers contained in the Reports do not necessarily reflect the opinion of the AWI.

Editor

Dr. Horst Bornemann

Editorial editing and layout

Birgit Reimann

Alfred-Wegener-Institut  
Helmholtz-Zentrum für Polar- und Meeresforschung  
Am Handelshafen 12  
27570 Bremerhaven  
Germany

[www.awi.de](http://www.awi.de)  
[www.awi.de/en/reports](http://www.awi.de/en/reports)

The first or editing author of an issue of Reports on Polar and Marine Research ensures that he possesses all rights of the opus, and transfers all rights to the AWI, including those associated with the co-authors. The non-exclusive right of use (einfaches Nutzungsrecht) remains with the author unless stated otherwise. The AWI reserves the right to publish the submitted articles in its repository ePIC (electronic Publication Information Center, see inside page of verso) with the option to "print-on-demand".

*Titel: Das Vegetationsuntersuchungs-Team der Expedition "Chukotka 2018" blickt auf seinem Rückweg zum Feldlager auf den See Ilirney, Tschukotka, von dem lange Sedimentkerne geborgen werden konnten  
(Foto: Luise Schulte, AWI).*

*Cover: On its way returning to the field camp, the vegetation survey team of the expedition "Chukotka 2018" is looking at the lake Ilirney, Chukotka, of which long sediment cores could be retrieved  
(Photo: Luise Schulte, AWI).*

# **Russian-German Cooperation: Expeditions to Siberia in 2018**

---

**Edited by**

**Stefan Kruse, Dmitry Bolshiyarov, Mikhail Grigoriev,  
Anne Morgenstern, Luidmila Pestryakova, Leonid Tsibizov,  
and Annegret Udke**

**Please cite or link this publication using the identifiers**

**<http://hdl.handle.net/10013/epic.ece0c6cc-8e97-4850-a23c-ebc1ede9eafc> and  
[https://doi.org/10.2312/BzPM\\_0734\\_2019](https://doi.org/10.2312/BzPM_0734_2019)**

**ISSN 1866-3192**

# **Expeditions to Siberia in 2018**

**Research Station Samoylov Island and Lena Delta 05.04. - 15.09.2018**

**Expedition to Chukotka and Central Yakutia 29.06. - 21.08.2018**

## **Chief scientists**

**Dmitry Bolshiyarov (AARI), Svetlana Evgrafova (SIF), Alexey Fage (IPGG, NSU),  
Mikhail Grigoriev (MPI, IPGG, NEFU), Birgit Heim (AWI), Ulrike Herzsuh (AWI),  
Annellen Kahl (EPFL), Christian Knoblauch (UHH), Liudmila Lebedeva (MPI),  
Anne Morgenstern (AWI), Luidmila Pestryakova (NEFU),  
Aline Plötz (AWI), Lasse Sander (AWI), Nikolay Sennikov (IPGG, NSU),  
Jens Strauss (AWI), Sebastian Wetterich (AWI)**

# Contents

<b>1 Introduction</b>	<b>3</b>
<b>2 Research Station Samoylov Island and Lena Delta</b>	<b>10</b>
2.1 Samoylov Deep Drilling Spring Campaign 2018	11
2.1.1 Introduction	12
2.1.2 Study region	15
2.1.3 Field methods and sampling strategy	16
2.1.4 Preliminary results	19
2.2 New long-term permafrost borehole installation	24
2.3 Temperature monitoring on Samoylov and Kurungnakh Islands	28
2.4 SaLTO Observatory fully operational after major upgrade	30
2.5 Monitoring Lena River water at Research Station Samoylov Island	33
2.6 Winter hydrological and hydrobiological investigations on the Lena Delta channels and Samoylov Island lakes	37
2.7 Hydrological measurements in the Olenekskaya Channel	42
2.8 Isotopic composition of the snow cover on Samoylov Island and its modification in spring	44
2.9 Water vapour isotope analyses on Samoylov Island	50
2.10 Studying the spatial variability on Samoylov Island: analysis of CO <sub>2</sub> fluxes, precipitation and snow cover simulation	52
2.11 Greenhouse gas release from buried soil: field incubation study	56
2.12 Spatial and temporal distribution of recently assimilated carbon dioxide at the soil-plant interface	59
2.13 Source assessment of carbon emissions from polygonal tundra and ice complex deposits using <sup>14</sup> C analysis	61
2.14 Soil moisture and vegetation effects on carbon dioxide and methane fluxes in a transect through an eroding permafrost landscape on Kurungnakh	65
2.15 Investigations of snow cover and vegetation evolution from spring to summer using time-lapse cameras	68
2.16 KoPf - assessing above-ground and below-ground carbon in the central Lena Delta	73
2.17 Dendrochronological potential of tundra shrubs in the vicinity of Samoylov Island	80
2.18 Large drained lake basin in the south-eastern part of Kurungnakh Island as seen on geophysical data and preliminary geomorphological study	83
2.19 Shallow seismic survey of different permafrost types on Samoylov and Kurungnakh Islands	87
2.20 Study of sub-bottom talik in the Lena River Delta by the ERT method	94
2.21 Seismicity of the Laptev Sea Rift	97
2.22 Permafrost research on Sobo-Sise Island (Lena Delta)	102
2.23 Water tracks at the lower Lena River basin: results of field studies 2018	114
2.24 New geological, paleontological, and paleobotanical data from natural sections of Paleozoic, Mesozoic and Cenozoic sedimentary formations on Lena River main channel and Olenekskaya, Trofimovskaya and Bykovskaya channels, banks and islands	117
2.24.1 Paleozoic part	117
2.24.2 Mesozoic part	117
2.24.3 Cenozoic part	121

2.25	Paleomagnetic studies of Late Devonian volcanogenic and Early Carboniferous sedimentary complexes . . . . .	125
2.26	Investigations into coupled coastal lagoon and beach-ridge systems in Buor Khaya Bay, southern Laptev Sea . . . . .	127
2.27	Botanical survey of vascular plants in the southern Buor Khaya Bay . . . . .	129
<b>3</b>	<b>Expedition to Chukotka and Central Yakutia: Modern vegetation studies and lake sediment coring at the Tundra-Taiga-Transition zone in Chukotka and Yakutia</b>	<b>136</b>
3.1	Introduction . . . . .	137
3.2	Glacial lake coring and treeline forest analyses at the northeastern treeline extension in Chukotka .	139
3.3	Sampling mixed-species boreal forests affected by disturbances and mountain lake mountain lake and alas lake coring in Central Yakutia . . . . .	148
<b>4</b>	<b>Appendix</b>	<b>154</b>
A.1	List of participants . . . . .	155
A.2	Supplementary material to Lena 2018 Expedition . . . . .	161
A.3	Supplementary material to Chukotka 2018 Expedition . . . . .	249

# Chapter 1

## Introduction

*Stefan Kruse*<sup>1</sup>, *Dmitry Bolshiyarov*<sup>2</sup>, *Mikhail Grigoriev*<sup>3,4,5</sup>, *Anne Morgenstern*<sup>1</sup>, *Luidmila Pestryakova*<sup>5</sup>, *Leonid Tsibizov*<sup>4</sup>

<sup>1</sup> Alfred Wegener Institute Helmholtz Center for Polar and Marine Research, Potsdam, Germany

<sup>2</sup> Arctic and Antarctic Research Institute, St. Petersburg, Russian Federation

<sup>3</sup> Melnikov Permafrost Institute, Siberian Branch, Russian Academy of Sciences, Yakutsk, Russian Federation

<sup>4</sup> Trofimuk Institute for Petroleum Geology and Geophysics, Siberian Branch, Russian Academy of Sciences, Russian Federation

<sup>5</sup> Federal State Autonomous Educational Institution of Higher Education "M.K. Ammosov North-Eastern Federal University", Yakutsk, Russian Federation

### Overview

This report provides an overview of the study locations, scientific objectives and field activities of the joint Russian-German expeditions to Siberia in 2018. While most expeditions covered investigations of the biology, geology, geomorphology, coastal dynamics, ecology and paleoenvironment of the Lena Delta region, with a focus on Samoylov Island, others led to the tundra taiga ecotone of Chukotka and Central Yakutia.

Co-operative Russian-German geoscientific research in Siberia resulted in annual expeditions to Yakutia and the Siberian Arctic since 1993. An expedition to the Lena River Delta in 1998 within the framework of the Russian-German Cooperation SYSTEM LAPTEV SEA, supported by the research ministries of both countries was the first in the series of annual joint Russian-German expeditions LENA. This first expedition laid the foundation for the establishment of a permafrost observatory on Samoylov Island in the central Lena Delta and the operation of a research station, which has been serving as a scientific and logistical base for the LENA expeditions ever since. Permafrost conditions, micrometeorology, trace gas exchange, biology, and many other parameters are monitored at long-term measurement sites on the island and have been providing important data for the expeditions and the research community as a whole, for example through publication via data repositories such as PANGAEA (<https://www.pangaea.de/>) or integration into international data bases, such as the Global Terrestrial Network for Permafrost (GTN-P; <http://gtnp.arcticportal.org/>).

In 2018, the LENA expedition covered the period from early April to mid of September. It was coordinated by Guido Grosse (Alfred Wegener Institute Helmholtz Center for Polar and Marine Research - AWI, Potsdam), Dmitry Bolshiyarov (Arctic and Antarctic Research Institute - AARI, St. Petersburg) and Mikhail N. Grigoriev (Melnikov Permafrost Institute, Siberian Branch, Russian Academy of Sciences - MPI SB RAS, Yakutsk, North Eastern Federal University - NEFU, Yakutsk) and led by Dmitry Bolshiyarov and Waldemar Schneider (AWI, Potsdam).



Figure 1.1: *Samoylov Island and Lena Delta Campaign Logo - Samoylov Deep Drilling Spring Campaign Logo*

The Research Station Samoylov Island is operated by the Trofimuk Institute for Petroleum Geology and Geophysics, Siberian Branch, Russian Academy of Sciences (IPGG SB RAS), and provided a logistics staging base, laboratories for field work and accommodation for the scientists, technicians and students.

In addition to research on Samoylov Island, field sites included other locations within the Lena River Delta and adjacent to it. Larger efforts focused on Samoylov Deep Drilling Campaign in April to investigate deep permafrost conditions and the development of the delta. Additional expeditions set out to Sobo-Sise, Sardakh, Tit-Ary Island and to Buor Khaya Bay in July and August.

Furthermore, the CHUKOTKA expedition includes field work in July and August that extends long lasting multi-proxy studies of Siberian landscapes across and ahead of the arctic treeline. It was coordinated by Prof. Dr. Ulrike Herzschuh (Alfred Wegener Institute Helmholtz Center for Polar and Marine Research - AWI, Potsdam) and Prof. Dr. Luidmila A. Pestryakova (North Eastern Federal University - NEFU, Yakutsk). The second chapter is separated into two parts of the expedition, tundra to taiga analyses and glacial lake deep drilling in Chukotka (section 3.2), and boreal forests and mountain lake coring in Yakutia (section 3.3).



Figure 1.2: *Chukotka 2018 Campaign Logo*

Expedition logos are presented in Figures 1.1 and 1.2. Participants and their affiliations are listed in the appendix, which also lists the collected samples and measurements made in 2018. This report contains contributions from the participants. The authors are responsible for content and correctness.



### Expedition Lena 2018 – Participants and itinerary

94 scientists, technicians and students participated in the LENA 2018 expedition, of which 51 were based at Russian research institutions and universities, and 34 were from German, six from Swiss, two from Polish and one from British research institutions and universities. Group photos for April, July, August and September are presented in Figure 1.3, 1.4 and 1.5.

Jens Strauss (AWI Potsdam) and Mikhail Grigoriev (MPI Yakutsk) led the Samoylov Deep Drilling Campaign, which was taking place from April 5<sup>th</sup> to April 27<sup>th</sup>, 2018, on Samoylov Island. In total, a group of 12 participants took part in the drilling campaign (Figure 1.6).

Four land expeditions took place in and around the Lena Delta in July and April. The expeditions to Sardakh (July 22<sup>th</sup> to August 15<sup>th</sup>) and Tit-Ary Islands were planned and undertaken by the Novosibirsk State University, Russia.

From August 3<sup>rd</sup> to August 16<sup>th</sup>, six scientists worked at Buor Khaya Bay in the southern Laptev Sea under the direction of Lasse Sander (AWI, Sylt) (Figure 1.7). An expedition to Sobo-Sise Island with seven participants was led by Sebastian Wetterich (AWI, Potsdam) from July 4<sup>th</sup> to August 10<sup>th</sup> (Figure 1.8).



Figure 1.3: *April team at Research Station Samoylov Island*



Figure 1.4: August team at Research Station Samoylov Island



Figure 1.5: September team at Research Station Samoylov Island



Figure 1.6: Participants of Samoylov Deep Drilling Campaign



Figure 1.7: Members of expedition to Buor Khaya Bay



Figure 1.8: *Sobo-Sise expedition members*

#### **Expedition Chukotka 2018 — Participants and itinerary**

20 scientists and students participated the Chukotka 2018 expedition. Nine were based at the Alfred Wegener Institute Helmholtz Centre for Polar and Marine Research in Potsdam and eleven at the Ammosov North-Eastern Federal University in Yakutsk and the St. Petersburg University in Russia. Group photos of both parts are presented in Figure 1.9 and 1.10.



Figure 1.9: *Chukotka expedition members – part 1*



Figure 1.10: *Chukotka expedition members – part 2*

### **Acknowledgements**

The LENA and CHUKOTKA 2018 expeditions depended on essential support of the Russian and German organizing institutions, funding agencies, authorities and individuals. In particular, we would like to express our appreciation to the staff of the Research Station Samoylov Island, the Lena Delta Reserve, the Tiksi Hydrobase, and the Arctica GeoCenter.

## **Chapter 2**

### **Research Station Samoylov Island and Lena Delta**

Edited by: Dmitry Bolshiyarov, Svetlana Evgrafova, Alexey Faguet, Mikhail Grigoriev, Birgit Heim, Annelen Kahl, Christian Knoblauch, Liudmila Lebedeva, Anne Morgenstern, Lasse Sander, Nikolay Sennikov, Jens Strauss, Leonid Tsibizov, Sebastian Wetterich

## 2.1 Samoylov Deep Drilling Spring Campaign 2018

*Loeka L. Jongejans*<sup>1,2</sup>, (*Volkmar Assmann*<sup>1</sup>, *Julia Boike*<sup>1</sup>: not in the field), *Dmitry Bolshiyarov*<sup>5</sup>, (*Niko Bornemann*<sup>1</sup>: not in the field), *Boris Grigoriev*<sup>6</sup>, *Mikhail Grigoriev*<sup>3,4</sup>, *Andrey Kartoziia*<sup>4,7,8</sup>, *Georgii Maksimov*<sup>3,4</sup>, *Semen Ostreldin*<sup>6</sup>, *Stanislav Ostreldin*<sup>6</sup>, *Waldemar Schneider*<sup>1</sup>, (*Peter Schreiber*<sup>1</sup>, *Leonid Tsibizov*<sup>4,7</sup>: not in the field) and *Jens Strauss*<sup>1</sup>

<sup>1</sup> Alfred Wegener Institute Helmholtz Center for Polar and Marine Research, Potsdam, Germany

<sup>2</sup> University of Potsdam, Potsdam, Germany

<sup>3</sup> Melnikov Permafrost Institute, Siberian Branch, Russian Academy of Sciences, Yakutsk, Russian Federation

<sup>4</sup> Trofimuk Institute for Petroleum Geology and Geophysics, Siberian Branch, Russian Academy of Sciences, Russian Federation

<sup>5</sup> Arctic and Antarctic Research Institute, St. Petersburg, Russian Federation

<sup>6</sup> Federal State Autonomous Educational Institution of Higher Education "M.K. Ammosov North-Eastern Federal University", Yakutsk, Russian Federation

<sup>7</sup> V.S. Sobolev Institute of Geology and Mineralogy, Siberian Branch, Russian Academy of Sciences, Novosibirsk, Russian Federation

<sup>8</sup> Novosibirsk State University, Novosibirsk, Russian Federation

### Fieldwork period and location

From April 06<sup>th</sup> to April 27<sup>th</sup>, 2018 (on Samoylov Island)



## 2.1.1 Introduction

### General scientific rationale and objectives

Permafrost thaw is associated with impacts on climate, land surface and coastal and river bank structures. Processes such as thermokarst and thermo-erosion lead to ground subsidence, which can have drastic effects on the topography. One of the main drivers of surface subsidence vulnerability is the sedimentological composition, including ground ice content, and the temperature state of permafrost.

This drilling campaign aimed to retrieve a deep, frozen sediment core from Samoylov Island to cover several scientific disciplines including geocryology, sedimentology and geochemistry. This campaign provides sample material from much greater depths (65.7 m) than previous boreholes on the island (27 m in 2006) and the analysis of the sediments will therefore lead to a better understanding of the deep permafrost deposits on Samoylov Island. Furthermore, a temperature chain was installed in the borehole for long-term temperature monitoring (see section 2.2). Therefore, the campaign consists of several work packages:

- Work package 1: Cryostratigraphy and lithology of Samoylov deep permafrost
- Work package 2: Biogeochemical characterization of deep delta sediments
- Work package 3: Late Quaternary environmental variability in the central Lena Delta
- Work package 4: Permafrost temperature observatory (in 2019)

### Expedition itinerary and general logistics

The field work took place on Samoylov Island in April 2018. The drilling team consisted of 10 people from 6 different institutions in Germany and Russia (Figure 2.1.1 and Figure 2.1.2). The team was accommodated on the Research Station Samoylov Island (Figure 2.1.3). The team and the drilling rig (placed on a truck) were transferred from Tiksi over the Lena by tracked vehicles (Vestikhods) and trucks. The drilling rig and the equipment were set up at the borehole location (approximately 800 m from the station) as well as a tent for describing the cores and a bigger tent for shelter (Figure 2.1.4). Field work materials were transported between the station and the borehole location by tracked vehicles (Figure 2.1.5). A borehole was drilled, after which initial temperatures were measured and a geophone was installed (Table 2.1.1). Unfortunately, the geophone was broken during installation of the temperature chains. The core material was shipped over the Lena to the Melnikov Permafrost Institute in Yakutsk.



Figure 2.1.1: Participants at borehole from left to right: Dmitry Bolshiyarov, Waldemar Schneider, Semen Ostreldin, Boris Grigoriev, Jens Strauss, Stanislav Ostreldin, Mikhail Grigoriev, Georgii Maksimov and Fedor Sellyakhov; Missing: Loeka Jongejans and Andrey Kartoziia. Photo by Anne Morgenstern





Figure 2.1.2: Participants in upper row from left to right: Boris Grigoriev, Stanislav Ostrelidin, Dmitry Bolshiyarov, Jens Strauss, Semen Ostrelidin, Ivan, Andrey Kartozia; bottom row from left to right: Mikhail Grigoriev, Georgii Maksimov and Loeka Jongejans. Photo by Lutz Beckebanze



Figure 2.1.3: Research Station Samoylov Island. Photo by Loeka Jongejans

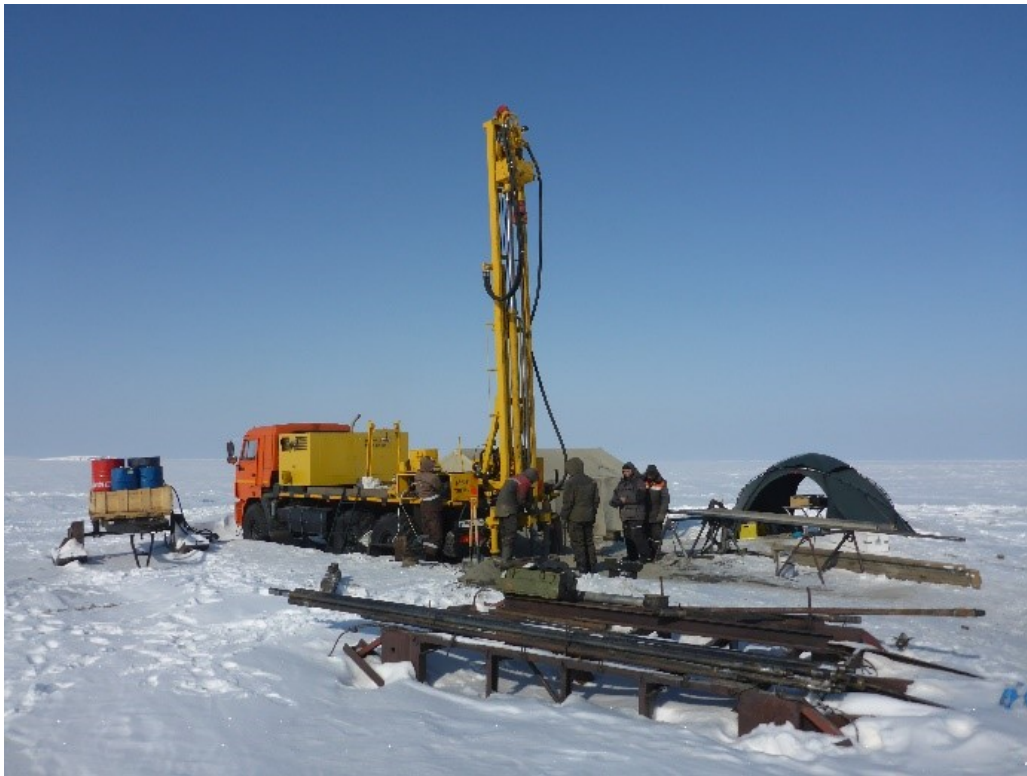


Figure 2.1.4: *Drilling rig on borehole location with tents. Photo by Jens Strauss*



Figure 2.1.5: *Tracked vehicle transporting sample boxes. Photo by Loeka Jongejans*

Table 2.1.1: Time table of field work

Date	Task
April 13 <sup>th</sup> , 2018	Beginning of drilling; cleaning, photographing, describing and packing of cores; field subsampling AARI
April 20 <sup>th</sup> , 2018	End of drilling
April 26 <sup>th</sup> , 2018	Temperature measurement down in the new borehole to the bottom right after drilling
April 26 <sup>th</sup> , 2018	Installing container with geophones (60 mm in diameter) at the borehole bottom
July 2018	Shipping cores to ice cellar of MPI-Y
August 2018	Cutting cores at Melnikov Permafrost Institute and sending samples to partner institutes (AWI, IPGG, MPI-Y)
July 11 <sup>th</sup> 2018	Installing temperature chains and taking station borehole temperature measurements, see section 2.2

## 2.1.2 Study region

### Samoylov Island

Samoylov Island (N 72.36998°, E 126.47532°) (Figure 2.1.6) is situated in the Lena Delta (northeast of Siberia), the largest river delta in the Arctic. The first research activities started in the second half of the 19<sup>th</sup> Century, when Nikolai Jürgens, Alexander von Bunge and Adolph Eigner started their meteorological and magnetic measurements on the island (Barr and Lüdecke 2010). A research station was built in 1998 on the location of a previously built building of the Lena Delta Nature Reserve. This station is and was used in summer by Russian and German scientific institutes. A new research station, which can host up to 20 scientists, was built in 2013 and is operated by the IPGG (Figure 2.1.3). The station is used all-year round for research expeditions from spring to autumn primarily organized by AWI, AARI and MPI-Y.

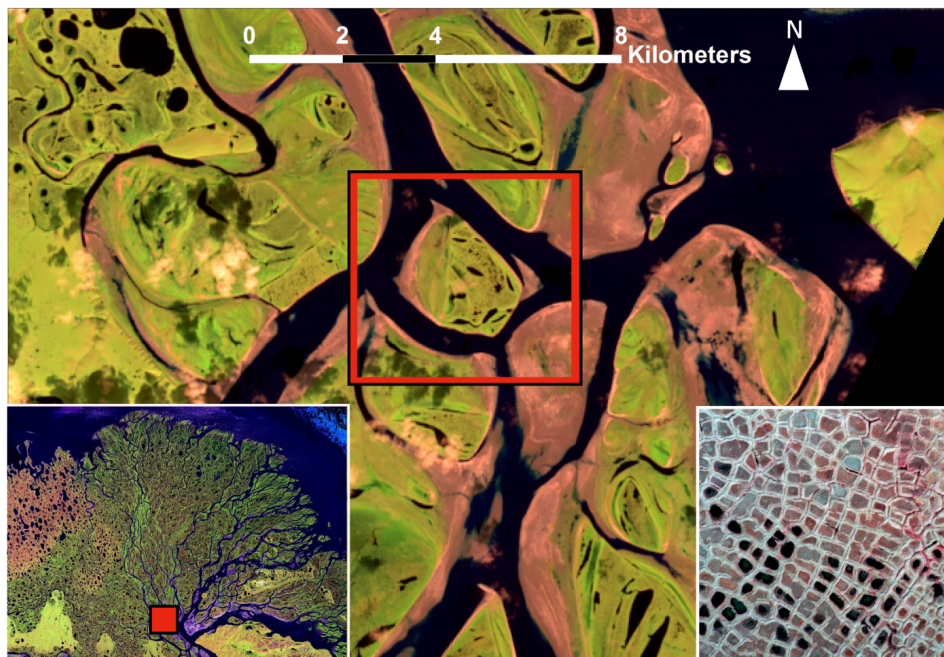


Figure 2.1.6: Background picture: Samoylov Island in Lena Delta, indicated by red square. Lower left corner: Lena Delta Samoylov Island indicated by red square. Lower right corner: polygonal tundra. Source: Landsat 8 image, USGS/NASA (background picture), Landsat 7 image from the July 27<sup>th</sup>, 2000, USGS/NASA (lower left corner) and CrestoAleina et al. (2013) (lower right corner).

## Geological and geographical background

Samoylov Island is situated in one of the main channels of the Lena Delta (Figure 2.1.6). Neotectonics block-movement, caused by high seismicity, formed the Lena Delta island archipelago, consisting of over 1500 islands, during the Holocene (Are and Reimnitz 2000) and can be divided into three river terraces. Samoylov island is situated on the first terrace, which is characterized by ice-wedge polygonal tundra, large thermokarst lakes and active flood plains (Boike et al. 2013). The island is located in the zone of continuous permafrost with a thickness of about 500 to 600 m (Romanovskii and Hubberten 2001). It is composed mainly of middle Holocene deposits (Hubberten et al. 2006) and consists of two parts: the western part (3.4 km<sup>2</sup>, 1 to 5 m a.s.l.), which is the modern floodplain and is flooded annually in spring, and the eastern part (4.1 km<sup>2</sup>, 10 to 16 m a.s.l.), which is characterized by wet polygonal tundra (Boike et al. 2008). The polygonal tundra has a microrelief with elevation differences of 0.5 m due to the presence of low-centered ice wedge polygons (Figure 2.1.6) (Boike et al. 2008). The Lena Delta Region has a dry continental climate with low temperatures (mean annual air temperature: -14.7 °C) and low precipitation (mean annual precipitation: 190 mm) (Hubberten et al. 2006). The permafrost temperatures on Samoylov Island are extremely low (mean annual temperature at the top: -10.1 °C) (Boike et al. 2008).

## Research activities on the island

Several weather stations (soil and climate stations and eddy covariance stations) were installed on the island in 1998 and 2006, measuring climatic parameters such as air temperature, radiation and wind speed and direction. Many field investigations, manual as well as automated, have been performed to measure a wide range of parameters such as vegetation and snow distribution, active layer thickness, lake water level and temperature (Boike et al. 2013).

A previous sediment core was taken in 2006 on the southeastern part of Samoylov Island, close to the station (N 72.36956°, E 126.47511°) in the spring of 2006 to a depth of 27 m. A temperature chain with 23 temperature sensors was installed in the summer of 2006 in the borehole (Boike et al. 2013).

### 2.1.3 Field methods and sampling strategy

#### Samoylov deep drilling

We chose the borehole location (N 72.37697°, E 126.48056°) (Figure 2.1.7) on the eastern and higher part of the island, which is not flooded during spring. However, in order not to disturb the weather stations and other measurement devices on the east side, we stayed as far to the west as possible. The sampling location is characterized by low-centered ice-wedge polygons, which are mostly filled with water in summer time. Hence, we picked the borehole location on the edge of a polygonal rim, so that we would not drill directly in the ice wedge and have no stagnating water in summer.

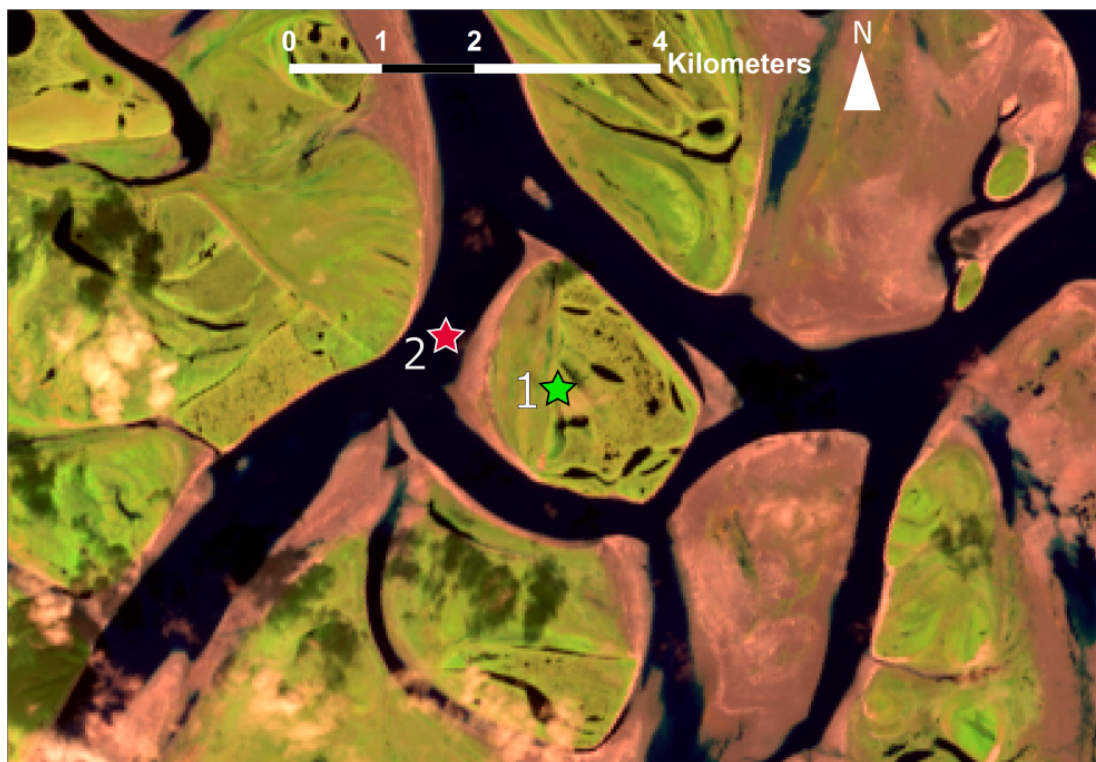


Figure 2.1.7: Samoylov Island with borehole location of Samoylov Deep Drilling (1; green star) and Lena River drilling (2; red star). Source: Landsat 8 image, USGS/NASA (background picture)

The borehole was drilled using a URB2-4T drilling rig (Figure 2.1.4) which is operated by two hydraulic cylinders that control the rotating hollow drill rods (approximately 4 m long) and a core barrel (approximately 3.5 m) into the frozen sediments. More drilling rods were placed on the top as the borehole became deeper. For the upper part, a drilling head with the largest diameter (146 mm) was used, after which a smaller diameter was chosen (127 and 108 mm) (Figure 2.1.8).

#### *Core material*

The core material was retrieved inside the core barrel and brought to the surface by removing the drilling rods one by one. The hole was then covered to prevent disturbance of the borehole, and the core material was removed from the core barrel using (a combination of) continuous or abrupt vibration and heating. The core (mostly around 1 to 2 m long) was then brought into the tent, where it was cleaned, photographed and described. The core profile description included sediments, ground ice and organic matter properties (see subsection 2.1.4). The borehole depth was compared to the core length every time so that potential core loss was logged. The core material was packed in tube foil and labeled and stored in thermoboxes.

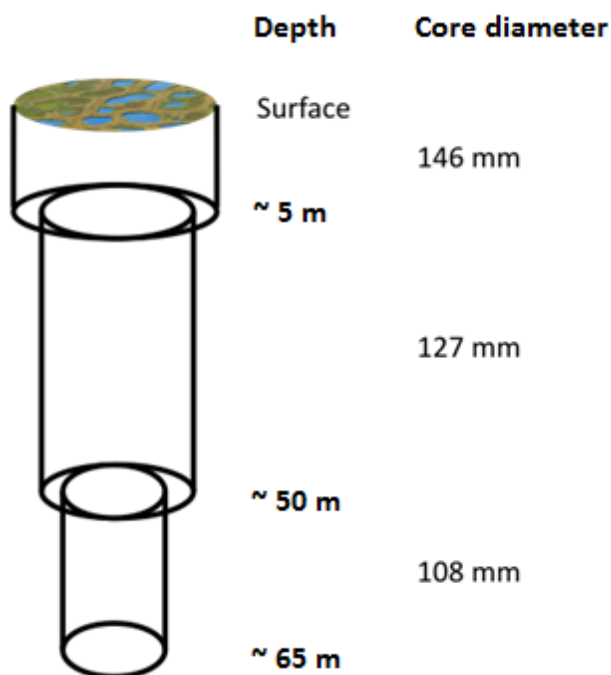


Figure 2.1.8: Schematic overview of borehole (lateral view) with core barrel diameter per depth interval

The sample cores were kept frozen before and during transport by ship to Yakutsk, where they were stored in the ice cellar. In August 2018, the cores were sawn into halves in the ice cellar in Yakutsk and repacked. One half was packed for transport to AWI, whereas the other half of the material was subsampled by the IPGG, AARI and MPI-Y. The core material for AWI is planned to be transported to Potsdam in December 2018, where it will be described in more detail and subsampled for laboratory analyses (Work packages 1-3).

*Temperature chains*

A core barrel was placed in the upper few meters of the borehole to prevent disturbance. A temperature chain was installed in July 2018 (Work package 4) (Figure 2.1.9). The details of the installation and setup are described in the summer expedition report 2018 (see section 2.2).

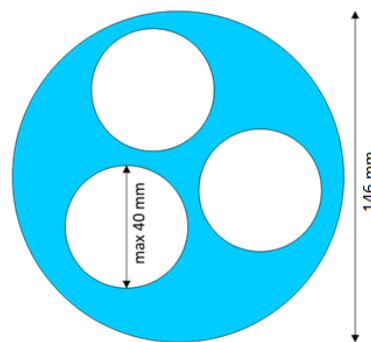


Figure 2.1.9: Schematic overview of the borehole (top view) with smaller tubes for temperature chains

**Lena River drilling**

An additional borehole was made in the Tumatskaya channel of the Lena, just west of Samoylov Island (Figure 2.1.7). The borehole was made in a shallow part of the river so that the ice was ground to the bottom. The same steps in core collection and description were performed as described in the previous chapter.

**Water sampling close to Stolb Island**

As part of the Changing Arctic Ocean NERC project CACOON (Changing Arctic Carbon cycle in the cOastal Ocean Near-shore), we collected water samples below the ice close to Stolb Island (N 2.39501°, E 126.68014°, Figure 2.1.10). This sampling was done in six repetition at three depths (3, 5 and 7 m) on April 8, 12, 16, 19, 22

and 26<sup>th</sup>. We filtered the water for dissolved and particulate organic carbon. Also, we took and froze an original sample. The samples were labelled L18 (Lena 2018) - 01 - (for 1 sampling) - 03 - (for the 3 m depth).



Figure 2.1.10: Picture of water sampling close to Stolb Island. Photo by Jens Strauss

## 2.1.4 Preliminary results

### Samoylov deep permafrost sediments

Sediment, ground ice and organic material properties were described of the sediment core (Table A.2.1). An initial stratigraphy is shown in Figure 2.1.11. Pictures of special features are shown in Appendix 3.

#### *Sediments*

The upper part of the core (0 to 23 m) shows quite some variation in texture (sand, peat dominated sand, sandy silt). Especially the upper 10 m are very organic rich with many wooden remains up to 10 cm long (Figure A.2-1) in the first 4 meters, and more peaty remains and peat inclusions (at approximately 12 m) lower on (Figure 2.1.11). The lower part (23 m and down) of the core is dominated by coarse sand. From 30 to 45 m, the coarse sand contains many oxidized spots (Figure A.2-2). In the lower part, especially from 45 m, many pebbles are present (Figure A.2-3), some even bigger than the core barrel diameter. Organic-rich layers are visible around 35 (Figure A.2-4), 45 and 50 m.

#### *Cryostructure*

Most of the core was retrieved in a frozen state (Figure 2.1.11). However, from 50 m and deeper, the material was mainly unfrozen due to drilling heat. As the drill got deeper into the sediments with many pebbles, a lot of the sediments was ground by the drill and blown out of the borehole by the air pressure through the drilling rods. To avoid the loss of material, we continued drilling without using air pressure, which led to the buildup of drilling heat, thawing the sediments.

Although we drilled on the edge of a polygonal rim so that we would not drill in the ice-wedge, we drilled through the wing of the ice-wedge. In general, the sediments were quite ice-rich, but the structure of the ice was not always visible. The cryostructure includes ice lenses (macro lenses indicated in Figure 2.1.11) and ice bands. Also, vertical ice bands were present in some ice-rich parts of the core (6, 23.5, 27, 28-30, 32 and 48 m). Furthermore, polosatic structures were visible around 27 m (Figure A.2-5). Pure freshwater ice was present at

around 22 m (Figure A.2-6). In two areas (at around 30 and 38 m), we noted the contact of silty and coarse sand, which we identified as cryoturbation (Figure A.2-7).

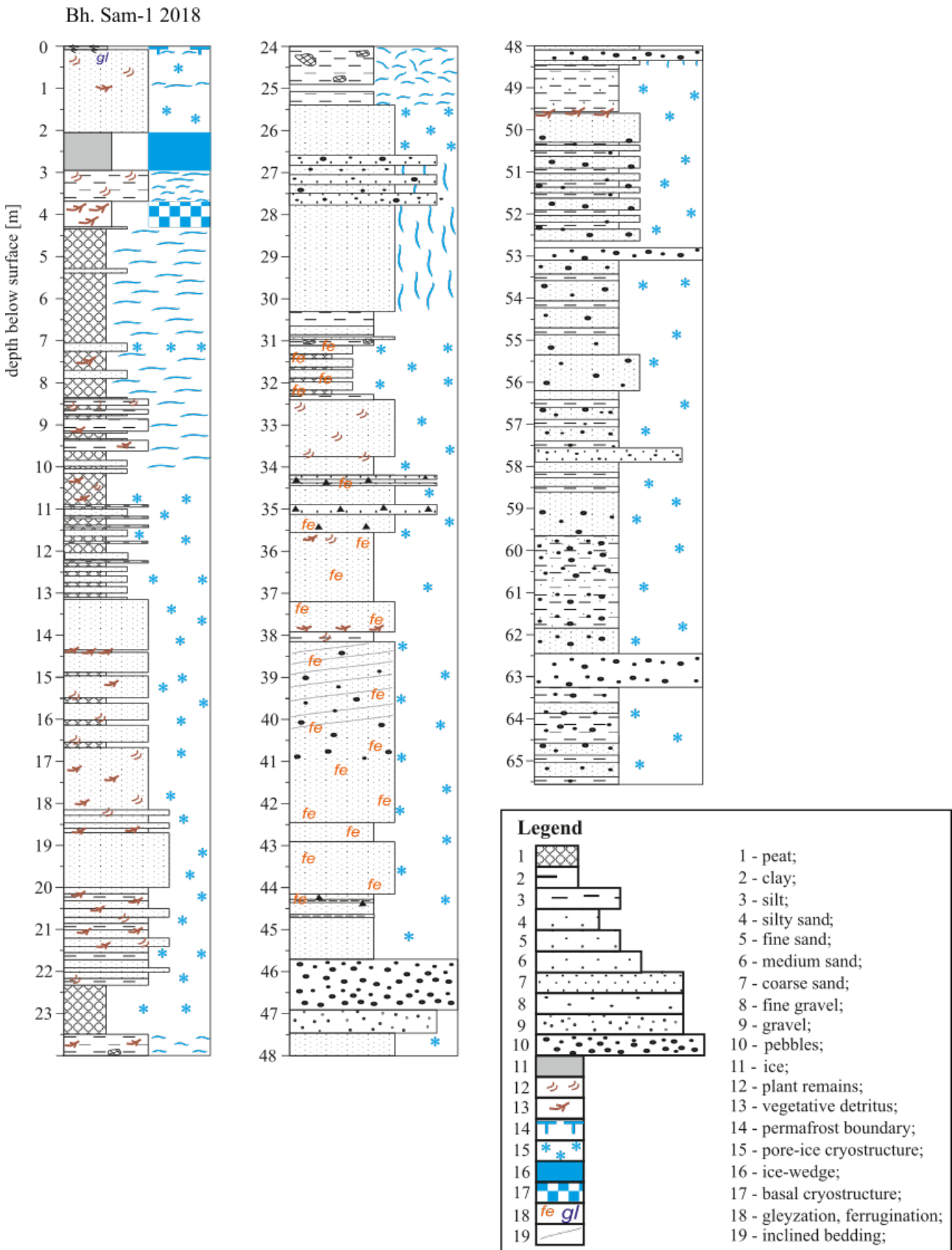


Figure 2.1.11: Stratigraphy of deep permafrost sediment core. Graph by Georgii Maximov



### Magnetic susceptibility

The volumetric magnetic susceptibility ( $K$ ) of the sediment cores was measured in the field in April 2018 (Figure 2.1.12a). The magnetic susceptibility (given in SI unit) is dependent on the concentration and type of magnetic minerals. Therefore, it can give insights in different sediment layers with different mineral composition (DaSilva et al. 2015; Wang and Evans 1997). The magnetic susceptibility ranges from 0 to  $5.1 \cdot 10^{-3}$  SI and shows most variation in the bottom part (65 to 50 m) (Figure 2.1.12a).

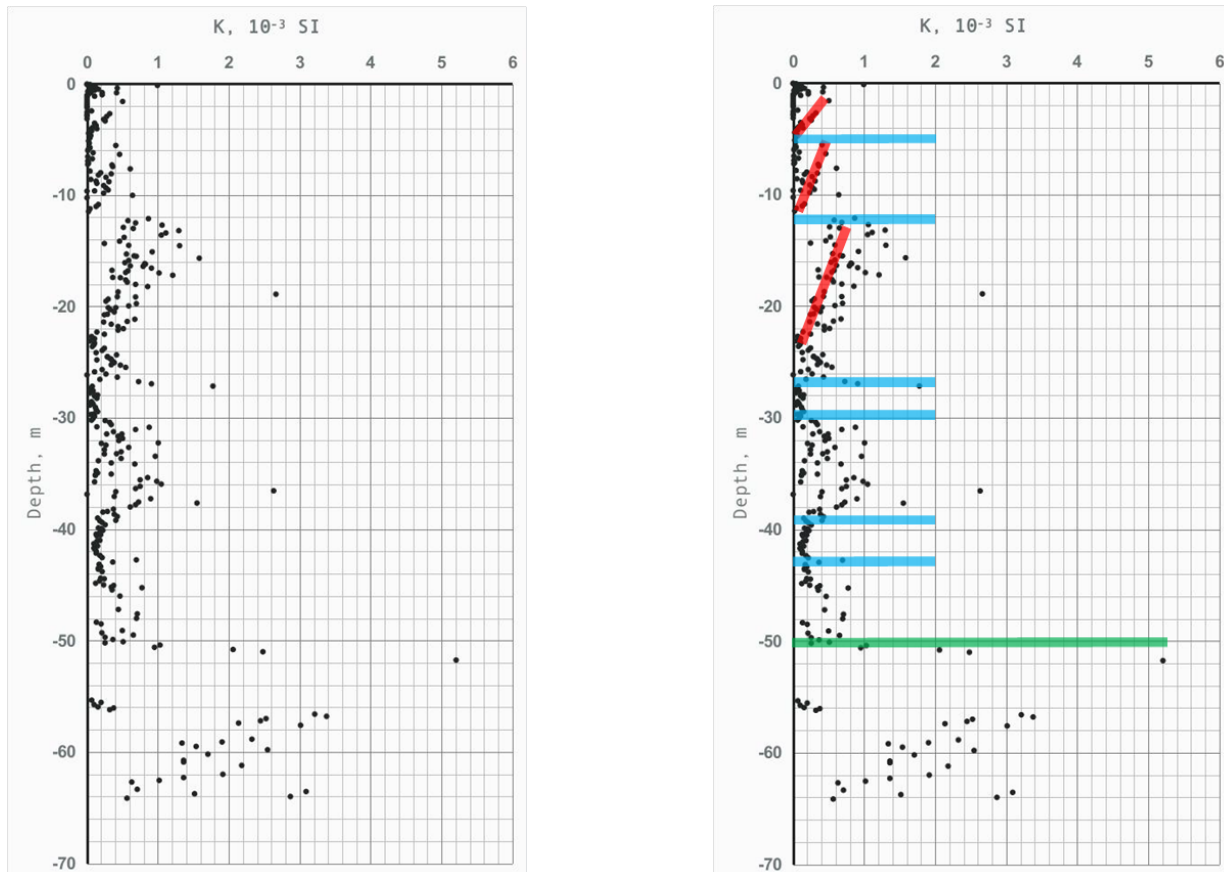


Figure 2.1.12: *Magnetic susceptibility of Samoylov deep sediment core; left) Raw data and right) interpretation*

The first interpretation was made by the IPGG (L. Tsibizov) (Figure 2.1.12b). Several trends were distinguished of decreasing values by increasing depth (red lines), where low values are likely related to high ice content or sandy layers whereas high values could correspond to intensive fluvial sedimentation or a change of sedimentation type (low concentration of magnetic minerals). Transitions within the data are shown with blue lines. The higher values and higher variability in the deposits below 50 m (below the green line) suggests these sediments have a different sediment source. Otherwise, it could also point to higher sedimentation rates. For further interpretation, lithology and grain size data will be included after laboratory analyses.

### Ground temperature

Initial temperature measurements were taken in the borehole using a 61 m long chain with 17 temperature loggers (every 0.5 m in the top and every 5 m below) (Figure 2.1.13). The temperature decreases from the surface to the lowest value at a depth of 2 m ( $-13.4^{\circ}\text{C}$ ), then increases to the maximum at 10 m deep ( $-7.6^{\circ}\text{C}$ ), after which it stabilizes at ( $-8.5^{\circ}\text{C}$ ). As the measurements were taken only a few days after finishing the drilling, this initial temperature record is overestimated because of the drilling heat. Measurement that were taken in summer with the newly installed chain, are described in the summer expedition report 2018, as well as a comparison with the old borehole (see section 2.2).

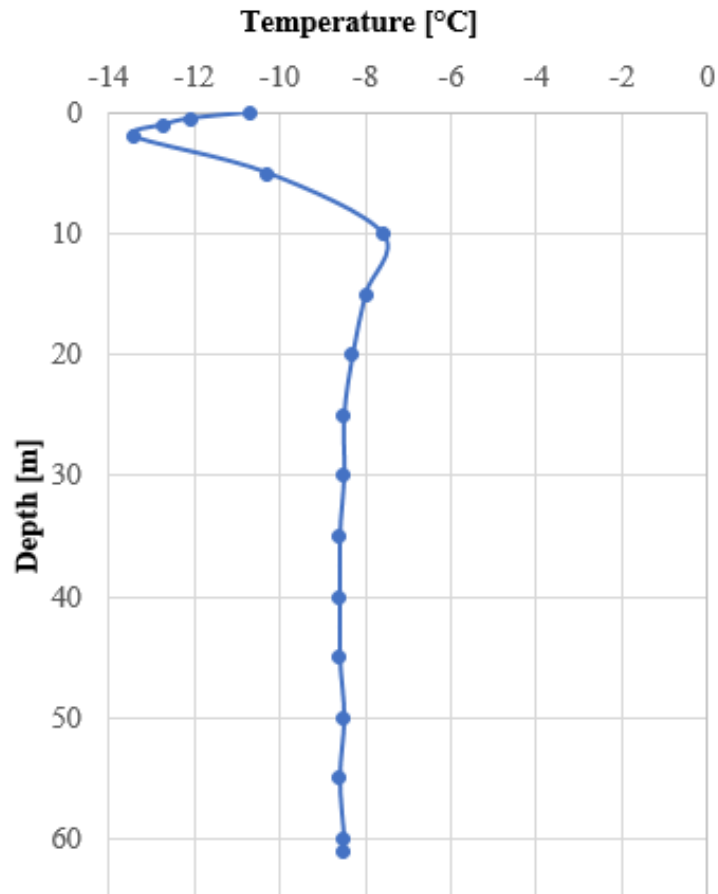


Figure 2.1.13: Initial temperature profile in borehole. Measured on April 26<sup>th</sup>, 2018

### Lena River sediments

Sediment, ground ice and organic material properties of the sediment core were described during fieldwork (A.2.2). An initial stratigraphy is shown in Figure 2.1.14.

#### Sediments

The upper 30 cm was snow cover. All depths were measured from the snow surface. The river ice was 60 cm thick and grounded to the bottom. The ice was clear with a few horizontal cracks and small bubbles from 30 to 47 cm. Sediments were retrieved to a depth of 23.8 m. The sediments were dominated by fine to medium sand Figure 2.1.14. We found peat layers from 100 to 150 cm, 875 to 910 cm, 1650 to 1700 cm and organic-rich layers from 730 to 1095 cm, around 1400 cm and 2155 to 2380 cm.

#### Cryostructure

The upper 5 m were frozen. Macro lenses were visible in the first 3 m, as well as around 600 cm. We found ice bands up to 3 mm thick around 860 to 875 cm and from 1322 to 1428 cm. From 5 to 20 m, silty parts were unfrozen whereas the sandy parts were frozen. Water coming out of the borehole while drilling suggests that the transition from frozen to unfrozen sediments was around 20 m. It is likely that the talik under the Lena channel here bulges to the sides of the channel. By using just the drilling rods without conserving the sediments, we tried to reach the permafrost table below the talik. However, likely due to the pollution of the drilling rods, we were not able to go deeper than 30 m. This is possibly the permafrost table.

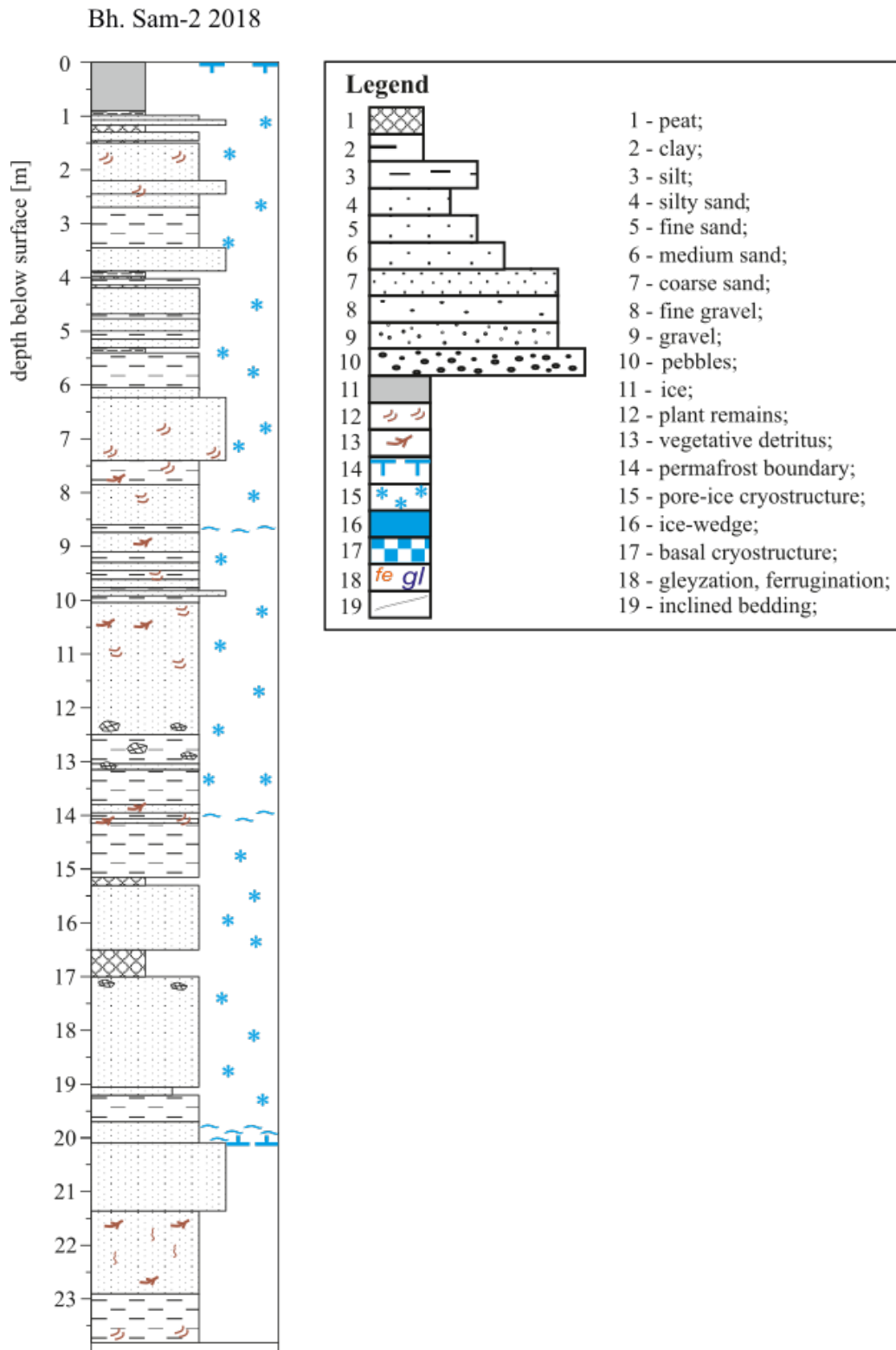


Figure 2.1.14: Stratigraphy of Lena River permafrost sediment core. Graph by Georgii Maximov

## 2.2 New long-term permafrost borehole installation

*Niko Bornemann*<sup>1</sup>, *Peter Schreiber*<sup>1</sup>, *Volkmar Assmann*<sup>1</sup>, (*Waldemar Schneider*<sup>1</sup>: not in the field), *Mikhail Grigoriev*<sup>4,5</sup>, *Dmitry Bolshiyarov*<sup>3</sup>, *Jens Strauss*<sup>1</sup>, *Loeka Jongejans*<sup>1</sup>, (*Julia Boike*<sup>1</sup>: not in the field), *Leonid Tsibizov*<sup>5,6</sup>, *Andrey Kartoziia*<sup>5,6,7</sup>, (*Dmitriy Auynov*<sup>5</sup>: not in the field)

<sup>1</sup> Alfred Wegener Institute Helmholtz Center for Polar and Marine Research, Potsdam, Germany

<sup>2</sup> St. Petersburg State University, St. Petersburg, Russian Federation

<sup>3</sup> Arctic and Antarctic Research Institute, St. Petersburg, Russian Federation

<sup>4</sup> Melnikov Permafrost Institute, Siberian Branch, Russian Academy of Sciences, Yakutsk, Russian Federation

<sup>5</sup> Trofimuk Institute for Petroleum Geology and Geophysics, Siberian Branch, Russian Academy of Sciences, Russian Federation

<sup>6</sup> Novosibirsk State University, Novosibirsk, Russian Federation

<sup>7</sup> V.S. Sobolev Institute of Geology and Mineralogy, Siberian Branch, Russian Academy of Sciences, Novosibirsk, Russian Federation

### Fieldwork period and location

From June 11<sup>th</sup> to July 04<sup>th</sup>, 2018 (on Samoylov Island)

### Objectives

Establishment of a long term permafrost temperature observatory on Samoylov Island at N 72.376972°, E 126.480556°



Figure 2.2.1: Figure shows the study site Samoylov island and the location of the borehole (61 m borehole, 2018) in yellow. Source of figure: Google Earth.

### Methods

#### Installation description

A metal core barrel was placed after drilling (spring 2018, this report chapter section 2.1) in the upper few meters of the borehole to prevent disturbance by the surrounding. This tube has a diameter of 168 mm outside (154 mm inside), total length 3000 mm (550 mm above ground 2450 mm in ground) and wall thickness of 7 mm. In summer 2018 three polyethylene pipes (according to DIN 8074 PN 12.5 hart) were installed in the borehole (outer diameter 40 mm and inner 37 mm) closed with a cap to reduce air circulation (Figure 2.2.2).

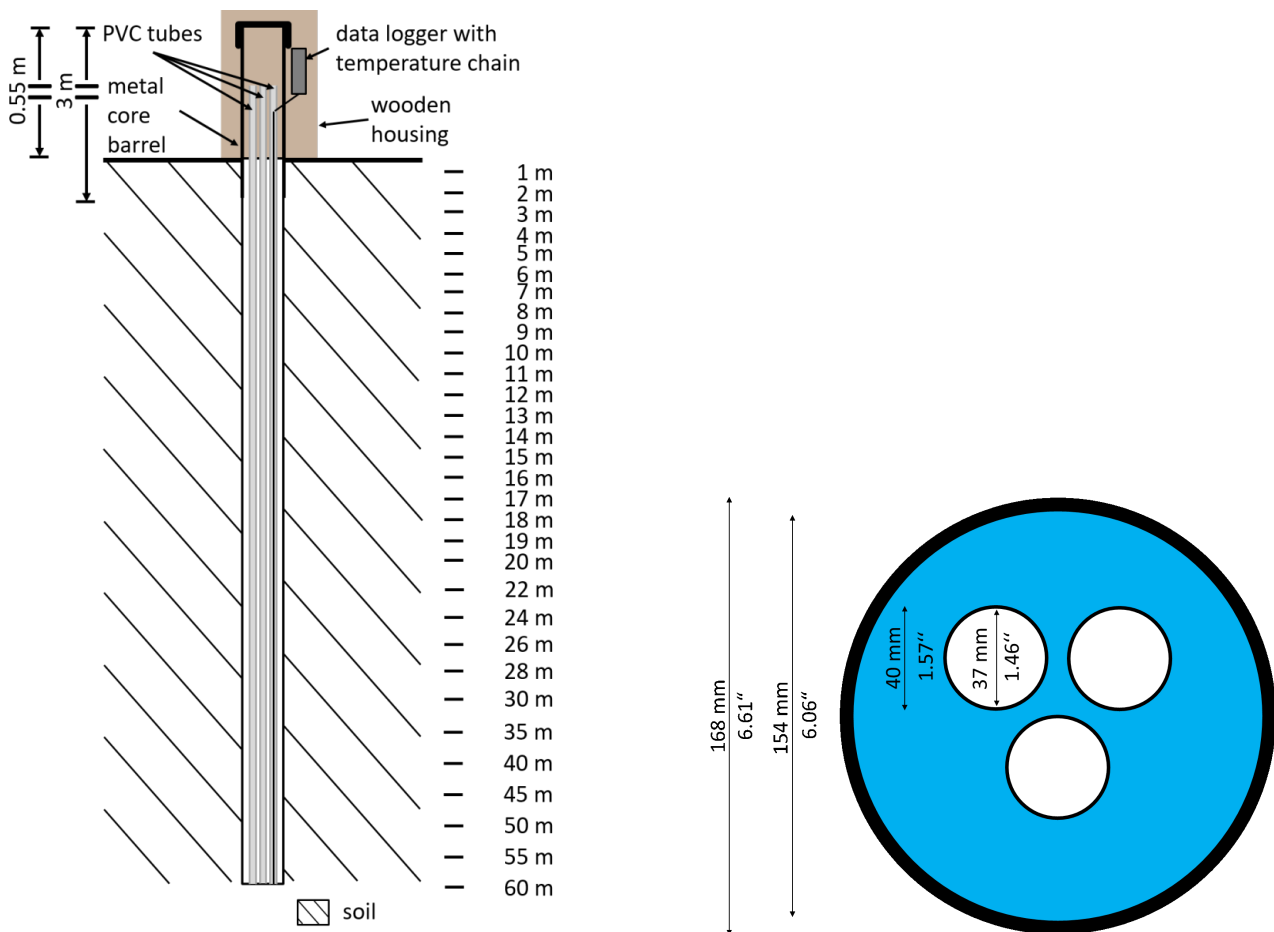


Figure 2.2.2: Schematic overview of the borehole a) (side view) borehole with housing and setting of temperature chain b) (top view) borehole with smaller tubes inside for measurement devices

The three tubes provide independent access to permit additional (geophysical and calibration) measurements to be made in the future. The remaining air space in the borehole around the PE tubes will be backfilled with dry sand in winter or summer 2020 to reduce the airspace around the measurement equipment. On the July 11<sup>th</sup>, a datalogger (M-Log5W, GeoPrecision GmbH, Germany) and temperature chain (Ultra Precision Temperature Sensor Pt100, GeoPrecision GmbH, Germany) with 31 temperature sensors was permanently installed (Figure 2.2.3). The accuracy of temperature Sensor is  $\pm 0.05^\circ\text{C}$  between  $-20$  to  $25^\circ\text{C}$ ,  $\pm 0.1^\circ\text{C}$  from  $-30$  to  $-40^\circ\text{C}$  and  $\pm 0.25^\circ\text{C}$  from  $-40$  to  $85^\circ\text{C}$ , the resolution is  $0.001^\circ\text{C}$ . The depth of the 31 sensors is 1, 2, 3, 4, 5, 6, 7, 8, 9, 10, 11, 12, 13, 14, 15, 16, 17, 18, 19, 20, 22, 24, 26, 28, 30, 35, 40, 45, 50, 55 and 60 m below the ground surface and will continuously measure every hour. To protect the borehole and metal pipe from solar radiation a wooden housing was placed above the setup. A wooden boardwalk leads to the borehole to prevent the surrounding vegetation from degradation during maintaining events (Figure 2.2.1).



Figure 2.2.3: Installation of the new borehole on July 9<sup>th</sup>, 2018. Photo by Niko Bornemann



Figure 2.2.4: Picture of the installation with housing and boardwalk. Photo by Niko Bornemann

### Preliminary results

A first comparison of the borehole temperature data of the 27 m borehole drilled in 2006 (Boike et al. 2019) and from 2018 were made for the August 2<sup>nd</sup>, 2007, and 2018. The temperatures in 20.75 m (27 m borehole, 2006) was with  $-8.96^{\circ}\text{C}$  a bit lower as at 20.0 m (new 61 m borehole, 2018) with  $-8.42^{\circ}\text{C}$  but  $\sim 1.0\text{ K}$  lower as the temperature in 2018 of the 2006 drilled borehole with  $-7.40^{\circ}\text{C}$  (Figure 2.2.5).

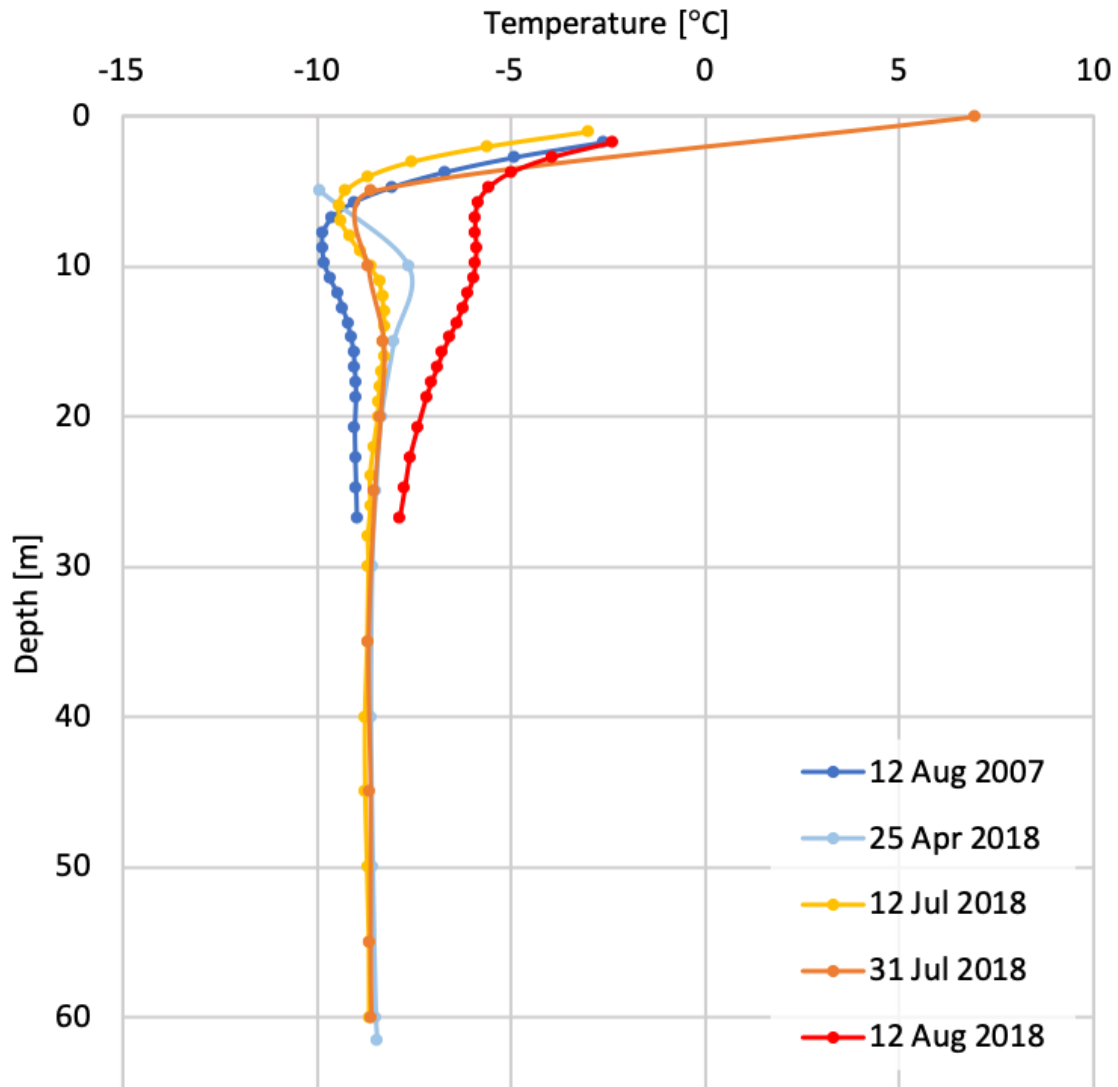


Figure 2.2.5: The temperature profile comparison on August 12<sup>th</sup>, 2007, of 27 m borehole (drilled 2006, dark blue), temperature profile of 27 m borehole in 2018 (red) and temperature profile of 61 m borehole (drilled 2018, light blue, yellow and orange) in April and July 2018. First measurement right after drilling were done by G. Maximov (Figure 2.1.13).

## 2.3 Temperature monitoring on Samoylov and Kurungnakh Islands

Leonid Tsibizov <sup>1,2</sup>, Andrey Kartoziia <sup>1,2,3</sup>, (Dmitriy Auynov <sup>1</sup>: not in the field)

<sup>1</sup> Trofimuk Institute for Petroleum Geology and Geophysics, Siberian Branch, Russian Academy of Sciences, Russian Federation

<sup>2</sup> Novosibirsk State University, Novosibirsk, Russian Federation

<sup>3</sup> V.S. Sobolev Institute of Geology and Mineralogy, Siberian Branch, Russian Academy of Sciences, Novosibirsk, Russian Federation

### Fieldwork period and location

From July 22<sup>th</sup> to August 10<sup>th</sup>, 2018 (on Samoylov Island and Kurungnakh Island)

### Objectives

Long-term temperature monitoring is a direct method for study of permafrost state changes. We use borehole temperature chain (60 m) on Samoylov Island to study temperature changes at different depth and shallow chains (1 m) on different permafrost objects to detect short-term processes in active layer. Beyond that shallow chains were used in order to obtain a high resolution data from the surface layer, which is necessary for calibration of new experimental method (Institute of Physics SB RAS) - remote sensing of surface permafrost layer properties (temperature, electrical permittivity, water content) based on detection of GNSS signal dissipation.

### Methods

Temperature monitoring on Samoylov and Kurungnakh Islands is conducted with temperature stations ASTM developed in IPGG SB RAS. One of such stations was installed on a new borehole on Samoylov Island (N 72.380574°, E 126.483801°), which was drilled in April 2018. First measurement was done in April after drilling, data logger was installed in July and operates starting from this time. The station chain is 60 m long and contains 13 DC18B20 sensors with 5 m distance between the sensors. Measuring period of the station is 6 hours, uncertainty of each measurement is 0.1 °C (due to additional calibration, see section 2.1 and 2.2).

Several shallow temperature stations were installed on Kurungnakh island for active layer temperature state monitoring. Length of their temperature chain is 100 cm with 10 cm distance between the sensors, measuring period is 4 hours. Such monitoring was started in 2016 on alas in the southern part of the island (3 stations) and on the Ice complex (2 stations). Then in 2017, 2 stations were moved from the Ice complex to the "southern" alas. One of these stations (T1, see the list below) was destroyed in 2017 by unknown local beast (Figure 2.3.1).

In 2018 2 stations (T3 and T5) were recharged and leaved on the "southern" alas (T5 was moved at a distance of several meters) and 2 (T2 and T4) were moved to the Ice complex surface in the nearby of another big drained alas in southern part of Kurungnakh (where the GNSS sensor was installed). Their chains were shorten to 50 cm (5 cm distance between the sensors) - upper sensor is on 10 cm above the surface, lower -40 cm deep. The stations were installed within pilot study area in the nearby of GNSS sensor (Figure 2.3.2).

Shallow temperature station list:

T1 (N 72.28911°, E 126,18870°) - destroyed in July 2017

T2 (N 72.28974°, E 126,18681°) - moved in 2018 to (N 72.30047°, E 126.22682°)

T3 (N 72.29131°, E 126,18640°)

T4 (N 72.28960°, E 126,18300°) - moved in 2018 to (N 72.30010°, E 126.22580°)

T5 (N 72.29101°, E 126,18035°) - moved in 2018 to (N 72.29059°, E 126.18093°)

### Preliminary results

First results from the borehole on Samoylov Island are provided in Figure 2.2.5.





Figure 2.3.1: *Temperature station destroyed by local beast*

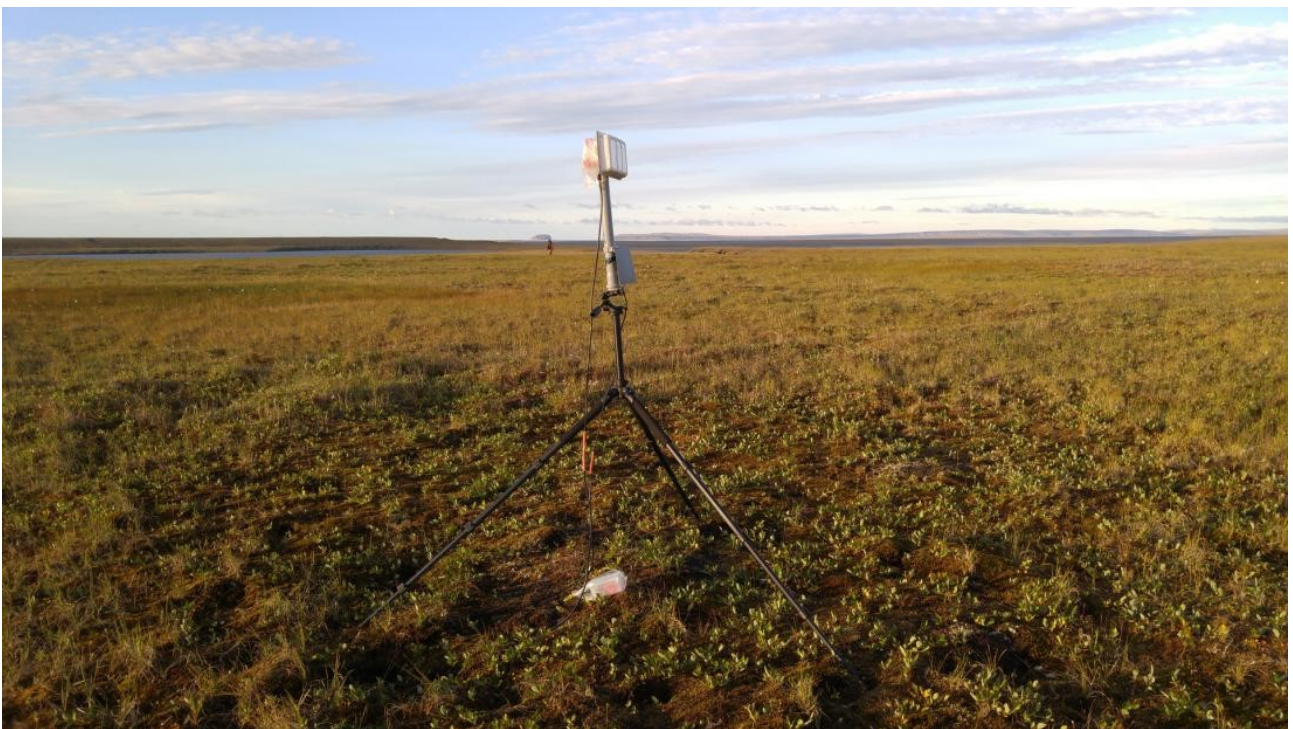


Figure 2.3.2: *Experimental station for remote permafrost surface parameters sensing*

## 2.4 SaLTO Observatory fully operational after major upgrade

Lutz Beckebanze <sup>1</sup>, Christian Wille <sup>2</sup>, Peter Schreiber <sup>3</sup>, Niko Bornemann <sup>3</sup>, Norman Rüggen <sup>1</sup>, Oliver Kaufmann <sup>1</sup>, Sergey Pravkin <sup>4,5</sup>, Volkmar Assmann <sup>3</sup>, (Julia Boike <sup>3</sup>, Torsten Sachs <sup>2</sup>, Lars Kutzbach <sup>1</sup>: not in the field)

<sup>1</sup> Institute of Soil Science, Universität Hamburg, Hamburg, Germany

<sup>2</sup> GFZ German Research Centre for Geoscience Helmholtz Centre Potsdam, Potsdam, Germany

<sup>3</sup> Alfred Wegener Institute Helmholtz Center for Polar and Marine Research, Potsdam, Germany

<sup>4</sup> St. Petersburg State University, St. Petersburg, Russian Federation

<sup>5</sup> Arctic and Antarctic Research Institute, St. Petersburg, Russian Federation

### Fieldwork period and location

From April 18<sup>th</sup> to April 27<sup>th</sup>, 2018 (on Research Station Samoylov Island)

From June 11<sup>th</sup> to July 14<sup>th</sup>, 2018 (on Research Station Samoylov Island)

From September 3<sup>rd</sup> to September 20<sup>th</sup>, 2018 (near Research Station Samoylov Island)

### Objectives

The **Samoylov Long-Term Observatory** (SaLTO) aims to continue the existing long-term observation of vertical carbon and energy fluxes as well as meteorological, hydrological, and permafrost conditions on Samoylov Island. This continuous time series will provide unique insights into the change of the permafrost landscape on Samoylov Island. Especially long time series of the vertical fluxes of carbon (CO<sub>2</sub> and CH<sub>4</sub>) are required in order to detect inter-annual variability and long-term changes in the carbon balance.

In 1998, the long-term observation of the meteorological and hydrological conditions as well as 2002 the vertical fluxes of carbon and energy using the micrometeorological eddy-covariance method started in the center of Samoylov Island. However, in the past years, the 10-meter tower holding the above-ground measurement instruments slowly subsided into the tundra, therefore came to the end of its lifetime, and needed replacement. In 2017, a field lab in the shape of an igloo was installed nearby the existing observatory tower (Figure 2.4.1). This field lab provides excellent conditions for high precision instruments that are used e.g. for a high quality eddy-covariance flux estimation of carbon and energy. In the previous field season of 2016, a new 10-meter measurement tower was installed next to the platform for the igloo and about 50 m away from the old tower (Figure 2.4.2).

After a successful test of the temperature and moisture conditions inside the field lab during the winter of 2017/2018, sensitive measurement instruments could be installed in the field lab. Therefore, the old 10-meter tower including the measurement instruments were dismantled during the field season of 2018 and new measurement instruments were reinstalled at the new 10-meter tower and in the field lab, respectively.

### Fieldwork summary

#### *April*

During the expedition in April 2018, the necessary maintenance of the measurement instruments at the old 10-meter tower were carried out. This included the installation of the open-path methane gas analyzer Li-7700, which is not suitable for winter operation and thus hibernates at the research station. Additionally, all data from the winter season of 2017/2018 was downloaded from the loggers and stored on backup hard drives in the station.

#### *June to July*

During the expedition in June and July, the closed path eddy covariance system was moved from the old tower to the new tower and igloo. A conduit was installed between igloo and tower for the save installation of cables and gas sampling tubes. The closed-path eddy covariance (EC) system for the measurement of fluxes of CO<sub>2</sub>, H<sub>2</sub>O, and CH<sub>4</sub> started operation on July 1<sup>st</sup>. Additionally, an open-path EC system for the measurement of fluxes of CO<sub>2</sub> and H<sub>2</sub>O was installed on the new tower, which started operation on June 20<sup>th</sup>. The Igloo was equipped

with an air conditioning system to provide stable temperature conditions for the installed scientific devices. Furthermore, we installed infrastructure to access and backup the data of the research stations via a wireless data network including network storage space. All the necessary maintenance of meteorological, hydrological, and permafrost measurement devices were carried out on all running stations. Some of the radiation and wind sensors were moved from the old to the new tower.

### September

During September, the old eddy covariance tower was dismantled and the running measurement systems prepared for winter operation. Additionally, last samples from a  $^{13}\text{C}$  labelling experiment were taken on the flood plain and on the river terrace and the site was restored. Samples and instruments that needed maintenance were prepared for shipping to Germany.

### Preliminary results

In the winter of 2017/ 2018 and during the field season of 2018, all measurement instruments performed without major failures. The availability of the data from the old and new 10-meter tower is presented in Table 2.4.1.

Table 2.4.1: Data availability at the old and new 10-meter tower

Data Type	Data availability from the old tower	Data availability from the new tower
1-minute meteorological data	21.09.2017 – 05.09.2018	19.09.2017 – ongoing
30-minute meteorological data	21.09.2017 – 05.09.2018	19.09.2017 – ongoing
30-minute soil data	21.09.2017 – ongoing	-
Open-path EC CO <sub>2</sub> and H <sub>2</sub> O	21.09.2017 – 05.09.2018	20.06.2018 – ongoing
Open-path EC CH <sub>4</sub>	20.04.2018 – 05.09.2018	-
Closed-path EC CO <sub>2</sub> , H <sub>2</sub> O, CH <sub>4</sub>	21.09.2017 -29.06.2018	01.07.2018 – ongoing



Figure 2.4.1: Igloo and new tower with meteorological instruments in April 2018

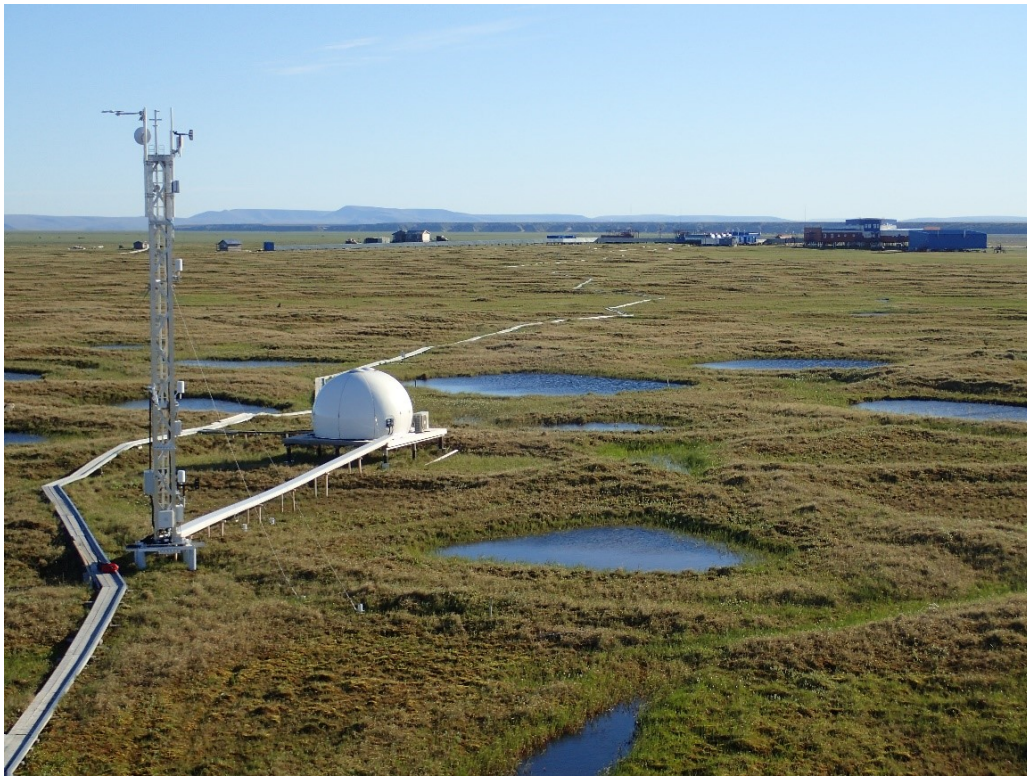


Figure 2.4.2: *Igloo and new tower with meteorological and eddy covariance instruments in June 2018 seen from the old tower*

## 2.5 Monitoring Lena River water at Research Station Samoylov Island

*Bennet Juhls*<sup>1</sup>, (*Paul Overduin*<sup>2</sup>: not in the field), *Anne Morgenstern*<sup>2</sup>, (*Jens Hölemann*<sup>3</sup>: not in the field), *Andrei Astapov*<sup>4</sup>, (*Vasily Povazhniy*<sup>5</sup>: not in the field), *Birgit Heim*<sup>2</sup>, (*Antje Eulenburg*<sup>2</sup>: not in the field), *Hanno Meyer*<sup>2</sup>

<sup>1</sup> Institute of Space Sciences, Freie Universität Berlin, Berlin, Germany

<sup>2</sup> Alfred Wegener Institute Helmholtz Center for Polar and Marine Research, Potsdam, Germany

<sup>3</sup> Alfred Wegener Institute Helmholtz Centre for Polar and Marine Research, Bremerhaven, Germany

<sup>4</sup> Research Station Samoylov Island, Trofimuk Institute for Petroleum Geology and Geophysics, Siberian Branch, Russian Academy of Sciences, Russian Federation

<sup>5</sup> Otto Schmidt Laboratory for Polar and Marine Research, Arctic and Antarctic Research Institute, St. Petersburg, Russian Federation

### Fieldwork period and location

From April 04<sup>th</sup>, 2018 to March 31<sup>st</sup>, 2019 (at Research Station Samoylov Island)

### Objectives

A number of studies predict an increase of carbon export to the Arctic Ocean from rivers due to rapidly changing climate in the Arctic (Camill 2005; Freeman et al. 2001; Frey and Smith 2005). One possible reason for the increase of carbon export is thawing permafrost, which can lead to a mobilization of previously frozen dissolved organic matter (DOM). The Lena River delivers about one fifth of all river water to the Arctic Ocean and is the main source of DOM in the Laptev Sea shelf (Thibodeau et al. 2014). The discharge of the Lena River and the DOM concentration shows an extreme seasonality. Scarce measurements of DOC and the colored fraction of DOM (CDOM) (>8 samples/year) were previously used to estimate fluxes to the Arctic Ocean for the whole year based on a proportional connection between DOM and discharge (Stedmon et al. 2011). Such estimations can potentially result in large errors. Longer sampling periods and higher sampling frequency are needed.

The Research Station Samoylov Island provides a unique opportunity to run a long-term monitoring for Lena River water hydrogeochemistry, because of its location in the central Lena River Delta close to the main channel and its year-round operation by station staff, who can conduct the sampling throughout the year. In April 2018 the monitoring program started (table 2.5.1). It will improve the understanding of seasonal variations of fluxes transported by the Lena River. The over-arching goal is to create a long-term data series, the results of which can provide a reference for all works of the Lena expedition related to hydrogeochemical investigations in the region and baseline for future change detection.

Table 2.5.1: The timing of the sampling efforts in the first field year of the monitoring program

Date	Itinerary
Dec 2017	initiation, preparation of sampling procedure
Feb 2018	Transport of sampling material (first 50 sets) to Samoylov with spring freight
April 2018	Kick-off sample
June 2018	Additional studies on Samoylov by Bennet Juhls
July 2018	Arrival of first season samples in St. Petersburg
Oct 2018	Arrival of first season samples in Potsdam / St. Petersburg
Feb 2019	Re-assessment of sampling protocol after 1 year of data

## Methods

Sampling design aimed at achieving a high-resolution record of constituents of Lena River water over annual cycles. Sampling frequency was chosen to be frequent enough to capture inter-seasonal variability as well as event-driven changes in water composition, such as the spring freshet, storm surges, and ice dynamics. Once established, it became practical to sample twice weekly during the open water season and less frequently (approximately weekly) during the ice season.

The sampling site is located close (walking distance) to the Research Station Samoylov Island at a major branch of the Lena River, the Olenyokskaya Channel. Sampling was carried out mostly from a small boat in the center of the channel during the open water season and from the ice surface when it allowed traffic (Figure 2.5.1). It is important to mention that samples were not taken from the main Lena River channel. Analyzed parameters are therefore restricted to dissolved constituents, with the tacit assumption that dissolved concentrations near Samoylov Island are similar to those of the main channel. The dependence of suspended material concentrations on flowpath and water velocity make it unlikely that the same assumption can be made. The similarity of Samoylov samples to the main river channel will be tested in subsequent field seasons.



Figure 2.5.1: Location of the sampling site close to the Research Station Samoylov Island. During ice conditions, an ice hole was drilled using an auger ice drill and the water sample was taken from that hole after carefully cleaning the ice-flush from the hole.

Sampling and further processing of samples were done as described in Figure 2.5.2. It was conducted by designated station staff, who was thoroughly trained by the science team during the first sampling events in April 2018.


Each sampling event included filling out a form recording the coordinates of sampling, the time of sampling and the results of *in situ* measurements. Temperature and electrical conductivity were measured *in situ*. Changing shoreline position and the presence of ice on the beach mandated a flexible approach to sampling. The sampling forms include a map/image of the southwestern portion of Samoylov Island on which the exact site could be recorded together with any other observations.

Samples were gathered in a 1 L bottle and then split, filtered, conserved and stored for transport to the laboratories in Saint Petersburg and Potsdam, where subsequent analyses will be conducted. Sub-samples were collected for measurements of several parameters, such as temperature, conductivity, DOC (dissolved organic carbon), spectral CDOM absorption (aCDOM), dissolved and total nutrients, and stable isotopes (Table 2.5.2 and A.2.3).

Lena River water sampling instructions 26.03.2018 Bennet Juhs


**Take:**

1 L sample bottle,  
Conductivity meter,  
sample sheet + pen,  
and go to river shore



**Sampling**

1) Sample water into bottle and rinse the bottle two times with lid  
2) Sample 1 Liter Lena water




**Conductivity & Temp.**

1) Measure Conductivity & Temperature in in river directly  
2) Note on sampling sheet  
3) Go back to station




**Clean Syringe**

1) Fill syringe with 20 ml sample water  
2) Pull out syringe to the end and rinse water



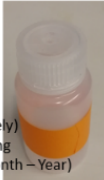
**Isotopes**

1) Rinse isotope bottle (Green, 30ml) with sample water  
2) Fill isotope bottle with unfiltered water to the top  
3) Label bottle with running number + Date ( Day – Month – Year)




**Total nutrients**

1) Take Nutrients bottle (orange, 60 ml)  
2) Rinse bottle with 20 ml sample water  
3) Fill bottle (not completely)  
4) Label bottle with running number + Date ( Day – Month – Year)



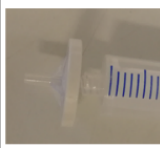
**Rest Sample**

1) Take rest sample bottle (yellow, 60 ml)  
2) Rinse bottle with 20 ml sample water  
3) Fill bottle (not completely)  
4) Label bottle with running number + Date ( Day – Month – Year)



**Syringe filter**

**Attention:**  
If new filter is used (because filter is dirty), new filter needs to be rinsed  
Use for at least every sample day new filter



Lena River water sampling instructions Bennet Juhs

**Dissolved Nutrients**

1) Take 20ml sample water into syringe  
Mount filter  
Rinse water through filter (cleaning)  
Remove filter  
2) Take 50ml water into syringe  
Mount rinsed filter  
3) Filtrate 10ml into sample bottle (white, 60ml)  
4) Rinse sample bottle  
5) Filtrate rest 50 ml into bottle (fill not completely)  
6) Label bottle with running number + Date ( Day – Month – Year)




**DOC**

1) If new filter: Take 10ml sample water into syringe  
Mount filter  
Rinse water through filter (cleaning)  
Remove filter  
2) Take 30ml water into syringe  
3) Mount rinsed filter  
4) Filtrate 10ml into sample bottle (white, 20ml)  
5) Filtrate rest 20 ml to bottle (leave 10% space)  
6) Label bottle with running number + Date ( Day – Month – Year)




**CDOM**

1) If new filter: Take 20ml sample water into syringe  
Mount filter  
Rinse water through filter (cleaning)  
Remove filter  
2) Take 60ml water into syringe  
3) Mount rinsed filter  
4) Filtrate 10ml into sample bottle (white, 50ml)  
5) Rinse sample bottle  
6) Filtrate rest 50 ml into bottle (fill not completely)  
6) Label bottle with running number + Date ( Day – Month – Year)




**Acidify DOC sample**

1) Take on lab gloves & safety glasses  
2) Take eppendorf pipette and mount new pipette tip  
3) Take ca. 25µl HCl (30% suprapur) into pipette  
4) Fill HCl into glas vial  
5) close vial with lid and shake



**Fill sample sheet**



**Store samples**

Isotopes  
CDOM  
DOC  
Rest sample  
Dark & cold (+4°C) → Fridge

**Store samples**

Total Nutrients  
Dissolved Nutrients  
Frozen (-20°C) → Freezer



Figure 2.5.2: Sampling and processing protocol

Table 2.5.2: Overview of measurements and su bsamples for dissolved constituent concentrations

Parameter	Units	Partner for analyses
Temperature	°C	<i>in situ</i>
Conductivity	µS/cm	<i>in situ</i>
DOC	mg/L or µmol1/L	AWI, Potsdam
CDOM	1/m	OSL, St. Petersburg
Dissolved nutrients	µmol1/L, µg/L	OSL, St. Petersburg
Total nutrients	µmol1/L, µg/L	OSL, St. Petersburg
Stable Isotopes	Per mille SMOW	AWI, Potsdam
CDOM EEM (fDOM)		DTU, Copenhagen
Rest sample (60ml)		

In June, additional measurements for light absorption and attenuation were done using an WetLabs AC-S Spectrophotometer. Different filter types and filter pore sizes were tested and compared to each other. Four different filters were used: 0.8 CA, 0.7 GF/F, 0.45 CA and 0.22 CA and filtered and unfiltered absorption and attenuation was measured with the AC-S (Figure 2.5.3, Table A.2.4).

The results of this data will provide information about differences in concentrations of dissolved organic matter dependent on the filter size and type and allows a comparison of the data to previous and future studies.

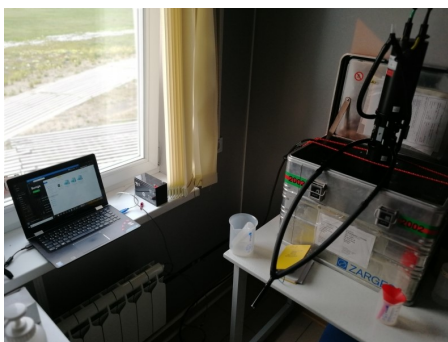


Figure 2.5.3: AC-S bench-top method, measuring absorption and attenuation of unfiltered and filtered water samples

**Preliminary results**

First sample sets were transported to Germany in October 2018 and all parameters listed in Table 2.5.2 were analyzed. Preliminary results show a very strong seasonality of all parameters. Dissolved organic matter concentrations (DOC, CDOM) follow the seasonality of the Lena River discharge with highest concentrations during the river ice break up and lowest concentrations during the winter under ice flow.

Conductivity drops rapidly with onset of the river ice break-up and reaches its minimum shortly after the maximum river discharge in the first week of June. Temperatures of the Lena River increase with a week delay after the maximum river discharge (Figure 2.5.4). We aim to continue these observations with small adaptations and hope to start a long term observation dataset which can potentially provide insight about changing transport of matter from land to sea with ongoing Arctic warming and thawing permafrost.

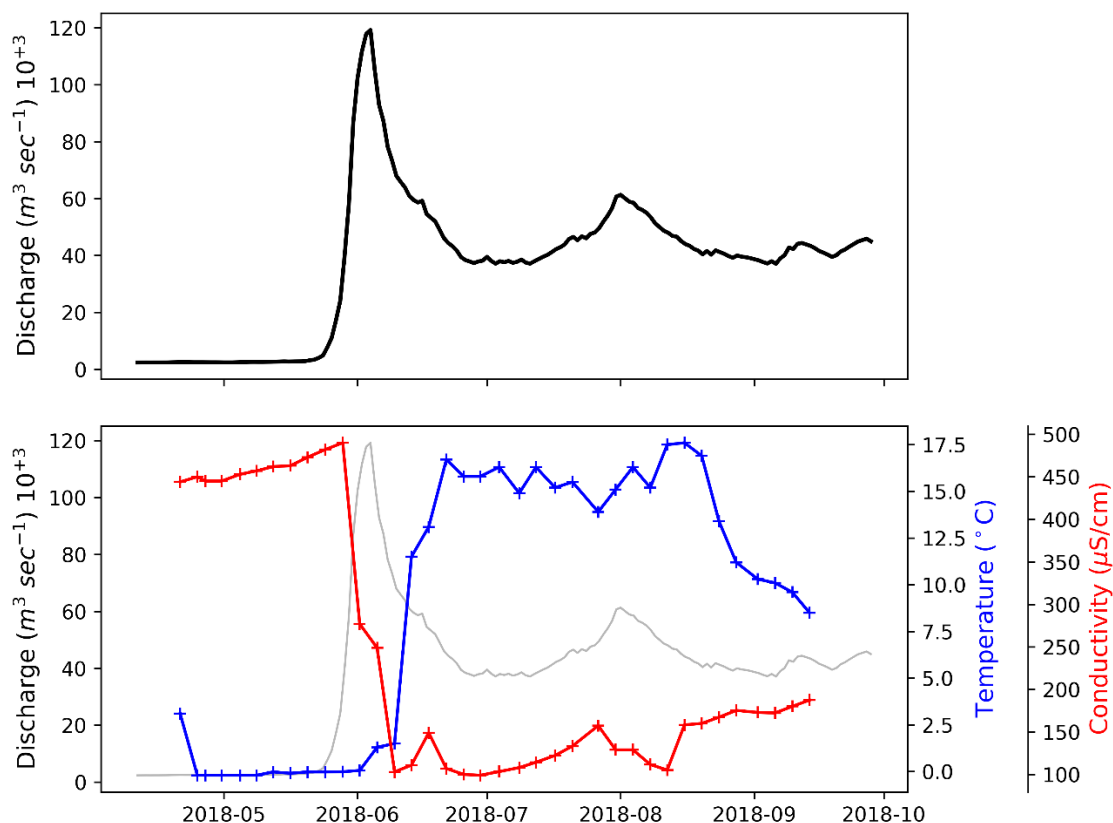


Figure 2.5.4: Upper figure shows the discharge of the Lena River at the Kusur station (data from ArcticGRO, Shiklomanov et al. 2018). Lower figure shows the temperature (blue) and the conductivity (red).



## 2.6 Winter hydrological and hydrobiological investigations on the Lena Delta channels and Samoylov Island lakes

Irina Fedorova <sup>1</sup>, Larisa Frolova <sup>2</sup>, (Gulnara Nigamatzyanova <sup>2</sup>: not in the field)

<sup>1</sup> St. Petersburg State University, St. Petersburg, Russian Federation

<sup>2</sup> Kazan Federal University, Kazan, Russian Federation

### Fieldwork period and location

From April 15<sup>th</sup> to May 01<sup>st</sup> 2018 (Main Channel of the Lena River, Bykovskaya, Olenekskaya and Tumatskaya Channels, Lakes on Samoylov Island)

### Objectives

Field measurements were focused on prolongation of winter monitoring and receiving new information about winter hydrological, hydrochemical, and hydrobiological parameters in the channels and lakes of the Lena River Delta. These observations were done in April 2015, 2016 and 2017, to reveal interannual variability. Some additional hydrometrical and hydrological characteristics had been measured in comparison with 2015, 2016, and 2017. Water discharge of the Lena River was measured on Main Channel, Bykovskaya, Olenekskaya and Tumatskaya Channels of the delta. The monitoring of ice thickness on lakes of Samoylov Island and under ice hydrochemistry were also extended. Hydrobiological studies included the study of zooplankton composition and its quantitative characteristics in different types of water bodies and channels of the Lena River Delta.

### Methods

#### 1. Measurement of winter water discharge

Water discharge measurements were carried out in three Lena River channels (Bykovskaya, Olenekskaya and Tumatskaya) as well as on a profile across the main channel, 4.7 km upstream of Stolb Island (Figure 2.6.1). Profiles were located at representative (standard) channel positions where Russian Hydrometeorological Service has been measuring since 1951 (for the main channel and Bykovskaya Channel) and since 1977 (for Trofimovskaya and Tumatskaya Channel). Time schedule of measurements in April 2017 is presented in Table A.2.5. Hydrometrical work included measuring of a snow thickness. After drilling ice-holes with a moto auger, a stick measured the ice thickness; the water depth (H) was determined by echo sounder Garmin 521s. Water velocity (v) were determined with an ISP-1 current meter on the several verticals and standard horizons: (0.15H, 0.65H and 0.85H under ice). Afterwards water samples were taken near the surface (0.15H), at intermediate depths (0.65H) and near the bottom (0.85H) (Table A.2.6). Amount of verticals on a channel were determined according to the channel width but not than 500 m between verticals. Water discharge (Q) will be calculated by the equation  $Q = F * v$ , were  $F$  means a square of a channel profile (Fedorova et al. 2015).

#### 2. Water sampling in the channels and lakes, laboratory analysis

Samples for total suspended matter were collected in chosen verticals and horizons (on different water depths) of the River channel profiles and lakes of Samoylov Island (Figure 2.6.2). Water samples were collected by plastic water sampler of HidroBios (<https://www.hydrobios.de/de/>) with a volume 2.5 L. Conductivity and dissolved oxygen O<sub>2</sub> were measured in a field by the Hanna company portative loggers. For a turbidity water was filtered in the laboratory through a pre-prepared paper filters (diameter 10 cm) to "Kuprin" filtration device or through glass microfiber or polycarbonate filters (GF pore size of 0.45 nm, diameter 4.7 cm and PC) with vacuum system. Paper filter were used for the turbidity receiving; PC filters and GF filters – for following geochemistry analyses.). Further filters were dried and weighed in the laboratory. Turbidity was determined as the difference between full and empty the filter divided by the volume of the sample. According to the calculated water discharge and turbidity, suspended supply will be determined. pH and RedOx potential Eh was measured in the laboratory with multiparametrical device (WTW 340i). All sample for further hydrochemical analyses were filtrated through cellulose acetate (cations, anions, isotopes) or glass (DOC, CDOM) filters.

Samples for cations and DOC were preserved with 65% HNO<sub>3</sub> and 30% HCl and stored in 4 °C. Nutrient samples were kept frozen. These samples were transported to St. Petersburg for later analyses

### 3. Sample locations

Hydrobiological samples were taken in three thermokarst lakes of Samoylov Island and in Bykovskaya, Oleneskaya and Tumatskaya Channels. Sampling of zooplankton was carried out by filtering with the help of the Epstein plankton net (mesh size is 100 µm, diameter 19 cm) and was fixed with 70% alcohol or 4% borax-buffered formalin. Hydrobiology analyses including microscopy and calculation of indexes were carried out according to standard methods (Konstantinov 1986). The main structural characteristics of zooplankton communities were analyzed. The assessment of water quality was carried out on the basis of on the Pantle–Buck saprobity index in Sádeček's modification and the Zelinka and Marwan saprobity index (Sládeček 1973; Zelinka 1961). The trophic status of the reservoirs was determined by the Shannon's diversity index on the basis of the zooplankton biomass data (Shannon 1949).

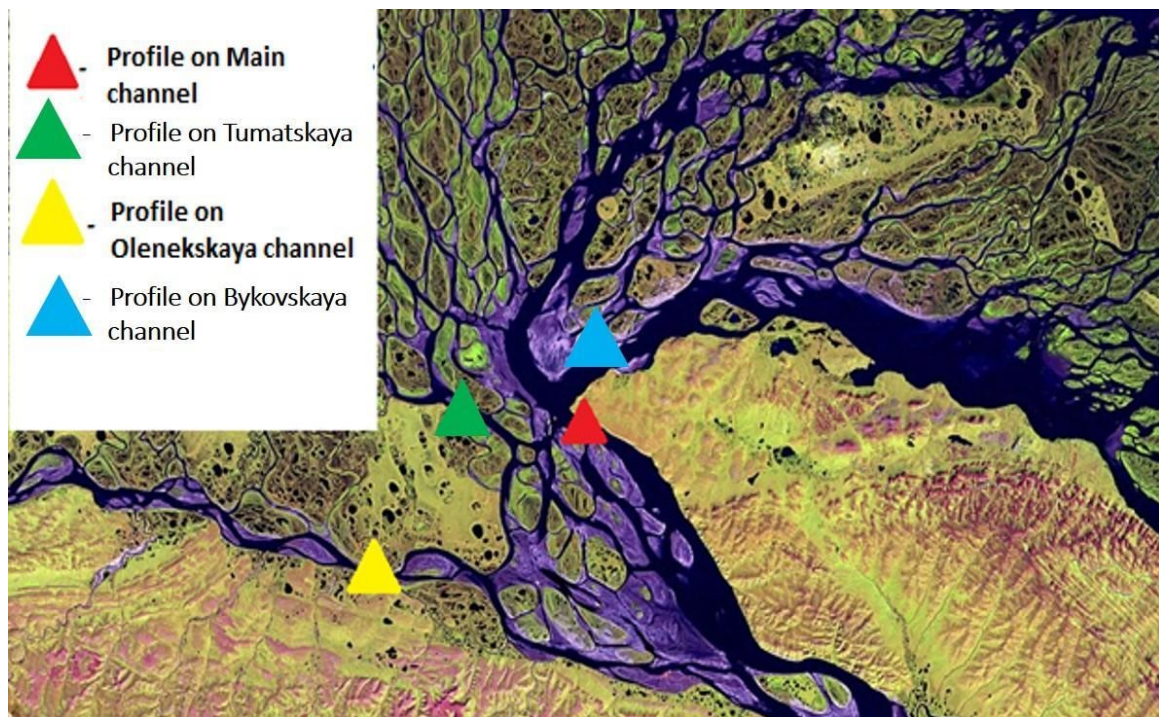


Figure 2.6.1: Location of the sampling transects on the Lena River channels

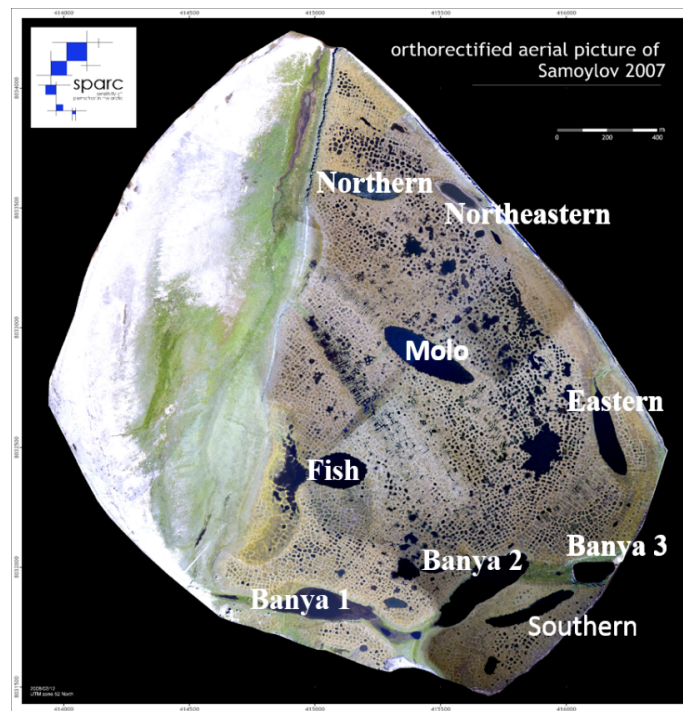


Figure 2.6.2: Sampled lakes on Samoylov Island

### Preliminary results

In April 2018 hydrological field measurements were carried out to extend previous investigations and included standard hydrometrical measurements.

We measured water and sediment discharge on the Main Channel, Bykovskaya, Oleneskaya and Tumatskaya branches in winter at low discharge.

Ice thickness on the channels ranged from 1.6 m on the vertical 2 of the Main Channel to 2.15 m near the right bank of Bykovskaya (Table A.2.5). Ice thickness of lakes value from 1.40 m to 2.20 m on Molo and Northern Lakes correspondingly. Maximal snow thickness on ice was reaches 0.9 m on Lakes (Eastern Lake) and 0.65 m on channels (Tumatskaya) that is less than in April 2017. On the Bykovskaya Channel as well as on Northern and Southern lakes most stations were without snow at all. Profile of the Main Channel gauge line is on the Figure 2.6.3.

Maximal water depth was observed in the Main Channel of the Lena River; 28.3 m (vertical 3), while the Oleneskaya Channel was only approximately 3.1 m deep. Water level of channels was on (“+”) and under (“-”) ice surface (Table A.2.5). Water velocity in channels was 0.131 m/s maximum in the Main Channel, maximum 0.176 m/s in the Bykovskaya Channel, 0.043 m/s in Oleneskaya Channel, and no velocity was measured in Tumatskaya Channel (Table A.2.6). The velocities were a little bit less than in April 2017.

Temperature of water in channels was about 1 °C, in lacustrine water temperature value from –0.1 °C (in Banya 2 and Banya 3 lakes) to 2.6 °C (in Northern lake) (Table A.2.7, A.2.9).

Comparative value for hydrochemical parameters of channels and lakes are in the Table A.2.9. Conductivity of channels was much higher than in lakes except Banya 1 lake with conductivity 466  $\mu\text{S}/\text{cm}$ . Minimum value is 110  $\mu\text{S}/\text{cm}$  for Banya 2. Sometimes conductivity of lakes is in 4 times less than for channels (Table A.2.8, A.2.9 and Figure 2.6.4). It is very important to know that when measured on site at low water temperature (about –0.1 °C) the value should be corrected to standard temperature (25 °C). For example, observed conductivity 272.1 with temperature –0.7 °C will have normalized meaning 560.3  $\mu\text{S}/\text{cm}$ . Channel water conductivity ranged not significant 424 to 371  $\mu\text{S}/\text{cm}$ .

pH was neutral in all channels and sub acid for several lakes (Table A.2.9). Dissolved oxygen concentration for lacustrine water had a higher variation from 3.87 (Banya 1 lake) to 13.43 mg/L (Banya 2 lake). Dissolved oxygen in channels' water had 7.7 to 8.16 mg/L meanings.

Quite interesting results can be found on RedOx potential Eh (mV) analyses (Table A.2.9, 2.6.1 and Figure 2.6.5). For most part of lakes Eh had values 5-32 Eh positive meanings. It means oxidizing-reduction conditions with unstable hydrochemical regime and variable content of hydrogen sulfide H<sub>2</sub>S and oxygen in water. All riverine water and Banya 1 Lake had negative Eh; reduction conditions with possibility of hydrogen sulfide H<sub>2</sub>S in water.

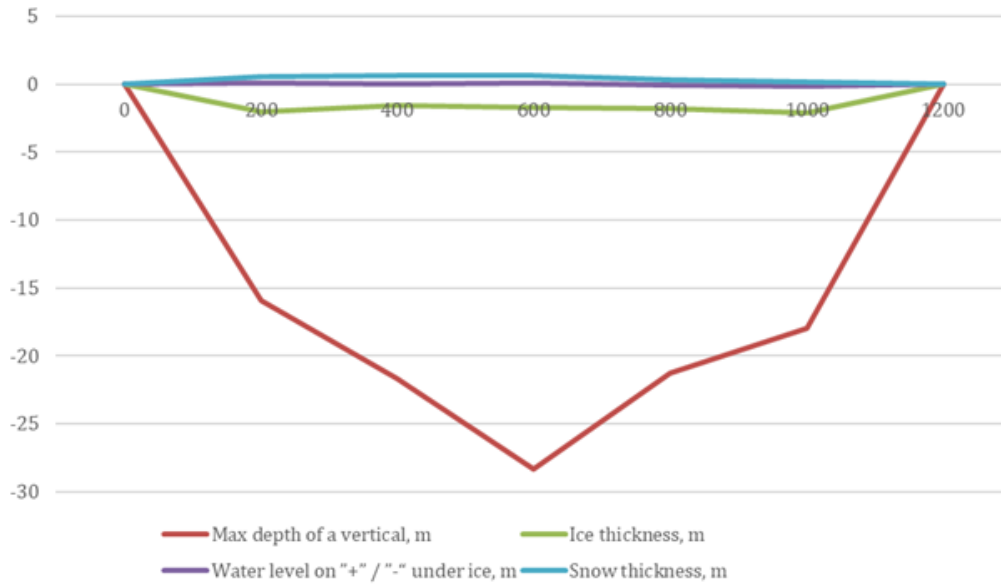


Figure 2.6.3: Profile of the Main Channel

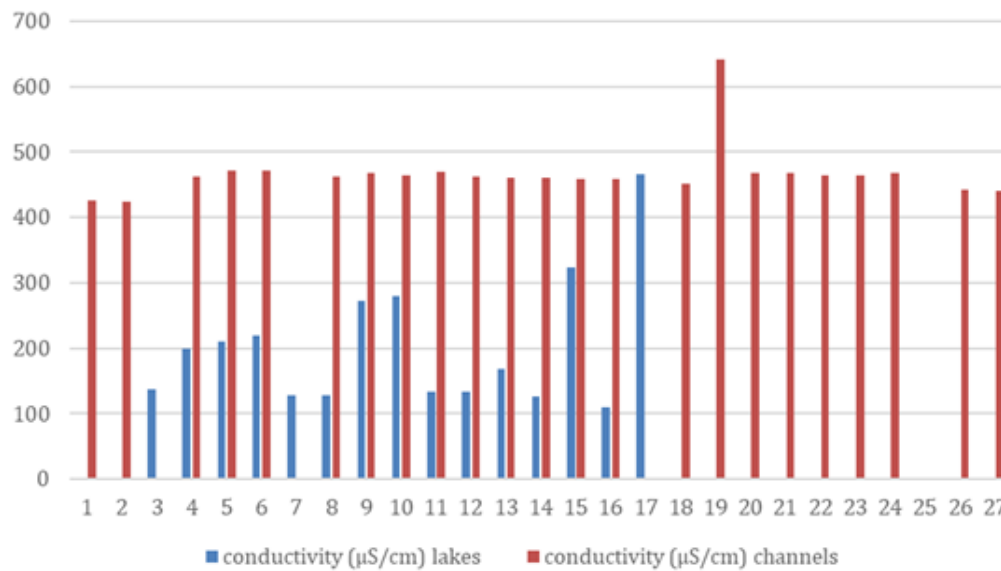


Figure 2.6.4: Conductivity of lakes and channels of the Lena Delta in April 2018

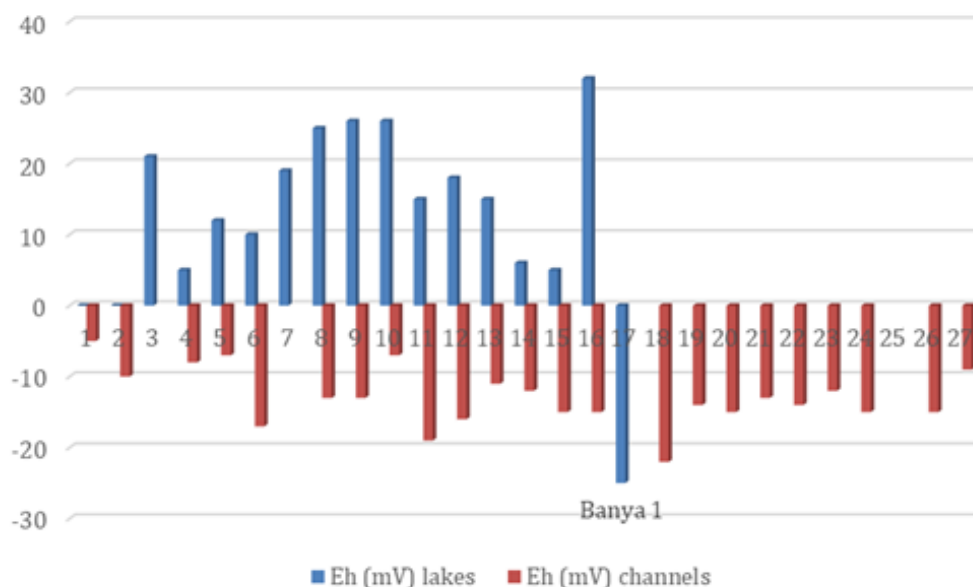


Figure 2.6.5: Redox potential Eh (mV) of lakes and channels

Table 2.6.1: Comparison of hydrochemical parameters of lakes and channels

Objects	water temperature [°C]		pH		Eh [mV]		conductivity [μS/cm]		Dissolved oxygen water [mg/L]	
	min	max	min	max	min	max	min	max	min	max
Lakes	-0.1	2.6	6.48	7.45	-25	32	110	466	3.87	13.43
Channels	1.2	1.5	7.16	7.33	-22	-5	424	471	7.7	8.16

#### Preliminary results of spring zooplankton analysis

Spring zooplankton in the Lena Delta channels and studied thermokarst lakes was represented by extremely low number of taxa (12 taxa). The zooplankton species composition was dominated by *Rotifera*. The abundance of zooplankton of lakes were determined by juvenile stages of copepods. The zooplankton abundance in channels was determined by *Rotifera*, the biomass by copepods. The average values of zooplankton abundance was 4.9 thousand ind./m<sup>3</sup> and biomass - 29.2 mg/m. The values of the Shannon-Weaver species diversity indices was relatively low; 1.60 for lakes and 0.54 for channels, indicating low species diversity of zooplankton communities. The level of saprobity index characterizes the lakes and channels as oligo saprobic according to the Pantle–Buck saprobity index in Sládeček's modification (S=1.40 for lakes and 1.49 for channels). In accordance with the Zelinka and Marwan saprobity index the studied lakes and channels were characterized as oligo saprobic with a deviation in  $\beta$ -mesosaprobic zone. Among the main species dominating in frequency of occurrence and quantitative indicators in all types of lakes were *Kellicotia longispina* (Kellikot, 1879), *Eudiaptomus graciloides* (Lilljeborg, 1888). Juvenile stages of copepods, *Conochilus unicornis* (Rousselet, 1892) and *Keratella cochlearis* (Gosse, 1851) were noted in most samples.

Thus, the investigated spring zooplankton of lakes and channels of the Lena River Delta was estimated as quite poor in species diversity. The dominant species were cold-water, typical components of the zooplankton in northern waters.

## 2.7 Hydrological measurements in the Olenekskaya Channel

*Dmitriy Bolshiyakov<sup>1</sup>, Vyacheslav Polyakov<sup>1</sup>*

<sup>1</sup> Arctic and Antarctic Research Institute, St. Petersburg, Russian Federation

### Fieldwork period and location

From July 08<sup>th</sup> to July 13<sup>th</sup>, 2018 (Olenekskaya Channel (N 72.30111°, E 126.08497°), Gusinka site (N 72.49844°, E 125.23772°), and Chay-Tumus site (N 72.36131°, E 125.66614°))

### Objectives

The aim of hydrological measurements in the Olenekskaya Channel was to confirm the loss of water flow from the beginning of the channel to the middle part of the channel, which was observed in previous years. It was planned to measure the flow of water in the Olenekskaya Channel in three sections: main Olenekskaya, Chay-Tumus and Gusinka (Figure 2.7.1).

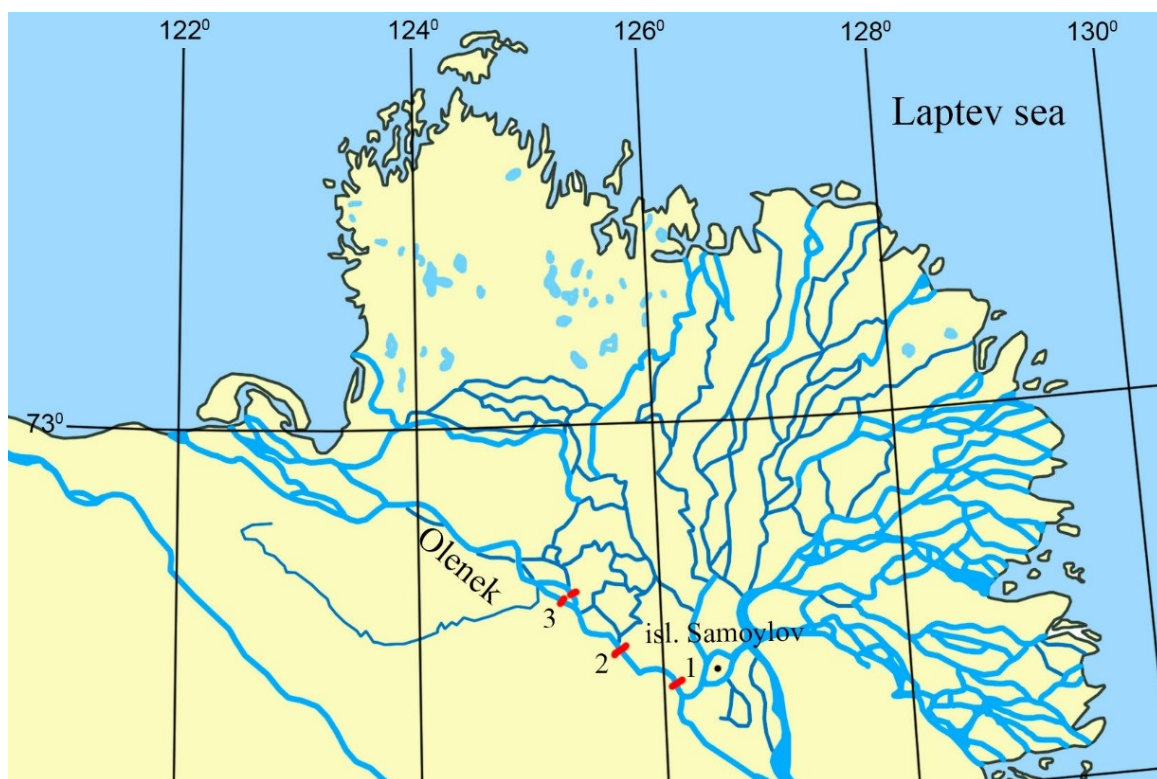


Figure 2.7.1: The study sites of the Lena River Delta. 1- Main Channel (Olenekskaya); 2- Chay-Tumus; 3- Gusinka.

### Methods

The measurements of water speed were carried out from a rubber boat using the GR-21M hydrological current meter, checked on May 15<sup>th</sup>, 2018, by the State Hydrological Institute of the Russian Federation.

The measurements of the main Olenekskaya Channel (N 72.30111°, E 126.08497°) were performed on July 9<sup>th</sup>, 2018, at the Gusinka site (N 72.498444°, E 125.237722°) on July 12<sup>th</sup>, 2018, and the Chay-Tumus site (N 72.36131°, E 125.66614°) on July 8<sup>th</sup>, 2018, and July 13<sup>th</sup>, 2018. The Olenekskaya Channel in the main section and on the Chay Tumus flows in one channel. At the Gusinka site, there are two channels (Figure 2.7.2), which required measurements on two gauge lines.

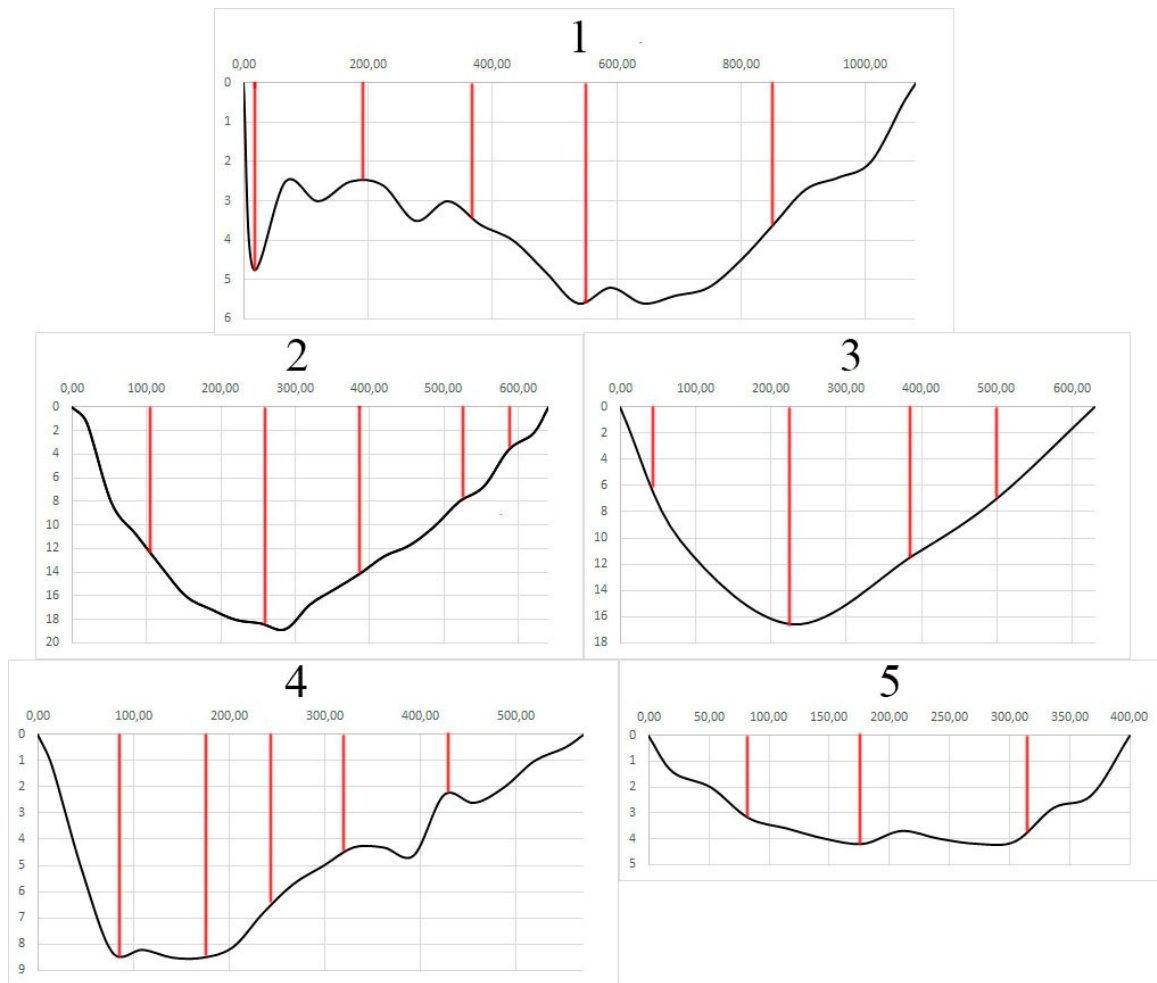


Figure 2.7.2: Water flow measurement results of study sites. 1 – Main Olenekskaya channel; 2,3 – Chay Tumus; 4,5 – Gusinka.

### Preliminary results

The results of measured water flows are presented in Table 2.7.1. The measurements were carried out in different phases of the sea level. On the Olenekskaya Channel, on July 8<sup>th</sup> 2018, and on July 9<sup>th</sup> 2018, measurements took place during the decline of the water level in the channel (up to 20 cm/d). The measurements on July 12<sup>th</sup> and 13<sup>th</sup>, 2018, occurred during the rise of the water level (only 5 to 7 cm/d), but the wind surge during a storm with northwesterly winds caused clear water recharge and slower flow rates, which can be seen when comparing the flow rates of Chay Tumus.

Table 2.7.1: The results of measured water flows

Channel	Date	Water discharge [m <sup>3</sup> /s]
Olenekskaya (main gauge line)	09.07.2018	2022.9
Olenekskaya (Chai-Tumus gauge line)	08.07.2018	2658.7
Olenekskaya (Chai-Tumus gauge line)	13.07.2018	1343.5
Olenekskaya (Gusinka gauge line)	12.07.2018	1765.6

In the Olenekskaya Channel, water flow changes significantly as a result of wind surges and drifts. Longer and frequent hydrometric measurements are required to detect flow changes along the flow path.

## 2.8 Isotopic composition of the snow cover on Samoylov Island and its modification in spring

Thomas Opel<sup>1,2</sup>, Hanno Meyer<sup>2</sup>

<sup>1</sup> Permafrost Laboratory, Department of Geography, University of Sussex, Brighton, United Kingdom

<sup>2</sup> Alfred Wegener Institute Helmholtz Center for Polar and Marine Research, Potsdam, Germany

### Fieldwork period and location

From April 18<sup>th</sup> to May 13<sup>th</sup>, 2018 (on Samoylov Island)

### Objectives

(1) The main objective of this research team is an improved understanding of how modern wedge-ice formation is related to the snow-cover transformation in spring and how the stable-isotope signal is transferred from snow into ice wedges in the polygonal tundra of Samoylov Island.

Over the last years, polygonal ice wedges from Arctic permafrost regions have been increasingly utilized as climate archives because they preserve the stable isotope composition of oxygen ( $\delta^{18}\text{O}$ ) and hydrogen ( $\delta\text{D}$ ) over long periods. Due to their specific formation conditions, in particular frost cracking due to thermal contraction and frost-crack filling by snowmelt, ice wedges are strictly confined to the cold period of the year when precipitation falls as snow (hereafter referred to as winter). Their stable-isotope composition provides unique paleoclimate information (i.e. past temperatures) that is not or not adequately captured by other climate archives in the Arctic, which record mainly summer climate conditions (Meyer et al. 2015).

For a better deployment of ice-wedge-based isotope data towards a calibration to temperatures, an improved understanding of the involved processes such as sublimation, wind drift, depth hoar formation, and snowmelt, and in particular their impact on the stable isotope composition of the remaining snow cover is urgently needed.

(2) A second objective of the research group is to investigate frost cracking and crack infill processes. To date, there is only insufficient knowledge of frost crack dynamics, i.e. timing, spatial and temporal patterns of frequency, width, depth, development in winter and spring, potential plugs blocking the frost crack and the filling process.

(3) The third objective of the research group is to improve the understanding of the modern isotope hydrology with a focus on the differential wintertime freezing of different water bodies, such as shallow polygonal ponds, thermokarst lakes as well as the Lena River.

### Methods

#### (1) Snow studies

The snow studies built on earlier work on Samoylov Island in 2013 and 2016: They comprised the repeated detailed survey and sampling of a snow profile across a snow-covered low-center polygon with a diameter of about 20 m. The polygonal pond has a diameter of about 13 m and according to coring results from 2016 (LD16-BH-1A) and 2018 (LD18-BH-2, see below) the water depth is about 40 cm. The polygon walls are up to about 30 cm elevated above the frozen pond. The polygon walls are up to about 5 m wide, show clearly developed troughs, and are vegetated with mosses, herbaceous shrubs (*Carex*, *Salix*), sedges and lichens of 3 to 10 cm height.

The 21 m long snow profile in E-W direction was selected on April 19<sup>th</sup> and marked every meter by numbered poles (from 0 to 21, Figure 2.8.1). The sampling site is identical to LD13-SP-8 from the Lena 2013 expedition and LD16-SP-1 from the Lena 2016 expedition and situated between N 72.3705°, E 126.482037° and N 72.37055°, E 126.48265°.

At the profile the following working steps were carried out: (1) Measurements of snow cover thickness, (2) Detailed visual description of the snow cover incl a detailed photo documentation, (3) Sampling of the entire snow cover with a liner tube, (4) Detailed snow sampling of single horizons, (5) Snow temperature measurements, and (6) Snow density measurements.





Figure 2.8.1: Selected snow profile LD18-SP-1 on April 19<sup>th</sup> before sampling

The snow profile was repeatedly sampled on April 19<sup>th</sup>/20<sup>th</sup> (as LD18-SP-1), on April 26<sup>th</sup>/27<sup>th</sup> (as LD18-SP-2), on May 2<sup>nd</sup>/4<sup>th</sup> (as LD18-SP-3), and on May 9<sup>th</sup>/10<sup>th</sup> (as LD18-SP-4). On April 23<sup>rd</sup> a core of 1.05 m length (LD18-BH-1) was drilled using a Kovacs Mark III corer from a snow drift close to the Samoylov Station, in order to test for older snow from the preceding winter. Additionally, snow pits were sampled across Samoylov Island in connection with frost-crack studies.

### (2) Frost crack and crack infill studies

To investigate frost cracking and crack infill processes we carried out surveys and sampling focusing on troughs of polygon rims. After removing the snow cover, we determined the state of frost cracks (i.e. open, closed, filled, plugged, not cracked) of this winter using different tools such as spatula and wire (approximately 3 mm in diameter) and measured widths and depths. Furthermore, the snow cover above the trough was described and sampled with a particular focus on depth hoar and ice layers. Additionally, we sampled ice accretions in polygonal troughs potentially plugging the cracks. In total, 27 frost cracks and corresponding snow pits were studied and sampled (47 samples of snow, 33 samples of depth hoar, 15 samples of ice).

### (3) Drilling cores of pond, lake and river ice

The ice covers on polygonal ponds, thermokarst lakes and the Lena River were drilled with an ice drill Kovacs Mark III. All these coring positions are indicative of the respective freezing conditions and processes (open vs. closed system freezing) since last fall and winter that are archived in the lake, pond or river ice stable isotopes. On April 23<sup>rd</sup>, the polygonal pond belonging to the investigated snow profile was cored and yielded an ice core of 40 cm (LD18-BH-2). On April 24<sup>th</sup>, a 2.01 m long ice core (LD18-BH-3) was drilled at Shallow Lake at N 72.375169°, E 126.511306°. Additionally, a sample of the still unfrozen water under the ice was taken. On April 29<sup>th</sup>, Molo Lake (N 72.377942°, E 126.497124°) was cored and two cores were retrieved: LD18-BH-4 (1.81 m) and LD18-BH-5 (0.51 m long, from 1.30 to 1.81 m depth). Fish Lake (N 72.373781°, E 126.487333°) was also drilled on April 29<sup>th</sup> and two cores were retrieved: LD18-BH-6 (1.50 m) and LD18-BH-7 (1.23 m). Additionally, a sample of unfrozen water was taken. On May 4<sup>th</sup>, a 1.44 m long core (LD18-BH-8) was drilled from the Lena River at N 72.367545°, E 126.468242° as well as a sample of unfrozen river water taken. On May 6<sup>th</sup>, Shallow Lake (N 72.375011°, E 126.510853°) was revisited to drill another 1.63 m core (LD18-BH-9) and another sample of unfrozen lake water was taken. Additionally, a core of 1.01 m length (LD18-BH-10) from a polygonal pond close to the snow profile (N 72.370755°, E 126.482865°) was drilled. On May 7<sup>th</sup>, Kurungnakh Island was visited to drill two cores from two thermokarst lakes: LD18-BH-11 (1.93 m) at N 72.297046°, E 126.118249° and LD18-BH-12 (2.01 m) at N 72.295004°, E 126.204703°, complemented by a sample of unfrozen lake water.

## Preliminary results

All samples are listed in Table A.2.10 in the Appendix.

### (1) Snow studies

On April 19<sup>th</sup>, the snow cover thickness along our profile varied between 9 cm on the western polygon wall and 32 cm in the polygon center (mean 23 cm). Depth hoar in the lowest part of the snow profile accounted for between 2 and 20 cm (mean 8 cm). The snow temperature was relatively uniform and varied between  $-10.9^{\circ}\text{C}$  in 5 cm depth and  $-13.5^{\circ}\text{C}$  at 30 cm depth above the pond ice. The mean density of the complete snow cover (based on liner tube samples every meter) yielded  $284 \text{ kgm}^3$ . This and the following density values have to be treated with caution as sometimes the depth hoar proportion of the snow cover may be not sampled completely. An earlier melt event manifested in a thin ice layer within the snow cover.

Snowfall and in particular snow drift due to heavy wind changed the snow cover significantly until the next study of the snow profile (Figures 2.8.2, 2.8.3). On April 25<sup>th</sup>, the snow cover thickness varied between 10 cm on the western wall and 58 cm in the polygon center (mean 39 cm). The depth hoar thickness varied between 3 and 24 cm (mean 10 cm). The mean snow density was  $291 \text{ kgm}^3$ .

Further snow drift and snow fall occurred over the next days. A low-pressure system with temperatures up to  $2^{\circ}\text{C}$  and bringing some rain passed Samoylov Island on May 1<sup>st</sup>/2<sup>nd</sup> and lead to changes in snow cover stratigraphy on the tundra surface. Dry and soft snow turned into wet snow before changing to hard and compact layers. Generally, a slightly reduced snow cover could be observed particularly on polygon walls (Figures 2.8.2, 2.8.3). Along our profile this was mainly reflected on the eastern polygon wall. On May 2<sup>nd</sup>, the snow cover thickness of our snow profile varied between 7 and 62 cm (mean 40 cm). The depth hoar thickness varied between 0 and 23.5 cm (mean 9 cm). The mean snow density increased to  $314 \text{ kgm}^3$ . The snow temperature varied between  $-12.1^{\circ}\text{C}$  close to the frozen ground and  $-3.9^{\circ}\text{C}$  close to the snow surface).

Only slight changes could be observed until the last sampling of the snow profile (Figures 2.8.2, 2.8.3). On May 9<sup>th</sup>, the snow cover thickness varied between 4.5 cm on the eastern polygon wall and 59 cm in the polygon center (mean 39 cm). The depth hoar varied between 0 and 22 cm (mean 10 cm). Even though the ice layer frequency has increased, the mean snow density decreased to  $297 \text{ kgm}^3$ . During daytime sampling the snow temperature varied between  $-0.4^{\circ}\text{C}$  close to the snow surface and  $-10.8^{\circ}\text{C}$  close to the frozen ground.

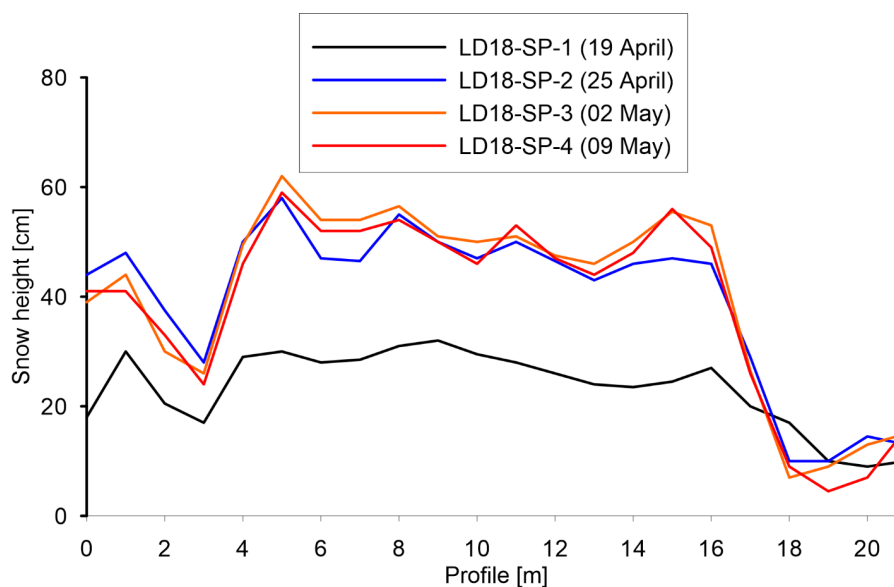


Figure 2.8.2: Snow cover thickness along the studied profile on April 19<sup>th</sup>, April 25<sup>th</sup>, May 02<sup>nd</sup>, and May 11<sup>th</sup>. Note that the topography of the polygon was not considered in this figure. The polygon walls (up to about 30 cm high) are represented by the profile sections 0 to 4 m (east) and 17 to 21 m (west).

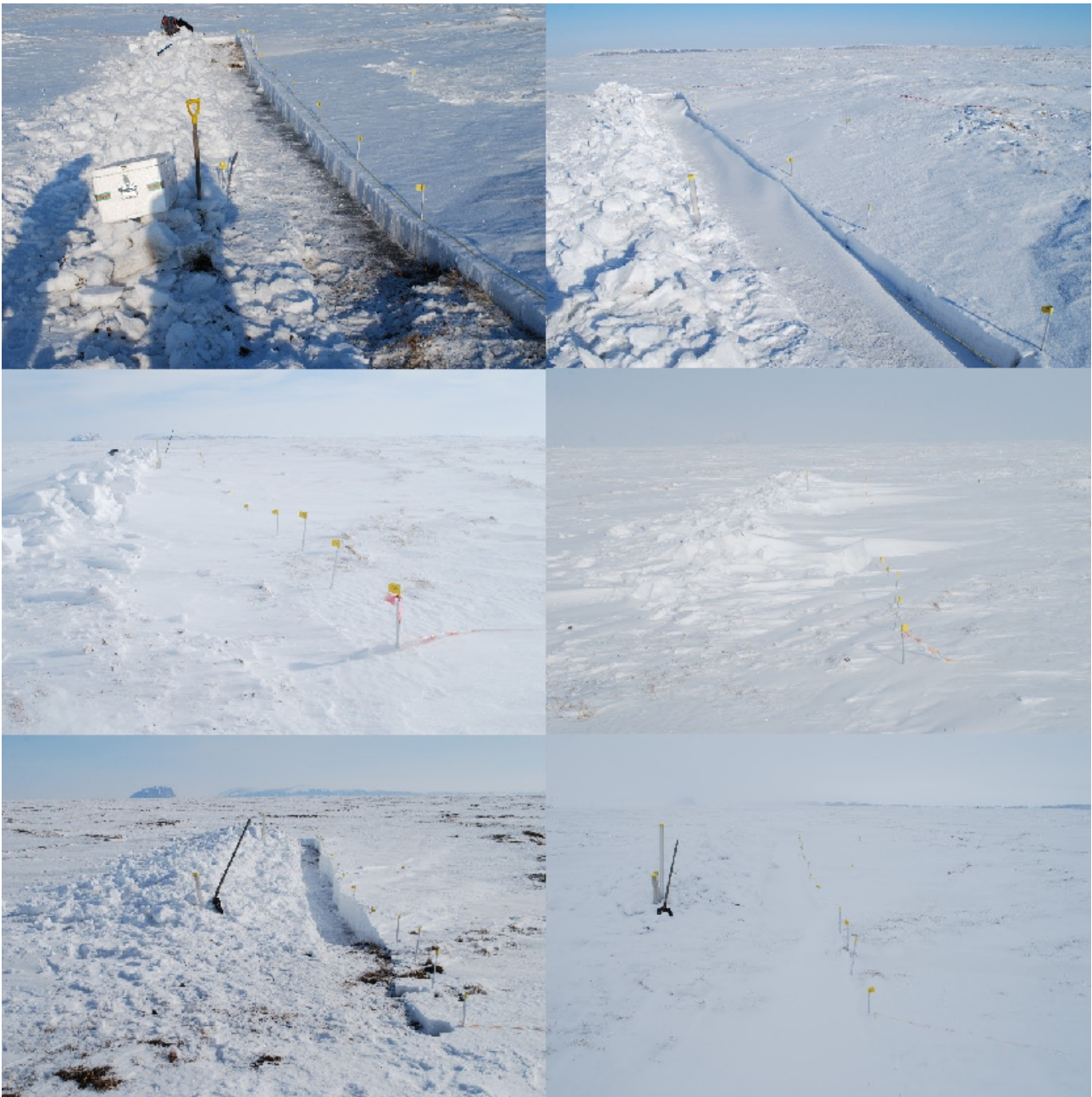


Figure 2.8.3: The studied snow profile on April 19<sup>th</sup> (top left), April 22<sup>nd</sup> (top right), April 26<sup>th</sup> (middle left), April 28<sup>th</sup> (middle right), May 4<sup>th</sup> (bottom left) and May 11<sup>th</sup> (bottom right)

(2) Frost crack and crack infill studies

The field observations clearly showed that no frost cracks were visible at the snow surface at the beginning of the fieldwork. This changed only after the melting/rain event on May 1<sup>st</sup>/2<sup>nd</sup>, when some cracks, formerly hidden in the snow cover, became detectable. Only in some cases, frost cracks of the preceding winter could be found at all. These frost cracks were up to 3 cm wide at the ground surface, but mostly between 0.5 and 0.8 cm (Figure 2.8.4).



Figure 2.8.4: Top view of a frost crack in a polygonal trough

The frost cracks detected were mostly sealed or plugged with ice accretions in a depth of about 20 cm, corresponding to the approximate position of the permafrost table. Only for one crack a depth of about 1 m could be detected using the steel wire probe. In snow pits above polygonal troughs, sometime ground frost cracks extended into the deeper depth hoar and snow layers, and partly into ice layers in the snow cover (Figure 2.8.5).

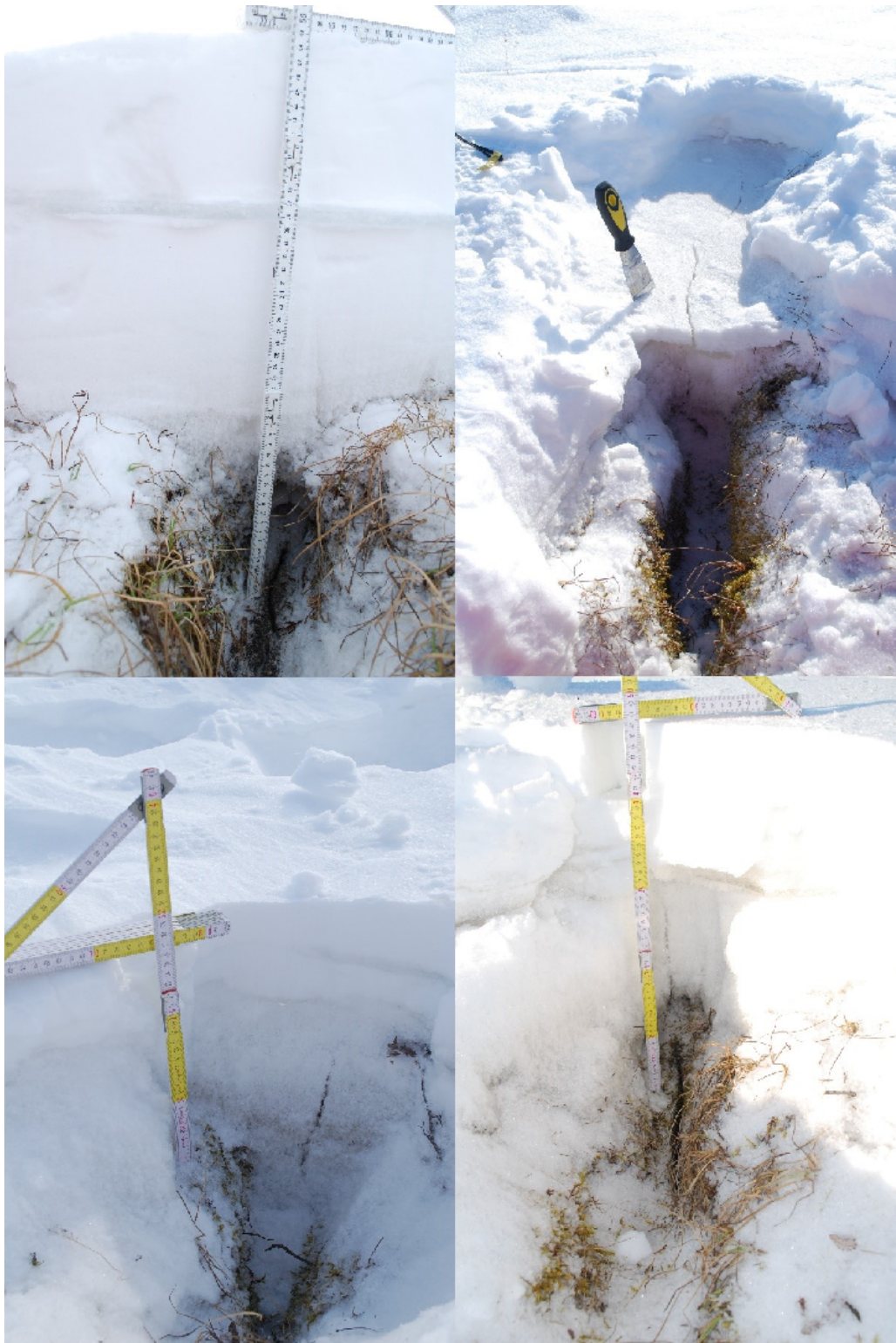


Figure 2.8.5: Different examples of frost cracks extending into the snow cover, consisting of depth hoar in the lower part and fresher snow in the upper part, sometimes also ice layers.

### Acknowledgements

A part of this research has received funding from the European Union's Horizon 2020 project INTERACT, under grant agreement No 730938.

## 2.9 Water vapour isotope analyses on Samoylov Island

Hanno Meyer <sup>1</sup>, (Jean-Louis Bonne <sup>2</sup>, Martin Werner <sup>2</sup>, Sepp Kipfstuhl <sup>2</sup>, Benjamin Rabe <sup>2</sup>, Melanie Behrens <sup>2</sup>, Lutz Schönike <sup>1</sup>: not in the field)

<sup>1</sup> Alfred Wegener Institute Helmholtz Center for Polar and Marine Research, Potsdam, Germany

<sup>2</sup> Alfred Wegener Institute Helmholtz Centre for Polar and Marine Research, Bremerhaven, Germany

### Fieldwork period and location

From April 18<sup>th</sup> to May 13<sup>th</sup>, 2018 (on Samoylov Island)

### Objectives

The project ISOARC, supported by AWI strategy fund, aims at understanding the water transport pathways in the Arctic with a focus on Northern Eurasia. The *in situ* water vapour isotopic analysers, installed at Research Station Samoylov Island and on-board Polarstern in July 2015, and associated with a network of ground stations in Eurasian Arctic from collaborating institutes, provide a dataset of specific humidity, H<sub>2</sub><sup>18</sup>O and HDO, covering an approximately 6000 km transect of the eastern Arctic. This will allow for a quantitative assessment of the Eurasian Arctic water cycle, its isotopic variations and imprint in various climate archives.

### Methods

A Cavity Ring Down Spectroscopy (CRDS) analyser (Picarro, Inc. L2140-i) has been running continuously since July 2015. It alternately measures stable oxygen and hydrogen isotopes of either ambient air (sampled through a heated tube, with an inlet located at about 5 meters height above ground level) or air coming from one of the two custom-made calibration units. Two independent calibration systems have been installed for a better resilience of the instrument: a vaporizer system allowing for a four-point calibration and a custom-made dew point generator, later named "bubbler", allowing for a one-point standard calibration. Two types of calibrations are performed: (i) correction of the humidity concentration-dependence by measuring each standard across a range of humidity values covering the expected ambient air humidity values, and (ii) repeated corrections of the deviation from the VSMOW-SLAP scale by fitting a linear regression between the known values and the measured values of a set of water standards, also allowing for the correction of the instrumental drift.

Troubles with the heating system directly pointing to the L2140i analyser lead to a data gap between April 14<sup>th</sup>-18<sup>th</sup>, 2018. The system showed an error message (safety mode because too high cavity and DAS temperatures) and stopped working with the room being at more than 30 °C. After switching off the heater and cooling down the container room, where the analyzer is situated, and after a computer restart the system started working again.

All the capillaries were cut and all calibration lines were dried for future use. Furthermore, the UltraTorr connector for the temperature safety in the bubbler cooler box was fixed. The Valco-Tee connection of Line 3B was renewed. All standards of bubbler and vaporiser were subsampled for testing the stability of the standards over time. The bubbler was refilled with 150 mL of standard T27 Mix (open bottle), and an additional sample was taken for calibration. For all standard lines and the bubbler, isotope-humidity response curves were measured for different humidity levels between 30.000 and 1.000 ppm with similar results as last year (Bonne et al. 2018). Having a satisfying quality dry air source as a carrier gas is a requirement for water vapour measurements, especially in winter when ambient air has a very low humidity. For this purpose, the chemical dessiccant (Drierite) in the dry air inlet line has been exchanged and the old batch dried for future use. In order to attempt limiting the frequency of clogging of the fused silica capillaries, which are used to deliver liquid water standards for the calibration, filters have been exchanged after the dry air source to prevent particles from entering the calibration unit. Additionally, a routine maintenance of all consumables has been done on site in May 2018.

### Preliminary results

Data acquired since July 2015, as shown on Figure 2.9.1, clearly depict variability on multiple time scales. Yearly cycles on specific humidity and  $\delta^{18}\text{O}$  reveal seasonal variations of large amplitudes. Synoptic events lead to strong isotopic changes within a few days, which might be related to variations of the moisture sources.

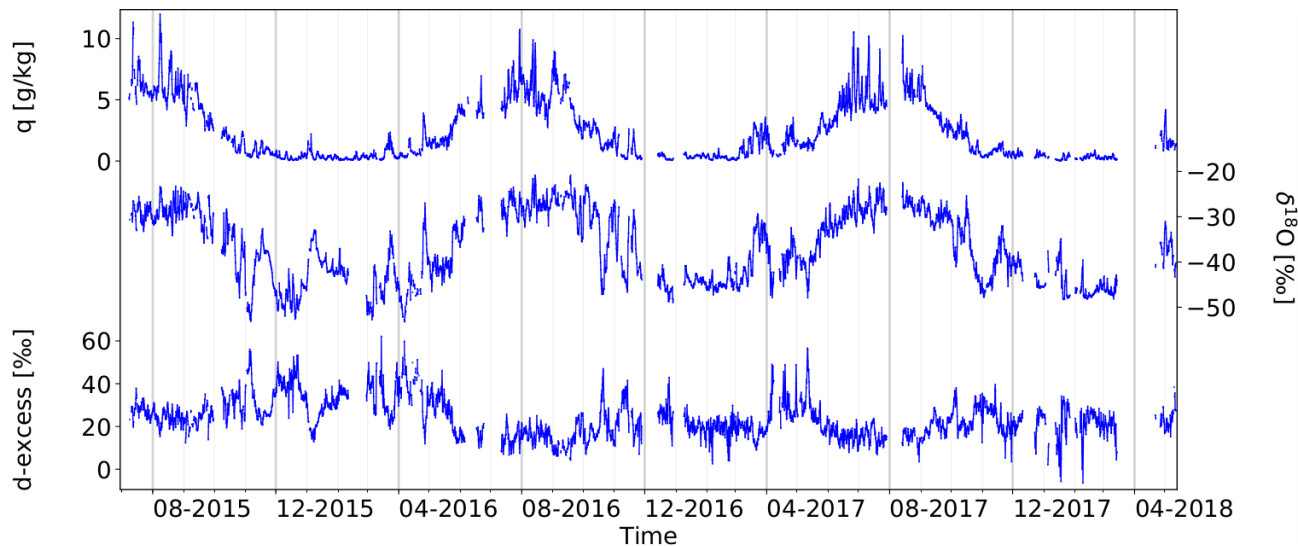


Figure 2.9.1: Time series of water vapour isotopic observations on Samoylov Island from July 1<sup>st</sup>, 2015, to May 13<sup>th</sup>, 2018

## 2.10 Studying the spatial variability on Samoylov Island: analysis of CO<sub>2</sub> fluxes, precipitation and snow cover simulation

Xavier Buchwalder <sup>1</sup>, Annina Riedhauser <sup>1</sup>, Nicolas Jullien <sup>1</sup>, Flore Chappuis <sup>1</sup>, Franziska Gerber <sup>1,2</sup>, Annelen Kahl <sup>1,2</sup>

<sup>1</sup> École Polytechnique Fédérale de Lausanne, Lausanne, Switzerland

<sup>2</sup> WSL Institute for Snow and Avalance Research SLF, Davos, Switzerland

### Fieldwork period and location

From August 23<sup>th</sup> to September 14<sup>th</sup>, 2018 (on Samoylov Island)

### Objectives

The objective for the group of students that we were was to have a first contact with the field work in the great North as well as deepening the understanding of the island that we had from previous year students. The research this year focused on assessing and analysing the spatial variability on the island. We tried to separate different types of soils and terrain, and study their differences as well as their reaction to the meteorological conditions. The measurements and analysis were then implemented into the snow cover model SNOWPACK to test its use in Arctic areas.

As a group of students, the expedition had also a pedagogical objective, Andreii Kartoziya from Novosibirsk University taught us about the geology of the region as well as helped us understanding its characteristics. As a first contact with the scientific world, we also had the opportunity to help the scientists present on the station in their work.

### Field work summary and preliminary results

Three meteorological stations (Sensorscope) have been used to measure air, surface and subsurface temperature, relative humidity, wind speed and direction, incoming shortwave radiation, and precipitation with a tipping bucket. The stations have been installed in the polygonal tundra, the floodplain and the sandy beach. These stations provided useful data to mostly complement the ones we collected by other means.

The other instruments used to measure precipitation were two PARSIVEL Disdrometers that were placed on the floodplain and the polygonal tundra. They provided a much more precise precipitation measurement than the classical tipping bucket used for most of the sampling around the world. A picture of both instruments is shown in Figure 2.10.1 and the comparison of the rain accumulation is shown in Figure 2.10.2. The PARSIVEL in the polygonal tundra was installed semi-permanently to measure precipitation during the winter 2018/19 and is located at N 72.370139°, E 126.479806°.





Figure 2.10.1: *Sensorscope station and PARSIVEL disdrometer*

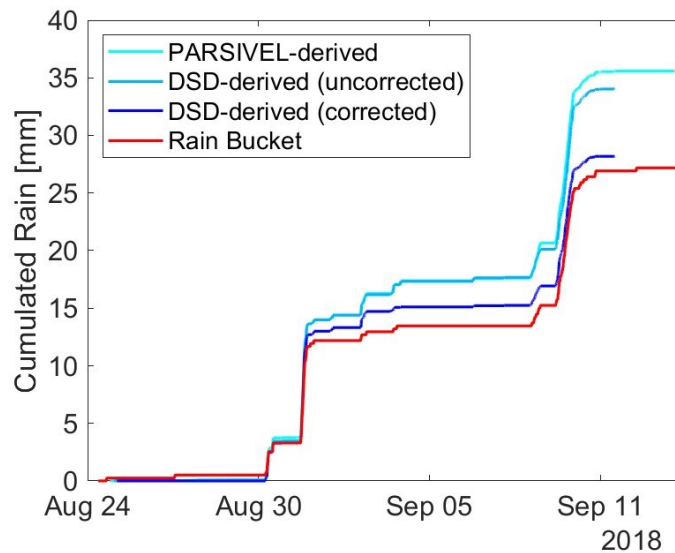


Figure 2.10.2: *Comparison of precipitation measurements between the rain bucket and the uncorrected and corrected PARSIVEL values*

A second part of the project was to test the SNOWPACK model (Bartelt and Lehning 2002) in Arctic conditions. This model was developed to simulate the snow cover and Alpine permafrost, but is in need of testing for different conditions. To improve the simulation, we measured several characteristics of the soils we were testing, the

density, the water content and the type of soil. We complemented it with data gathered in Langer et al. (2013). This was implemented in the model to provide a simulation as close to reality as possible. In addition to it, we used meteorological data collected on the island by Julia Boike from 2002 to 2017 (Boike et al. 2019) to have a local and precise measurement of the evolution of the weather over the years. The results of a simulation of the snow cover from 2002 to 2017 is shown in Figure 2.10.3.

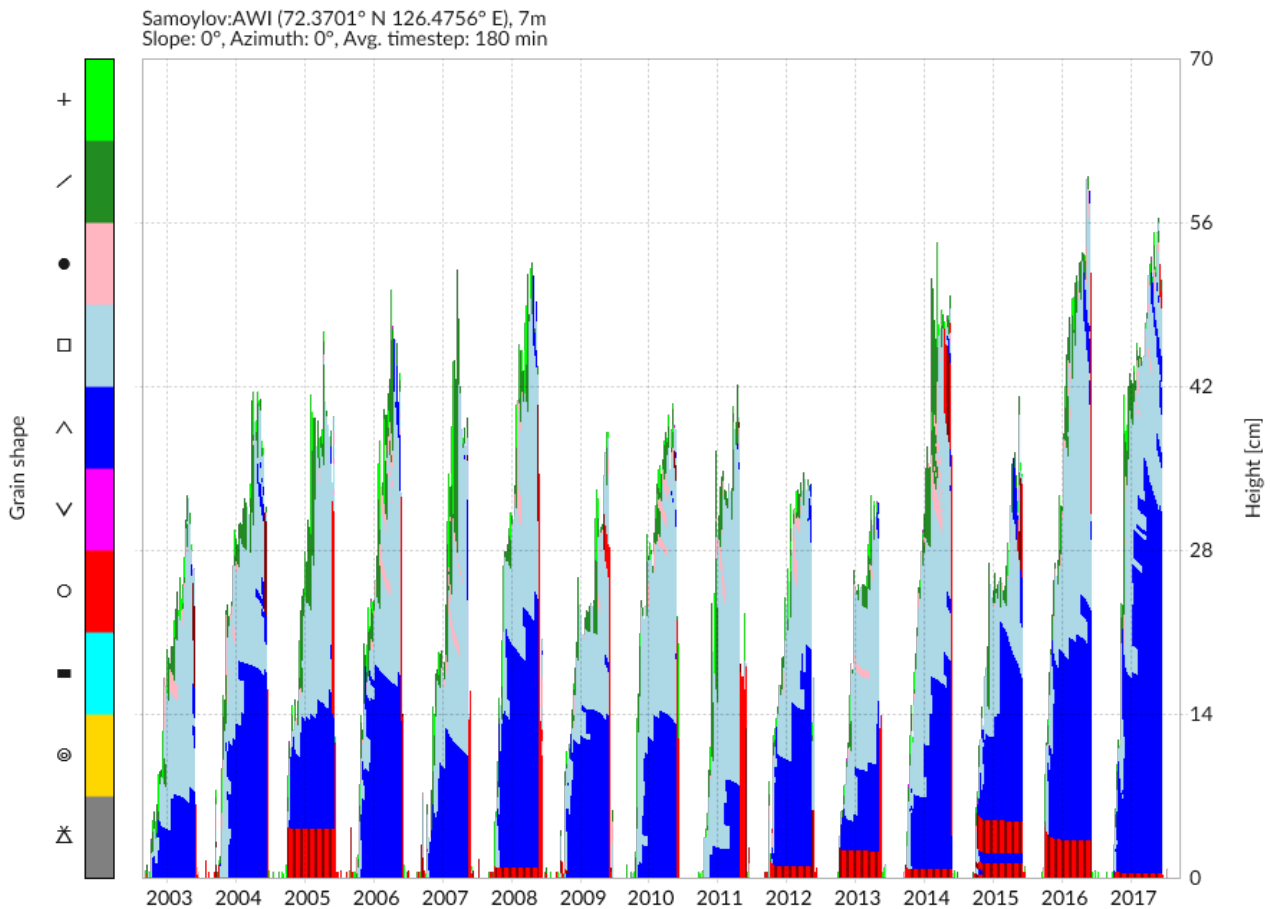


Figure 2.10.3: *SNOWPACK simulation of the grain shapes in the snow cover from 2003 to 2017*

A third part of the project was to analyse the CO<sub>2</sub> fluxes on the island. It was decided to separate them like we did with the Sensorscope stations, i.e. between the different regions of Samoylov Island (sandy beach, floodplain and polygonal tundra). Two different kind of measurements were performed. We set up one stationary sampling zone per soil type (reference plot), to which we added one random measurement per available day. A map of the measurements is shown in Fig 2.10.4. We added temperature and soil moisture data to all these CO<sub>2</sub> fluxes. Using both it was attempted to predict the CO<sub>2</sub> flux, and then compare it with the measured fluxes. A map showing the success rate of the method is shown in Fig. 2.10.5.

Details of the various measurement campaigns, the collected data and the subsequent analysis are described in a full project report, submitted by the students (in case of interested please contact: Xavier.buchwalder@epfl.ch). In addition to the field work performed for our interests, we had the chance to help different scientists from AWI on their missions, we wish to thank Christian, Aline, Oliver and many others for letting us join and help them a little bit in their work on the different islands.

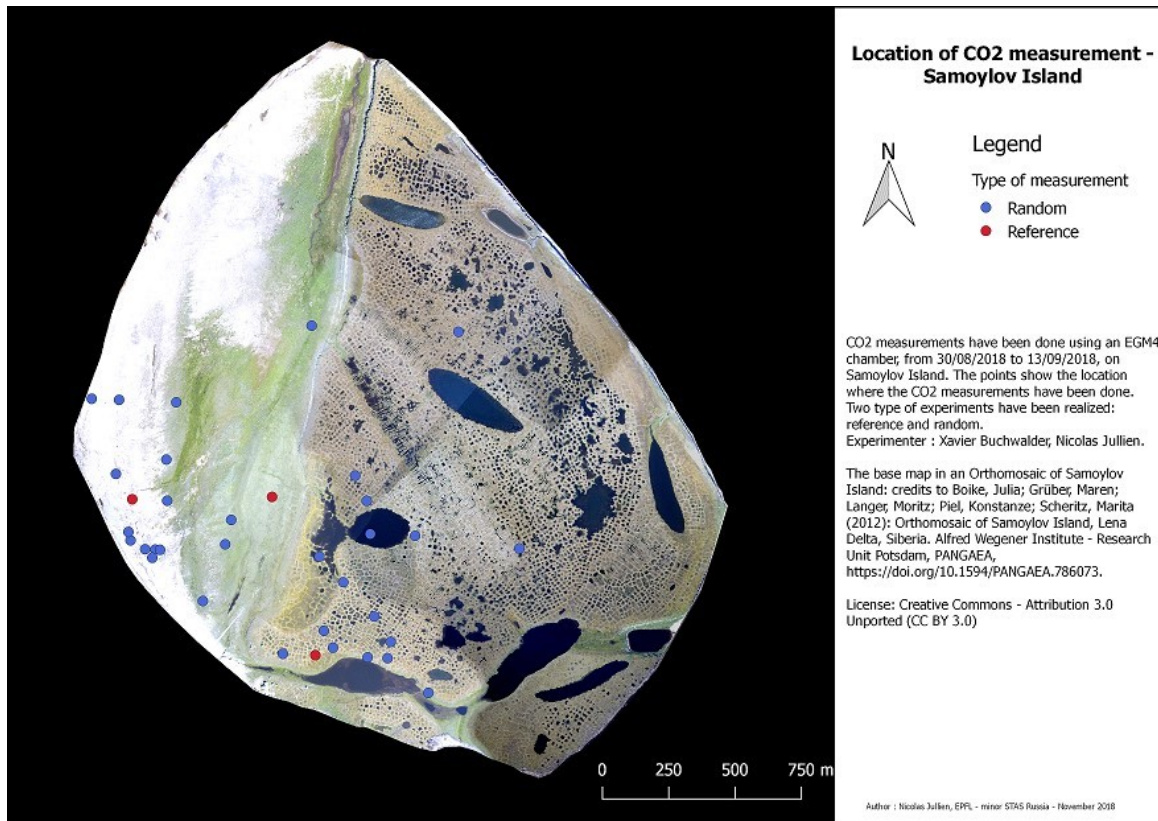


Figure 2.10.4: Location of the random and reference plots used for CO<sub>2</sub> fluxes measurements

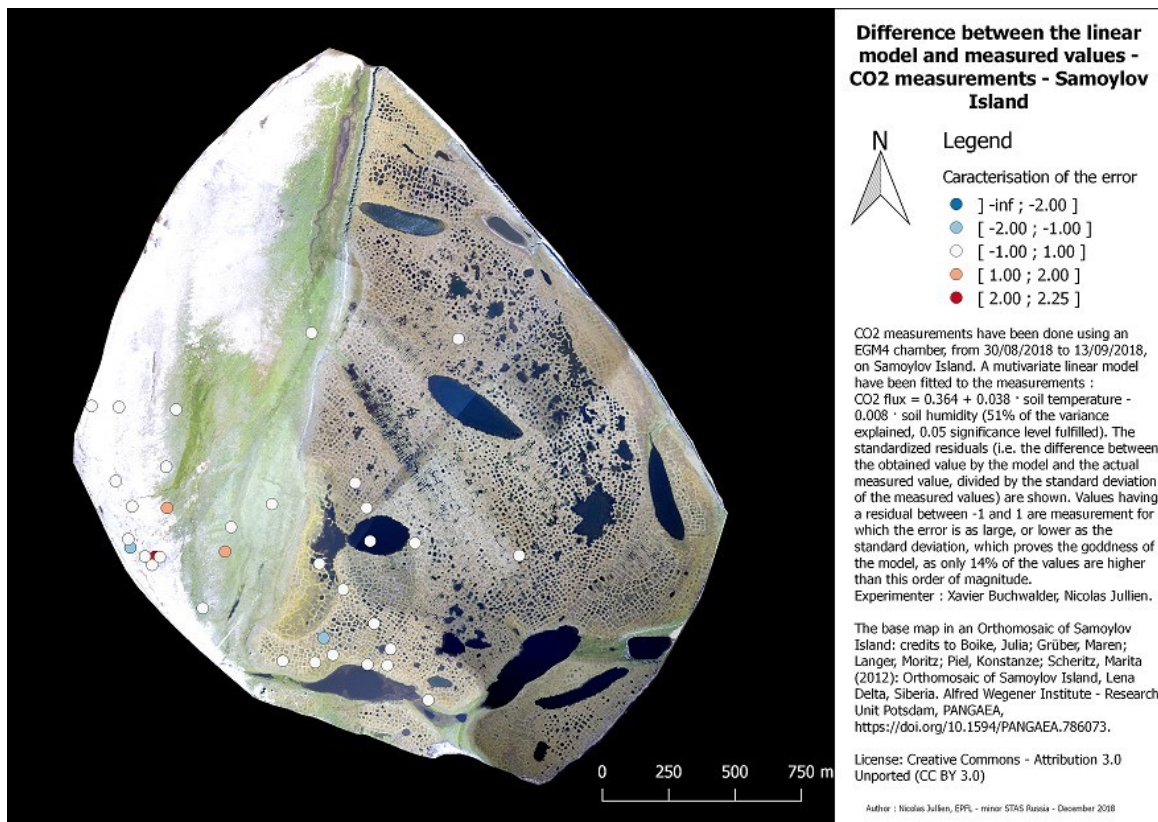


Figure 2.10.5: Map of the comparison between predicted and measured values of CO<sub>2</sub> fluxes, red and orange is overestimation, and blue is underestimation of the flux

## 2.11 Greenhouse gas release from buried soil: field incubation study

Svetlana Evgrafova <sup>1,2</sup>, Valeriy Kadutskiy <sup>2</sup>, Birgit Heim <sup>3</sup>

<sup>1</sup> Sukachev Institute of Forest, Siberian Branch, Russian Academy of Sciences, Krasnoyarsk, Russian Federation

<sup>2</sup> Siberian Federal University, Krasnoyarsk, Russian Federation

<sup>3</sup> Alfred Wegener Institute Helmholtz Center for Polar and Marine Research, Potsdam, Germany

### Fieldwork period and location

From July 31<sup>st</sup> to September 03<sup>rd</sup>, 2018 (on Samoylov Island)

### Objectives

To measure the microbial response and associated carbon release in gaseous forms (CO<sub>2</sub>, CH<sub>4</sub>) from organic matter that has been permanently frozen, we performed an *in situ* field-based incubation experiment in a rim of an ice-wedge polygon on Samoylov Island near Research Station Samoylov Island.

The basic research question is how fast thawed buried organic matter can be mineralized under *in situ* conditions to CO<sub>2</sub> and CH<sub>4</sub>.

### Methods

Frozen buried soil was taken from Holocene permafrost that had been exposed by erosion of the Lena riverbank. We transferred the material partly to the top of the active layer and partly into the subsoil in a rim of an ice-wedge polygon. Detailed experiment design described in Strauss et al. (2018). The intention was that formerly frozen soil was moved to the active layer, while still residing in the subsoil to mimic cryoturbation processes, or was exposed to the soil surface to simulate eroded riverbank. Experiment location and view from the top see (Figure 2.11.1). The experiment was installed in August 2015 (plots with buried soil covered by living groundcover of 5 cm thickness), and in August, 2016 (plots with uncovered buried soil). During August 2018, we measured CO<sub>2</sub> and CH<sub>4</sub> efflux from experimental plots using gas chromatograph installed in Samoylov's lab in order to continue monitoring of greenhouse gas release from buried soil.

CO<sub>2</sub> and CH<sub>4</sub> fluxes were measured by a closed chamber technique. Samples of formerly buried soil were taken to characterize chemical and microbiological properties. Additional gas samples were taken for the measurement of  $\delta^{13}\text{C}$  in the laboratory at the Institute of Forest, Krasnoyarsk, Russia. Soil temperature was measured daily at noon using a Campbell data logger (Campbell Scientific, Ltd., USA) that was permanently installed with 5 sensors in different soil depth. Air temperature during gas sampling was recorded by the weather station at Research Station Samoylov Island. The active layer thickness was measured manually using a metal probe.



Figure 2.11.1: *Field-based incubation experiment: view from the top and location on Samoylov Island. A - part of experiment simulated eroded river bank (Exp\_open), B - part of experiment simulated cryoturbation (Exp\_covered), C - Campbell data logger (sensors are installed on neighboring ice-wedge polygon)*

### Preliminary results

CO<sub>2</sub> and CH<sub>4</sub> released from the experimental plots were sampled every second day during August, 2018, measured using gas chromatograph and quantified according to Lal (2016). Preliminary results showed that in comparison to previous data obtained in 2015-2017, CH<sub>4</sub> release from cryoturbation simulation experiment was lower in plots contained buried soil than in disturbance control plots. In contrast, CH<sub>4</sub> release from eroded river bank experiment showed higher values that were registered in 2015-2017 (Figure 2.11.2, A). CO<sub>2</sub> release from both variant of the experiment was distinctly larger in plots contained buried soil than in disturbance control plots during the whole period of monitoring in August 2018. We should mention that this fact was registered first time over the whole period of CO<sub>2</sub> release monitoring from the experiment installation (Figure 2.11.2, B).

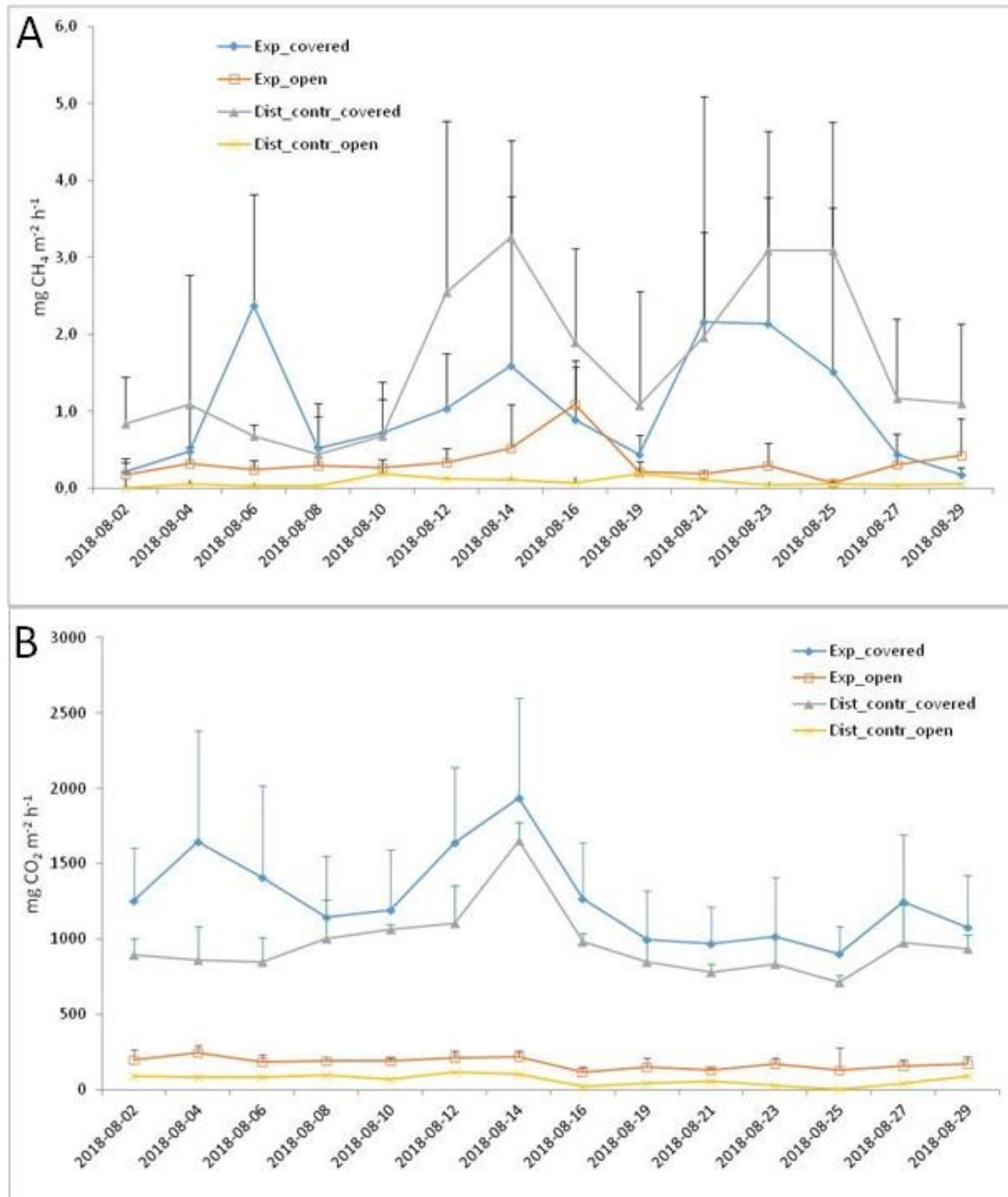


Figure 2.11.2: Release of CH<sub>4</sub> (A) and CO<sub>2</sub> (B) over time from soil in a field-based experiment. Legend: *Exp\_covered*: mean value between plots with buried soil covered by groundcover (5 cm thickness); *Exp\_open*: mean value between plots with uncovered buried soil; *Dist\_contr\_covered*: mean value between plots without buried soil covered by groundcover (5 cm thickness); *Dist\_contr\_open*: uncovered plots without buried soil. Bars indicate standard deviations (n=3).

## 2.12 Spatial and temporal distribution of recently assimilated carbon dioxide at the soil-plant interface

*Tim Eckhardt*<sup>1,2</sup>, *Christian Knoblauch*<sup>1,2</sup>, *Philipp Wischhöfer*<sup>3</sup>, *Stine Holm*<sup>4</sup>, *Pavel Barsukov*<sup>5</sup>, *Nikolay Lashchinskiy*<sup>6</sup>, *Norman Rüggen*<sup>1,2</sup>, (*Eva-Maria Pfeiffer*<sup>1,2</sup>: not in the field)

<sup>1</sup> Institute of Soil Science, Universität Hamburg, Hamburg, Germany

<sup>2</sup> Center for Earth System Research and Sustainability, Universität Hamburg, Hamburg, Germany

<sup>3</sup> Institute of Geology and Mineralogy, University of Cologne, Cologne, Germany

<sup>4</sup> Section of Geomicrobiology, GFZ German Research Centre for Geoscience Helmholtz Centre Potsdam, Potsdam, Germany

<sup>5</sup> Institute of Soil Science and Agrochemistry, Siberian Branch, Russian Academy of Sciences, Novosibirsk, Russian Federation

<sup>6</sup> Central Siberian Botanical Garden, Siberian Branch, Russian Academy of Sciences, Novosibirsk, Russian Federation

### Fieldwork period and location

From July 11<sup>th</sup> to September 20<sup>th</sup>, 2018 (on the Floodplain (N 72.37692°, E 126.48230°) and the first River Terrace (N 72.37494°, E 126.47775°) of Samoylov Island)

### Objectives

The overall objective of our fieldwork is to gain a deeper understanding of the processes of carbon (C) turnover in the coupled system soil-vegetation-atmosphere. Therefore, we conducted a tracer experiment where we provided <sup>13</sup>C-labelled CO<sub>2</sub> for plant photosynthesis to follow the flux of atmospheric CO<sub>2</sub> on its pathway through the vegetation into the plant and soil and subsequently out of the soil into the atmosphere as CO<sub>2</sub> and CH<sub>4</sub>. The experiment was conducted by closed chamber measurements at two sites that differed in vegetation and soil properties. The overall research questions are i) How much recently assimilated CO<sub>2</sub> enters the soil via autotrophic respiration? ii) How high is the turnover of recently assimilated C in the soil within a vegetation period? iii) Are there differences in C sequestration between sites of the polygonal tundra and the floodplain and which parameter are causing this difference? iv) Are the study sites a source or sink for atmospheric C during the vegetation period?

### Methods

The experiments were conducted in close cooperation between the project partners of the KoPf project from the University of Cologne, the GFZ German Research Centre for Geosciences, Universität Hamburg and Russian partners from Novosibirsk. The experiments started at the beginning of July and samples were taken until mid-September 2018 (Figure 2.12.1). To provide plants with <sup>13</sup>C-enriched CO<sub>2</sub> for photosynthesis, a closed chamber measurement system was used.

The experiment was conducted at two sites with similar hydrologic conditions, but different vegetation and soil conditions: a water-saturated polygon center in the polygonal tundra and a water-saturated site on a floodplain. After the <sup>13</sup>C-CO<sub>2</sub> pulse labelling, samples were taken at both sites on a regular basis until the end of the vegetation period. These samples comprised plant leaves and roots as well as soil and water. Furthermore, respiration fluxes were measured regularly and gas samples for isotope analysis were taken (Figure 2.12.2). Close to the labelled sites control sites without <sup>13</sup>C-CO<sub>2</sub> labelling were established and regularly sampled (see Table A.2.11). Additionally, 50 cm deep soil cores were taken at both study sites and the vegetation composition was analyzed.

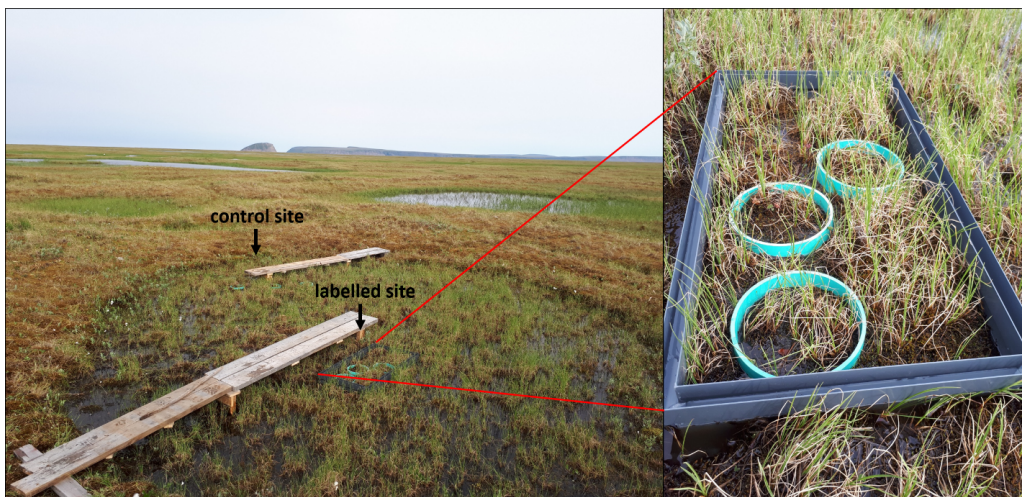


Figure 2.12.1: The sampling site at the polygonal tundra on Samoylov Island

**Preliminary results**

The soil and vegetation composition differed between the two study sites. While sedges (mainly *Carex concolor*) and mosses (*Meesia triquetra*, *Scorpidium scorpioides*, *Drepanocladus revolvens*) dominated the polygon center, a shrub-moss (*Salix glauca*, *Meesia triquetra*) community with less abundant sedges (*Carex concolor*) dominated the site at the floodplain.

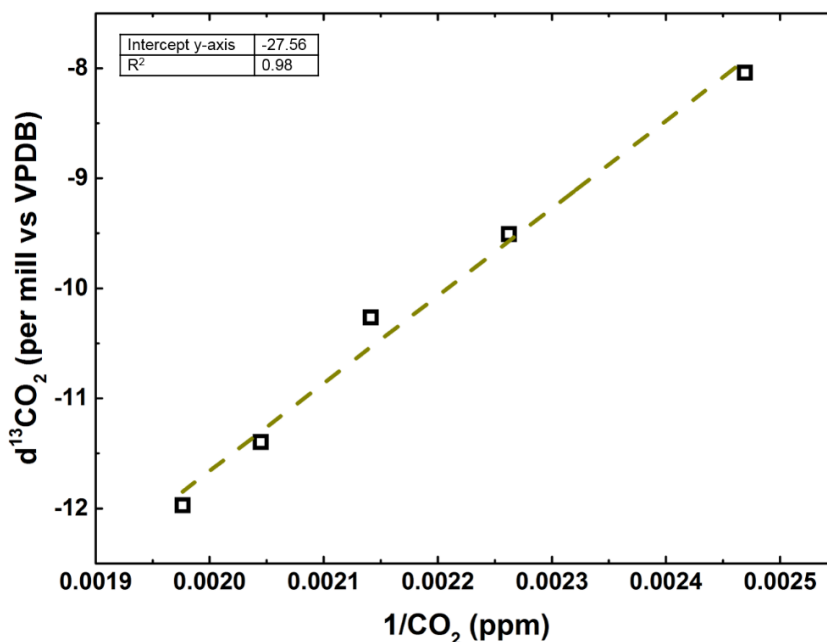


Figure 2.12.2: Keeling plot of the respired CO<sub>2</sub> from the control site at the polygon center

The ecosystem respiration fluxes at the polygon center and the floodplain were within the same range. The first measurements of the  $\delta^{13}\text{C}$  signatures of the respired CO<sub>2</sub> for the control sites (-27.56‰ VPDB) show that the values are close to the  $\delta^{13}\text{C}$  signatures of soil organic matter in the polygon centers on Samoylov (-28‰ to -30‰ VPDB, Knoblauch et al. 2015). These first results demonstrate the applicability of Keeling plots for determining the isotopic composition of ecosystem respiration fluxes at these sites (Figure 2.12.2).



## 2.13 Source assessment of carbon emissions from polygonal tundra and ice complex deposits using $^{14}\text{C}$ analysis

Jan Melchert <sup>1</sup>, Philipp Wischhöfer <sup>1</sup>, Stine Holm <sup>2</sup>, (Janet Rethemeyer <sup>1</sup>: not in the field)

<sup>1</sup> Institute of Geology and Mineralogy, University of Cologne, Cologne, Germany

<sup>2</sup> GFZ German Research Centre for Geoscience Helmholtz Centre Potsdam, Potsdam, Germany

### Fieldwork period and location

From July 15<sup>th</sup> to August 29<sup>th</sup>, 2018 (on Samoylov Island and Kurungnakh Island)

### Objectives

Yedoma deposits that developed during the last glacial period and early Holocene in unglaciated areas of the circum-arctic region have been a carbon sink for millennia. They are particularly prone to rapid degradation due to global warming because of their high ice content. Ground ice thaw causes thermokarst and erosion processes exposing the previously frozen organic material (OM) to microbial degradation, which finally results in the release of greenhouse gasses (GHG) including  $\text{CO}_2$  and  $\text{CH}_4$  into the atmosphere.

In order to understand how rapid the OM in Yedoma deposits may be mineralized and released as  $\text{CO}_2$  upon thaw, we investigate the carbon isotopic composition ( $^{13}\text{C}$ ,  $^{14}\text{C}$ ) of the  $\text{CO}_2$  released from a retrogressive thaw slump in the Yedoma deposits on Kurungnakh Island in the Lena River Delta. Additionally, we analyze the quality of the OM using elemental and lipid biomarker analysis, which will give us information on the stage of OM degradation as well as on carbon sources that are preferentially respired as  $\text{CO}_2$ . In addition, we investigate  $\text{CO}_2$  emitted from the active layer of different polygons on Samoylov Island.

The results of our three-year field study (2016-2018) document distinct changes of the thaw slump including its rapid erosion and colonization of the bare sediments by plants, which is also reflected by variable  $^{14}\text{C}$  contents of the  $\text{CO}_2$  released at some sites.

### Fieldwork summary

During our expedition to the Lena Delta from July until August 2018, we sampled  $\text{CO}_2$ , sediments, and dissolved organic carbon (DOC) from different sites on the thaw slump on Kurungnakh Island as well as from different polygons on Samoylov Island (Table 2.13.1).

#### *Kurungnakh Island*

The study sites on the thaw slump shown in Figure 2.13.2 included freshly exposed Yedoma sediments, i.e. thaw mounds (Baidzerakhs), and sediments at the thaw slump bottom where Yedoma was mixed with Holocene material.  $\text{CO}_2$  was sampled for  $^{14}\text{C}$  analysis from the non-vegetated sediment surface using closed, dark respiration chambers and from deeper part of the thawed sediment (down to 58 cm of depth) using passive  $\text{CO}_2$  depth samplers (Fig. 2.13.1). The  $\text{CO}_2$  was trapped on molecular sieves coupled to the sampling devices. The passive depth samplers were deployed for about 20 days. In addition, atmospheric  $\text{CO}_2$  samples were taken from the Holocene terrace above the thaw slump.  $\text{CO}_2$  fluxes were measured during  $\text{CO}_2$  sampling using a LICOR 840A infrared gas analyzer. The measurement time was kept shorter than five minutes in order not to disturb  $\text{CO}_2$  fluxes from the sediment.

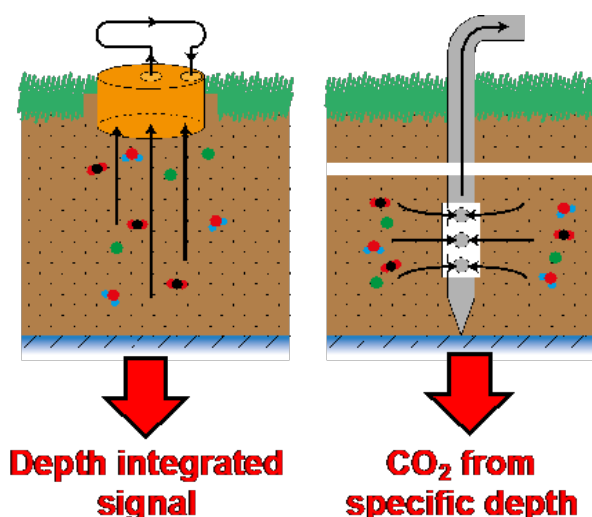


Figure 2.13.1:  $\text{CO}_2$  was collected with respiration chambers and depth samplers and trapped on molecular sieves for  $^{14}\text{C}$  analysis at CologneAMS.

At all sites, temperature depth profiles were measured at the day of  $\text{CO}_2$  sampling. Sediment samples were collected for lipid and  $^{14}\text{C}$  analysis in 10 cm depth intervals from pits that were dug close to the  $\text{CO}_2$  sampling sites down to the permafrost table. DOC samples of about 600 ml were collected using rhizons (2.5 mm diameter, 0.15  $\mu\text{m}$  pore size; Rhizosphere Research).

#### Samoylov Island

On Samoylov Island, we sampled  $\text{CO}_2$ , soil, DOC and particulate organic carbon (POC) from elevated polygonal rims and depressed polygon centers (Table 2.13.1). Respiration chambers were placed on non-vegetated sites to collect heterotrophically respired  $\text{CO}_2$  from trenched subplots of the polygon rim and center of site TiP (Table 2.13.1), where the living biomass had been removed. Passive depth samplers were deployed for 20 days to collect  $\text{CO}_2$  from the bottom of the active layer close to the permafrost table from both, polygon rims and centers. At each site, temperature profiles were measured on the day of  $\text{CO}_2$  sampling and soil samples were collected from the active layer down to the permafrost table (10 cm depth intervals) near the site where  $\text{CO}_2$  was sampled. Water samples were collected from water saturated polygon centers for filtration to recover DOC and particulate organic carbon (POC). DOC from dry polygon centers and rims was sampled from the base of the active layer using rhizons. From polygon centers, water was extracted via perforated steel tubes and subsequently filtered to separate DOC and POC.

Table 2.13.1: Overview of sampling locations and type of samples collected during our 2018's field campaign

Site ID	Name	Latitude [ $^{\circ}\text{N}$ ]	Longitude [ $^{\circ}\text{E}$ ]	Sample material
Samoylov Island*				
FLP	Fish Lake Polygon	72.37278	126.48512	DOC, soil
FLP2	Fish Lake Polygon 2	72.37220	126.48920	DOC soil
TiP	Tim's Polygon	72.37407	126.49731	DOC, $\text{CO}_2$ , soil
Kurungnakh Island				
KUP	Kurungnakh Polygon	72.32343	126.22298	DOC, sediment
KUP2	Kurungnakh Polygon 2	72.32520	126.26561	DOC, sediment
TSB 1	Thaw slump bottom (K4)	72.33900	126.29207	DOC, $\text{CO}_2$ , sediment
TM 1	Thaw slump, thaw mound (K7)	72.33923	126.29290	DOC, $\text{CO}_2$ , sediment
TM 2	Thaw slump, thaw mound (KX)	72.33920	126.29199	DOC, $\text{CO}_2$ , sediment

\*Additional POC samples were taken from polygon centers.

### Preliminary results

Figure 2.13.2 shows how rapidly the thaw slump on Kurungnakh Island has changed during three years. The photos taken in August 2016, 2017, and 2018 reflect not only the fast changes of the relief but also the rapid plant colonization of the bare sediments exposed as thaw mounds.



Figure 2.13.2: *Thaw slump on Kurungnakh Island. Photos were taken annually in August and show relief changes and progressing plant colonization on the slump.*

Figure 2.13.3 summarizes our first three-year data set for two sites of the thaw slump on Kurungnakh Island including  $^{14}\text{CO}_2$  results for samples taken with respiration chambers (2016 to 2018) and with depth samplers (2018).

The  $^{14}\text{CO}_2$  results obtained for samples taken with respiration chambers from the thaw slump bottom (TSB 1; July 2018) vary in a narrow range of 2,100 yrs up to 2,600 yrs from 2016 until 2018. The  $^{14}\text{CO}_2$  values for the thaw mound (TM 2) show a much larger scatter between the three years in the range of 1,060 yrs to 7,970 yrs. All  $^{14}\text{CO}_2$  results obtained so far are much younger than the  $^{14}\text{C}$  age of the bulk sediment. The  $\text{CO}_2$  collected with depth samplers is much older (up to 17,850 yrs at TSB 1) and very similar to the  $^{14}\text{C}$  ages of the bulk sedimentary OM and the DOC collected from similar depth intervals. These preliminary results suggest that  $\text{CO}_2$  collected with respiration chambers potentially includes considerable contributions of atmospheric  $\text{CO}_2$  in the pore space of the surface sediment.

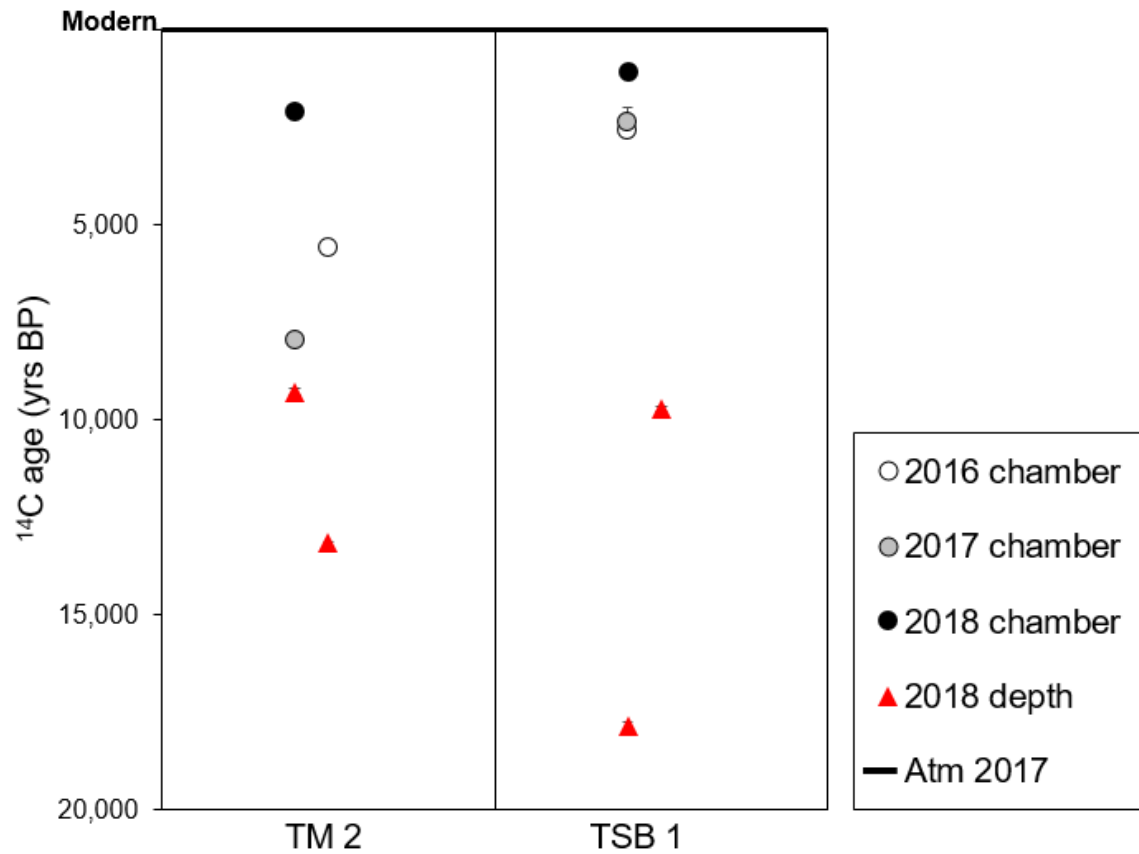


Figure 2.13.3:  $^{14}\text{C}$  ages (uncalibrated) of  $\text{CO}_2$  collected with respiration chambers (2016 to 2018) and depth samplers (2018) from thaw mounds (TM) and the thaw slump bottom (TSB) on Kurungnakh Island. The solid black line indicates the atmospheric  $^{14}\text{CO}_2$  content in 2017.

## 2.14 Soil moisture and vegetation effects on carbon dioxide and methane fluxes in a transect through an eroding permafrost landscape on Kurungnakh

Christian Knoblauch <sup>1,2</sup>, Tim Eckhardt <sup>1,2</sup>, Pavel Barsukov <sup>3</sup>, Nikolay Lashchinskiy <sup>4</sup>,  
(Eva-Maria Pfeiffer <sup>1,2</sup>: not in the field)

<sup>1</sup> Institute of Soil Science, Universität Hamburg, Hamburg, Germany

<sup>2</sup> Center for Earth System Research and Sustainability, Universität Hamburg, Hamburg, Germany

<sup>3</sup> Institute of Soil Science and Agrochemistry, Siberian Branch, Russian Academy of Sciences, Novosibirsk, Russian Federation

<sup>4</sup> Central Siberian Botanical Garden, Siberian Branch, Russian Academy of Sciences, Novosibirsk, Russian Federation

### Fieldwork period and location

From July 04<sup>th</sup> to July 29<sup>th</sup>, 2018 (on Kurungnakh Island)

### Objectives

The objectives of the field work on Kurungnakh was to quantify the impact of vegetation composition and soil moisture on methane, and carbon dioxide (CO<sub>2</sub>) fluxes in a tundra landscape affected by thermokarst.

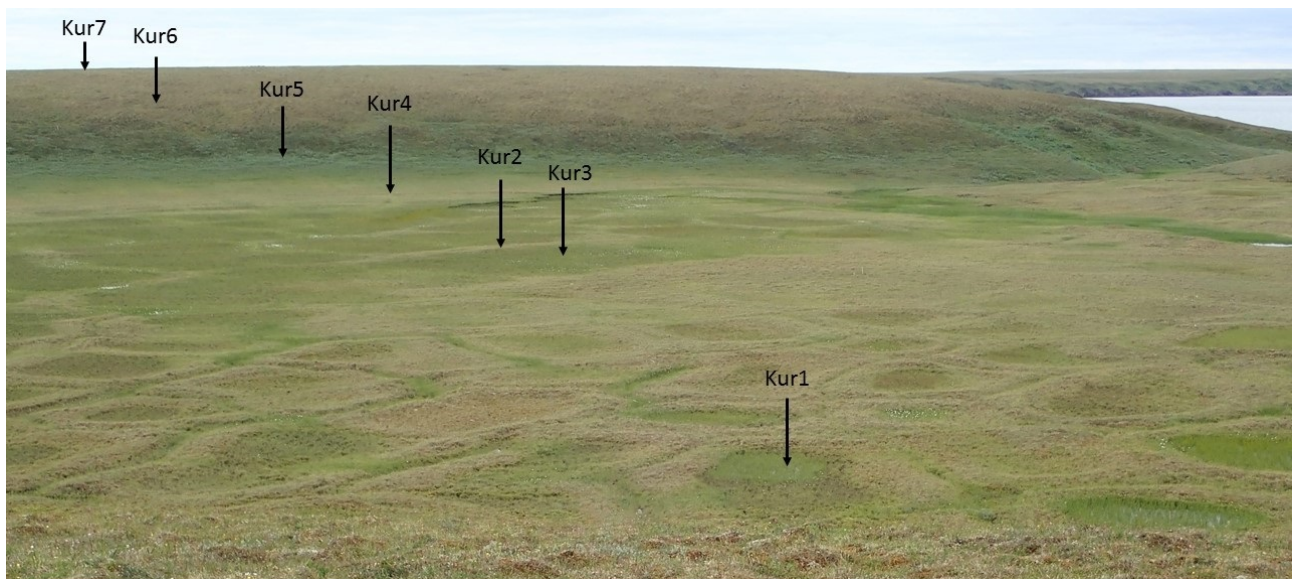


Figure 2.14.1: Position of the samples sites in the transect through a thermokarst depression on Kurungnakh Island

### Methods

Carbon dioxide and methane fluxes were measured at seven different sites (Table 2.14.1) in a transect from the bottom of a thermokarst depression (alas) to the surface tundra plain unaffected by thermokarst (Figure 2.14.1). The study sites in the transect were selected based on their vegetation composition to consider all main plant functional types in the study area. Methane fluxes and ecosystem respiration CO<sub>2</sub> fluxes were determined with opaque chambers (20 cm height) followed by measurements of net ecosystem exchange (NEE) CO<sub>2</sub> fluxes with transparent chambers (30 cm height). Gas fluxes were quantified over a period of five minutes using a portable greenhouse gas analyser (UGGA, Los Gatos Research, USA). Furthermore, the vegetation composition was determined at the end of the measurement period in each of the frames used for gas flux measurements.

### Preliminary results

Soil moisture and vegetation composition differed substantially between the different study sites (Table 2.14.1). While the water saturated polygonal centres (site Kur1 and Kur3) were dominated by sedges (*Carex concolor* and *C. rariflora*) and graminoids (*Eriophorum angustifolium*), at the dryer polygon rim (Kur2) also dwarf shrubs (*Salix pulchra*) appeared. Site Kur4 at the rise of the thermokarst depression (Figure 2.14.1) showed water saturation at the bottom of the active layer and the vascular plant composition was dominated by sedges (*Carex concolor*) and dwarf shrubs (*Arctous alpina*). Site Kur5 at the bottom of the slope showed the deepest thaw depth (>40 cm), standing water at the bottom of the active layer and a vascular plants community that was clearly dominated by *Salix glauca*. The well-drained sites Kur6 and Kur7 showed no free water in the profile and their vegetation was dominated by dwarf evergreen shrub (*Cassiope tetragona*), graminoids (*Luzula sibirica*) and herbs (*Tofieldia coccinea*).

Table 2.14.1: Position of the sampling sites and their most abundant species

Site	Latitude [°N]	Longitude [°E]	Water table	Dominant plant species
Kur1	72.29108	126.18755	5 cm above soil surface	<i>Carex concolor</i> <i>Eriophorum angustifolium</i>
Kur2	72.29059	126.18457	No standing water in active layer (>20 cm)	<i>Carex concolor</i> <i>Salix pulchra</i> <i>Hylocomium splendens</i>
Kur3	72.29065	126.18451	5 cm above soil surface	<i>Carex rariflora</i> <i>Aulacomnium turgidum</i>
Kur4	72.29034	126.18209	Bottom of active layer (20 cm)	<i>Carex concolor</i> <i>Arctous alpina</i> <i>Tomentypnum nitens</i>
Kur5	72.29031	126.18141	50 cm below soil surface	<i>Salix glauca</i> <i>Astragalus frigidus</i> <i>Hylocomium splendens</i>
Kur6	72.28992	126.18076	No standing water in active layer (>48 cm)	<i>Cassiope tetragona</i> <i>Luzula sibirica</i> <i>Hylocomium splendens</i> <i>Dactylina arctica</i>
Kur7	72.28927	126.18021	No standing water in active layer (>35 cm)	<i>Tofieldia coccinea</i> <i>Dryas punctata</i> <i>Hylocomium splendens</i>

Carbon dioxide and methane fluxes differed substantially between the different sampling sites. Figure 2.14.2 presents exemplarily CO<sub>2</sub> and methane fluxes measured on July 27<sup>th</sup>, 2018. While, as expected, the highest methane fluxes were observed from the water saturated polygonal centres, the dry sites Kur6 and Kur7 at the top of the slopes and the plain were weak sinks for atmospheric methane. Maximum methane emissions at Kur1 were substantially higher than fluxes measured in polygonal centres at the nearby Samoylov Island (Knoblauch et al. 2015; Kutzbach et al. 2004; Wagner et al. 2003). The dry sites Kur2, Kur6 and Kur7 were all net sources for CO<sub>2</sub> even under light conditions (NEE >0), which demonstrates that release of CO<sub>2</sub> through plant respiration and heterotrophic respiration was higher than CO<sub>2</sub> uptake by photosynthesis. In contrast, the wetter sites were all net sinks for CO<sub>2</sub> with highest uptake fluxes in the sedge and graminoid dominated polygonal centre of Kur1 (−4.430 mg CO<sub>2</sub>-C m<sup>−2</sup> d<sup>−1</sup>) and the willow dominated site Kur5 at the bottom of the thermokarst depression (−3.547 mg CO<sub>2</sub>-C m<sup>−2</sup> d<sup>−1</sup>).

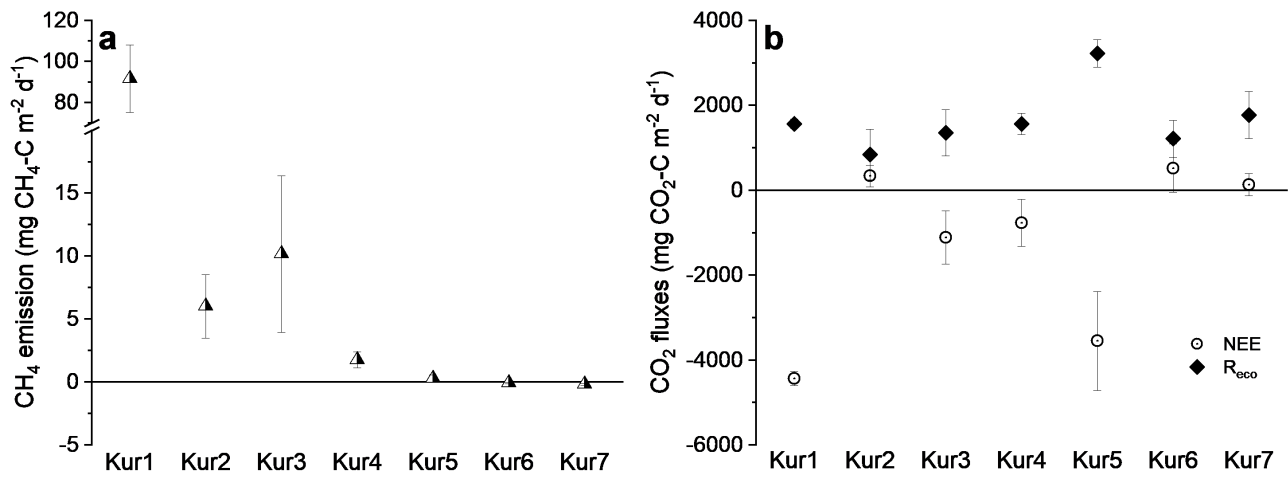


Figure 2.14.2: Methane (a) and CO<sub>2</sub> (b) fluxes measured on July 27<sup>th</sup>, 2018, in a transect through a thermokarst depression. Carbon dioxide fluxes were measured under dark conditions (Reco) and light conditions (NEE).

## 2.15 Investigations of snow cover and vegetation evolution from spring to summer using time-lapse cameras

Anne Morgenstern <sup>1</sup>, Till Hainbach <sup>1,2</sup>, Birgit Heim <sup>1</sup>

<sup>1</sup> Alfred Wegener Institute Helmholtz Center for Polar and Marine Research, Potsdam, Germany

<sup>2</sup> Institute for Geosciences, University of Potsdam, Potsdam, Germany

### Fieldwork period and location

From April 18<sup>th</sup> to April 26<sup>th</sup>, 2018 (on Kurungnakh Island)

### Objectives

Snow plays a key role in the thermal regime of permafrost, as well as for the supply of water for vegetation and for erosional processes. Besides areal coverage, snow depth and snow water equivalent (SWE) are the most important parameters for snow cover investigations as they define the insulation properties and the amount of stored water, respectively. Across arctic lowlands, however, the snow cover is very heterogeneous reaching from a few centimeters on flat elevated areas to several meters in local depressions or valleys. This leads to greatly varying water content within the snow cover. Furthermore, snow cover and its properties develop differently throughout the spring snowmelt period in different landscape units and relief settings. Standard remote-sensing products like NDSI (Normalized Difference Snow Index)-based snow cover of multispectral satellite imagery lack the temporal continuity needed for short time scale observations such as snow melt. Therefore, a higher temporal resolution is needed for the spatial analysis of seasonal snow cover evolution. Additional ground-based image acquisitions across landscapes at remote locations such as using continuous time series of Time-Lapse Cameras (TLC) can help to close the gaps in-between consecutive satellite images.

Our fieldwork aimed at answering the question how snow influences the development of thermal erosion of Yedoma-type Ice Complex deposits. Several sites on Kurungnakh Island that are affected by thermal erosion of Yedoma-type Ice Complex deposits served as key sites for the quantification of:

- the spatial distribution of the snow cover depending on different relief settings,
- snow water equivalent of the snow cover,
- the temporal evolution of the snow cover during snow melt

The set-up of TLC systems will also support investigations on how spatio-temporal snow dynamics influence the timing of physiological plant processes. Vegetation in turn captures snow and alters snow structure and in turn may determine the spatial melt-out patterns of the snow cover.

With our field investigations and the set-up of the TLC camera monitoring network we aim to investigate the spatial and temporal scales of snow characteristics in the central Lena Delta that are relevant across scales from a few square meters to the landscape scale covering hundreds of square meters.

### Methods

Our field work was separated into two main parts: (1) installation of automated Time-Lapse Cameras (TLC) for remote ground-based landscape monitoring of the spring and summer season and (2) obtain field data for the description and quantification of snow cover properties including snow water equivalent (SWE), snow depth and thickness of the depth hoar layer, snow pit description and snow sampling for isotope analyses.

We installed ten time-lapse cameras at several key sites covering different relief settings on Kurungnakh Island, i.e. different types of thermo-erosional valleys and flat terrain of Yedoma uplands (Figure 2.15.1, Table 2.15.1). KUR-TLC-0A is overlooking a steeply dissected thermo-erosional valley with active erosion of its steep unvegetated slopes and wetland vegetation on the valley floor. KUR-TLC-1A is overlooking a softly dissected valley system with zonal tussock tundra vegetation. KUR-TLC-2B was installed centrally on the Yedoma upland overlooking flat terrain with prostrate shrub tundra. Four cameras KUR-TLC-3A, KUR-TLC-3IIA, KUR-TLC-4A,



KUR-TLC-4B were installed around a complex thermo-erosion valley system. KUR-TLC-5B was installed on the eastern rim of the large discharge valley draining all the catchments from Western Kurungnakh (main valley). The TLC was looking northwards across the valley including monitoring of the slopes covered with high shrubs larger than 1 m height. KUR-TLC-6B was overlooking the drainage valley of Lucky Lake. Since many years TLCs have continuously been monitoring the micrometeorological measurement fields on Samoylov Island. We also installed SAM-TLC-1B on another Holocene terrace with polygonal wet tundra landscape. This Holocene terrace landscape element covers more square kilometer than Samoylov Island and will be used for investigating kilometer-scale operational remote sensing products on vegetation and SWE.



Figure 2.15.1: Positions of time-lapse cameras installed on Kurungnakh Island for the monitoring of snow cover and vegetation evolution from spring to summer 2018. Background Image Sentinel-2 Quasi True Color Composite from August 26<sup>th</sup>, 2018. Time Lapse Camera Codes are provided in Table 2.15.1.

Table 2.15.1: Positions of time-lapse cameras installed on Kurungnakh Island for the monitoring of snow cover and vegetation evolution from spring to summer 2018. Geographic coordinates of Latitude and Longitude are given in decimal degree with reference WGS84.

Time Lapse Camera (TLC) Code	Latitude [°N]	Longitude [°E]
KUR-TLC-0A	72.37296	126.24855
KUR-TLC-1A	72.36462	126.25537
KUR-TLC-2B	72.35117	126.17661
KUR-TLC-3A	72.33397	126.27685
KUR-TLC-3IIA	72.33359	126.27782
KUR-TLC-4A	72.33201	126.28027
KUR-TLC-4B	72.33201	126.28027
KUR-TLC-5B	72.33277	126.05894
KUR-TLC-6B	72.2942	126.1512
SAM-TLC-1B	72.3793	126.39009

The cameras (Brinno TLC200 in weather resistant housing ATH110) were installed mounted (using Netatmo Weather Station Mount) onto a 2 m profiled aluminum pole, which was drilled approximately 1 m into the ground (Figure 2.15.2).



Figure 2.15.2: *Two time-lapse cameras installed on one aluminum pole directed at different sections of a steep thermo-erosional valley on Kurungnakh Island*

Snow depth and SWE measurements were conducted strategically along cross-valley transects (e.g. Figure 2.15.3) as well as randomly, covering the most common terrain types on Kurungnakh Island: Yedomu upland, gentle slopes, steep newly eroded slopes (as accessible), valley troughs and water tracks. We used a 3 m avalanche probe for simple snow depth measurements and a snow water equivalent snow probe (Model WS-43). Within the thermo-erosional valleys snow accumulation often exceeded 3 m. In order to determine snow depth here, we measured the surface position of the snow cover along cross sections, where high-resolution elevation measurements were conducted without snow in previous summer campaigns.

Snow samples retrieved during snow water equivalent measurements were partially collected for analysis of the isotopic composition.

In addition, one snow pit was dug close to camera site KUR-TLC-1A on the valley floor. The description of snow characteristics followed the snow description chart by the WSL Institute for Snow and Avalanche Research SLF, Davos, Switzerland. This included the determination of snow temperature and density, hardness of snow layers, shape and size of snow-crystals, on which basis individual snow layers were defined. Snow samples through the snow profile were collected for determination of the isotopic composition.

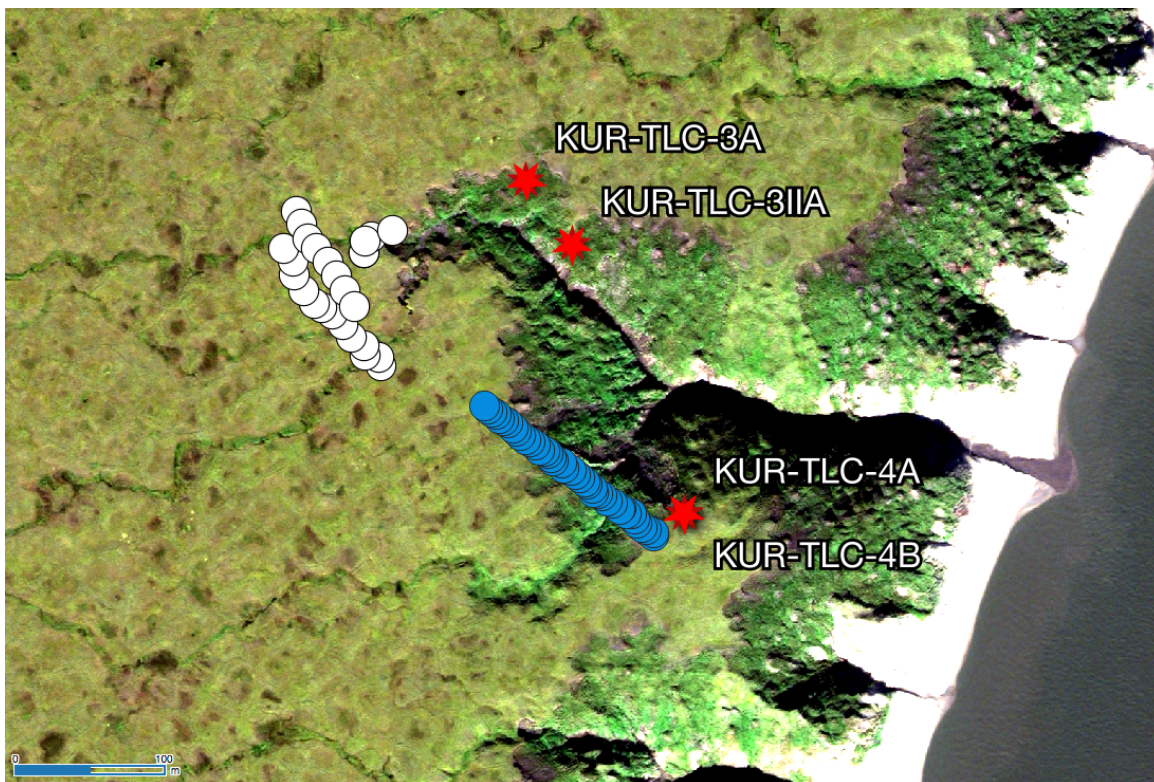


Figure 2.15.3: Location of profiles for the measurement of snow depth using an avalanche probe (blue) and measurements of snow water equivalent and snow depth using the WS-43 snow probe (white) across branches and water tracks of a thermo-erosional gully at the eastern coast of Kurunghakh Island. Background Image GeoEye Quasi True Color Composite

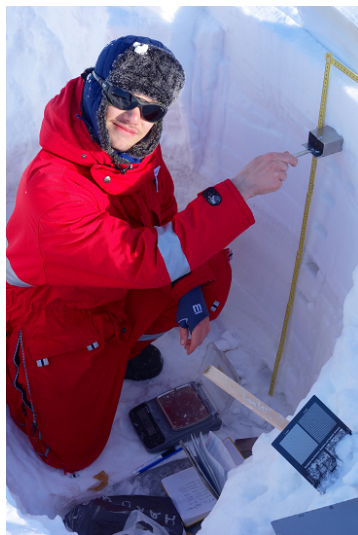


Figure 2.15.4: Till Hainbach in the snow pit studying a vertical snow profile close to the camera site KUR-TLC-1A



Figure 2.15.5: Birgit Heim (right) and Till Hainbach (left) measuring snow depth and SWE on polygonal tundra terrain close to the camera site KUR-TLC-0A

### Preliminary results

Generally, the snow distribution on Kurungnakh Island follows a specific pattern determined by the prevailing wind direction, the geographic position, relief and to a lesser degree vegetation. The snow cover was sparse to not present on south facing slopes, especially where the surrounding relief provided a large contact surface for wind blowouts. In contrast, shaded and/or protected areas (e.g. valley troughs or leewards facing slopes) could accumulate significant amount of snow. Leewards cliffs were typically characterized by formation of large cornices (tens to hundreds of meters long, put to several meters thick). On flat surfaces, thick layers of wind-crusting snow defined the visual nature of the landscape.

In addition, snow accumulated on the lee of tussocks whereas on the windward side the snow cover was blown away. This is, however, only true for areas where the average snow depth did not exceed the tussock height. Therefore, the visibility of tussocks can be seen as a landmark for snow cover thickness.

The majority of the TLCs operated through the time of snow melt and the time of vegetation leaf out and shooting (Figure 2.15.6, Table A.2.12). However, the most wind-exposed TLCs around the thermo-erosional valley could only monitor until the last days of May due to limited power supply. The cameras close to the Lena River were covered with droppings by birds that used the poles for several days in June. Image acquisition was thereby interrupted until the next rain event washed the camera lenses free again.

The final snow melt out at landscape scale across Kurungnakh Island occurred within a few days at the end of May (Table A.2.12). Similarly, the leaf out and shooting of vegetation occurred at landscape scale across Kurungnakh Island around 10 days after the final snow melt (Table A.2.12).



Figure 2.15.6: Example from time-lapse camera snapshots on snow melt, leaf out and shooting from landscape and plots

## 2.16 KoPf - assessing above-ground and below-ground carbon in the central Lena Delta

Birgit Heim <sup>1</sup>, Matthias Fuchs <sup>1</sup>, Iuliia Shevtsova <sup>1</sup>, Alexandra Runge <sup>1</sup>, (Ulrike Herzschuh <sup>1,2</sup>, Guido Grosse <sup>1,2</sup>: not in the field)

<sup>1</sup> Alfred Wegener Institute Helmholtz Center for Polar and Marine Research, Potsdam, Germany

<sup>2</sup> University of Potsdam, Potsdam, Germany

### Fieldwork period and location

From July 31<sup>st</sup> to September 03<sup>rd</sup>, 2018 (in the central Lena River Delta)

### Main Objectives

Our specific research questions for the Lena Delta region are:

- What are the relevant vegetation communities and their spatial coverage in the central Lena Delta?
- What are the relevant subground soil and permafrost characteristics and their spatial coverage in the central Lena Delta?
- Can we develop transfer functions between plant cover data, vegetation biomass and subground properties?
- What are the spectral characteristics of the relevant surface types in the central Lena Delta?

Field survey was carried out, plots on vegetation and field spectrometry were established and permafrost, soil and vegetation species and biomass samples were collected in the central Lena Delta, on Samoylov Island, the neighboring floodplains and Kurungnakh Island (Figure 2.16.1, Table A.2.16). Samoylov Island is built up by a Holocene river terrace (1<sup>st</sup> Lena Delta terrace) with polygonal wet tundra and the active sandy floodplain with elevations from 1 to 13 m a.s.l, Kurungnakh Island is part of the 3<sup>rd</sup> and highest geomorphological terrace in the Lena Delta with heights of 30 to 55 m a.s.l. (Morgenstern et al. 2011). Kurungnakh Island has at the base fluvial sandy sediments but is mostly composed of ice rich Yedoma (Schirrmeister et al. 2003; Schwamborn et al. 2002) with shrubby tundra on its upland plateau.

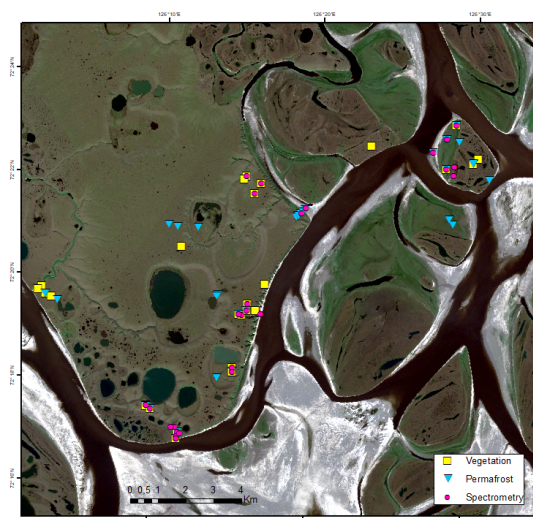


Figure 2.16.1: KoPf 'assessing above-ground and below-ground carbon': All sample locations (vegetation field survey, permafrost coring, field spectrometry) in the central Lena Delta, mainly on Samoylov and Kurungnakh Islands during August 2018

## PERMAFROST

### Objectives

We collected permafrost soil cores down to a depth of 100 cm to link the below-ground carbon with vegetation coverage and above-ground vegetation biomass. Previous studies that investigated soil organic carbon and nitrogen stocks in the central Lena Delta on Kurungnakh (Siewert et al. 2016) and Samoylov Island (Zubrzycki et al. 2013) focused on the below-ground carbon quantification. In this study we will deeply investigate the relation to above ground biomass to use vegetation characteristics and surface reflectance as a proxy for below-ground carbon. Therefore, we collected permafrost cores in plots where a detailed vegetation survey and biomass sampling was carried out (Figure 2.16.1, A.2.16). We also cored permafrost cores in cooperation with the IPGG Novosibirsk, Russia on a pingo where IPGG carried out geophysical measurements and we cored permafrost cores in cooperation with the GFZ (Microbiology) on Kurungnakh at an active permafrost degradation site.

### Methods

Sampling took place in August 2018. Before sampling the permafrost, the active layer was excavated, described and sampled with a fixed volume cylinder (volume 250 cm<sup>3</sup>). After sampling the active layer material permafrost was sampled by drilling with a modified, snow, ice, and permafrost (SIPRE) auger (Jon Holmgren's Machine Shop, Fairbanks) down to one meter below surface (Figure 2.16.2). The soil cores have a diameter of 3 inch (7.62 cm). The frozen cores were described including macroscopic sediment characteristics and facies, cryostratigraphy according to Frensh and Shur (2010) and plant macrofossils. Cores were subsampled in 5 to 10 cm increments according to facies horizons and transported to the laboratory facilities at AWI Potsdam.

- active layer sampling
- soil description, soil sampling
- permafrost coring down to 1 meter, visual permafrost core description, permafrost core sampling
- sampling organic-rich layers for radiocarbon dating



Figure 2.16.2: *Left: SIPRE permafrost drilling on Kurungnakh Island. Photo by Stine Hol; Middle: Active layer profile. Photo by Matthias Fuchs; Right: Permafrost core. Photo by Matthias Fuchs*

### Preliminary results

In total 35 sites were sampled in the central Lena Delta across Samoylov and Kurungnakh Islands and 338 soil samples collected (Figure 2.16.3, Table A.2.13).



Figure 2.16.3: Permafrost core and soil sample locations in the central Lena Delta mainly on Samoylov Island and Kurungnakh Island during August 2018

Cores with the signature KUR18 were collected on Kurungnakh Island, cores with the signature SAM18 were collected on Samoylov, or its neighboring floodplain islands. The expedition team sampled more than 100 kilograms soil material and more than 33 m of soil cores. We plan to analyze the samples at AWI Potsdam for total carbon (TC), total organic carbon (TOC), total nitrogen (TN) and grain size. The sample water and ice contents will be determined by the weighting before and after freeze-drying.

## VEGETATION

### Objectives

Vegetation is one important part of high-latitude permafrost landscapes that reflects climatic changes. Prevailing vegetation types in the Lena Delta are polygonal tundra, tussock tundra, wet sedge and moss-dominated tundra on Yedoma upland on undisturbed terrains. Disturbed terrains are frequently characterized by high vegetation biomass, e.g. shrub communities with individuals taller than half a meter densely grow on floodplains, at the rim of thermokarst basins, in thermoerosion valleys.

We plan to upscale vegetation cover and *in situ* biomass estimates from harvesting to remote-sensing derived above-ground biomass and above ground carbon stocks and also link to subground soil and permafrost properties. The vegetation field survey will provide qualitative and quantitative data on vegetation to link to field spectrometry (Figure 2.16.1, Table A.2.16). We will use Landsat-8 OLI and Sentinel-2 sensors for the spatial upscaling providing mapped fields of biomass (and above-ground carbon as higher level product) on 10 x 10 m (Sentinel-2) and 30 x 30 m (Landsat) grid cell spatial resolution.



Figure 2.16.4: Vegetation plot locations in the central Lena Delta mainly on on Samoylov Island and Kurungnakh Island during August 2018

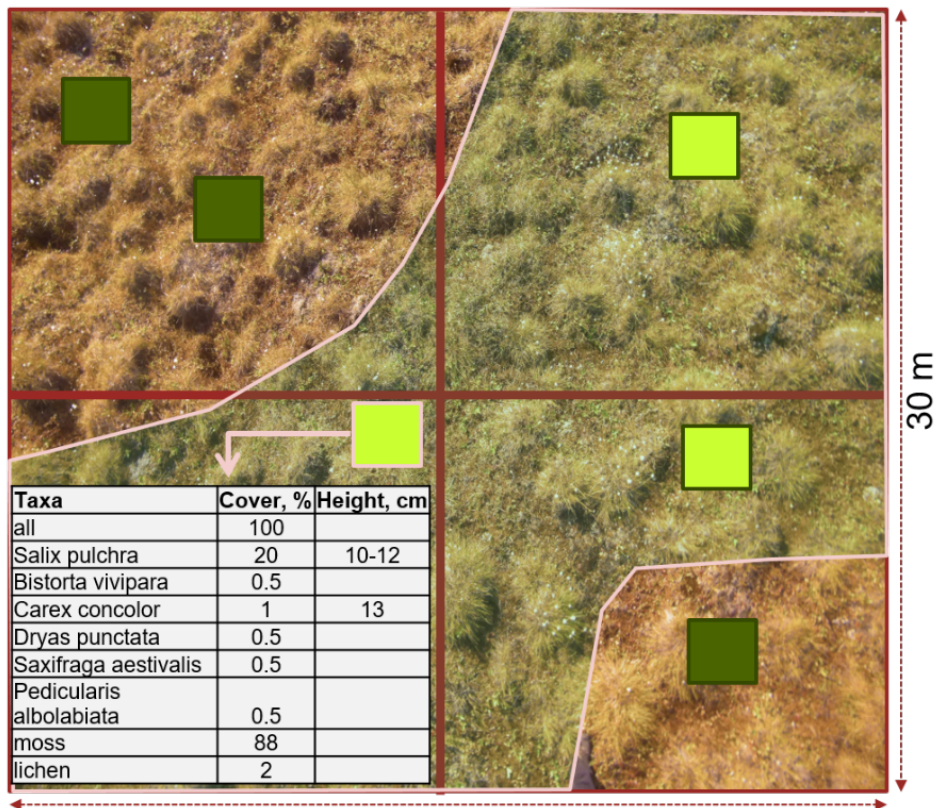


Figure 2.16.5: 30 m x 30 m vegetation plot set up with 2 m x 2 m subplots for vegetation cover estimation and biomass sampling on 0.5 m x 0.5 m inside the 2 m x 2 m subplots



## Methods

We established 27 30 m x 30 m vegetation plots (Figure 2.16.4, 2.16.5) that we mapped with high-spatial resolution using visible and near infrared wavelength cameras on telescopic stick. Vegetation cover and floristic composition were described on smaller subplots of 2 m x 2 m within each of the 30 m x 30 m plots according to the number of vegetation types that occurred at that site. This accounted in case of three vegetation types and three subplots per type for up to nine subplots for one site. Vegetation was estimated in percentage of projective cover on each 2 m x 2 m subplot (in general and by taxa found). Vegetation heights were recorded as well. For each specific vegetation type from one plot per vegetation type biomass was sampled (dominant taxa, not dominated taxa collected together in one sample "rest" and moss & lichen) on 0.5 m x 0.5 m inside the 2 m x 2 m subplot. Fresh biomass was weighted optimally directly in the field and subsampled.

- vegetation plot analyses (plant communities, protective coverage estimation)
- mapping of 30 m x 30 m plots with Visible and Near Infrared cameras on a telescopic stick
- sampling above ground biomass - moss, lichen, vascular plants (by dominant taxa and as rest) in selected representative subplots

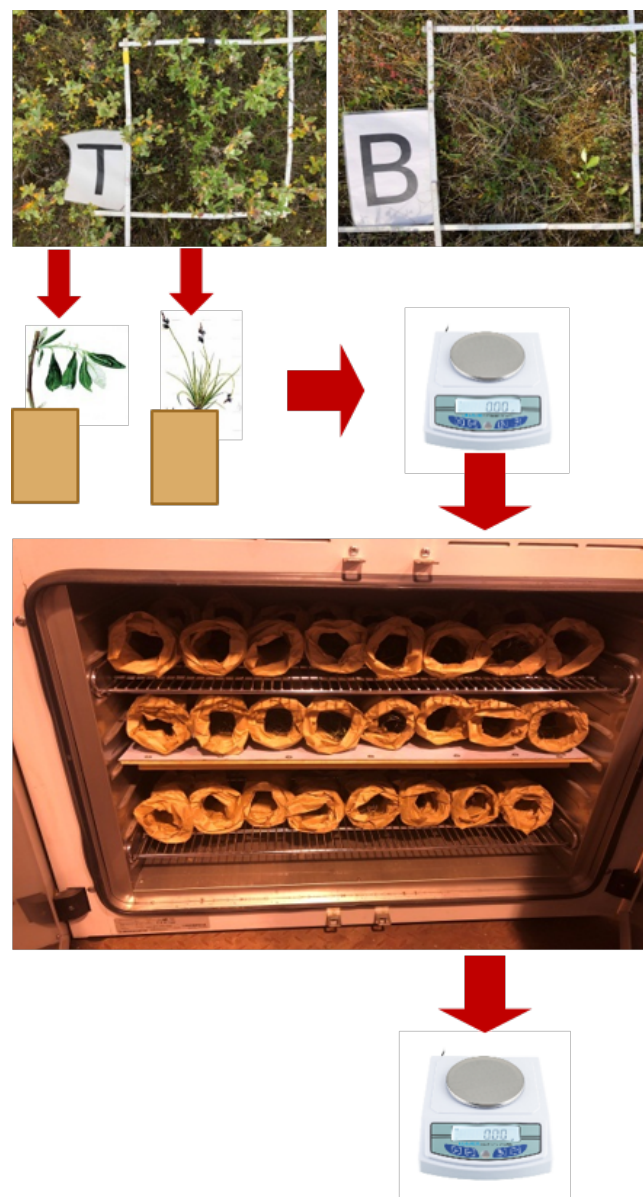


Figure 2.16.6: Scheme of biomass samples handling procedure on the Lena Delta 18 expedition

The subsamples after weighting were dried 2-4 days in a warm dry place, then for ca. 24 hours in the oven at a temperature of 60 °C and re-weighted (Figure 2.16.6). Dry weight was corrected using the fresh weight of initial sample and subsample and recalculated into kg/m<sup>2</sup>.

### **Preliminary results**

In total 27 sites were sampled across Samoylov and Kurungnakh Islands and 174 biomass samples (excluding high shrub samples which consist of 15 specific biomass samples) were collected (Figure 2.16.4, Table A.2.14).

## **SPECTROMETRY**

### **Objectives**

The Lena Delta 2018 August expedition included hyperspectral field measurements. The aim was to conduct spectral surface reflectance surveys of different homogenous vegetation areas on different permafrost landforms to establish a representative spectral reflectance database. Previously only one study with hyperspectral field spectrometry was conducted in the Lena Delta in 2005, which includes a few measurements on Samoylov and Kurungnakh-Island but the main focus was in the North west of the Lena Delta on the 2<sup>nd</sup> geomorphological terrace on Turakh-Sise, Ebe-Basyn-Sise and Khardang-Sise (Ulrich et al. 2009). Additionally to this, we took sun photometer measurements throughout the expedition, which will be used for atmospheric correction of satellite images, in this case Sentinel-2 images.

### **Methods**

We conducted field-spectrometry measurements with the Spectral Evolution SR-2500 with a 1.5 m Fiber Optic Cable. The instrument is calibrated to a spectral radiance range of 350 to 2.500 nm. We operated the field-spectrometer with a handheld Getac Rugged Notebook. For the surface reflectance spectral measurements we identified homogenous plots with a size of 30 m x 30 m. Most of the field-spectrometry surveys used the plots for vegetation and biomass sampling, some are independent from the biomass sampling survey but overlap with the permafrost soil coring (Figure 2.16.1, Table A.2.16). The surveys took place between 10 am to 3 pm in order to collect field-spectrometry measurements around noon. Individual results will have to take into account the acquisition time and the resulting sun angle influencing the measurements. Within the 30 x 30 m plots 100 individual measurements, randomly scattered across the plot, were taken. At the start and at the end of each survey the system was referenced by measuring the back reflected radiance from a Zenith Lite™ Diffuse Reflectance Target of 50% reflectivity. The grey reference measurements were repeated when weather conditions changed throughout an individual plot survey. The data was acquired by using the fibre optic cable with a handheld trigger, which was held at an arms-length away and at shoulder height, at about 1 m to the ground (see Figure 2.16.7). In addition to this, we recorded the weather conditions during the measurements with sky photos and took landscape and plot photos from all four corners of the 30 x 30 m plot.

For the sun photometer measurements we used the Calitoo system for measuring aerosol optical thickness. We took sun photometer measurements on days with good-weather and with either a Sentinel-2 or Landsat-8 acquisition scheduled for that day. We took repeated measurements from 8.30 am to 3 pm.

- spectral surface reflectance field measurements from 30 x 30 m plots across a range of vegetation types (plant communities, coverage) and natural surfaces (e.g. sand)
- field spectrometry measurements at vegetation plots with sampled communities, coverage and biomass
- field spectrometry measurements at additional sites of soil sampling and permafrost coring with photo documentation of the 30 x 30 m plot



Figure 2.16.7: Spectral Evolution SR-2500 field-spectrometer measurement set-up. Photos by Matthias Fuchs

**Preliminary Results**

In total we took 28 hyperspectral field measurements across Samoylov and Kurungnakh Islands (Figure 2.16.8). Four plots were measured twice with a two weeks delay, therefore depicting the changes in reflectance signature due to the starting autumn senescence. The sampling plots with the signature identifier SAM18 were collected on Samoylov and those with KUR18 on Kurungnakh (Table A.2.15).

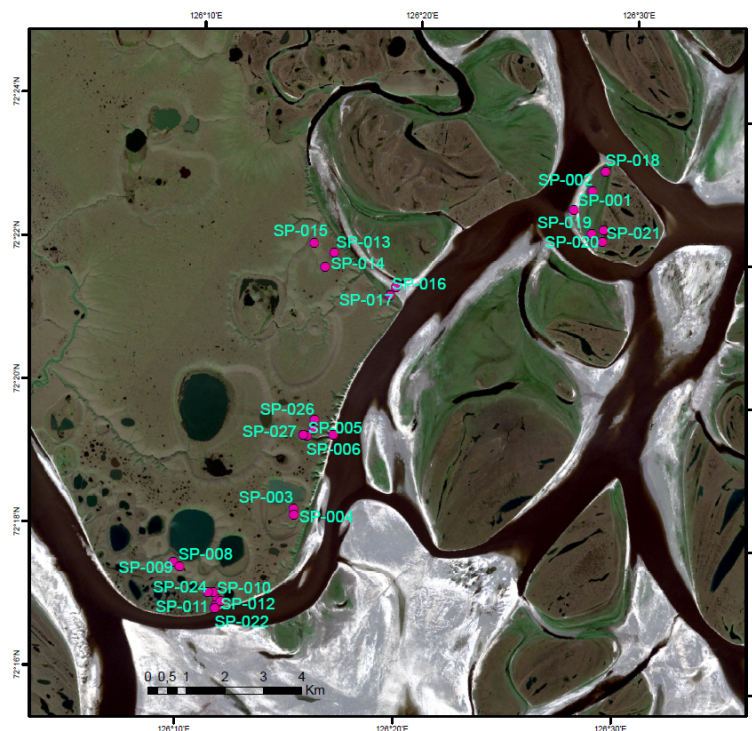


Figure 2.16.8: Field spectrometer plot locations in the central Lena Delta mainly on on Samoylov Island and Kurungnakh Island during August 2018

## 2.17 Dendrochronological potential of tundra shrubs in the vicinity of Samoylov Island

Agata Buchwal<sup>1</sup>, Grzegorz Rachlewicz<sup>1,2</sup>, Birgit Heim<sup>3</sup>

<sup>1</sup> Adam Mickiewicz University, Poznan, Poland

<sup>2</sup> Xi'an Jiaotong-Liverpool University, Suzhou, China

<sup>3</sup> Alfred Wegener Institute Helmholtz Center for Polar and Marine Research, Potsdam, Germany

### Fieldwork period and location

From August 15<sup>th</sup> to August 30<sup>th</sup>, 2018 (in the central Lena Delta)

### Objectives

Our specific research questions are:

- What are the main climatic drivers of shrub growth in Lena Delta?
- What are the trends of shrub growth in the Lena Delta region under on-going climate change and associated local disturbances of permafrost?

### Methods

For climate-growth relationship, we have sampled two major shrub species *Betula* and *Salix*. *Salix* samples were acquired in Samoylov Island, whereas *Betula nana* mainly on Kurungnakh Island. Additionally two other species were sampled for assessment of dendrochronological potential, namely *Rhododendron* and *Alnus* (Table A.2.17). Also one tree species, i.e. *Larix*, was sampled in one of the northernmost location known from literature (N 72°) (Figure 2.17.1).

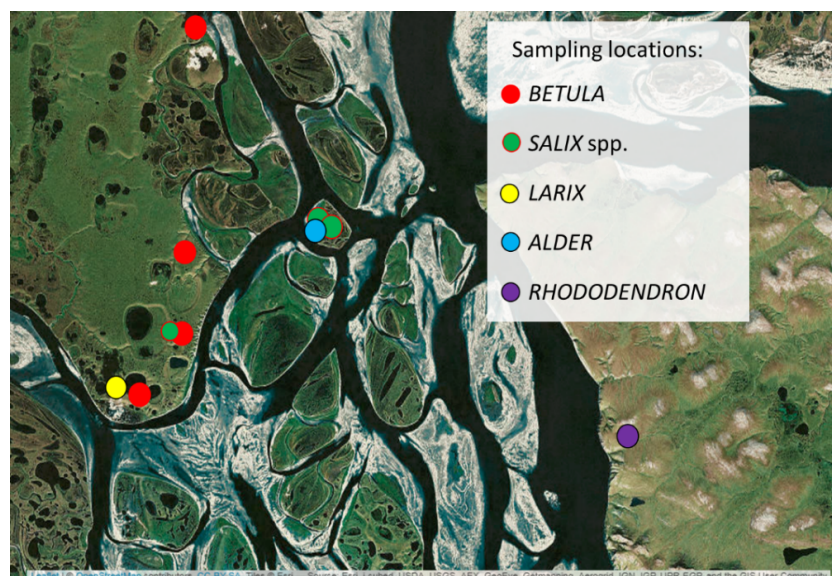


Figure 2.17.1: Overview of shrub genus sampling location performed in the central Lena Delta in August 2018

Over 150 shrub samples were acquired in total. Shrubs were sampled in various environmental settings: Yedoma Ice Complex, flood plain, recently drained thermokarst lake. Each shrub was sampled including below-ground parts (i.e., main root) and up to two main above-ground shoots. At each shrub sampling location, active layer depth was measured using a pin-probe. In the Research Station Samoylov Island laboratory all shrubs were dried in room temperature. Then from each shrub multiple specimens were acquired according to serial sectioning procedure. Other laboratory analyses, i.e., thin sections preparation and growth rings measurements (Figure 2.17.2), are conducted in the DendroLab in Adam Mickiewicz University (Poznan, Poland).

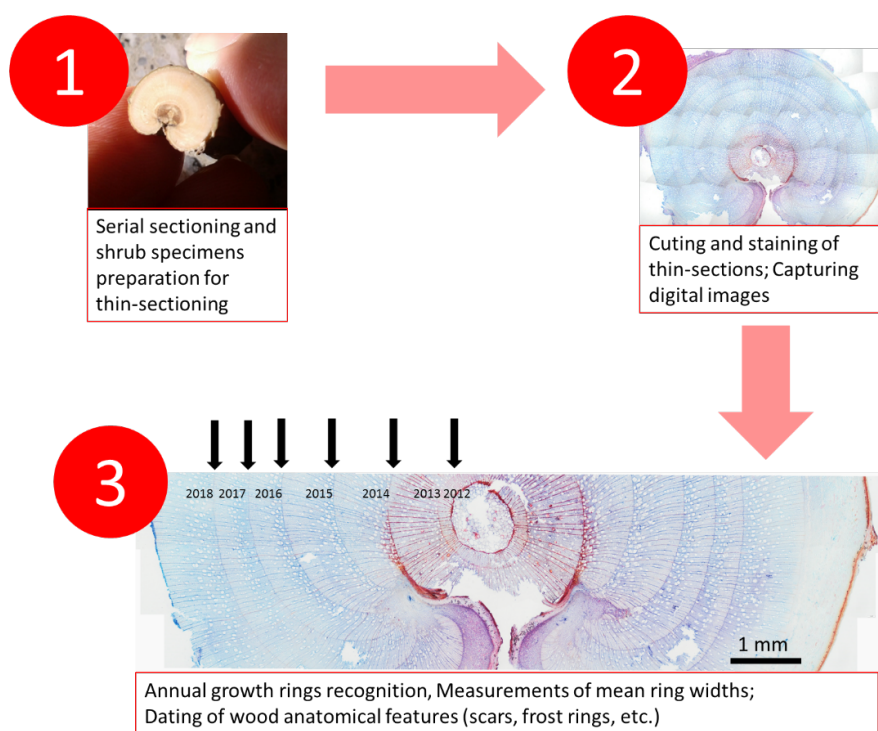


Figure 2.17.2: Shrub processing workflow. Stage 1: performed at Research Station Samoylov Island; Stage 2 and 3: performed in Adam Mickiewicz University DendroLab (Poznan, Poland)

**Preliminary results**

Recently drained lake (N 72.32388°, E 126.25084°)

In order to estimate the age of a possible thermokarst lake drainage event *Salix spp.* shrubs were sampled in so called recently drained lake, located in Eastern Kurungnakh Island.

Growth ring measurements performed on 28 shrubs (stem base specimens) revealed that shrub ages are fairly equal, no matter from which topographic positions the shrubs were sampled (Figure 2.17.3). The maximum *Salix spp.* shrub age revealed for this site so far is 21 years (Table 2.17.1).

Table 2.17.1: Overview of *Salix spp.* shrub age estimates assessed as number of annual growth rings. Shrubs were sampled in three topographic positions (see Figure 2.17.3A)

Lake Bottom (1S)		Lower shrubline (2S)		Upper shrubline (3S)	
shrub ID	# rings	shrub ID	# rings	shrub ID	# rings
1S01	17	2S01	18	3S01	20
1S02	19	2S02	20	3S02	19
1S03	16	2S04	18	3S04	19
1S04	17	2S05	18	3S05	19
1S05	14	2S06	18	3S06	21
1S06	17	2S07	21	3S07	19
1S07	20	2S08	18	3S08	15
1S08	16	2S09	18	3S09	19
1S09	18	2S10	18	3S10	18
1S10	17				

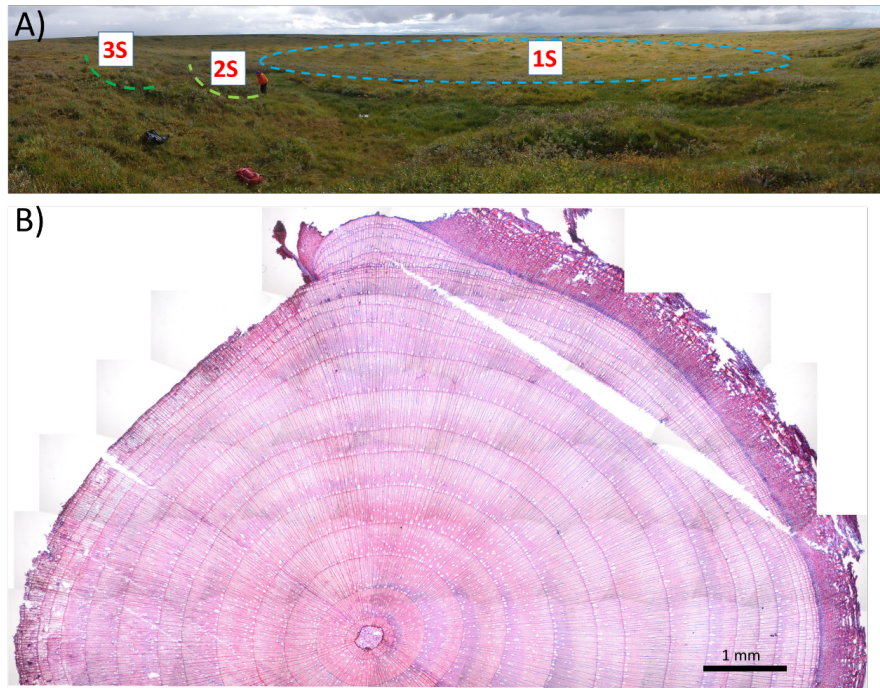


Figure 2.17.3: A) *Salix* spp. sampling plots within a recently drained lake in Eastern Kurungnakh Island: 1S - bottom of the lake, 2S - lower shrubline, 3S - upper shrubline; B) cross-sectional cut of *Salix* stem base section after staining with 21 annual growth rings and a scar visible in the upper part of the section together with the group of 8 wedging rings located in the outermost part

#### Acknowledgements

The research leading to these results has received funding from the European Union's Horizon 2020 project INTERACT, under grant agreement No. 730938.

## 2.18 Large drained lake basin in the south-eastern part of Kurungnakh Island as seen on geophysical data and preliminary geomorphological study

Alexey Faguet <sup>1,2</sup>, Andrey Kartoziia <sup>1,2,3</sup>, Egor Esin <sup>1,2</sup>, Anna Zaplavnova <sup>1,2</sup>, Nikolai Laschinskiy <sup>4</sup>

<sup>1</sup> Trofimuk Institute for Petroleum Geology and Geophysics, Siberian Branch, Russian Academy of Sciences, Russian Federation

<sup>2</sup> Novosibirsk State University, Novosibirsk, Russian Federation

<sup>3</sup> V.S. Sobolev Institute of Geology and Mineralogy, Siberian Branch, Russian Academy of Sciences, Novosibirsk, Russian Federation

<sup>4</sup> Central Siberian Botanical Garden, Siberian Branch, Russian Academy of Sciences, Novosibirsk, Russian Federation

### Fieldwork period and location

From July 19<sup>th</sup> to August 19<sup>th</sup>, 2018 (on Kurungnakh Island)

### Objectives

Multidisciplinary approach towards permafrost studies, correlation of data from various methods. With this objective, we study typical objects in the region using a variety of geophysical, geological, geobotanical and soil methods combined with remote sensing.

### Methods

1. Electrical resistivity tomography (ERT): SibER-48 (<http://nemfis.ru>) at 5 and 10 m step (45 and 90 meters penetration depth, correspondingly). Schlumberger, dipole-axis, pole-dipole arrays.
2. Geological observations in outcrops.
3. Geobotanical studies. The main task of the field work on Kurungnakh Island was to collect data about vegetation of two alas depressions different in size and age in order to create vegetation maps of these depressions. Before the field trip two alases were selected based on an UAV image. In each alas two transects were performed from north to south and from east to west. On each transect all visible vegetation types were described by standard method on sample plots 10 x 10 m. Additional vegetation which was present in alases but was not crossed by transects was also described.

### Preliminary results

#### *ERT studies*

A long ERT profile through the large drained lake basin has been recorded. The profile is shown in Fig. 2.18.1. The ERT profile revealed the structure of the basin to the depth of 80 m (Figure 2.18.2). The ERT data correspond with available data on Kurungnakh Island thermokarst lake basins structure (Morgenstern et al. 2011).



Figure 2.18.1: Large, partially drained thermokarst lake basin and ERT profile (white line).

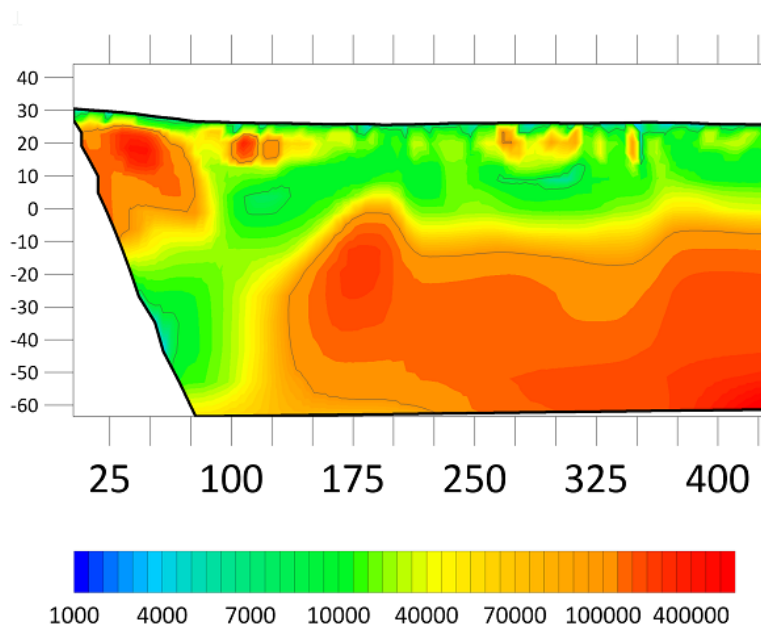


Figure 2.18.2: Fragment of the ERT cross section: resistivity in  $\Omega$ . Alas slope is seen on the left side. Green zone in the lower-left part is probably an anomaly from the still present thermokarst lake. Green color in the upper part of the cross sections – taberites and possibly thermokarst lake deposits. Thin orange inclusions in the upper part – refrozen lake sediments with ice wedges already present. Orange-red zone in the lower part of the cross section – frozen sand that underlies yedoma ice complex.

*Geological studies*

The task was a geomorphological description of micro-landforms, which are present in the studied thermokarst lake basin. Studies showed relationships between alas micro-landforms, geology setting, geophysical charac-



teristics of permafrost, as well as geobotany.

We studied alas micro-topography by means of geographic information system (GIS)-analysis of UAV remote sensing data and field observations. For these, we used the software package ArcGIS 10.2.2 by ESRI. In addition, we studied geological sections in Kurunghakh Island coastal outcrops to acquire a more precise definition of geological settings.

We revealed and described a number of land units that correspond to specific morphometry characteristics of analyzed surfaces, and reflect the development history the alas. For example, we identified several alas floor levels, a coastline of modern lake, pingo, slopes etc. In addition, we interpreted geophysical data based on present geological sections, and knowledge about the geology of the southeastern part of Kurunghakh Island.

#### *Geobotany*

We made 74 standard geobotanical descriptions.

The main vegetation type on flat drained surfaces around alases is tussock tundra with *Eriophorum vaginatum* as being dominant. The nanorelief on these flat surfaces consists of tussocks from 60 up to 100 cm in diameter and 0.3 to 0.5 m height, which make it difficult to see polygonal structures on the soil surface. The observed plant indicators of this surface are the two dominant species of zonal tundra, *Betula exilis* and *Eriophorum vaginatum*. Alas slopes of different orientation and inclination together with alas bottoms provide new habitats and support higher biodiversity in comparison to the flat mainland. The vegetation of these habitats includes different tundra types, fens and mires and aquatic communities. Also places with long-lasting snow are covered by specific vegetation type - willow thickets with *Salix glauca*. The vegetation dynamics in alas depressions follow an one-way successional sequence and could be used for the prediction of future landscape changes. Two vegetation maps of the studied alases are presented in Figure 2.18.3.

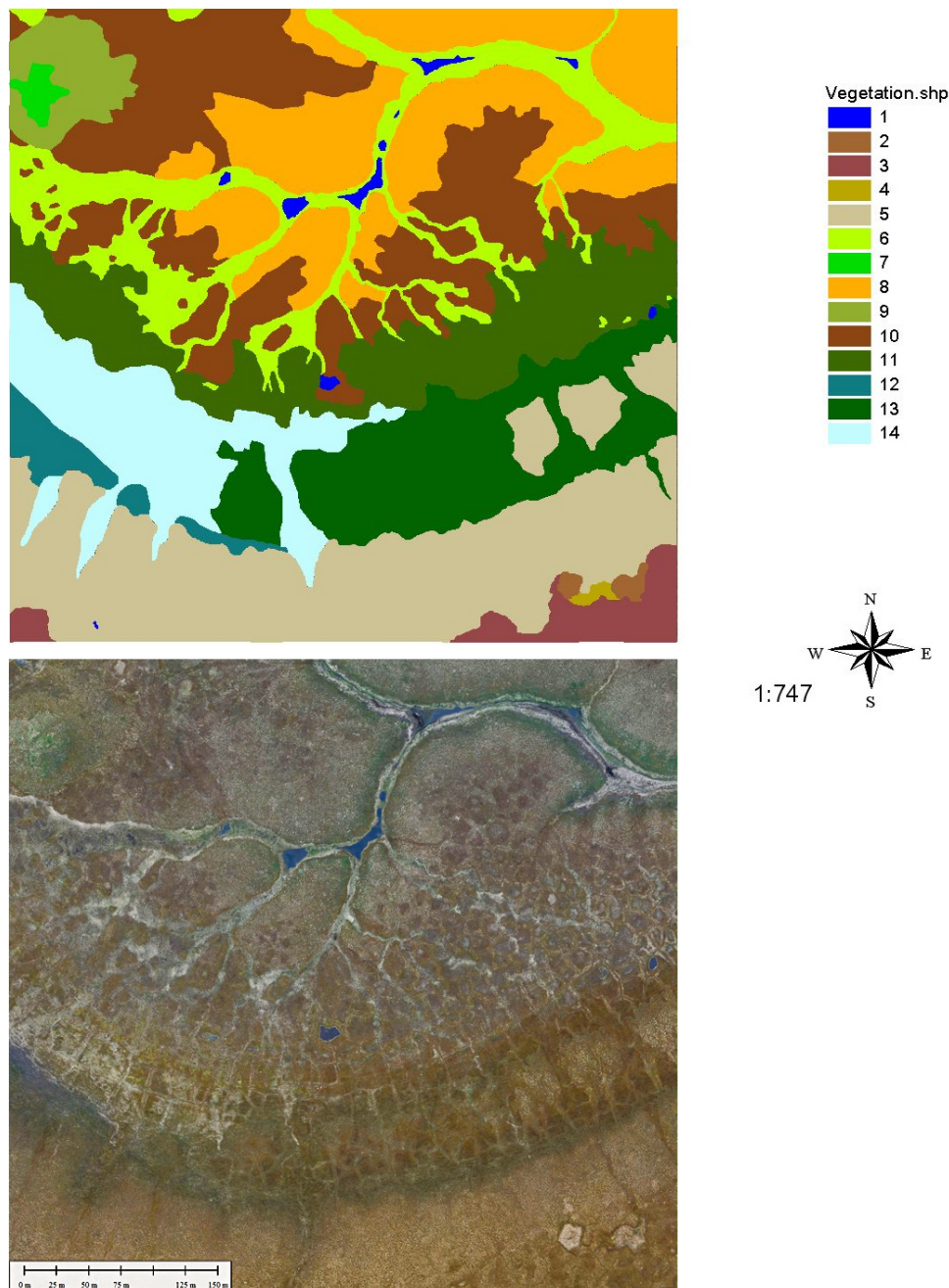


Figure 2.18.3: Vegetation map of the alas number 1 and UAV image of the same place.

*Legend: 1. Open water bodies. 2. Sage mires in low-centered polygons on the flat mainland. 3. Polygonal tundra with Eriophorum vaginatum and Carex concolor on the flat mainland. 4. Wet tundra (with Aulacomnium palustre) in small depressions on the flat mainland. 5. Tussock tundra (with Eriophorum vaginatum and Cassiope tetragona) on gentle slopes. 6. Semiaquatic vegetation along streams, small lakes and galleys (with Eriophorum angustifolium and Arctophyla fulva). 7. Grassland (with Arctagrostis latifolia) on the top of pingo. 8. Tussock tundra (with Eriophorum vaginatum and Hylocomium splendens) on elevated well-drained parts of alas bottom. 9. Hummock tundra (with Artemisia tilesii and Cassiope tetragona) on the slopes of the degraded pingo. 10. Complex of wet tundra (with Carex concolor and green mosses) and sage mires (with Carex rariflora and Tomentypnum nitens). 11. Complex of sage mires (with Carex concolor, C. rariflora, Eriophorum angustifolium and Tomentypnum nitens). 12. Willow thickets (with Salix glauca and green mosses). 13. Tussock tundra (with Cassiope tetragona) on the alas slopes. 14. Wet tundra (with Aulacomnium palustre) on the alas slopes.*

## 2.19 Shallow seismic survey of different permafrost types on Samoylov and Kurungnakh Islands

Gleb Chernyshov <sup>1,2</sup>, Egor Esin <sup>1,2</sup>, (Petr Dergach <sup>1,2</sup>: not in the field)

<sup>1</sup> Trofimuk Institute for Petroleum Geology and Geophysics, Siberian Branch, Russian Academy of Sciences, Russian Federation

<sup>2</sup> Novosibirsk State University, Novosibirsk, Russian Federation

### Fieldwork period and location

From July 17<sup>th</sup> to August 18<sup>th</sup>, 2018 (on Samoylov Island and Kurungnakh Island)

### Objectives

The main goal of our research on the islands Samoylov and Kurungnakh is to test shallow seismic surveys when studying different types of permafrost. Therefore, we study typical objects in the region using standard methods of seismic exploration and data processing.

### Methods

1. 2D active seismic survey: "Lakkolit24-M2" (<https://geodevice.ru>) with different source/receiver steps (2 to 10 m). A 3 kg sledgehammer was used as a seismic source. Acquisition geometry primarily depended on permafrost depth, as well as on surface conditions and required resolution of the seismic section.
2. Passive seismic monitoring: "Baykal-ASN86", GeoSpace "GS-One".

### Preliminary results

#### 2D active seismic survey

On *Samoylov Island* seismic exploration work was carried out at three sites (Figure 2.19.1): 1) wet polygons near the borehole, 2) dry polygons near Samoylov Research Station, and 3) bottom part of the island.

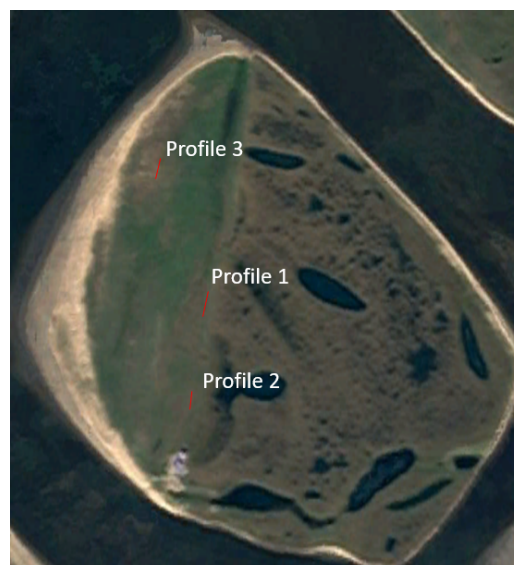


Figure 2.19.1: Fieldwork map on Samoylov Island: Profile 1 - polygons near the borehole, Profile 2 – dry polygons near Research Station Samoylov Island, Profile 3 – bottom part of the island

Profile 1. The profile passed along the cliff avoiding flooded areas. Acquisition geometry: profile length – 115 m, source step – 10 m (16 sources), receiver step – 5 m (24 receivers). At each point of the source, 5–7 records were made and the records summarized (Figure 2.19.2).

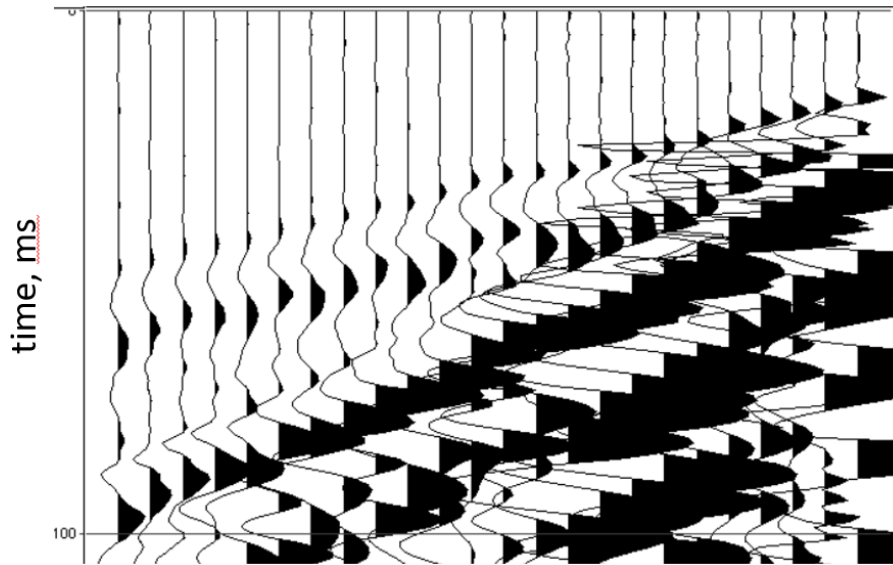


Figure 2.19.2: Seismogram for the source point at 240 m

For each seismogram, the times of first arrivals were determined. For the obtained set of hodographs, a plus-minus method (Hagedoorn 1959) was used to construct a velocity section of seismic waves (Figure 2.19.3). We interpret the high-velocity layer (3.400 m/s) as permafrost rocks.

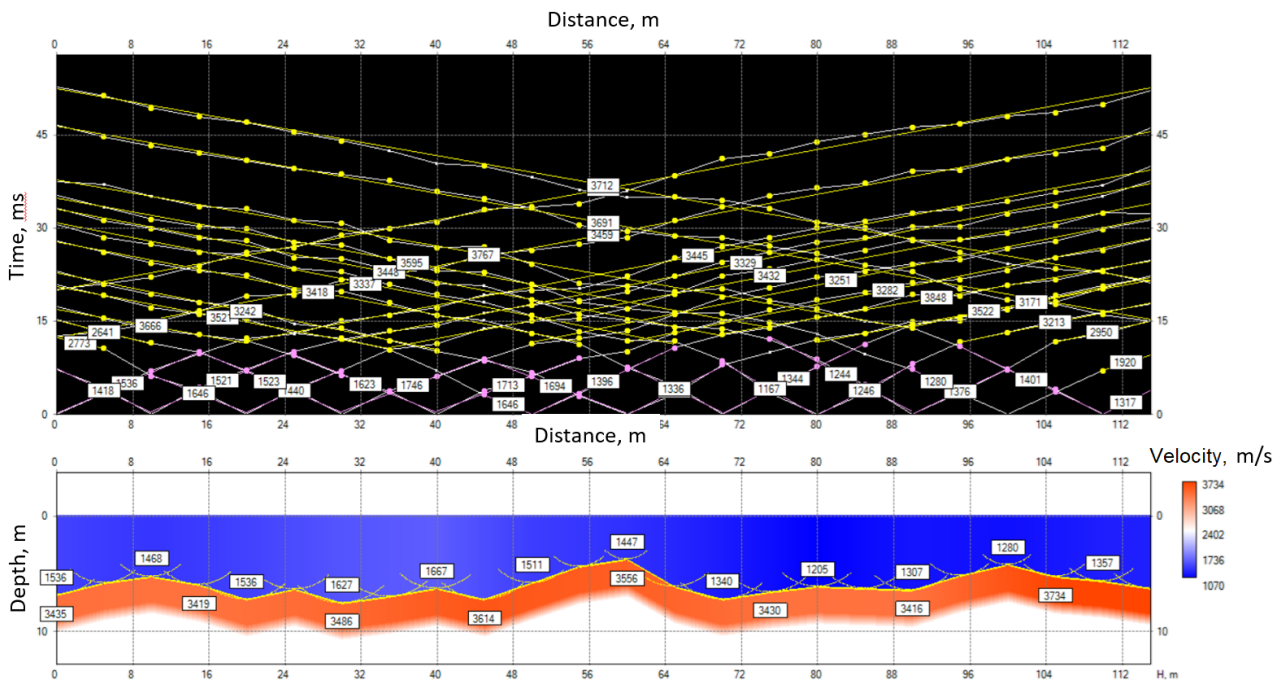


Figure 2.19.3: Set of hodographs and velocity section for the Profile 1, values indicate seismic wave velocities

Profile 2. The profile crossed several dry polygons. Acquisition geometry: profile length – 46 m, source step – 4 m (15 sources), receiver step – 2 m (24). At each point of the source, 5–7 records were made and the records summarized (Figure 2.19.4).

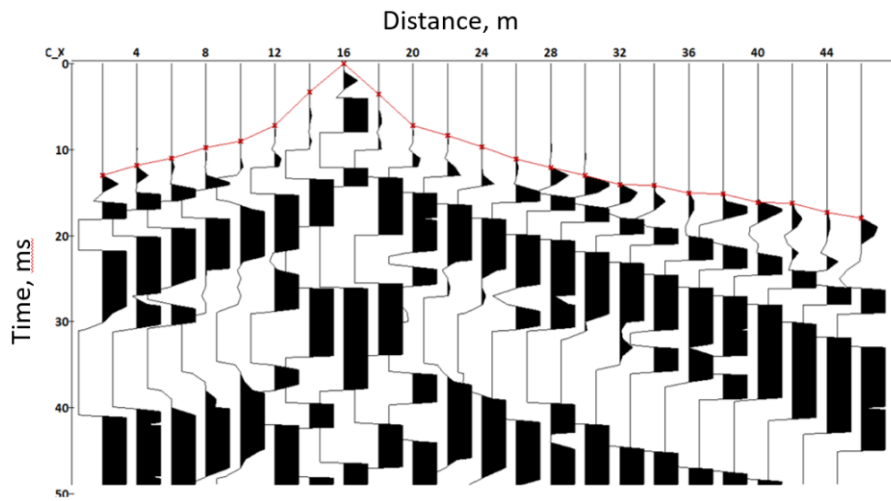


Figure 2.19.4: Seismogram for the source point at 16 m, the hodograph of the first entries is shown in red

A set of first-arrival hodographs and a section of seismic velocities were obtained following processing as shown for Profile 1.

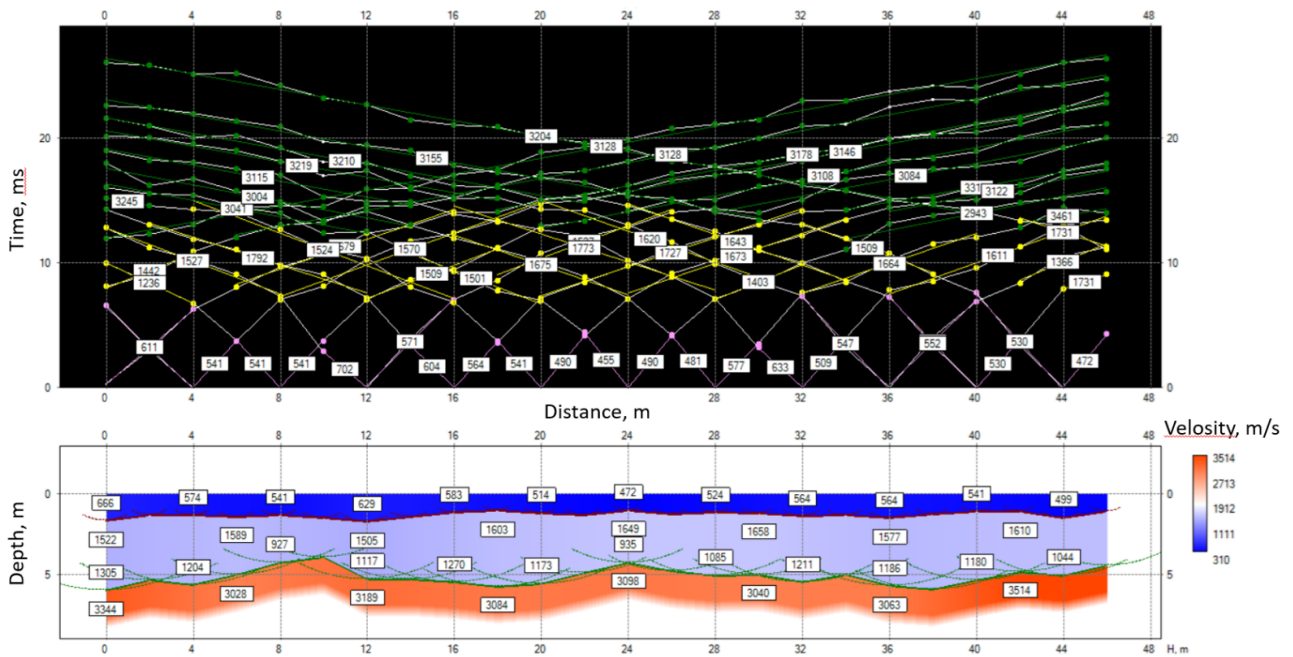


Figure 2.19.5: Set of hodographs and velocity section for Profile 2, values indicate seismic wave velocities

Profile 3. Acquisition geometry: profile length – 57.5 m, source step – 7.5 m (9 sources), receiver step – 2.5 m (24). At each point of the source, 5-7 records were made and the records summarized. Figure 2.19.6 shows the results of the processed data.

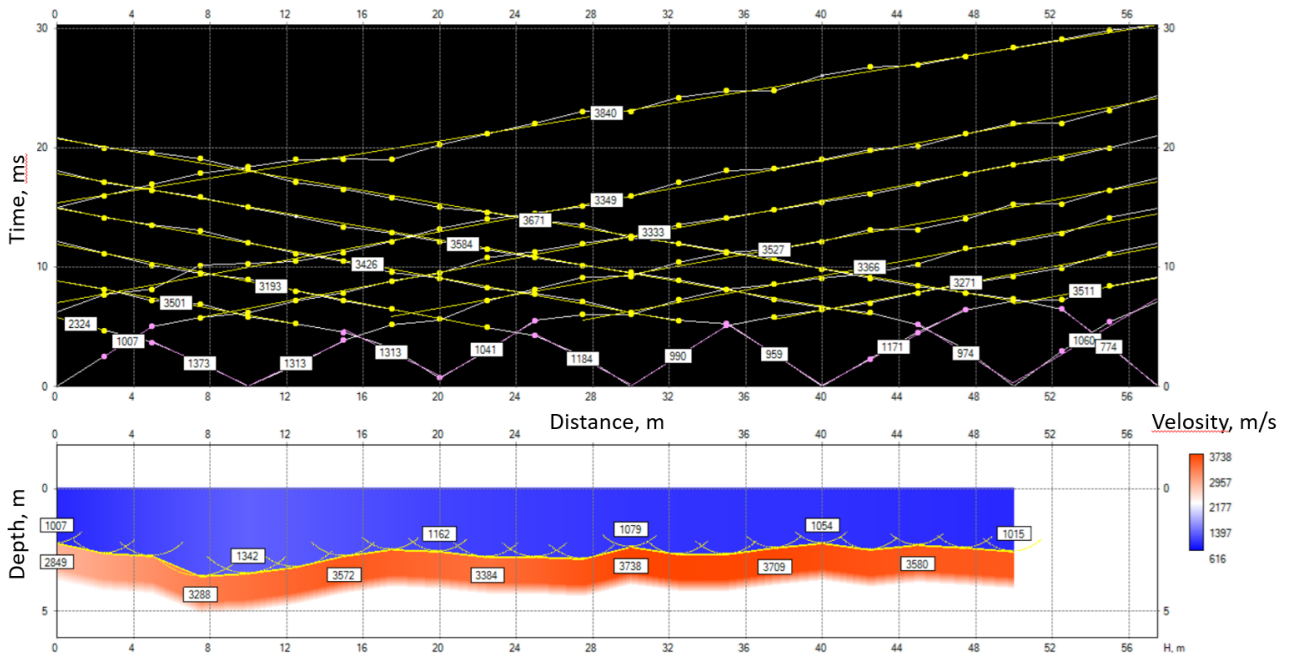


Figure 2.19.6: Set of hodographs and velocity section for Profile 3, values indicate seismic wave velocities

On Kurungnakh Island, seismic exploration work was carried out at two sites (Figure 2.19.7): 1) “Yedoma” Ice Complex, and 2) alas slope.

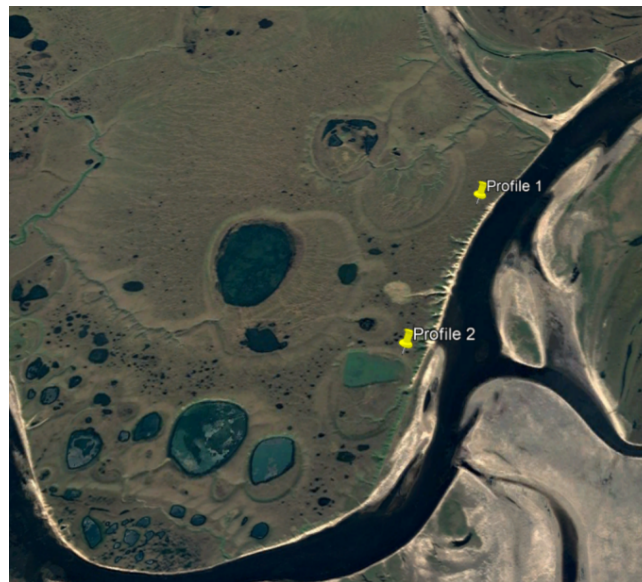


Figure 2.19.7: Fieldwork map of Kurungnakh Island: Profile 1 - polygons near the borehole, Profile 2 – alas slope

*Profile 1.* The profile was laid parallel to the cliff. Acquisition geometry: profile length – 115 m, source step – 10 m (16 sources), receiver step – 5 m (24). At each point of the source, 7-10 records were made and the records summarized (Figure 2.19.8).

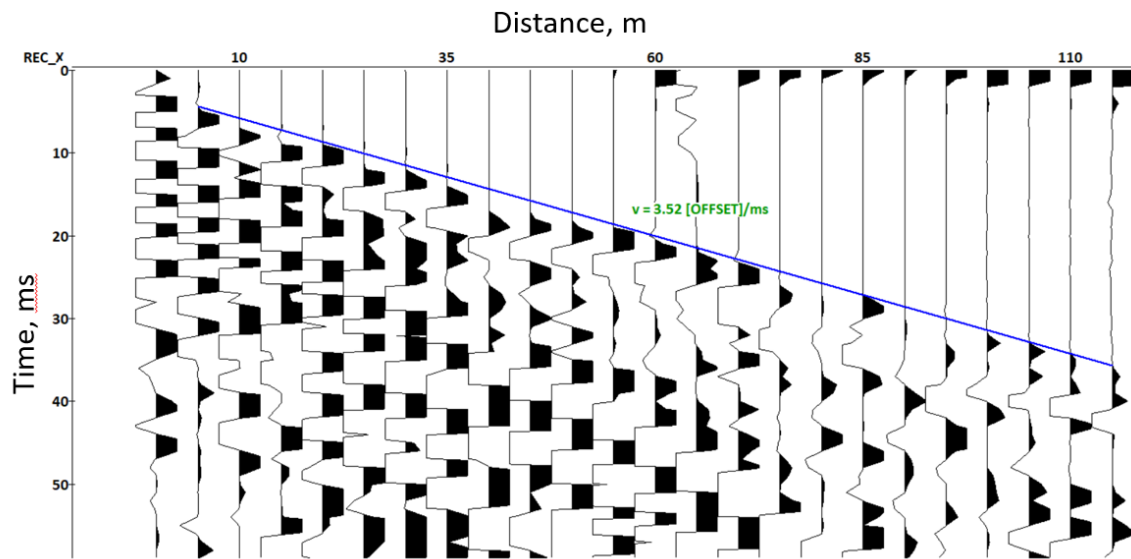


Figure 2.19.8: Seismogram for the source point at 0 m, the hodograph of the first entries is shown in blue, the velocity of forward wave is shown in green

The first-time arrivals do not carry information about the deep structure, since the high-speed permafrost (3.5 km/s) occurring at the surface is violating the conditions for the formation of head waves from boundaries located in the depth.

*Profile 2.* The profile was laid parallel to the cliff. Acquisition geometry: profile length – 115 m, source step – 10 m (16 sources), receiver step – 5 m (24). At each point of the source, 7-10 records were made and the records summarized (Figure 2.19.9).

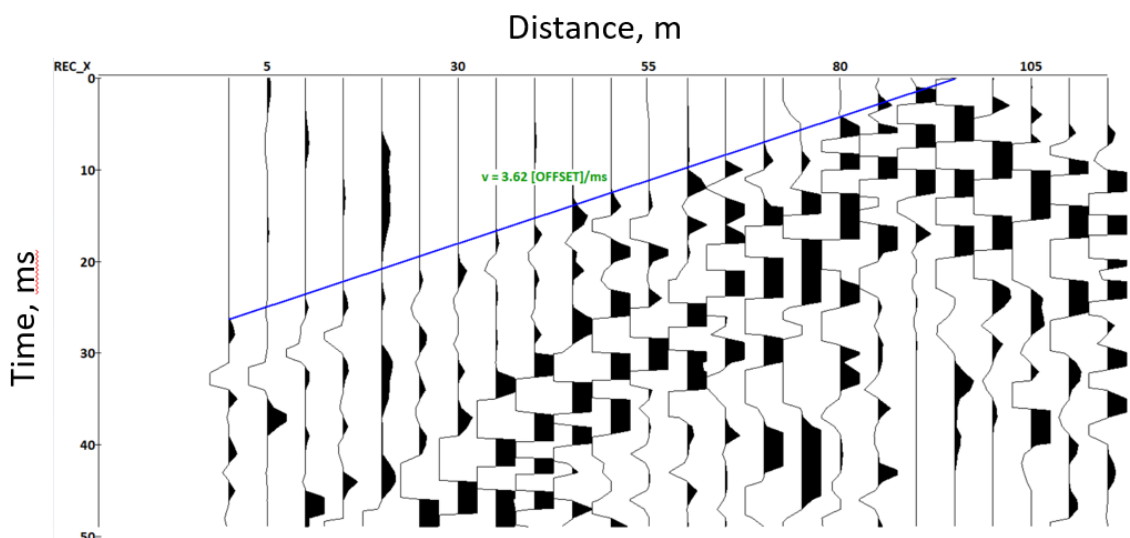


Figure 2.19.9: Seismogram for the source point at 95 m, the hodograph of the first entries is shown in blue, the velocity of forward wave is shown in green

For this data set, the same situation is observed as for Profile 1 (Kurungnakh Island). It is impossible to build a deep structure from the first arrival times. We encountered the same situation for the profile near the borehole on the Samoylov Island, which passed through the flooded polygons. However, in this report, data are not provided due to bad quality.

#### *Passive seismic monitoring*

Autonomous seismic recorders were installed for a period of 10 days on Profile 1 (Samoylov Island). The data were obtained in order to build a near-surface seismic section using the interferometry method. In the process of analyzing the data, other features of the signal were identified.

During the processing of passive seismic data, the signals from 9 earthquakes were found in continuous 10-days records. The example of the signal from a local earthquake is presented in Figure 2.19.10. By using the difference in arrival times of S- and P-waves, the hypocentral distance was estimated: 10 to 15 km.

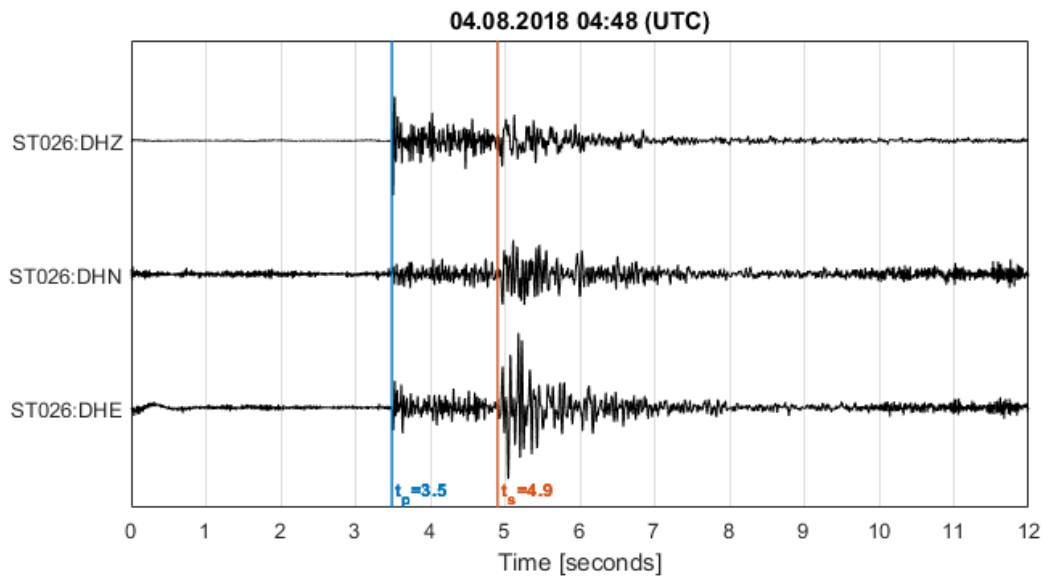


Figure 2.19.10: Example of a local earthquake record. Hypocentral distance 10 to 15 km

The example of the record of a regional earthquake is presented in Figure 2.19.11. In this case, the hypocentral distance was 220 to 280 km.

Figure 2.19.12 illustrates an example of the record of a large earthquake with higher hypocentral distance. In this case, the seismometer bandwidth (0.5 to 250 hertz) was not enough to record the low-frequency component of the signal (which corresponds to the S-wave). In this regard, it was not sufficient to estimate the hypocentral distance.



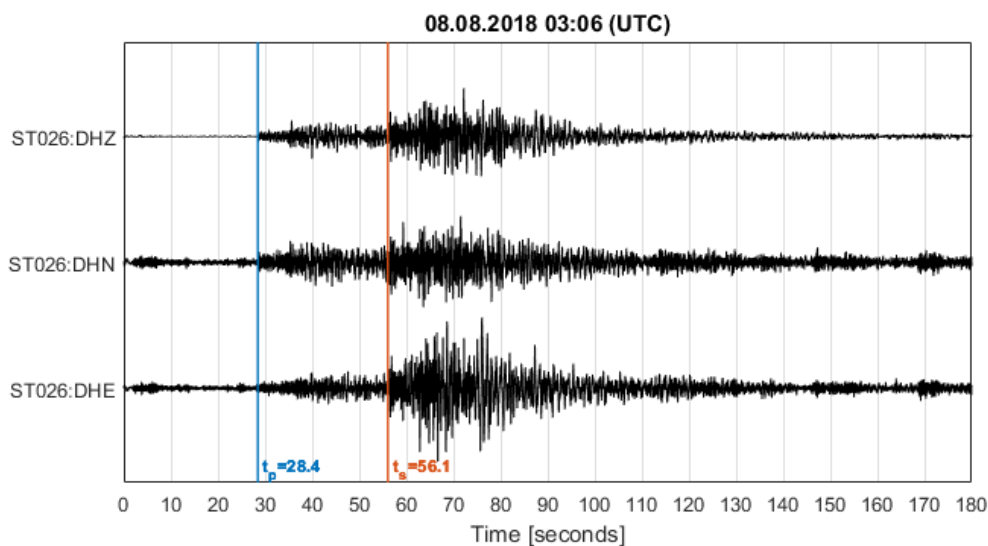


Figure 2.19.11: Example of a regional earthquake record. Hypocentral distance 220 to 280 km

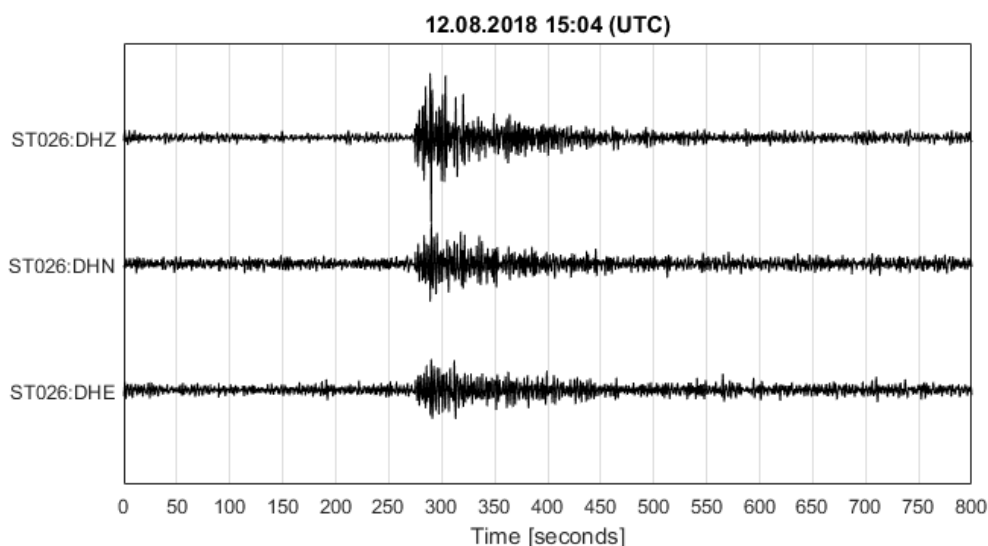


Figure 2.19.12: Example of a far earthquake record

It can be noticed that the records from the horizontal components are characterized by a much higher level of noise than the records of the vertical component. Probably, the reason for this effect is the seismometer installation problem due to the melting of the upper layer of loose sediments.

This problem can be solved by freezing of the borehole seismometers into wells 3 to 5 m deep. This will help to avoid the negative effects associated with seasonal melting of the top layer of loose sediments, and significantly improve the quality of the records. These experiments would be extremely useful for the development of methods of organizing seismological networks in areas of permafrost.

The Samoylov Island area is of great interest for seismological observations. According to the results of short-term observations, signals were recorded from both near local earthquakes with hypocentral distances of less than 15 km and from more distant regional earthquakes with hypocentral distances of 100 km or more.

To directly study the geodynamic situation in the Samoylov Island area, it is advisable to create a local seismological network. The observations can also be included in the existing regional network.

## 2.20 Study of sub-bottom talik in the Lena River Delta by the ERT method

Nikita Bobrov <sup>1</sup>, Dmitry Bolshiyarov <sup>2</sup>

<sup>1</sup> St. Petersburg State University, St. Petersburg, Russian Federation

<sup>2</sup> Arctic and Antarctic Research Institute, St. Petersburg, Russian Federation

### Fieldwork period and location

From July 06<sup>th</sup> to July 13<sup>th</sup>, 2018 (at Olenekskaya Channel)

### Objectives

One of the important scientific problems in permafrost regions is the identification of talik zones (i.e. rocks and sediments being in the thawed state among frozen environment), the determination of their sizes and association with the geological structure and the hydrological regime of the territory. This task becomes especially relevant in view of modern climatic changes that lead in the Arctic to an expansion of taliks, especially those related to the hydrological network. Hydrogenic taliks exist everywhere below the riverbeds in permafrost zone, but talik thickness is questionable in any particular case. Knowledge of this parameter is important for building models of heat balance in permafrost regions, assessment of the dynamics of hydrological processes and rate of change in the state of frozen ground.

The structure of the aquifer below the riverbed can be evaluated with the help of geophysical method – electrical resistivity tomography (ERT). The precondition for talik detection and determination of its shape and size with the use of ERT is substantial electrical resistivity difference between thawed and frozen sediments. The application of ERT can give us the representation of the geological section and the estimate of the earth's materials state (frozen or unfrozen) at a depth inaccessible for drilling with portable facilities. The program of the summer campaign in 2018 continued the year 2017 geophysical works and aimed at the evaluation the thickness of sub-bottom talik for better understanding of aquifer dynamic in the Lena Delta. In 2017, the works have been carried out at the Bolshaya Tumatskaya Channel near to Research Station Samoylov Island. In July, 2018, measurements were conducted at the Olenekskaya Channel near Chai-Tumus, including a 18 km profile along the river. In Figure 2.20.1 the location of geophysical profiles is presented.



Figure 2.20.1: Location of geophysical profiles (red lines) at the Olenekskaya Channel

## Methods

ERT measurements were carried out with Syscal Pro 48 instrument. Multi (10)-channel measurements in motion were conducted: the technique called CRP – Continuous Resistivity Profiling. The towed cable (streamer) of 240 m length with electrodes spacing equal to 10 m and dipole-dipole configuration of measurements were used. The length of source dipole AB was 20 m, the length of receiver dipole varied from 10 to 40 m, the offsets varied from 25 to 200 m. The estimated depth of investigation was about 70 m. The equipment was placed in the motor boat, with the help of which the streamer was towed. Measurements were made both along and across the river. Before the start of crosscut profiles the cable was laid out on the beach in the form of a snake. The drift of the streamer under the influence of the water flow definitely took place but was inessential for the task considered. The crosscut CRP profiles were complemented by stationary ERT soundings at the banks of the river, when the instrument was placed at the water edge; one cable with electrodes was submerged to the bottom of the river with the end of the cable anchored from inflatable boat and the other cable laid on the beach (Figure 2.20.2).



Figure 2.20.2: ERT sounding at the bank of the Olenekskaya Channel (profile 1). In the right photo the direction of the measurements line is denoted by the red dashes.

The measured voltages were transformed to the section of apparent resistivity, and then geoelectrical section was recovered through the inversion procedure.

## Preliminary results

2017 year CRP at the Bolshaya Tumatskaya Channel has found considerable growth of resistivity values at the depth of 40 to 50 m below the surface. Measurements in the year 2018 at the Olenekskaya Channel generally confirmed this result. Two cross-sections – near Chai-Tumus (profile 1) and along hydrological gauge line (profile 3) were obtained.

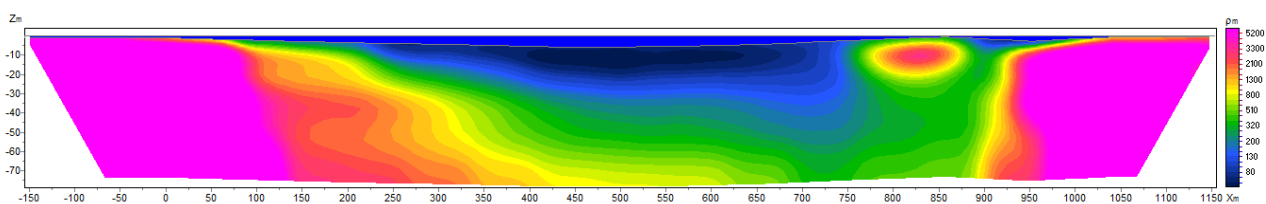


Figure 2.20.3: Resistivity section obtained as a result of combined CRP and land ERT data inversion for the profile 3. Horizontal scale – distance along the profile, m. Vertical scale – depth, m. The color scale in the right presents resistivity values. Bathymetry data are included, water is colored with blue (water resistivity  $100 \Omega m$  does not correspond to the color scale).

Between them one long upstream profile of 18 km length was passed (profile 2). At all profiles we can see increasing resistivity with the depth, which apparently corresponds to the transition from the talik to permafrost. In this case the thickness of sub-bottom talik is estimated as much as first tens of meters. This means that below this depth permafrost is presented almost everywhere under the channels of the Lena River Delta.

The result of 2D ERT data inversion for the profile 3 is given in the Figure 2.20.3. ZondRes2D program was used, and smoothness constrained inversion was performed with NLPCG algorithm, that uses the conjugate gradient method to solve a nonlinear optimization problem. Bathymetry data were included in the model as a-priory information. The water resistivity derived from direct conductivity measurements (about  $100 \Omega$ ) was fixed. Mean RMS error was about ten percent, which is rather big value for ERT, but one should keep in mind that CRP data obtained in motion has great dispersion due to impossibility of stacking.

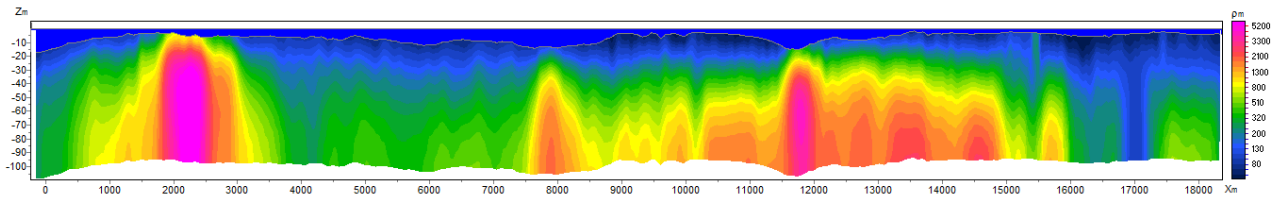


Figure 2.20.4: Resistivity section obtained as a result of CRP data inversion for 18 km profile 2 along the Olenekskaya Channel. Horizontal scale – distance along the profile, m. Vertical scale – depth, m. The color scale in the right presents resistivity values. Bathymetry data are included.

In the Figure 2.20.4 the geoelectrical section recovered along 18 km upstream profile is presented. One can see that it is rather complicated, and there is no direct correlation between river depth and the thickness of the talik. Apparently, local geological structure plays the main role.

So, the main results of geophysical studies of hydrogenic sub-bottom taliks in the Lena Delta can be summarized as follows:

- ERT measurements performed at the Lena River channels has found considerable growth of resistivity values at the depth of first tens of meters below the surface everywhere in the studied area.
- This increasing of resistivity apparently indicates that sub-bottom talik has limited thickness under the channels of the Lena Delta.
- The confirmation of this assumption can be done by special under channel drilling or seismic survey with adequate offsets.

### Acknowledgement

We thank Arctic and Antarctic Research Institute for the opportunity to take part in the “Lena-2018” expedition. Some results were obtained in the framework of the Russian Foundations for Basic Research project No. 18-05-60291. The research was performed with the use of the equipment provided by the Research park of St. Petersburg State University, Center for Geo-Environmental Research and Modeling (GEOMODEL). Special thanks to Waldemar Schneider and Dmitry Bolshiyarov for the help in organization of the fieldwork.

## 2.21 Seismicity of the Laptev Sea Rift

*Aline Ploetz*<sup>1</sup>, (*Boris Baranov*<sup>2</sup>: not in the field), *Tanja Fromm*<sup>1</sup>, (*Wolfram Geissler*<sup>1</sup>: not in the field), *Stepan Gukov*<sup>3</sup>, *Christian Haberland*<sup>4</sup>, *Frank Krüger*<sup>5</sup>, (*Artem Krylov*<sup>2</sup>: not in the field), *Dmitri Peresyphkin*<sup>3</sup>, *Sergey Petrunin*<sup>3</sup>, (*Sergey Shibaev*<sup>3</sup>: not in the field), *Rustam Tuktarov*<sup>3</sup>, (*Nikolay Tsukanov*<sup>2</sup>: not in the field) and *Daniel Vollmer*<sup>5</sup>

<sup>1</sup> Alfred Wegener Institute Helmholtz Centre for Polar and Marine Research, Bremerhaven, Germany

<sup>2</sup> Shirshov Institute of Oceanology of the Russian Academy of Science, Moscow, Russian Federation

<sup>3</sup> Yakutsk Branch Federal Research Centre Geophysical Survey, Russian Academy of Science, Yakutia, Russian Federation

<sup>4</sup> GFZ German Research Centre for Geoscience Helmholtz Centre Potsdam, Potsdam, Germany

<sup>5</sup> University of Potsdam, Potsdam, Germany

### Fieldwork period and location

From September 03<sup>th</sup> to September 16<sup>th</sup>, 2018 (in the Lena Delta, Tiksi and Buor-Khaya Bay)

### Objectives

The main objective of the ongoing study is to investigate the geodynamic processes of the continental Laptev Sea Rift and their major tectonic zones to better describe the amagmatic rifting and its consequences in an Arctic and global context. From the Arctic Ocean the ultra-slow spreading Gakkel ridge is propagating towards the continental slope of the Laptev Sea in North-East Siberia. In comparison to the Gakkel Ridge, which separates the North American plate from the Eurasian plate, the Laptev Sea region shows diffuse seismic activities. A few larger earthquakes located south-east to the Gakkel Ridge are suggested to define the further plate boundary (Fujita et al. 2009).

From the Laptev Sea shelf south to the coastal regions of the continent, focal depths increase from 10 to 25 km (Jemsek et al. 1986; Franke et al. 2000; Fujita et al. 2009). Data from local short-term studies in the 80ies, showed that there is abundant local seismicity (Kovachev et al. 1994 (eng. 1995); Avetisov 1999).

According to Sloan et al. (2011) the westernmost limit of seismicity is related to the thick lithosphere of the Siberian shield, which indicates some structural control on the recent tectonic activity. Franke et al. (2000) defined with nine teleseismic events the North-American-Eurasian pole of rotation west to the Cherskii mountains. Furthermore, they assume a separate microplate, based on the concentration of crustal extensions and seismicity to east and west of the Laptev Sea, respectively (Franke et al. 2000). Additional, focal mechanisms indicate changes between compressional and extensional tectonic phases over short distances. This might be a consequence of the fact that the pole of rotation is close to our study area, probably to the south of Lena delta (Gaina et al. 2002). It is up to now not known, if especially the southern Laptev Sea Rift is still in an extensional mode, or if compression already started and how the old continental lithosphere is eroded by the rifting process. This includes to verify the position of the rotation pole between the Eurasian and North-American plates and to prove or disprove, if an independent Laptev Sea microplate exists. Therefore, we are monitoring local earthquakes in the Laptev Sea and Lena Delta to fulfil the following objectives:

1. Location of microseismicity and its relationship with active faults. We want to identify seismologically active faults zones. In a first step, we deployed instruments in earthquake areas, which are already identified by the global seismological network, though with low spatial resolution.
2. Focal mechanisms. What is the present geodynamic setting, where is extension and where is compression in the Laptev Sea and in the Lena Delta region, where is the exact pole of rotation? What is the relation of the recent seismicity to pre-existing crustal and lithosphere structures (e.g., western Verkhoyansk Fold-and-Thrust Belt, Olenek Fault-Zone or South Anyui Suture)?

3. Lithosphere structure. It is interesting to note that despite the Cenozoic continental rifting in the Laptev Sea little volcanism is known. Thus, we like to compare the deep crustal and upper mantle structure with other continental rift systems (e.g. Afar) to enhance our understanding on the driving forces.



Figure 2.21.1: Global map with plate boundaries after Bird (2003) highlighted in red and the framed area of interest. Map of the study area showing the temporary station distribution for 2018/19, magenta triangles presents the network and the bullseye the seismic array. White triangles mark stations that were dismantled in 2017 and 2018.

### Methods and fieldwork summary

Like in the last two field-seasons (e.g. Geissler et al. 2017), we focused in the Lena Delta on the southern part of the Olenek fault zone close to the Research Station Samoylov Island. There, with the support of the Research Station Samoylov Island and their boat URAL, we re-installed two, dismantled two and maintained five seismic stations of the regional network (see Figure 2.21.1; Table A.2.18).

We did extend this network to the southeast to the Buor-Khaya Bay, to monitor the seismicity of the southern Laptev Sea in greater detail. Because of the weather, only three of the planned positions could be reached with the vessel NICOLE and alternatively overland two other positions with an all-terrain vehicle (see Figure 2.21.1; Table A.2.19). Unfortunately, two of the planned stations, placed on the north-eastern end of the bay, could not be deployed.



Figure 2.21.2: Panorama of the Buor-Khaya Bay, view from the station BK003. Photo by Tanja Fromm)

Furthermore, we maintained 13 stations of a 2 km aperture seismological array (see Figure 2.21.1; Table A.2.20). The array, located about 10 km east of Tiksi, monitors the wider area especially the Laptev Sea. Such an installation is logistically much easier to maintain than a distributed regional station network.



Figure 2.21.3: *left: C. Haberland and R. Tuktarov walking to maintain station LD019 - Norden-shield. Photo by Aline Ploetz; right: F. Krüger und S. Gukov setting up station BK003. Photo by Tanja Fromm*

All stations were equipped with MARK 3C 1s passive sensors, CUBE data acquisition systems and two 80 Ah batteries buried as deep as possible in the partially frozen ground (see Figure 2.21.2 and 2.21.3). This configuration was chosen to ensure minimum power consumption at low temperatures and worked well for the previous installations.

The data recovery was almost complete with nine months of data from 20 stations. In the array, we lost three external GPS antennas, due to animal activity. For these stations the time has to be calculated or modelled e.g. with a noise-correlation of other stations. Furthermore, we could identify 3 stations of the array which recorded on some components only frequencies greater than 10 Hz during the winter. This could be recognized by looking at a known teleseismic event (Figure 2.21.4). Until now, we are not sure what pre-filtered these recordings. From previous installation, we know that the temperature in the ground went down to  $-26^{\circ}\text{C}$ . A possible explanation could be leaking water into the seismometer that had frozen the components during the cold winter and manipulated the recordings.

The data acquisition stopped at most stations in late April due to the 32-Gbyte limitation of the CUBE data loggers. Most batteries could be reloaded (all were at or above 11.5 V capacity). Data are shared among the partners (Yakutsk, Moscow, Potsdam/ Bremerhaven).

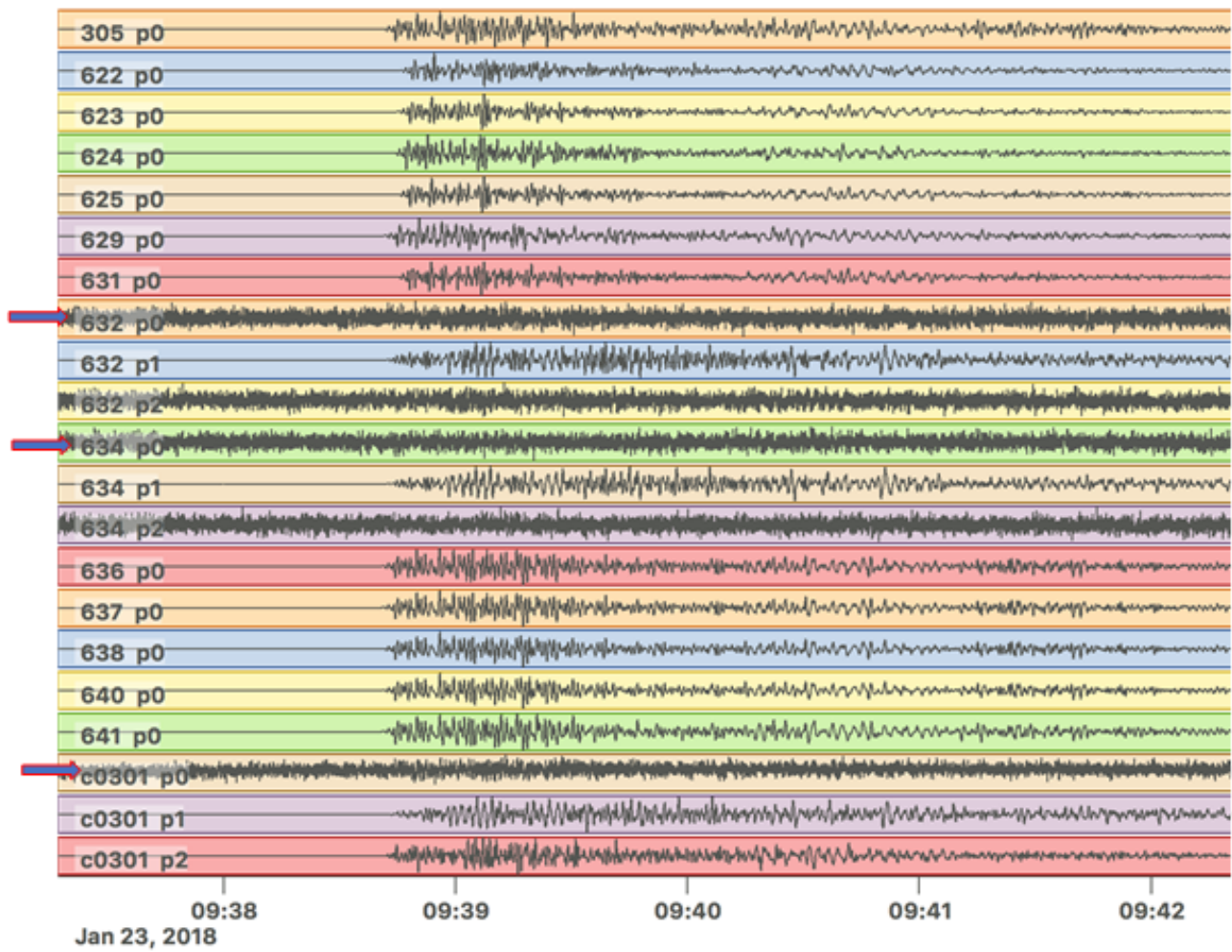


Figure 2.21.4: *Teleseismic event with a magnitude of 7.9 located to the Gulf of Alaska, recorded on stations in the Lena Delta network and the Tiksi-array. The three marked stations, plotted with multiple components, are not showing the estimated incoming low-frequency signal characteristic for such an earthquake.*



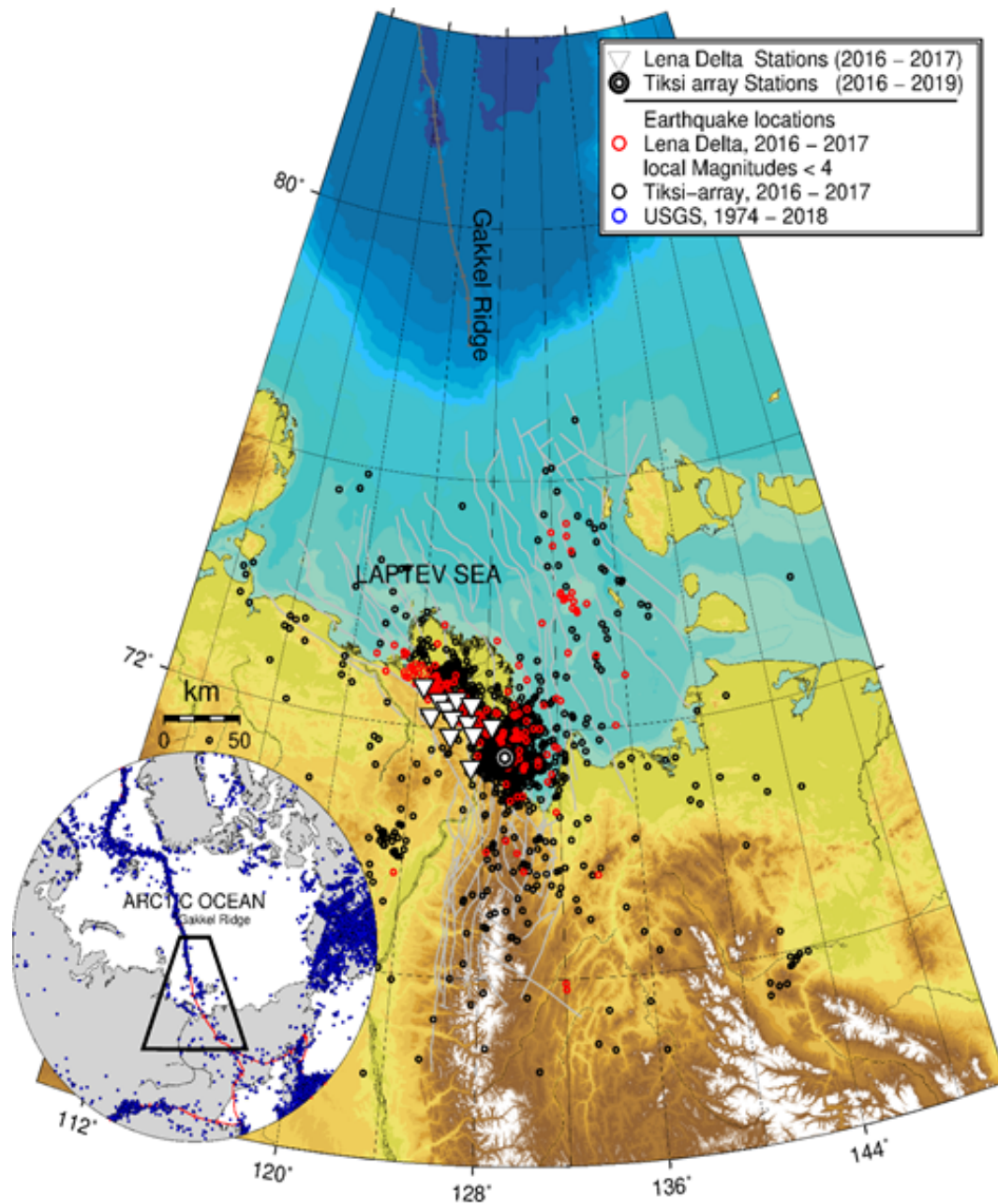


Figure 2.21.5: Regional map of the Laptev Sea showing the preliminary results of located earthquakes from the first recordings (2016 to 2017)

### Preliminary results

First location results of our data recorded from 2016 to 2017 show high seismicity in the Buor-Khaya Bay and the southern Lena Delta (Figure 2.21.5). We located several hundreds of earthquakes with the Lena Delta network and the Tiksi-array with local magnitudes  $mL < 4$ . Focal depths are mainly  $< 25$  km. It is however unclear if this seismicity marks a continuation of the Olenek fault in East-West direction or if it is caused by another fault in North-South direction.

### Acknowledgements

We are grateful to our Russian and German colleagues who worked in the field. Instruments were provided by Geophysical Instrument Pool Potsdam (GIPP). We thank the captain and crew of the vessel *NICOLE* from the Arctic Geo Centre Tiksi as well as all people of the Research Station Samoylov Island.

## 2.22 Permafrost research on Sobo-Sise Island (Lena Delta)

*Sebastian Wetterich*<sup>1</sup>, *Alexander Kizyakov*<sup>2</sup>, *Michael Fritz*<sup>1</sup>, *Aleksey Aksenov*<sup>3</sup>, *Lutz Schirrmeister*<sup>1</sup>,  
(*Thomas Opel*<sup>1,4</sup>: not in the field)

<sup>1</sup> Alfred Wegener Institute Helmholtz Center for Polar and Marine Research, Potsdam, Germany

<sup>2</sup> Faculty of Geography, Cryolithology and Glaciology Department, Lomonosov Moscow State University, Moscow, Russian Federation

<sup>3</sup> Arctic and Antarctic Research Institute, St. Petersburg, Russian Federation

<sup>4</sup> University of Sussex, Brighton, United Kingdom

### Fieldwork period and location

From July 11<sup>th</sup> to July 25<sup>th</sup>, 2018 (on Sobo-Sise; eastern Lena Delta)

### Objectives

The part of the LENA 2018 expedition on Sobo-Sise Island in the eastern Lena Delta took place from July 11<sup>th</sup> to July 25<sup>th</sup> 2018. The field team consisted of three AWI colleagues from the AWI Permafrost Research section and two Russian colleagues; Alexander Kizyakov from the Moscow State University and Aleksey Aksenov from the Arctic Antarctic Research Institute (Figure 2.22.1).



Figure 2.22.1: *Participants of the Sobo-Sise expedition 2018: S. Wetterich, A. Aksenov, L. Schirrmeister, M. Fritz, A. Kizyakov (from left to right)*

Sobo-Sise Island belongs to the third geomorphologic terrace of the Lena Delta. According to a landform classification by Fuchs et al. (2018) 43% of the land surface are occupied by Yedoma uplands and Yedoma slopes, 43% are thermokarst basins and 14% are lakes. The cliff is remarkable for its fast shore line retreat of up to 20 m/yr based on Landsat data (2000-2013; Nitze and Grosse 2016) and for substantial elevation change due to thaw subsidence of up to -2 cm/yr (based on Sentinel-1 InSAR, 2017) and up to -3.4 cm/yr (based on on-site rLiDAR) both indicating ongoing and fast permafrost degradation (Chen et al. 2018; Guenther et al. 2018).

In continuation of previous work on the island in 2014-16 the 2018 campaign focused on three major aims:

1. Cryolithological description and extensive sampling of the Yedoma Ice Complex (IC) and adjacent alas profiles to deduce paleoenvironmental information and organic matter (OM) data;

2. Geochemical characterisation, surface waters pathways by means of dissolved organic carbon (DOC), coloured dissolved organic matter (cDOM), hydrochemistry and stable water isotopes;
3. Active layer and thaw subsidence measurements in continuation of previous studies.

## Methods and fieldwork summary

### Permafrost sampling

Yedoma IC and alas profiles were taken at different positions of the river shore including both, vertical sediment profiles and horizontal ice-wedge profiles (Figure 2.22.2) to cover the entire exposed permafrost archive.



Figure 2.22.2: Location of sediment and wedge-ice profiles on Sobo-Sise Island (GeoEye-1 image of July 8<sup>th</sup>, 2014, synthesis of NIR+Red+Green)

The Yedoma IC exposed up to about 25 m above river level (arl) was cryolithologically described and sampled on rope by A. Kizyakov using hammer and axe to document and to obtain the material. Three overlapping 'windows' of sedimentary polygon fillings of the IC were sampled (SOB18-01: 24.1 to 15.7 m arl, SOB18-03: 18.2 to 10.2 m arl and SOB18-06: 13.4 to 0.9 m arl). The sampling totaled in 61 samples (Appendix A.2.21). Additionally, at profile SOB18-06 we took samples for detailed radiocarbon dating at 2.5 m arl within one peat horizon (samples SOB18-06-40 to SOB18-06-58). At profile SOB18-01 a core (SOB18-07) was drilled down to 1.7 m depth below surface (bs) using the SIPRE permafrost corer (Figure 2.22.3).

Profiles of alas deposits were sampled at three locations – east of the cliff (SOB18-04: 3.6 to 1.1 m arl, SOB18-05: 2.15 to 0.65 m arl) and west of the cliff (SOB18-10: 1.35 to 0.7 m arl). Sampling positions are shown in Figure 2.22.4. Detailed cryolithological descriptions are given in Appendix A.2.22.

The sedimentary material of the IC and alas profiles will be subject to sedimentological, OM, biomarker, paleo-bioindicators, ancient DNA analyses complemented by radiocarbon dating and stable isotope analyses of the intrasedimental ice. Ground ice content was already estimated in the field as weight difference of the sample after oven-drying (Appendix A.2.21).



Figure 2.22.3: Yedoma IC profiles studied at the Sobo-Sise cliff shown as (a) overview with the thermoerosional valleys incising the Yedoma cliff and draining into the Lena River, (b) detail of SOB18-06, (c) detail of SOB18-01 and SOB18-03 and (d) drilling of SOB18-07

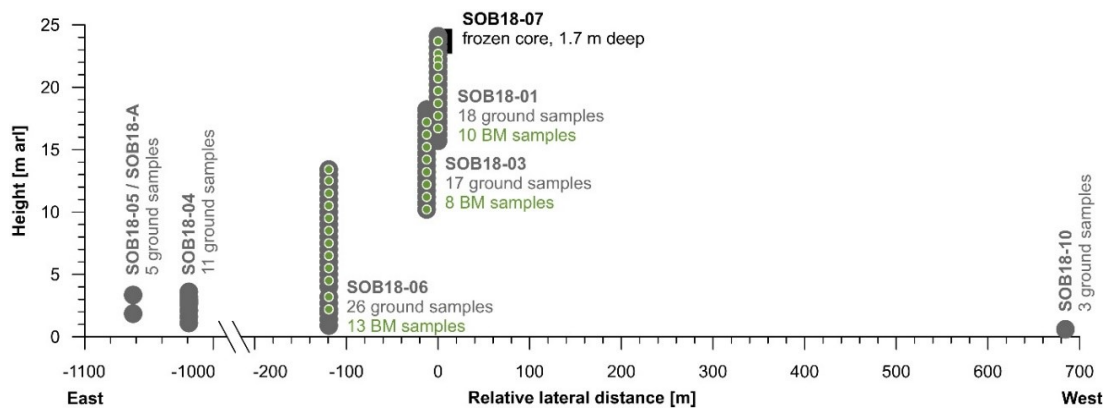


Figure 2.22.4: Sampling locations of sediment profiles on Sobo-Sise Island (BM – biomarker samples)

Three Yedoma IC ice wedge profiles were obtained at different heights above the river (Figure 2.22.5). SOB18-02 was taken at 19.7 m arl on rope by ice screw between the sediment profiles SOB18-01 and SOB18-03. The ice wedge profiles SOB18-08 and SOB18-09 were taken by chainsaw at 9.4 m arl and 2 m arl, respectively.

The detailed horizontal ice wedge profiles amounted to 250 samples and will be analysed for stable water isotopes (Appendix A.2.23). Additionally sampled ice blocks from the Yedoma IC profiles will be analysed for DOC and CO<sub>2</sub> radiocarbon ages.

The ice wedge SOB18-02 was sampled on rope by ice screws at 4.5 m bs between sediment profiles SOB18-01 and SOB18-03 (Figure 2.22.5a) over a width of 4.5 m with sample distance of 0.15 m. Single ice veins were 1 to 2 cm wide and contained numerous rounded bubbles (diameter 1 mm), partly elongated.

The ice wedge SOB18-08 was exposed between 0.4 and 1.6 m bs over a width of 4.6 m (Figure 2.22.5b) and covered by the active layer (0 to 0.2 m bs) and protective layer (0.2 to 0.4 m bs).

The ice wedge SOB18-09 was situated below a thermoerosional valley and sampled from the Lena River bank about 2 m arl over an apparent width of 3.9 m (Figure 2.22.5c). The wedge ice contained numerous rounded bubbles (diameter 1 to 2 mm) but elongated bubbled (diameter 1 mm) in its central part.

The approximately 2 m high and 1.2 m wide ice wedge was sampled in the profile SOB18-04 (Figure 2.22.5d). This ice wedge had several lateral shoulders that merged into ice-rich sediment layers. The ice contained numerous small air bubbles (>1 mm in diameter). Individual ice veins were difficult to recognize. Nine samples at 10 cm intervals were taken at 1.7 m bs. Left and right 10 cm distance from the ice wedge edge were left. In addition, a large sample was taken in the middle of the ice wedge at 1.9 m depth with the axe (Appendix A.2.23).



Figure 2.22.5: Ice wedge profiles studied at the Sobo-Sise cliff shown as (a) detail of SOB18-02, (b) detail of SOB18-08, (c) detail of SOB18-09 and (d) detail of SOB18-04.

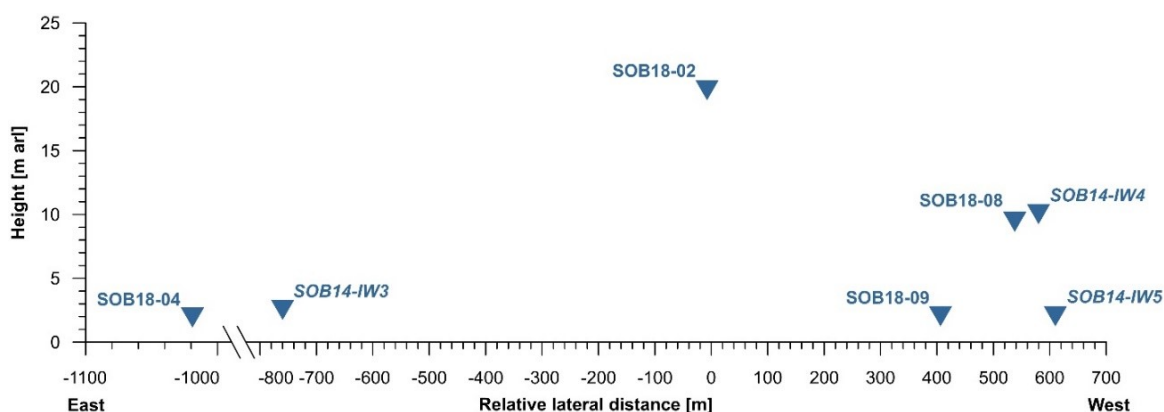


Figure 2.22.6: Sampling locations of wedge-ice profiles on Sobo-Sise Island (IW – ice wedge). Profiles samples in 2014 are indicated in italics. Note differing x-axis if compared to Figure 2.22.4.

Yet unpublished ice wedge sampling on Sobo-Sise Island conducted in 2014 by Thomas Opel is reported here to complement the study. The major aim of the ice-wedge studies during the expedition was to generate new ice-wedge stable-water isotope ( $\delta^{18}\text{O}$ ,  $\delta\text{D}$ , d excess) datasets for the reconstruction of past winter climate variability. Additional ice-wedge samples have been taken to test and compare different dating approaches for ground ice by  $^{36}\text{Cl}/\text{Cl}^-$  as well as radiocarbon dating of organic macro remains, DOC, and  $\text{CO}_2$  from air bubbles. In total, nine ice wedges have been studied and sampled in detail (blocks, slices). All ice-wedge blocks and slices were transported to Germany in frozen state for further sub-sampling in the cold lab. Additional ice-wedge samples were taken from several sediment cores along transects in the study areas. Several modern ice veins from recently growing ice wedges have been sampled as modern endmember. To characterise the general stable-isotope environment, precipitation as well as water from rivers, creeks, lakes, active layer have been sampled. In the following, it will be focused on the detailed ice-wedge studies.

On Sobo-Sise Island, ice wedges were studied in different landscape types and stratigraphic units: (1) Yedoma IC deposits (SOB14-IW3), late Glacial to Holocene thermokarst basins (SOB14-IW1, 2 and 5) and slope from Yedoma IC uplands and thermokarst basin (SOB14-IW4).

Two ice wedges SOB14-IW1 and SOB14-IW2 (Figure 2.22.7a, N 72.5219°, E 127.8572°) were studied directly beside sediment profile SOB14-01 of Jens Strauss in a thermokarst basin (alas) about 8 m arl. The ice-rich host sediments were grey sandy silts with table lenticular cryostructures and peat inclusions.

Ice wedge SOB14-IW1 was a syngenetic ice wedge mirroring the polygonal surface. It was up to 1.6 m wide. The wedge ice was milky white with clearly detectable ice veins of 0.5 to 1.5 cm width and many air bubbles. Two kinds of air bubbles have been found: small (up to 1 mm) round bubbles and vertically elongated bubbles up to 2 mm long. The wedge ice contained little amounts of sediments and organics. The ice wedge was cut perpendicular to its growth direction. In total, 7 blocks were cut from the ice wedge with a chain saw, five in a 1.2 m wide horizontal profile 1 m below surface (active layer depth 44 cm) and two additional blocks from below for dating purposes (Figure 2.22.7a).

Ice wedge SOB14-IW2 was a smaller ice wedge (about 20 cm wide), preliminary interpreted as second-order ice wedge dissecting the polygon. It was partly degraded. In the milky white wedge ice single ice veins (0.5 to 1 cm wide) could be clearly identified. Small spherical air bubbles of 0.5 to 1 mm in diameter as well as vertically elongated (up to 1 cm) were found. The ice was characterized by little amounts of sediments and organics. Two samples were taken by chain saw, representing the ice wedge itself and most likely refrozen standing water above.

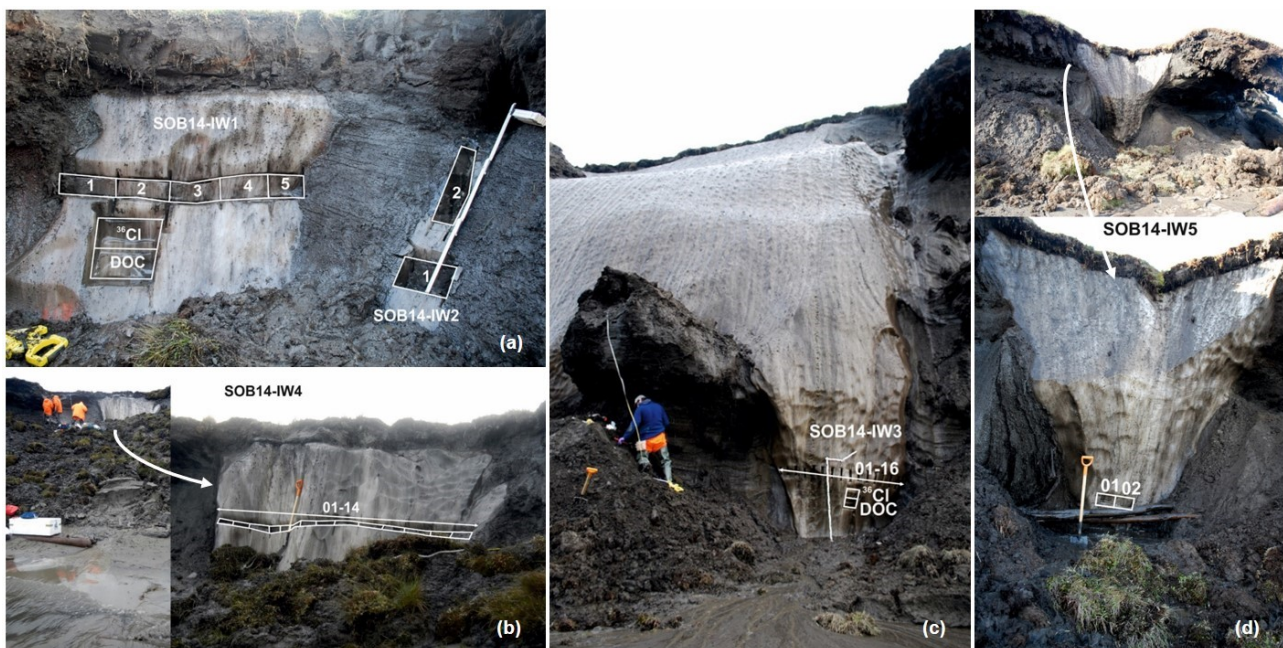


Figure 2.22.7: Ice wedges of the Sobo-Sise expedition 2014 (a) SOB14-IW1 and 2 in a thermokarst basin, (b) SOB14-IW3 in the lowest accessible part of the Yedoma IC, (c) SOB14-IW4 at the slope from Yedoma IC upland to thermokarst basin and (d) SOB14-IW5 at the lowest slope from Yedoma IC upland to thermokarst basin

Ice wedge SOB14-IW3 (Figure 2.22.7b, N 72.53581°, E 128.30054°) was studied directly beside sediment profile SOB14-02-A about 2.5 m arl. The ice-rich host sediments belong to the lowest accessible part of the Yedoma IC and were brownish to grey silts to sandy silts with structureless cryostructure at the bottom, lenticular cryostructure in the middle and ice bands and lenticular structure in the upper part of the profile. This profile was overlain by a distinct peat layer. At the left side of the ice wedge a vertical sand lense could be identified, likely pressed upwards due to ice-wedge growth. Ice wedge SOB14-IW3 was a syngenetic ice wedge of the Yedoma IC. It was about 2.7 m wide. The wedge ice was milky grey. Partly, single ice veins were clearly detectable and 0.5 to 1.5 cm wide. Very few sand veins could be found. The ice exhibited many air bubbles: (1) very small bubbles in the centre of single ice veins, (2) spherical bubbles 0.5 to 2 mm in diameter, and (3) elongated bubbles up to 1 cm long (diameter 0.5 to 2 mm). The amount of sediment and organics was low. 17 samples (vertical slices of 2 to 8 cm width, resolution 15 to 20 cm) in a horizontal profile were cut by chain saw, complemented by two blocks (Figure 2.22.7b).

Ice wedge SOB14-IW4 (Figure 2.22.7c, N 72.54262°, E 128.26814°) was studied directly beside sediment profile SOB14-03 at the slope from Yedoma IC upland to thermokarst basin. The ice-rich host sediments consisted of grey sandy silt in the lower part and silt in the upper part with peat lenses and a peat horizon. In the lower part a lenticular cryostructure was found and in the upper part a layered cryostructure. Ice wedge SOB14-IW4 was interpreted as syngenetic ice wedge. It was covered by 40 cm of sediment, whereof 35 cm represented the active layer. The ice was milky white with clearly detectable and partly cross-cutting ice veins up to 1 cm wide. The content in sediments and organics was very low whereas many elongated air bubbles up to 3 cm long could be found. About 1.6 m below surface 14 blocks were sampled in a horizontal profile of 3.6 m width (Figure 2.22.7c). As such an ice-wedge width is rather unlikely, we observed and sampled most likely an ice-wedge junction that appeared to be wider due to cutting and erosional (flowing water) effects. The stable-isotope data will help to solve this issue.

Ice wedge SOB14-IW5 (Figure 2.22.7d, N 72.54284°, E 128.26775°) was studied at the lowest part of the slope from Yedoma IC upland to thermokarst basin. The host sediments were grey silts and sands with ice bands, that were bend upwards in the immediate vicinity of the ice wedge and include woody remains as well as distinct peat layers.

Ice wedge SOB14-IW5 was sampled in its about 1 m wide lower part about 30 cm above the ice-wedge

toes, representing the initial ice-wedge stage (Figure 2.22.7d). Two blocks were cut. The wedge ice was milky white with very little organics and little sediment inclusions. Partly sand grains were found in the clearly detectable ice veins up to 1 cm wide and cross-cutting each other. The wedge ice was characterised by a lot of air bubbles that occurred in three types: (1) very tiny clouds of bubbles, (2) elongated bubbles (1.5 to 2.0 cm long, and 1 mm in diameter, and (3) spherical bubbles of about 1 mm in diameter.

Five additional samples were taken from modern ice veins from recently growing ice wedges in different locations of a huge thermokarst basin. Additional ice-wedge samples were taken from boreholes in transects from the Yedoma IC uplands to thermokarst basins (profiles SOB14-T1 and SOB14-T2).

### Geochemical investigations

Permafrost thaw and rapid erosion mobilize large quantities of sediment, carbon and nutrients into the aquatic ecosystem and ultimately into the nearshore zone of the Laptev Sea. The high Yedoma cliffs together with the Holocene cover deposits, exposed along the channels of Lena River Delta, export large volumes and masses of material into the aquatic environment. However, an integrated assessment of organic matter stocks, their lateral fluxes due to thaw and erosion and on the fate of eroded material in the aquatic environment is still missing and hampers our ability to quantify the contribution of lateral OM fluxes to the Arctic carbon cycle.

Hydroecological elements of the Lena Delta comprise the Lena River including its channels, the coastal waters, lakes and ponds, creeks and thermoerosional gullies, and meltwater streams from thawing permafrost cliffs (Figure 2.22.8, Figure 2.22.9, Figure 2.22.10). This study focused on creating the link between OM stocks and fluxes from the Yedoma cliff towards one of the main Lena River channels.



Figure 2.22.8: Location of surface water sampling on Sobo-Sise Island (GeoEye-1 image of July 8<sup>th</sup>, 2014, synthesis of NIR+Red+Green)





Figure 2.22.9: Examples of thermoerosional valleys showing (a, b) creek water ca. 50 m before it flows over the cliff into the Lena channel; valley at east end of Yedomia island (SOB18-SW-04, July 14<sup>th</sup>, 2018, 17:51), (c, d, e) a thermoerosional valley draining western edge of eastern alas right before it flows in the Lena channel; little creek ca. 100 m east of Yedomia cliff (SOB18-SW-10, July 17<sup>th</sup>, 2018, 14:51), (f, g, h) a thermoerosional valley of alas west of camp; central outflow right at the edge of alas into the Lena River (SOB18-SW-02, July 14<sup>th</sup>, 2019, 12:30) and (i, j, k) a thermo-erosional valley between the camp and the first permafrost sampling site above SOB18-01 (SOB18-SW-01, July 14<sup>th</sup>, 2018; 12:12)

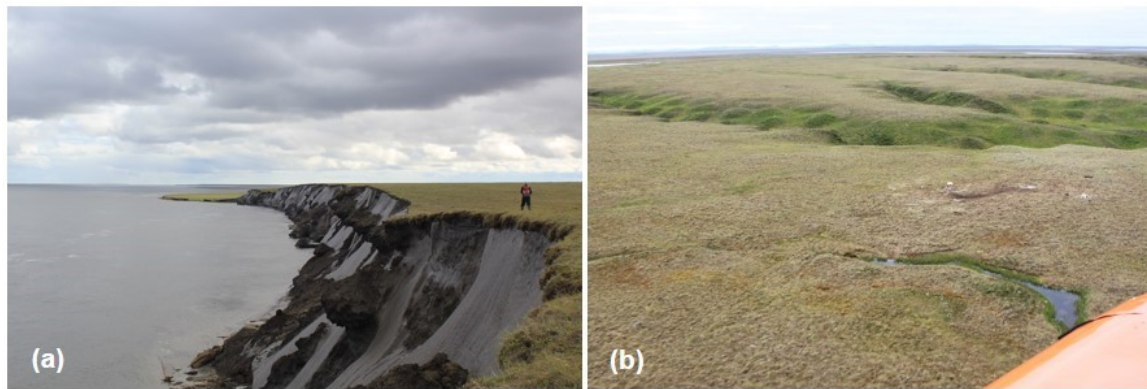


Figure 2.22.10: Examples of sampling sites and water bodies showing (a) the permafrost cliff, where permafrost outflow samples and river water samples have been taken directly at and below the headwall and (b) the interpolygonal pond at camp as seen from the helicopter (SOB18-SW-16, July 23<sup>th</sup>, 2018).

### Preliminary results

One major goal of this expedition to Sobo-Sise Island was to quantify OM stocks in (i) permafrost deposits and (ii) surface water bodies and to characterize the quality of the OM for a better understanding of the fate of OM from terrestrial permafrost towards the Arctic nearshore environment. Expected results are:

- particulate and dissolved carbon and nitrogen stocks of the late Pleistocene Yedoma and Holocene cover deposits on Sobo-Sise Island;
- biogeochemical characteristics of the late Pleistocene Yedoma and Holocene cover deposits on Sobo-Sise Island;
- dissolved organic carbon stocks in surface water bodies on Sobo-Sise Island;
- annual OM fluxes from Sobo-Sise Island based on erosion rates and OM stocks;
- quantitative information on OM degradation in surface water bodies.

Permafrost sampling of the Sobo-Sise cliff is described elsewhere in this report chapter (see section "Permafrost sampling"). Frozen samples were left to thaw overnight and supernatant water was decanted for the following analyses in descending order of priority depending on water availability: stable water isotopes, DOC concentration, cDOM, major anions and cations, pH and electrical conductivity (Appendix A.2.24). For surface water 250 mL glass bottles (Schott©) were used for sampling polygonal pond, creek water from thermoerosional valleys and Lena River water. Sample bottles were rinsed three times with sample water before sample collection. Nalgene HDPE bottles (1 l) were used for sampling permafrost meltwater from the headwall. A larger sample volume was required due to the high sediment load of sometimes greater than 50% in the suspension. Samples were filtered, split and chemically preserved for the different analyses directly in the field lab (Figure 2.22.11).

For stable water isotope analyses ( $\delta^{18}\text{O}$ ,  $\delta\text{D}$ ) unfiltered samples were directly filled in sample bottles. For DOC and cDOM analyses samples were filtered through pre-rinsed 0.7  $\mu\text{m}$  GF/F glass fiber filters attached to a rubber-free syringe. The liquids were filled in clear glass vials with screw caps and PTFE septum and amber glass vials for DOC and cDOM, respectively. DOC samples were acidified with HCl (30% suprapur). For major ion analyses samples were filtered through 0.45  $\mu\text{m}$  CA syringe filters and filled into sample bottles.  $\text{HNO}_3$  (65% suprapur) was added to cation samples. All samples were stored cool and dark. If possible and if enough sample material was available pH and electrical conductivity were determined in the field directly using a portable WTW multimeter.

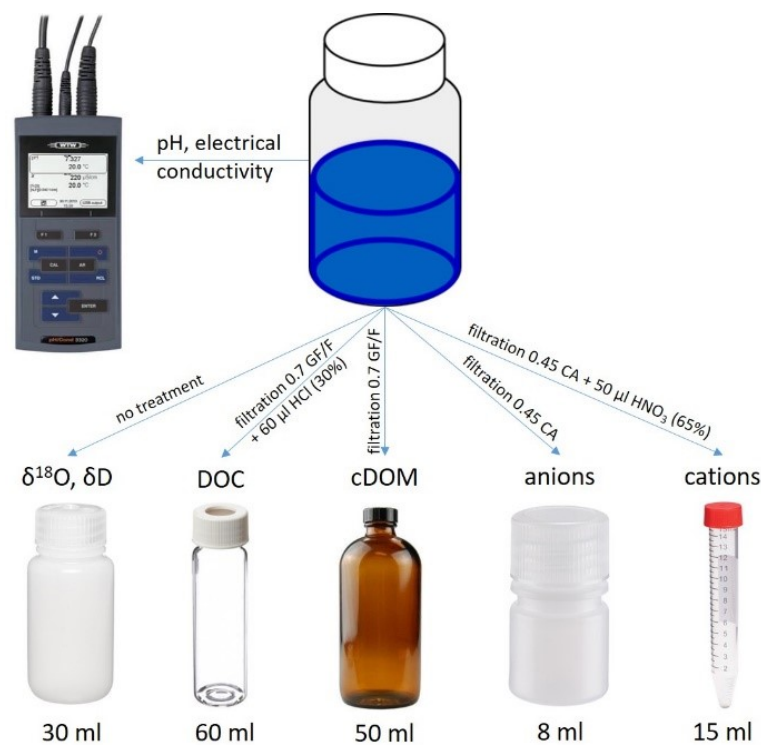


Figure 2.22.11: Scheme of water sample treatment and preservation

Field work resulted in:

- Four rain samples at different days for stable water isotopes to characterize modern precipitation;
- 16 surface water samples for pH, electrical conductivity, stable water isotopes, DOC concentration, cDOM, anions, cations:
  - polygonal pond (n=2)
  - creek water from thermoerosional valleys (n=5)
  - Lena River water (n=6)
  - Permafrost meltwater from headwall (n=3)
- meltwater samples from thawed permafrost samples for pH, electrical conductivity, stable water isotopes (n=102), DOC concentration (n=33), cDOM (n=21), anions (n=21), cations (n=21)
- meltwater from thawed ice wedge samples for stable water isotopes (n=84)

#### Active layer and thaw subsidence measurements

In continuation to active layer and thaw subsidence measurements in 2015-16 on Sobo-Sise Island (ref. F. Günther) in course of the PETA-CARB project, repetitions were undertaken on July 19<sup>th</sup>, 2018 (Figure 2.22.12).



Figure 2.22.12: Location of active layer profiles and thaw subsidence benchmark measurements on Sobo-Sise Island (GeoEye-1 image on July 8<sup>th</sup>, 2014, synthesis of NIR+Red+Green)

The benchmark measurements of relative heights above the vegetation surface are shown in sketches and photographs in Figure 2.22.13. For benchmarks #1 a small depression around was observed and captured in two measurements of 13.0 and 20.5 cm relative height above surface. Benchmark #2 revealed a value of 9.4 cm. Benchmark #3 was surrounded by a small water pool; the measure was 12.2 cm. Benchmark #4 was almost at the surface with values of 0.0 and 1.1 cm. Benchmark #5 was on one side surrounded by moss higher than the benchmark leading to a value of -3.0 cm and on the other side above the benchmark with 4.0 cm. Benchmark #6 was also from one side surrounded by water with 12 cm above the ground of the pool and 7.7 cm above the vegetation surface. The moss surrounding benchmark #7 was higher than the benchmark top resulting in a value of -3.0 cm.

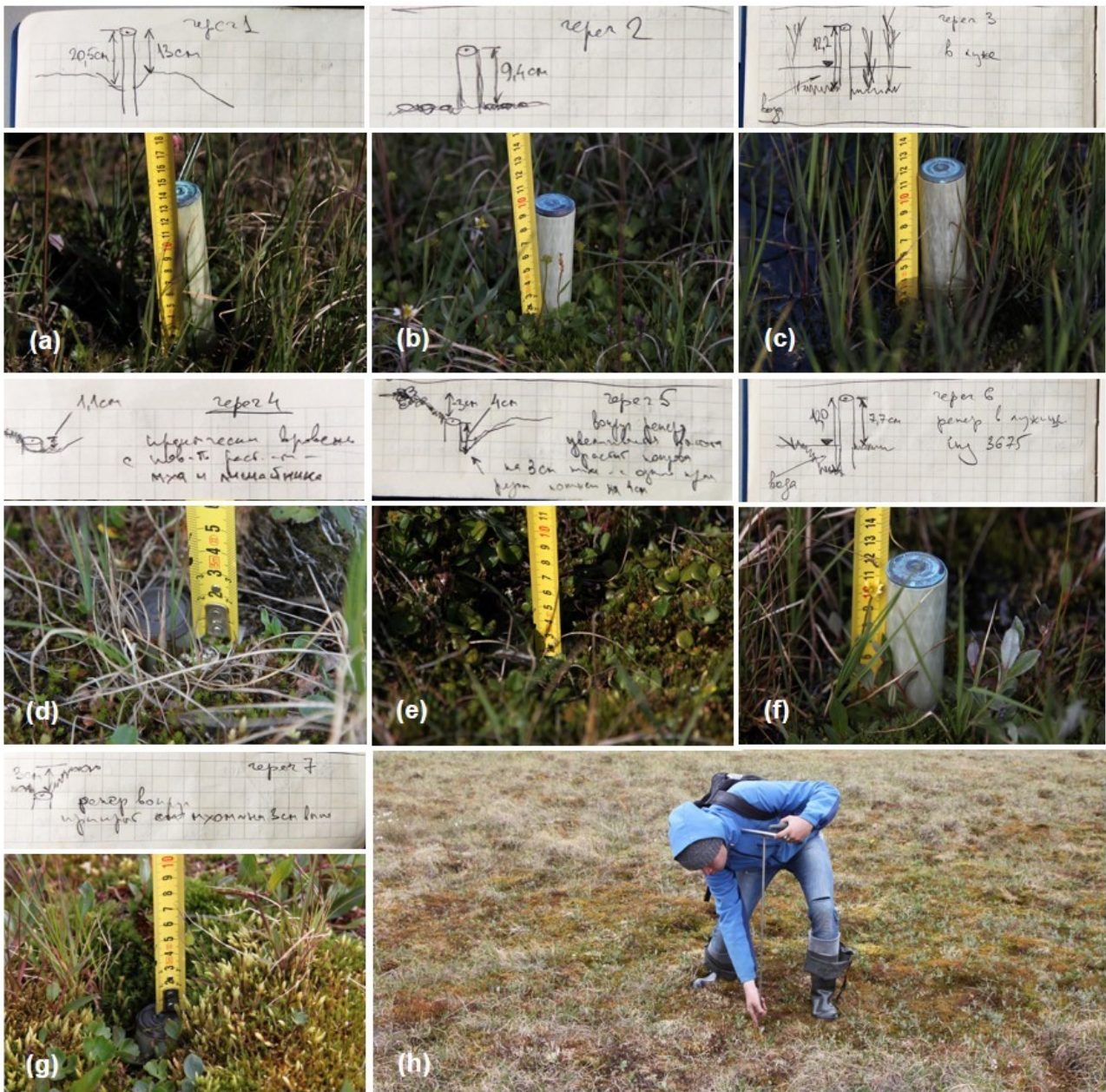


Figure 2.22.13: Thaw subsidence measurements on Sobo-Sise Island of (a) benchmark #1, (b) benchmark #2, (c) benchmark #3, (d) benchmark #4, (e) benchmark #5, (f) benchmark #6 and (g) benchmark #7. Figure (h) illustrates active layer depth measurements along the profiles shown in Figure 2.22.12.

## 2.23 Water tracks at the lower Lena River basin: results of field studies 2018

*Liudmila Lebedeva*<sup>1</sup>, *Anna Tarbeeva*<sup>2</sup>, *Vladimir Shamov*<sup>3,1</sup>, *Olga Makarieva*<sup>4,1</sup>

<sup>1</sup> Melnikov Permafrost Institute, Siberian Branch, Russian Academy of Sciences, Yakutsk, Russian Federation

<sup>2</sup> Lomonosov Moscow State University, Moscow, Russian Federation

<sup>3</sup> Pacific Institute of Geography, Vladivostok, Russia

<sup>4</sup> St. Petersburg State University, St. Petersburg, Russian Federation

### Fieldwork period and location

From August 01<sup>th</sup> to August 11<sup>th</sup>, 2018 (on Khabarovo (Stolb) meteorological station and around)

### Objectives

The main objective was to characterize hydrological and geomorphological functioning of water tracks. Geomorphological and hydrological functioning of such distinct features of the Arctic tundra as water tracks is important to understand and to be able to project their development in the future under climate change and anthropogenic influence.

### Methods

The water level, temperature and electrical conductivity at water tracks and creek were measured with 1-hour temporal resolution at three installed gauges (Figure 2.23.1). We also measured water discharge, active layer depth and ground temperature. Samples from water tracks, creeks, suprapermafrost ground water of the active layer, ground ice and snow were collected for hydrochemical and isotopic analysis. We made ground surface leveling and tacheometry surveys to determine the boundary of the watershed area of water track. Tracer experiments were carried out to estimate hydraulic conductivity of soil in watershed divides, on the slopes and in water tracks.

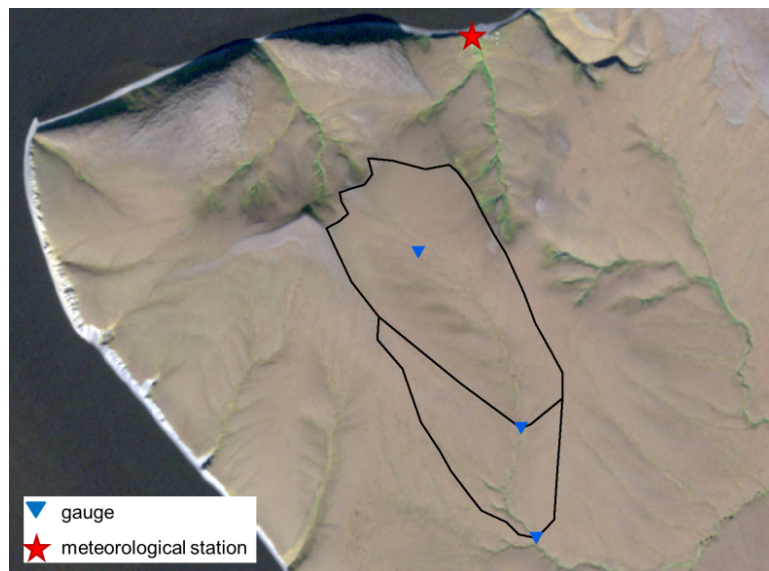


Figure 2.23.1: *Location of meteorological station and hydrological gauges*

## Preliminary results

Water tracks are distinct features of the hillslopes in the Arctic tundra. From hydrological point of view, water tracks are narrow bands of high soil moisture that route water downslope, in the absence of overland flow, through permafrost dominated soils (Gooseff et al. 2013). Geomorphologically water tracks are elements of a rudimentary channel network formed on the hillslopes, that never developed into a mature channel network because permafrost is limiting erosion (McNamara et al. 1998).

Water tracks were studied in Alaska, Canada and Antarctica. In Russia they were described as geomorphological phenomenon. Their hydrological role in Siberian tundra was not investigated. In other Arctic regions it was shown that water tracks as preferential subsurface flow paths dominate soil hydrology. They convey water downslope and impose significant control on the hydrologic response of watersheds. Water tracks affect active layer depth, water quality, vegetation distribution, microfauna and bacterial assemblages. They increase near-surface organic carbon concentrations, primary production and photosynthetic rates.

Field work in the low Lena River basin near Khabarovo (Stolb) meteorological station in August 2018 was a pilot study of water tracks in Siberian tundra.

The watershed area of the water track that was selected for the study was 0.015 km<sup>2</sup>, and the receiving nested creeks have watersheds with areas 1.41 and 2.07 km<sup>2</sup>. The slopes of the basin are composed of ice rich silt (up to 300% of dry weight). The Paleozoic rocks (aleurolites) are exposed in the upper part of the ridges and in the incised channel of the creek, where gravelly material appears in the sediments. The water track has a unexpressed channel with relative average depth of 0.5 m. The mean channel gradient in the water track is 0.082 m/m, mean active layer depth at the watershed at the beginning of August is 0.26 m. Altitudes are from 119 to 140 m a.s.l. Dominant vegetation is tussock tundra. The upper 10 cm of the soil profile is typically represented by moist moss and peat (Figure 2.23.2). There is water-saturated silty loam beneath the organic layer that lies on frozen ground with high ice content or on pure ice. While slopes mostly covered by organic and silty loam soils, patterned ground and frost mounds are found at the watershed divides. Active layer is water-saturated all over the watershed even at watershed divides after several weeks with no rain. Tracer experiment showed that the maximum hydraulic conductivity of the near surface deposits is in the watershed divides where pebbles are found within the active layer. The rough estimate of saturated hydraulic conductivity is 16 m/d. That is larger than in silty loam in slopes and water tracks almost in one order. Estimates of hydraulic conductivity for slopes and water tracks are 3.9 and 3.8 m/d accordingly.

During the observation period (August 1<sup>st</sup> to 11<sup>th</sup>, 2018) the air temperature increased in the absence of precipitation. Water level measured in the water track consistently increased during this period that can be explained by seasonal thawing of ice rich sediments (Figure 2.23.3). Water level in the receiving creek (watershed area 1.41 km<sup>2</sup>) also rose, but at a lower rate. Water level in the creek with a watershed area of 2.07 km<sup>2</sup> was stable. The water temperature at all gauges had a pronounced diurnal variation with amplitude of up to 3 °C and changed from 1.85 °C at the water track to 6.4 °C at the middle and 4.9 °C at the lower gauging stations. The decrease of the water temperature at the pebbly channel could be explained by local percolation of water through cold gravel sediments upstream the gauging station.

Water level at the water track showed diurnal variation with maximum during the night and minimum in a day time opposite to the diurnal cycle of air temperature. It could be explained by evaporation from the water track and nearby. Water level in the creek that receives a number of water tracks does not have such pronounced diurnal variation that suggests influence of other water sources apart from the water tracks.

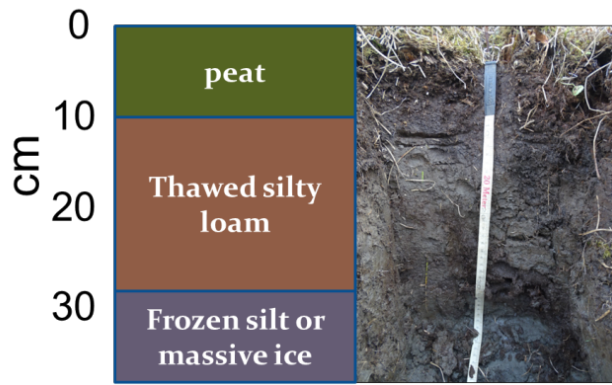


Figure 2.23.2: Typical soil profile

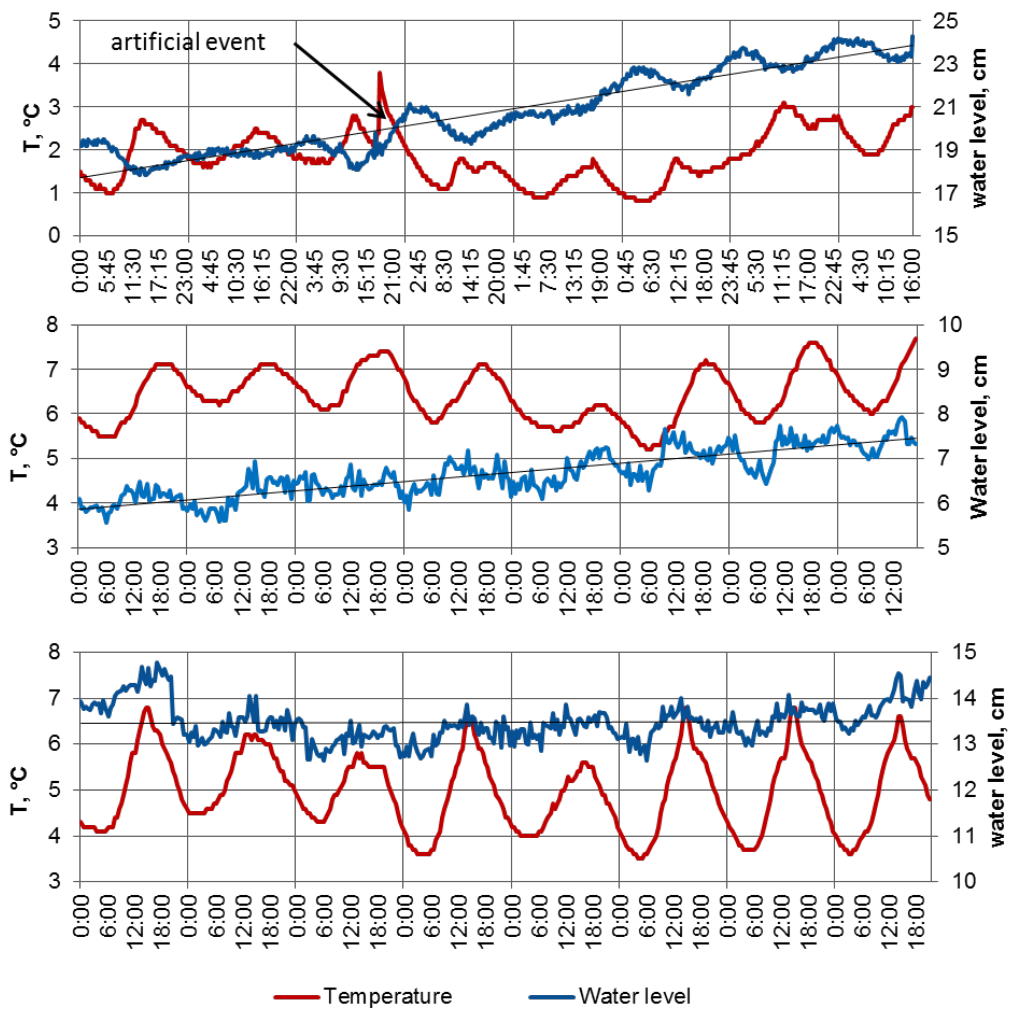


Figure 2.23.3: Water level and temperature at upper (graph on the top), middle (in the middle) and lower (graph at the bottom) gauges with half an hour temporal resolution, August 2<sup>nd</sup> to 9<sup>th</sup>, 2018



## 2.24 New geological, paleontological, and paleobotanical data from natural sections of Paleozoic, Mesozoic and Cenozoic sedimentary formations on Lena River main channel and Olenekskaya, Trofimovskaya and Bykovskaya channels, banks and islands

*Taras Gonta*<sup>1</sup>, *Andrey Kartoziia*<sup>1,2,4</sup>, *Raliya Khabibulina*<sup>1</sup>, *Leonid Khazin*<sup>1</sup>, *Irina Khazina*<sup>1</sup>, (*Igor Kosenko*<sup>1,4</sup>: not in the field), *Olga Kuzmina*<sup>1</sup>, *Nikolay Lashchinskiy*<sup>3</sup>, *Egor Metelkin*<sup>4</sup>, *Nikolay Sennikov*<sup>1</sup>, (*Olga Urman*<sup>1</sup>: not in the field)

<sup>1</sup> Trofimuk Institute for Petroleum Geology and Geophysics, Siberian Branch, Russian Academy of Sciences, Russian Federation

<sup>2</sup> V.S. Sobolev Institute of Geology and Mineralogy, Siberian Branch, Russian Academy of Sciences, Novosibirsk, Russian Federation

<sup>3</sup> Central Siberian Botanical Garden, Siberian Branch, Russian Academy of Sciences, Novosibirsk, Russian Federation

<sup>4</sup> Novosibirsk State University, Novosibirsk, Russian Federation

### 2.24.1 Paleozoic part

#### Fieldwork period and location

From August 26<sup>th</sup> to September 05<sup>th</sup>, 2018 (at Atyrdakh Formation)

#### Objectives

Comprehensive (paleontological, stratigraphic, sedimentological) study of the sections of the Atyrdakh Formation stratotype in order to reconstruct paleogeographic settings in the marginal part of the Siberian Craton in the Paleozoic.

- Detailed description of the section and its lithologic-sedimentological stratification
- Sampling of pebbles for micro- and macrofauna

#### Preliminary results

20 sections have been described including the stratotype section of Atyrdakh Formation.

More than 200 samples of carbonate pebbles have been sampled for micro- (ostracods, conodonts, radiolarians) and macrofauna (corals).

Drill samples have been found in the delta of the Lena River (on the peninsula Chai-Tumus).

### 2.24.2 Mesozoic part

#### Fieldwork period and location

From July 17<sup>th</sup> to August 13<sup>th</sup>, 2018 (on Cape Chekurovka and Chucha)

#### Objectives

Comprehensive study of Upper Jurassic – Lower Cretaceous marine deposits in the region of Chekurovka anticline (lower course of the Lena River, region of capes Chekurovka (N 70.96441°; E 127.51475°) and Chucha (N 70.79412°; E 127.61152°) (Figure 2.24.1).

- Redescription of Upper Jurassic (Volgian) – Lower Cretaceous (Ryazanian – Valanginian) sections on capes Chekurovka and Chucha.
- Sampling of macro- and microfauna, palynological samples and samples for organic geochemistry for clarification of regional stratigraphy and search of interregional stratigraphic markers.

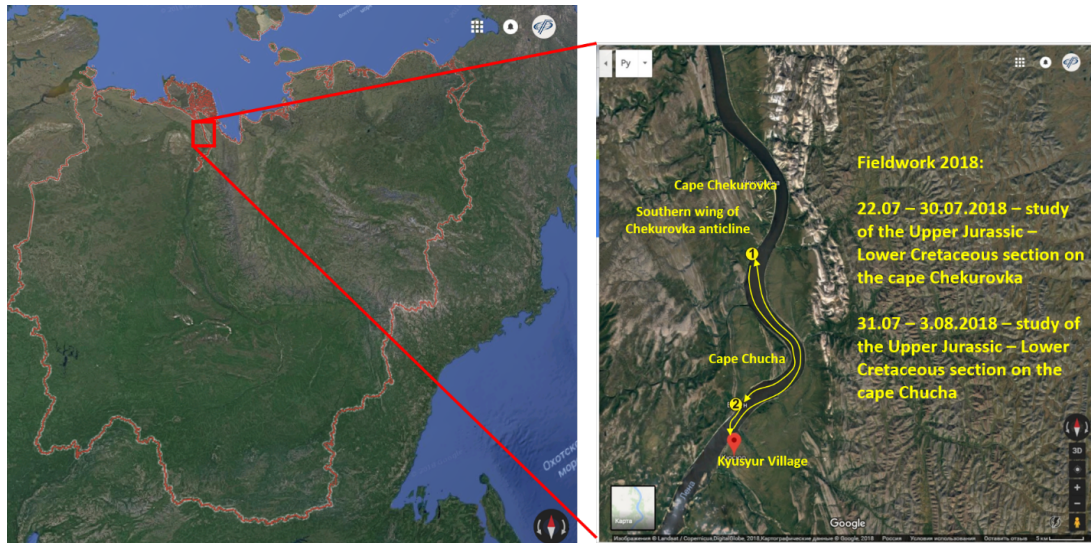


Figure 2.24.1: *Region of fieldworks*

### Methods

Both sections (Figures 2.24.2, 2.24.3, 2.24.4) have been described layer-by-layer. Sampling of macro- and microfossils, palynological samples and samples for geochemical analysis was carried out with an exact binding to the layers and lithological units. The most common macrofossils from studied sections represented by bivalves of the genus *Buchia* and ammonites. These fossils are very important for the stratigraphy of Upper Jurassic – Lower Cretaceous marine deposits. Special attention was paid to the study of Jurassic/Cretaceous boundary interval (Figure 2.24.2).



Figure 2.24.2: View on the Jurassic/Cretaceous boundary section on the cape Chekurovka



Figure 2.24.3: View on the Ryazanian part (units 33-34) of the Chekurovka section



Figure 2.24.4: View on the Upper Ryazanian part of the Chucha section

### Preliminary results

- The Upper Jurassic – Lower Cretaceous sections located on capes Chekurovka and Chucha has been described.
- Macro- and microfossils, samples for palynological and organic geochemical analysis have been collected.
- A total of 71 samples were taken for the macrofauna — mainly bivalves of the genus *Buchia* and ammonites; 31 samples were taken for the microfauna from the Chekurovka section, 30 samples from the Chucha section, the same number of samples were taken for the palynological analysis. 15 samples were transferred for geochemical analysis (Figure 2.24.5).



Figure 2.24.5: Field photos of some collected fossils from the sections Chekurovka and Chucha. Belemnite from the Ryazanian part of the Chucha section (A); ammonite from the Upper Ryazanian of the Chekurovka section (B); ammonites and bivalves *Bichia* from the Ryazanian part of the Chekurovka section (C); crinoids from the Upper Ryazanian of the Chekurovka section

### 2.24.3 Cenozoic part

#### Fieldwork period and location

From July 17<sup>th</sup> to August 25<sup>th</sup>, 2018 (on Sardakh Island)

#### Objectives

Multiproxy study of Cenozoic deposits of the Lena River Delta.

- Redescription of the section of the Neogene-Pleistocene Sardakh Formation on the Sardakh Island.
- Sampling of the I and III floodplain terraces on the Sardakh Island.

- Recent and subrecent microfauna and pollen samples collecting on the Kurungnakh, Sardakh and Samoylov Islands.
- Description of the section of the Paleogene deposits on the Bykovkaya channel.

### Methods

Sections were carefully cleaned to avoid contamination with allochthonous material. A detailed layer-by-layer description of the sediments was carried out, with the establishment of mineral-petrographic features, types of structures and textures, inclusions of organic residues. Sampling was carried out at certain intervals, depending on the thickness of the layers. The section of the I floodplain terrace on the Sardakh Island was sampled by continuous furrow method. Samples for modern microfauna were selected from various reservoirs on Samoylov Island using a plankton sieve. Samples for modern pollen were collected on the established grid on the islands of Sardakh, Samoylov and Kurungnakh with an attempt to cover all possible plant microhabitats.

### Preliminary results

- A section of Neogene-Pleistocene deposits on the Sardakh Island is described (N 72.57612°, E 127.191624°). At the base of the section, imprints of well-preserved broadleaf flora were found, their taxonomic identification was made. Palynology and microfauna samples were taken.
- The sections I and III of the floodplain terraces of the Lena River on the Sardakh Island are described. Palynology and microfauna samples were taken.
- A large number of recent and subrecent samples of flora and microfauna from the islands of Sardakh, Kurungnakh, Samoylov, and the coast of the Bykovskaya channel were selected.
- A section of Paleogene sediments exposed in the Bykovskaya channel near Bulunkan Bay is described (N 72.21666°, E 127.966664°). Palynology and microfauna samples taken. Coal interlayers containing amber inclusions have been found at the base of the section.

### Botany data

#### *Sardakh*

#### **Fieldwork period and location**

From July 22<sup>th</sup> to July 25<sup>th</sup>, 2018 (on Sardakh Island)

#### **Objectives**

There is not any available information about Sardakh Island vegetation. Nobody made a geobotanical survey of the island. So the main task of this field trip was to collect data about vegetation of the island and information about interconnections between vegetation and relief features.

#### **Methods**

Before field trip the island structure was examined on high-resolution satellite images. Set of sample sites in all habitats visible on an image were preformed for the field work in order to describe maximal diversity.

In the field, three main trips were made: one around the island and two others crossed the island in two directions with approximately right angle between them.

Geobotanical descriptions were made by standard method on sample plots 10 to 10 m. On each plot all vascular plants were listed with their phenological phase and abundance. Among mosses and lichens only abundant species which could be easily determined in the field were registered. In addition few specimens were collected for the farther determination in lab.

### Preliminary results

It was made 47 geobotanical descriptions with 116 species of higher vascular plants and about 40 species of mosses and lichens.

The main part of the island is presented by a rounded outcrop about 2 km in diameter elevated above river level by 20 to 25 m with steep cliffs. Its upper surface is flat and slightly concave to the center. In the central part there are two lakes and a big depression from former lake. Along the shoreline of the lakes aquatic vegetation with *Arctophila fulva* and *Eriophorum polystachyon* was described. The big depression in the central part of the island is covered by sedge mires with dense layer of green or *Sphagnum* mosses. The main vegetation on the rest of upper surface consists of polygonal complex of sedge mires and wet sedge tundra with dense moss layer. Near the edge of the upper surface a strip of about 300 to 500 m width occupied by zonal vegetation type – tussock tundra with *Eriophorum vaginatum*. This stripe dissected by narrow galleys with *Eriophorum polystachyon*-communities at the bottom and *Cassiope*-tundra on slopes. From the north and east sides outcrop contacted with small areas of the first terrace and floodplain. At the galley mouth on the floodplain surface quite often baidjarachs could be found with species-rich grasslands on their surface. Willow thickets and horsetail communities were described on the floodplain. First terrace was not investigated.

Collected data set is enough for the general characteristics of the vegetation on the upper surface of the outcrop. For the vegetation description of the whole island it is important to collect additional data from the first terrace, from cliffs and a bit more data for some vegetation types.

*Samoylov*

### Fieldwork period and location

From July 26<sup>th</sup> to August 14<sup>th</sup>, 2018 (on Samoylov Island)

### Objectives

The field work on Samoylov Island was a continuation of the botanical research started in 2017. The main task was to collect geobotanical information for the vegetation map based on detailed UAV image.

### Methods

Preliminary analysis of the data collected at 2017 allowed to determine parts of the island not visited last year and community types with insufficient data. Based on these information field trips were planned for the summer 2018 on the floodplain and on the first terrace at the eastern part of the island. Geobotanical descriptions were made by standard method on sample plots 10 to 10 m. Some questionable specimens of vascular plants and mosses were collected for further determination in lab.

### Preliminary results

It was made 47 standard geobotanical descriptions.

Based on field data preliminary legend for the vegetation map was created. Each legend element has characteristics of habitats, species composition and physiognomic features. For the most of legend elements specific colors or textures were determined on the UAV image. The whole legend consists of elements without any vegetation (sand beach and water bodies); elements of the anthropogenic infrastructure (buildings and roads) and different vegetation types. Among the latter, there are few types of pioneer vegetation, water vegetation, willow thickets, tundra and mires. In some cases especially for the water vegetation one element includes few community types because it was not possible to distinguish these types on the image.

The whole island flora consists of 143 vascular plant species which belong to 83 genera and 34 families. Ten leading families in terms of species richness include 100 species (70% of whole flora). 19 families presented by one or two species. The richest genera are: *Salix* (11 species), *Pedicularis* (9), *Carex* and *Saxifraga* (7 species each).

Vegetation structure strictly depends on relief position. According to main geomorphological surfaces two succession systems could be described. First one for the floodplain is one-way exogenous succession started

with pioneer vegetation just behind fresh sand bar on the river bank. Second succession system developed on the first terrace. It is reversible exogenous succession connected with polygonal structures and their development and degradation.



## 2.25 Paleomagnetic studies of Late Devonian volcanogenic and Early Carboniferous sedimentary complexes

*Nikolay Mikhailtsov*<sup>1,2</sup>, *Denis Avdeev*<sup>1,2</sup>

<sup>1</sup> Trofimuk Institute for Petroleum Geology and Geophysics, Siberian Branch, Russian Academy of Sciences, Russian Federation

<sup>2</sup> Novosibirsk State University, Novosibirsk, Russian Federation

### Fieldwork period and location

From August 04<sup>th</sup> to August 15<sup>th</sup>, 2018 (on America-Khay mountain (Kurungnakh Island) and on the right bank of the main course of the Lena River)

### Objectives

Paleomagnetic data provide paleotectonic and paleogeographic reconstructions with a quantitative information. Principal thing is availability of time-continuous bank of solid paleomagnetic determinations for large crustal blocks. The main goal of paleomagnetic research in the Lena Delta is to cover "gap" in paleomagnetic data for Siberian Platform nearby Devonian and Early Carboniferous time.

Tasks to the field work in 2018:

- additional study and additional paleomagnetic sampling of the volcanogenic-sedimentary section of the America-Khaya mountain (Upper Devonian), where previously good preliminary results were obtained;
- study with paleomagnetic sampling of the Bastakh formation (Early Carboniferous) on the right bank of the main course of the Lena River;
- pilot sampling of new objects and previously unstudied stratigraphic levels in the area in order to determine suitability for paleomagnetic study in subsequent field seasons.

### Methods

Methods used:

1. Visual observation and lithological description of the geological section.
2. Detailed (layer-to-layer) sampling of rocks for biostratigraphic analysis and for isotope-geochemical studies.
3. Sampling of oriented samples for paleomagnetic study.

The most common type of paleomagnetic sampling is using a gasoline-powered portable drilling apparatus with a water-cooled diamond bit. The diameter of cores is usually approximately 2.5 cm. After coring of the outcrop to a depth of 5 to 12 cm, an orientation stage is slipped over the sample while it is still attached to the outcrop at its base. Orientation stages have an inclinometer for determining inclination (dip) of the core axis and magnetic or sun compass (or both) for determining azimuth of core axis. The accuracy of orientation by such methods is about  $\pm 2^\circ$ . After orientation, the core is broken from the outcrop, marked for orientation and identification, and returned to the laboratory.

**Preliminary results**

1. The volcanic-sedimentary section of Mount America-Khaya has been studied in detail. It was established that there are three series of basalt flows in the section, slightly differing in morphology. The lower series lies directly on the most ancient levels of the late Devonian in the study area — a red-colored carbonate-sandy stratum of Frasnian age with an apparent thickness of about 50 m. All three series of basalts were sampled for paleomagnetic analysis and for petrological and geochemical studies. Detailed sampling was also carried out in the zone of exocontact basalts with underlying limestones and red sandstones.
2. A detailed layer-by-layer sampling for paleomagnetic studies in the stratotype section of the Bastakh Formation (Early Carboniferous) in outcrops on the right bank of the main course of the Lena River was performed. Four stratotypical levels were studied, as well as the previously unstudied lowermost levels, exposed at low water level in the river. Sampling of a penetrating doleritic dyke (presumably of Triassic age) and the zone of its exocontact was also performed.
3. Pilot testing of Early Permian rocks exposed upstream of Bastakh limestones was performed in order to determine their suitability for paleomagnetic study.

In total, 10 field routes were completed. Overall 225 oriented and non-oriented samples were taken for complex investigations.

## 2.26 Investigations into coupled coastal lagoon and beach-ridge systems in Buor Khaya Bay, southern Laptev Sea

Lasse Sander<sup>1</sup>, Ivan Khristoforov<sup>2</sup>, Kencheeri Danilov<sup>2</sup>, Olga Bolshiyanova<sup>3</sup>, Rune Michaelis<sup>1</sup>, Sergev Pravkin<sup>3,5</sup>, Svenja Papenmeier<sup>1,4</sup>

<sup>1</sup> Alfred Wegener Institute Helmholtz Centre for Polar and Marine Research, List/Sylt, Germany

<sup>2</sup> Melnikov Permafrost Institute, Siberian Branch, Russian Academy of Sciences, Yakutsk, Russian Federation

<sup>3</sup> Arctic and Antarctic Research Institute, St. Petersburg, Russian Federation

<sup>4</sup> Leibnitz Institute for Baltic Sea Research, Warnemünde, Germany

<sup>5</sup> St. Petersburg State University, St. Petersburg, Russian Federation

### Fieldwork period and location

From August 3<sup>rd</sup> to August 16<sup>th</sup>, 2018 (on Buor Khaya Bay, southern Laptev Sea)

### Objectives

Coupled coastal lagoon and beach-ridge systems have been shown to be complementary paleoenvironmental archives for the reconstruction of past coastal changes driven by marine forcing, such as relative sea level and wave climate changes (e.g. Sander et al. 2016). These and other similar coastal landforms are relatively abundant in the Siberian arctic and their potential is currently largely underused. In order to establish the value of the approach in the regional setting of the Laptev Sea, several potential field sites were visited during the LENA 2017 expedition (Sander et al. 2018). The focus of the expedition in 2018 has been (i) the collection of material for the establishment of age control on the prograded sequence of paleoshorelines (beach ridges), (ii) the collection of additional elevation data, and (iii) the survey of surface and subsurface characteristics of the coastal lagoons for two of the most promising sites (Figure 2.26.1). The aim of the study was to obtain robust information of the Holocene coastal evolution and relative sea level history of Buor Khaya Bay.

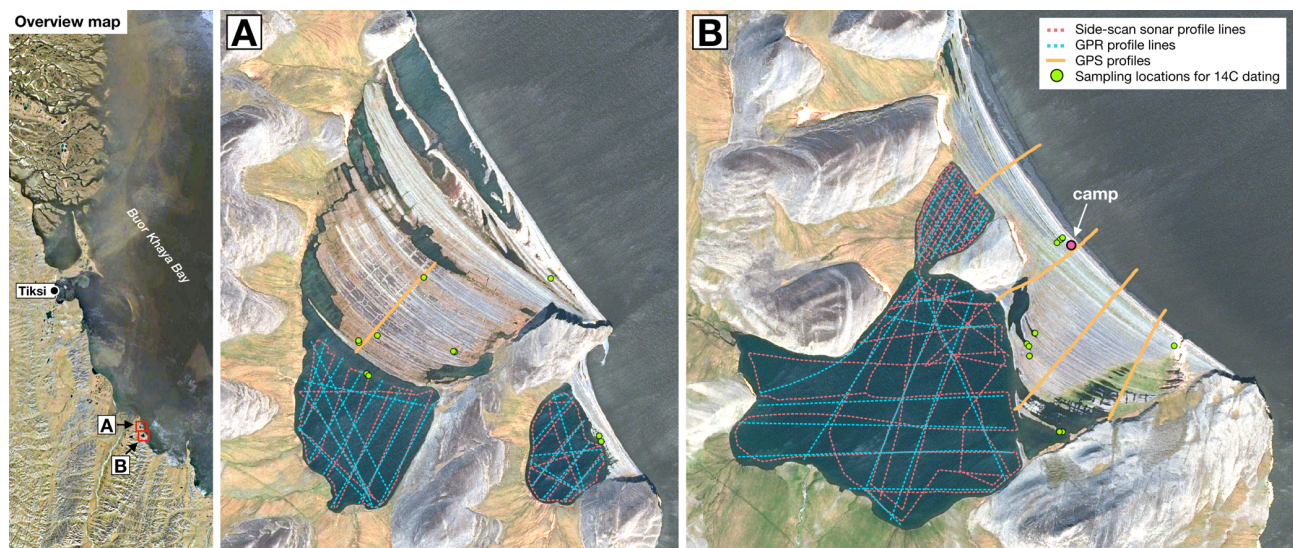


Figure 2.26.1: Overview map of the location of the studied field sites in Buor Khaya Bay (left); A: Northern beach ridge/lagoon system (Gavril-Kyuyele) and an additional small lagoon (Syrdyk-Kyuyel) (center); B: Southern beach ridge/lagoon system (Makhchar) with the location of the camp (right)

## Methods

Structured field observations on geomorphology, frost features, vegetation and grain-size distribution were conducted on the subaerial parts of the beach-ridge systems. GPS elevations were obtained along several cross-ridge transects. In order to construct a robust chronology for the formation of the systems, >50 wood samples were taken for radiocarbon dating and dendrochronological analysis. Ground penetrating radar (GPR) and side-scan sonar (SSS) surveys of three coastal lagoons were conducted from a rubber dinghy equipped with an outboard motor. High-frequency SSS data were collected using a laterally mounted Tristar Starfish 990F (Fig. 2.26.2C), with the objective to obtain information on the reflective properties of the surface of the lagoon floor. Ground truth was obtained using a simple underwater camera setup, based on a waterproof action camera and a diving torch (Figure 2.26.2E). GPR unshielded dipole antennas (50 and 100 MHz) served to obtain information about the bottom sediments by changing the amplitude and phase of the electromagnetic signal reflected from the boundary of the bottom contour. Development of methodical features of the application of the GPR method allowed to effectively use it for the study of the lagoon water bodies (Khristoforov and Omelyanenko 2018). The antennas were waterproofed and towed behind the dinghy (Figure 2.26.2A). The GPR data were processed using GeoScan32 software. With both methods combined, profile lines with a total length of >140 km were recorded.

## Preliminary results

Good GPR results were obtained for two of the lagoons and it was possible to identify bottom sediment and subsurface structures. An example of a GPR profile is shown in Figure 2.26.2B. The bottom water in the smallest lagoon (Syrdyk-Kyuyel) was too saline and it was therefore only possible to obtain data to a depth of c. 6 m. With water depths of >20 m, the lagoons are relatively deep in comparison of the open waters of Buor Khaya Bay (mostly <15 m). The lagoon floor is composed of bedrock, fine-grained sediment, and areas of coarse clastic deposition from either the direct weathering of bedrocks (regolith) or the local redeposition of weathered material by wave processes (Figure 2.26.2B). The fine-grained sedimentary infill on the lagoon floor is thin and appears to be partly mobile, suggesting a closure and separation of the lagoon environment from marine conditions by barrier formation rapidly after the stabilization of mean sea level around 6 kyr ago. Patterned frost features (polygons) were observed in shallow water at depths of up to c. 2 m below the current water level of the lagoons. Almost all GPR profiles show well-defined boundaries at an average depth of 7 m (see red line in Figure 2.26.2B). This boundary is sometimes divided into 2-3 boundaries at different depths. The average value of the amplitude of this boundary exceeds 3-4 times the noise level of electromagnetic waves in the water. This is probably due to a relatively sharp change in physical parameters, in particular water temperature and/or its mineralization. It is also possible that this is a halocline.

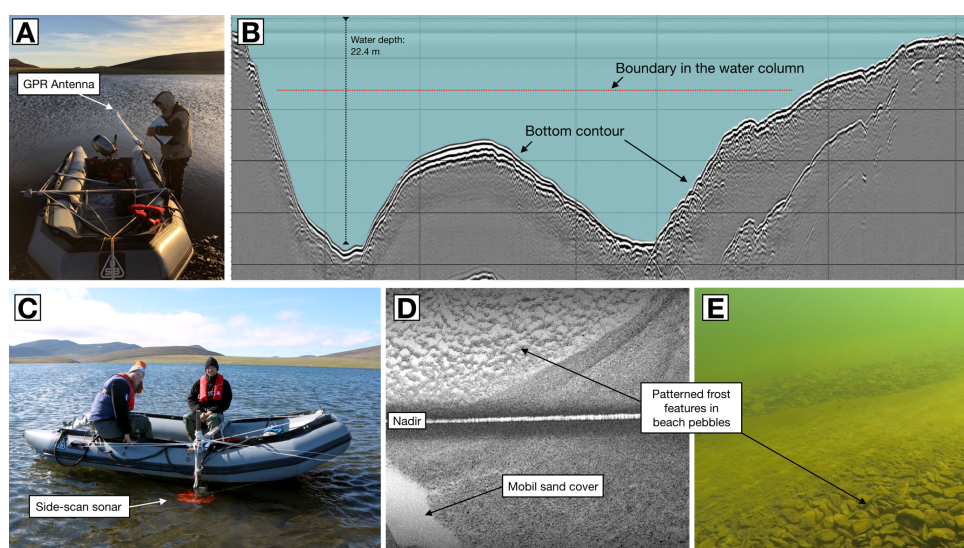


Figure 2.26.2: A - Setup of the GPR antenna, B - Example of the GPR data from the lagoon, C - Setup of the side-scan sonar, D - Example of sonar data from the lagoon floor, E - Example of underwater video data

## 2.27 Botanical survey of vascular plants in the southern Buor Khaya Bay

Olga Bolshiyanova <sup>1</sup>

<sup>1</sup> Arctic and Antarctic Research Institute, St. Petersburg, Russian Federation

### Fieldwork period and location

From August 3<sup>rd</sup> to August 16<sup>th</sup>, 2018 (on Buor Khaya Bay, southern Laptev Sea)

### Objectives

Systematic collection and description of tundra vegetation species.

### Methods

1. Plant collection
2. Drying in a herbarium press
3. Plant species identification
4. Creation of the herbarium

### Preliminary results

Vascular plants from a coastal setting in southern Buor Khaya Bay were collected and identified (Figure 2.27.1, 2.26). The collection of samples was conducted in the month of August during the blooming period in the tundra (Figure 2.27.2). The plants were collected, dried in a special herbarium press and identified. During the survey a few interesting species like *Coeloglossum viride* (L.) C. Hartm. (Figure 2.27.3) were found, a species which belongs to Orchidaceae family and included in Red List of Russia (Russian Red Book). Now the herbarium is in the collection of the Arctic and Antarctic Research Institute.

### Species List

*Aconogonon ochreatum* (L.) Hara  
*Arctous alpina* (L.) Nied.  
*Artemisia borealis* Pall.  
*Artemisia tilesii* Ledeb.  
*Astragalus alpinus* L. subsp. *arcticus* (Bunge) Hult.  
*Betula exilis* Sukaczew  
*Bistorta plumosa* (Small) D. Love  
*Bistorta vivipara* (L.) Gray  
*Caltha arctica* R. Br.  
*Cassiope tetragona* (L.) D. Don  
*Cerastium arcticum* Lange  
*Chamerion latifolium* (L.) Holub.  
*Chrysosplenium sibiricum* (Ser.) Charkev.  
*Claytonia joanneana* Schult.  
*Claytonia acutifolia* Pall. ex Schult.  
*Coeloglossum viride* (L.) C. Hartm.  
*Crepis chrysantha* (Ledeb.) Turcz.  
*Saxifraga cernua* L.  
*Diapensia obovata* (Fr. Schmidt) Nakai  
*Dryas punctata* Juz.  
*Empetrum nigrum* L.

*Eryophorum scheuchzeri* Hoop.  
*Gentiana algida* Pallas.  
*Lagotis minor* (Willd.) Standl.  
*Ledum palustre* L.  
*Minuartia arctica* (Stev. ex Ser.) Graebn.  
*Oxyria digyna* (L.) Hill.  
*Oxytropis nigrescens* (Pall.) Fisch.  
*Papaver lapponicum* (Tolm.) Nordh.  
*Pedicularis albolabiata* (Hult.) Ju. Kozhev.  
*Polemonium boreale* Adams  
*Rhodiola rosea* L. s. l.  
*Rubus chamaemorus* L.  
*Salix nummularia* Andress.  
*Sanguisorba officinalis* L.  
*Saussurea tilesii* Ledeb.  
*Saxifraga hirculus* L.  
*Saxifraga nelsoniana* D. Don  
*Saxifraga spinulosa* Adams  
*Silene stenophylla* Ledeb.  
*Vaccinium uliginosum* L.  
*Vaccinium vitis-idaea* L. ssp. *minus* (Lodd.) Worosch  
*Valeriana capitata* Pall. ex Link



Figure 2.27.1: View of the studied field site in Buor Khaya Bay



Figure 2.27.2: *Arctous alpina* (L.) Nied.



Figure 2.27.3: *Coeloglossum viride* (L.) C. Hartm.

## Bibliography

- Are F and Reimnitz E (2000) An Overview of the Lena River Delta Setting: Geology, Tectonics, Geomorphology, and Hydrology. *Journal of Coastal Research* 16:1083–1093.
- Avetisov GP (1999) Geodynamics of the zone of continental continuation of Mid-Arctic earthquakes belt (Laptev Sea). *Physics of the Earth and Planet Interior* 114:59–70. [https://doi.org/10.1016/S0031-9201\(99\)00046-1](https://doi.org/10.1016/S0031-9201(99)00046-1).
- Barr S and Lüdecke Cs (2010) *The History of the International Polar Years (IPYs)*. Springer.
- Bartelt P and Lehning M (2002) A physical SNOWPACK model for the Swiss avalanche warning: Part I numerical model. *Cold Regions Science and Technology* 35:123–145. [https://doi.org/10.1016/S0165-232X\(02\)00074-5](https://doi.org/10.1016/S0165-232X(02)00074-5).
- Bird P (2003) An updated digital model of the plate boundaries. *Geochemistry, geophysics, Geosystems* 4:1027. <https://doi.org/10.1029/2001GC000252>.
- Boike J, Kattenstroth B, Abramova K, Bornemann N, Chetverova A, Fedorova I, Fröb K, Grigoriev M, Grüber M, Kutzbach L, Langer M, Minke M, Muster S, Piel K, Pfeiffer E-M, Stoof G, Westermann S, Wischniewski K, Wille C, and Hubberten H-W (2013) Baseline characteristics of climate, permafrost and land cover from a new permafrost observatory in the Lena River Delta, Siberia (1998-2011). *Biogeosciences* 10:2105–2128. <https://doi.org/10.5194/bg-10-2105-2013>.
- Boike J, Nitzbon J, Anders K, Grigoriev M, Bolshiyarov D, Lander M, Lange S, Bornemann N, Morgenstern A, Schreiber P, Wille C, Chadburn S, Gouttevin L, Burke E, and Kutzbach L (2019) A 16-year record (2002–2017) of permafrost, active-layer, and meteorological conditions at the Samoylov Island Arctic permafrost research site, Lena River delta, northern Siberia: an opportunity to validate remote-sensing data and land surface, snow, and permafrost models. *Earth System Science Data* 11:261–299. <https://doi.org/10.5194/essd-11-261-2019>.
- Boike J, Wille C, and Abzinova A (2008) Climatology and summer energy and water balance of polygonal tundra in the Lena River Delta, Siberia. *Journal of Geophysical Research: Biogeosciences* 113. <https://doi.org/10.1029/2007JG000540>.
- Bonne J-L, Meyer H, and Hoffmann K (2018) *Russian-German Cooperation: Expeditions to Siberia in 2017*. Ed. by J Strauss, J Boike, DY Bolshiyarov, MN Grigoriev, H El.Hajj, A Morgenstern, PP Overduin, and A Udke. *Berichte zur Polar- und Meeresforschung = Reports on polar, marine research*, Bremerhaven, Alfred Wegener Institute for Polar, and Marine Research. Chap. ISOARC: Maintenance of the in situ water vapour isotopic analyser on Samoylov Island:296. [https://doi.org/10.2312/BzPM\\_0725\\_2018](https://doi.org/10.2312/BzPM_0725_2018).
- Camill P (2005) Permafrost Thaw Accelerates in the Boreal Peatlands During Late-20th Century Climate Warming. *Climate Change* 68:135–152. <https://doi.org/10.1007/s10584-005-4785-y>.
- Chen J, Günther F, Grosse G, Liu L, and Lin H (2018) Sentinel-1 InSAR Measurements of elevation changes over Yedoma uplands on Sobo-Sise Island, Lena Delta. *Remote Sensing* 10:1152. <https://doi.org/10.3390/rs10071152>.
- CrestoAleina F, Brovkin V, Muster S, Boike J, Kutzbach L, Sachs T, and Zuyev S (2013) A stochastic model for the polygonal tundra based on Poison-Voronoi diagrams. *Earth System Dynamics* 4:187–198. <https://doi.org/10.5194/esd-4-187-2013>.
- DaSilva AC, Whalen MT, Hladil J, Shadimova L, Chen D, Spassov S, Boulvain F, and Devleeschouwer X (2015) Magnetic susceptibility application: a window onto ancient environments and climatic variations: foreword. *Geological Society, London, Special Publications* 414. <https://doi.org/10.1144/SP414.12>.
- Fedorova I, Chetverova A, Bolshiyarov D, Makarov A, Boike J, Heim B, A Morgenstern., Overduin PP, Wegner C, Kashina V, Eulenburg A, Dobrotina E, and Sidorina I (2015) Lena Delta hydrology and geochemistry: Long-term hydrological data and recent field observations. *Biogeosciences* 12:345–363. <https://doi.org/10.5194/bg-12-345-2015>.



- Franke D, Krüger F, and Klinge K (2000) Tectonics of the Laptev Sea - Moma 'Rift' Region: investigation with Seismologic Broadband Data. *Journal of Seismology* 4. <https://doi.org/10.1023/A:1009866032111>.
- Freeman C, Evans CD, Montheith DT, Reynolds B, and Fenner N (2001) Export of organic carbon from peat soils. *Nature* 412:785–785. <https://doi.org/10.1038/35090628>.
- Frensh H and Shur Y (2010) The principle of cryostratigraphy. *Earth-Science Review* 101:190–206. <https://doi.org/10.1016/j.earscirev.2010.04.002>.
- Frey KA and Smith LC (2005) Amplified carbon release from vast West Siberian peatlands by 2100. *Geophysical Research Letters* 32. <https://doi.org/10.1029/2004GL022025>.
- Fuchs M, Grosse G, Strauss J, Günther F, Grigoriev MN, Maximov GM, and Hugelius G (2018) Carbon and nitrogen pools in thermokarst-affected permafrost landscapes in Arctic Siberia. *Biogeosciences* 15:953–971. <https://doi.org/10.5194/bg-15-953-2018>.
- Fujita KB, Kozmin BM, Mackey KG, Riegel SA, McLean MS, and Imeav VS (2009) Seismotectonics of the Chersky Seismic Belt, eastern Sakha Republic (Yakutia) and Magadan District. *Stephan Mueller Special Publication Series* 4:117–145. <https://doi.org/10.5194/smsps-4-117-2009>.
- Gaina C, Roest WR, and Müller RD (2002) Late Cretaceous-Cenozoic deformation of northeast Asia. *Earth Planet Science Letters* 197:273–286. [https://doi.org/10.1016/S0012-821X\(02\)00499-5](https://doi.org/10.1016/S0012-821X(02)00499-5).
- Geissler WH, Shibaev S, Haberland C, Petrunin S, Krueger F, Presypkin D, Vollmer D, Gukov S, Tuktarov R, and Baranov B (2017) Russian-German Cooperation: Expeditions to Siberia in 2016. Ed. by PP Overduin, F Blender, DY Bolshiyarov, MN Grigoriev, A Morgenstern, and H Meyer. Vol. 709. *Berichte zur Polar- und Meeresforschung*. Chap. Seismicity of the Laptev Sea Rift:103–107. [https://doi.org/10.2312/BzPM\\_0709\\_2017](https://doi.org/10.2312/BzPM_0709_2017).
- Gooseff M, Barrett J, and J Levy (2013) Shallow groundwater systems in a polar desert, MyMurde Dry Valleys, Antarctica. *Hydrogeological Journal* 21:171–183. <https://doi.org/10.1007/s10040-012-0926-3>.
- Guenther F, Grosse G, Maksimov G, Veremeeva A, Frincke A, Haghshenas HaghghiM, and Kizyakov A (2018) Repeat LiDAR for tracking extensive thaw subsidence on Yedomia uplands. *20 Years of LENA Expeditions:22–24*. URL: <http://hdl.handle.net/10013/epic.51566>.
- Hagedoorn JG (1959) The plus-minus method of interpreting seismic refraction sections. *Geophysical prospecting* 7:158–182. <https://doi.org/10.1111/j.1365-2478.1959.tb01460.x>.
- Hubberten H-W, Wagner D, Pfeiffer E-M, Boike J, and Gukov AY (2006) The Russian-German Research Station Samoylov, Lena Delta - A Key Site for Polar Research in the Siberian Arctic. *Alfred Wegener Institute for Polar and Marine Research & German Society of Polar Research, Bremerhaven*. URL: <http://hdl.handle.net/10013/epic.29916>.
- Jemsek JP, Bergman EA, Nabelek JL, and Solomon SC (1986) Focal depth and mechanisms of large earthquakes on the Arctic Mid-Ocean Ridge System. *Journal of Geophysical Research* 91:13993–14005. <https://doi.org/10.1029/JB091iB14p13993>.
- Khristoforov II and Omelyanenko AV (2018) Improving the Efficiency of Hydrological Investigations by Submersible Ground Penetrating Radar. *IEEE Geoscience and Remote Sensing Letters* 15:335–339. <https://doi.org/10.1109/LGRS.2017.2786858>.
- Knoblauch C, Spott O, Evgrafova S, Kutzbach L, and Pfeiffer E-M (2015) Regulation of methane production, oxidation and emission by vascular plants and bryophytes in ponds of the northeast Siberian polygonal tundra. *Journal of Geophysical Research: Biogeosciences* 120:2525–2541. <https://doi.org/10.1002/2015JG003053>.
- Konstantinov AS (1986) *Obshchaya gidrobiologiya: Uchebnoe posobie dlya studentov spets. vuz., Rossiya*:472.
- Kovachev SA, Kuzin IP, and Soloviev SL (1994 (eng. 1995)) Short-term study of microseismicity in the Guba Bourkhaya Laptev Sea, using ocean bottom Seismographs. *Physics of the Solid Earth* 30:647–658.
- Kutzbach L, Wagner D, and Pfeiffer E-M (2004) Effect of microrelief and vegetation on methane emissions from wet polygonal tundra, Lena Delta, Northern Siberia. *Biogeochemistry* 69. <https://doi.org/10.1023/B:BI0G.0000031053.81520.db>.
- Lal R (2016) *Encyclopedia of Soil Science, Third Edition*. Boca Raton: CRC Press:2804. ISBN: 9781498738903.
- Langer M, Westermann S, Heikenfeld M, Dorn W, and Boike J (2013) Satellite-based modeling of permafrost temperatures in a tundra lowland landscape. *Remote Sensing of Environment* 135:12–24. <https://doi.org/10.1016/j.rse.2013.03.011>.

- McNamara J, Kane D, and Hinzman L (1998) An analysis of streamflow hydrology in the Kuparuk River Basin, Arctic Alaska: a nested watershed approach. *Journal of Hydrology* 206:39–57. [https://doi.org/10.1016/S0022-1694\(98\)00083-3](https://doi.org/10.1016/S0022-1694(98)00083-3).
- Meyer H, Opel T, Laepple T, Dereviagin A, Hoffmann K, and Werner M (2015) Long-term winter warming trend in the Siberian Arctic during the mid- to late Holocene. *Nature Geoscience* 8:122–125. <https://doi.org/10.1038/NGEO2349>.
- Morgenstern A, Grosse G, Günther F, Fedorova I, and Schirrmeister L (2011) Spatial analyses of thermokarst lakes and basins in Yedoma landscapes of the Lena Delta. *The Cryosphere Discussions* 5:1495–1545. <https://doi.org/10.5194/tc-5-849-2011>.
- Nitze I and Grosse G (2016) Detection of landscape dynamics in the Arctic Lena Delta with temporally dense Landsat time-series stacks. *Remote Sensing of Environment* 181:27–41. <https://doi.org/10.1016/j.rse.2016.03.038>.
- Romanovskii NN and Hubberten H-W (2001) Results of permafrost modelling of the lowlands and shelf of the Laptev Sea region, Russia. *Permafrost and Periglacial Processes* 12:191–202. <https://doi.org/10.1002/ppp.387>.
- Sander L, Hede MU, Fruergaard M, Nielsen L, Clemmensen LB, Kroon A, Johannessen PN, Nielsen LH, and Pejrup M (2016) Coastal lagoons and beach ridges as complementary sedimentary archives for the reconstruction of Holocene relative sea-level changes. *Terra Nova* 28:43–49. <https://doi.org/10.1111/ter.12187>.
- Sander L, Michaelis R, Papenmeier S, Pravkin S, and Wiltshire KH (2018) Characteristics of wave-built sedimentary archives in Bour Khaya Bay. *Reports on polar and marine research, Bremerhaven, Alfred Wegener Institute for Polar and Marine Research* 725:108–110.
- Schirrmeister L, Grosse G, Schwamborn G, Andreev AA, and Meyer H (2003) Late Quaternary history of the accumulation plain North of the Chekanovsky Ridge (Lena Delta, Russia): A multidisciplinary approach. *Polar Geography* 27:277–319. URL: <http://hdl.handle.net/10013/epic.19953>.
- Schwamborn G, Rachold V, and Grigoriev MN (2002) Late Quaternary sedimentation history of the Lena Delta. *Quaternary International* 89:119–134. [https://doi.org/10.1016/S1040-6182\(01\)00084-2](https://doi.org/10.1016/S1040-6182(01)00084-2).
- Shannon C (1949) *The Mathematical Theory of Communication*. Urbana.
- Shiklomanov AI, Holmes RM, McClelland JW, Tank SE, and Spencer RGM (2018) Arctic Great Rivers Observatory. Discharge Dataset, Version 2018-12-01. Arctic Rivers. URL: <https://www.arcticgreatrivers.org/data>.
- Siewert MB, Hugelius G, Heim B, and Faucherre S (2016) Landscape control and vertical variability of soil carbon storage in permafrost-affected soils of the Lena River Delta. *Catena* 147:725–741. <https://doi.org/10.1016/j.catena.2016.07.048>.
- Sládeček V (1973) System of water quality from biological point of view. *Arch. Hydrobiol. Ergebnisse der Limnologie* 7:218. <https://doi.org/10.1002/iroh.19740590412>.
- Sloan RA, Jackson JA, McKenzie D, and Priestley K (2011) Earthquake depth distributions in central Asia and their relations with lithosphere thickness, shortening and extension. *Geophysical Journal Interior* 185:1–29. <https://doi.org/10.1111/j.1365-246X.2010.04882.x>.
- Stedmon CA., Amon RMW, Rinehart AJ, and Walker SA (2011) The supply and characteristics of colored dissolved organic matter (CDOM) in the Arctic Ocean: Pan Arctic trends and differences. *Marine Chemistry* 124:108–118. <https://doi.org/10.1016/J.MARCHEM.2010.12.007>.
- Strauss J, Boike J, Bolshiyarov DY, Grigoriev MN, El.Hajj H, Morgenstern A, Overduin PP, and Udke A (2018) Russian-German Cooperation: Expeditions to Siberia in 2017. *Berichte zur Polar- und Meeresforschung = Reports on polar and marine research, Bremerhaven, Alfred Wegener Institute for Polar and Marine Research* 725. [https://doi.org/10.2312/BzPM\\_0725\\_2018](https://doi.org/10.2312/BzPM_0725_2018).
- Thibodeau B, Bauch D, Kassens H, and Timokhov LA (2014) Interannual variations in river water content and distribution over the Laptev Sea between 2007 and 2011: The Arctic Dipole connection. *Geophysical Research Letters* 41:7237–7244. <https://doi.org/10.1002/2014GL061814>.
- Ulrich M, Grosse G, Chabrillat S, and Schirrmeister L (2009) Spectral characterization of periglacial surfaces and geomorphological units in the Arctic Lena Delta using field spectrometry and remote sensing. *Remote Sensing of Environment* 113:1220–1235. <https://doi.org/10.1016/j.rse.2009.02.009>.

- Wagner D, Kobabe S, Pfeiffer E-M, and Hubberten H-W (2003) Microbial controls on methane fluxes from a polygonal tundra of the Lena Delta, Siberia. *Permafrost and Periglacial Processes* 14:173–185. <https://doi.org/10.1002/ppp.443>.
- Wang Y and Evans ME (1997) Paleomagnetism of Canadian Arctic permafrost; Quaternary magnetostratigraphy of the Mackenzie Delta. *Canadian Journal of Earth Science* 34:135–139. <https://doi.org/10.1139/e17-011>.
- Zelinka M (1961) Zur Präzisierung der biologischen Klassifikation der Reinheit fließender Gewässer. *Arch. Hydrobiol.* 57:71–81.
- Zubrzycki S, Kutzbach L, Grosse G, Desyatkin A, and Pfeiffer E-M (2013) Organic carbon and total nitrogen stocks in soils of the Lena River Delta. *Biogeosciences* 10:3507–3524. <https://doi.org/10.5194/bg-10-3507-2013>.

## Chapter 3

### **Expedition to Chukotka and Central Yakutia: Modern vegetation studies and lake sediment coring at the Tundra-Taiga-Transition zone in Chukotka and Yakutia**

Edited by: *Stefan Kruse, Boris Biskaborn, Luidmila Pestryakova, Ulrike Herzschuh*

### 3.1 Introduction

Stefan Kruse <sup>1</sup>, Boris Biskaborn <sup>1</sup>, Luidmila Pestryakova <sup>3</sup>, Ulrike Herzschuh <sup>1,2</sup>

<sup>1</sup> Alfred Wegener Institute Helmholtz Center for Polar and Marine Research, Potsdam, Germany

<sup>2</sup> University of Potsdam, Potsdam, Germany

<sup>3</sup> Federal State Autonomous Educational Institution of Higher Education "M.K. Ammosov North-Eastern Federal University", Yakutsk, Russian Federation

The distribution areal of the northern tundra is vulnerable to global warming that drives the transition to open taiga forests (ACIA 2005). Forests in comparison to tundra is characterized with a lower albedo, and the resulting positive feedback loop of vegetation change and warming might lead to dramatic environmental changes in the Arctic (Bonan 2008). However, the speed of this tundra-taiga-transition is unknown and models predict only very uncertain future scenarios. Palaeoinformation about vegetation trajectories from earlier warming phases and interglacials/glacial cycles can help to assess legacies from the past that have still an impact on the current changes. Combining these with modern information and modelling (e.g. Kruse et al. 2016; Kruse et al. 2019; Epp et al. 2018), we aim to predict future treeline migrations and changes of ecosystem services, such as the potential of forests to hamper climate warming by carbon sequestration.

Ecosystem services of boreal forests are of critical importance for humanity and differ markedly between evergreen and summergreen needle-leaf forests. This expedition is part of the framework of the ERC consolidator grant GlacialLegacy within the timely questions will be addressed "Why is northern Asia dominated by summergreen boreal forests?" and "How will these larch forests change in the future?" with a coherent empirical and modelling approach integrating pollen data synthesis, sedimentary ancient DNA analyses, vegetation & biophysical survey and vegetation modelling.

Documented changes in vegetation across the Siberian treeline ecotone can be considered as a proxy for related changing variables, such as temperature and lake-water chemistry (Herzschuh et al. 2013), which in turn can affect microbial aquatic vegetation (like algae) in the embedded lakes. In order to reconstruct past dynamics in terrestrial and aquatic vegetation and their relationships to catchment and lake dynamics, we sampled sediment cores (short and long cores) from glacial and thermokarst lakes across the treeline ecotone. We will utilize pollen and sedimentary ancient DNA (sedaDNA) as well as sedimentological analyses (XRF, XRD, TOC, C/N, grain-size) for tracking variations in past vegetation communities and limnological responses across Holocene and late Pleistocene time scales. The reconstruction of terrestrial vegetation with pollen analyses will recover regional changes in plant communities, whereas local signals of vegetation change will be investigated using sedaDNA (e.g. Niemeyer et al. 2017). X-ray fluorescence (XRF) analyses will allow the reconstruction of lake-catchment-vegetation dynamics based on measured elements which will be supported by X-ray diffractometry (XRD), organic and grain-size data. Reconstructions of aquatic communities will contribute to the understanding of lake environmental changes and related evolutionary imprints on environmentally sensitive algae, like diatoms.

During the summer expedition we focused on the tundra-taiga transition zone in northeastern Siberia (Chukotka) for tundra associations that are successively replaced by summergreen larches along a bioclimatic gradient (Figure 3.1.1). We extended this gradient in Yakutia to capture the southwestwardly replacement of summergreen larch-dominated forests by evergreen taxa (*Picea*, *Pinus*, *Abies*), and sites having different disturbance histories (wildfire, wind throw, land-use). At each site visited, we conducted vegetation surveys for each dominant vegetation type, and if trees were present we recorded full forest inventories (sampling adapted from Kruse and Stoof-Leichsenring 2016). Plant material was collected from tree individuals and soil surface vegetation plots for the analyses of dendrochronology (similar to Wiczorek et al. 2017), modern genetics and biomass. For three-dimensional reconstructions of vegetation structure images were taken with an unmanned aerial vehicle (UAV). The soils were characterized and temperature and humidity profiles measured at different layers and transition zones from top to the permafrost table in addition to soil samples that were taken. All samples were brought to Potsdam for further processing in our laboratories.

To understand how larch stands modify the local hydrological and thermal conditions and whether this protects permafrost from degradation, further understanding of the heat and water exchange between the atmosphere and the permafrost is needed. The installation of two microclimate stations and further soil temperature sensors, as well as the sampling and describing of the forest and soil types across a transect in northeastern Siberia will provide data to study and understand the heat and water transfer processes in larch dominated boreal forest areas. Temperature sensors were buried in the ground in order to monitor the thermal state of the active layer and permafrost. The measurement set-up allows the calculation of a full energy and water balance. Additionally, two climate stations were set up in Chukotka and Southern Yakutia to collect meteorological field data such as temperature, humidity, radiation and wind data for at least the duration of one year.

This work adds to the extensive databases of Arctic lake, vegetation plots, and individual-tree measurements across the treeline in northeastern Siberia and permafrost areas of Russia.

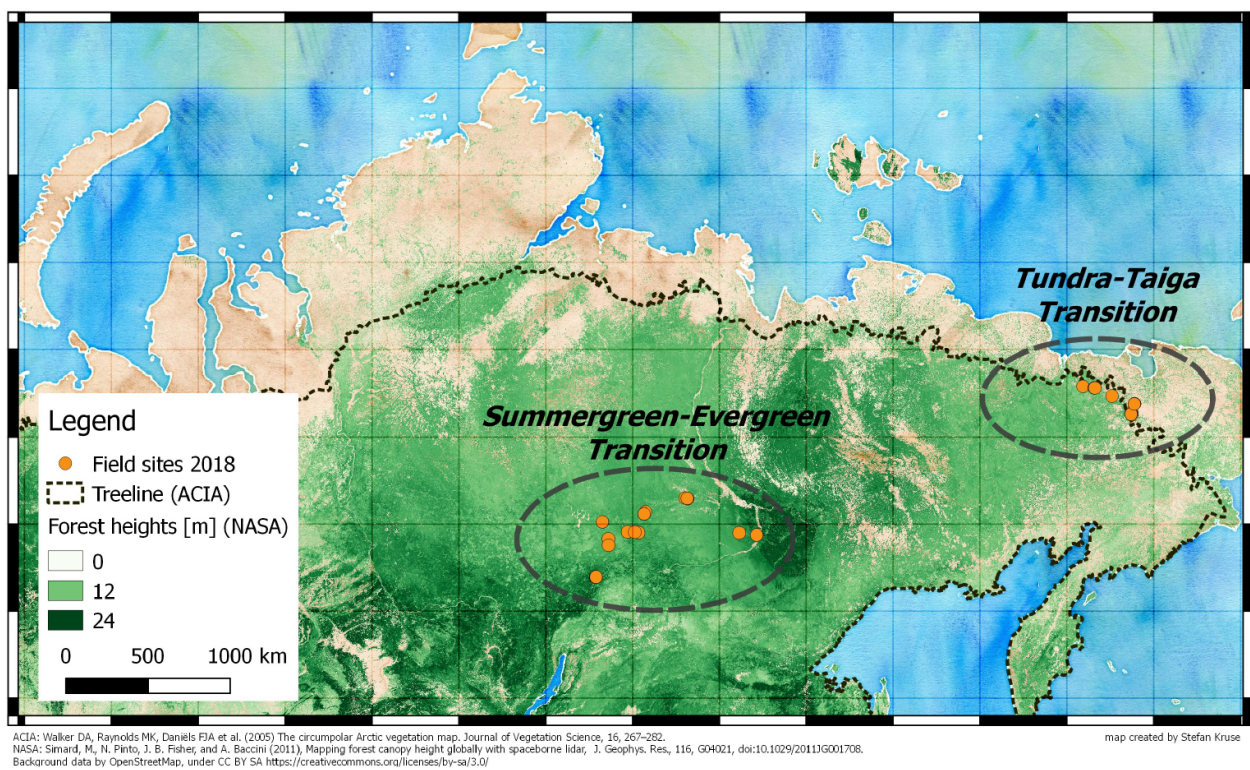


Figure 3.1.1: Overview map of field locations of the two parts of the expedition "CHUKOTKA 2018" visited in summer 2018

### 3.2 Glacial lake coring and treeline forest analyses at the northeastern treeline extension in Chukotka

*Boris K. Biskaborn*<sup>1</sup>, *Frederic Brieger*<sup>1</sup>, *Ulrike Herzsuh*<sup>1,3</sup>, *Stefan Kruse*<sup>1</sup>, *Luidmila Prestakova*<sup>2</sup>, *Iuliia Shevtsova*<sup>1</sup>, *Simone Stünzi*<sup>1</sup>, *Stuart Vyse*<sup>1</sup>, *Evgenii Zakharov*<sup>2</sup>

<sup>1</sup> Alfred Wegener Institute Helmholtz Center for Polar and Marine Research, Potsdam, Germany

<sup>2</sup> Federal State Autonomous Educational Institution of Higher Education "M.K. Ammosov North-Eastern Federal University", Yakutsk, Russian Federation

<sup>3</sup> University of Potsdam, Potsdam, Germany

#### Fieldwork period and location

From June 29<sup>th</sup> to July 24<sup>th</sup>, 2018 (at Lake Ilirney and Lake Rauchuagytgyn, westwards of Bilibino along the road towards Cherskii, Chukotka)

#### Objectives

This expedition to the treeline in northeast Siberia (Figure 3.1.1 & 3.2.1) complements a west–east transect across the Siberian tundra-taiga ecotone, in which similar regions have been visited in previous expeditions in 2011 & 2013 (lower Taimyr Peninsula), 2012 (along the Kolyma River), 2014 (Buor Khaya Peninsula) and 2016 (Chukotka, Kruse and Stoof-Leichsenring 2016).

Vegetation analyses were conducted at each vegetation plot along density gradients from tundra to taiga. In addition to the preceding studies, we aimed this year at assessing the full aboveground biomass as well as belowground carbon stocks so we took biomass samples from individual trees and shrubs, the surface vegetation and of the soils. Furthermore, we wanted to test the applicability of UAV-based imagery for the assessment of the 3D-structure of forests and the detection of single trees for upscaling plot information on larger areas.

Arctic lake system dynamics have been studied at AWI based on long-term cooperations with Russian partners, i.e. the Northeastern Federal University Yakutsk (NEFU). This initiative is related to the scientific programme of the AWI in PACES II, Topic 3.1: Circumpolar climate variability and global teleconnections at seasonal to orbital time scales. In forgoing years, AWI lake research in Russia has focused on Holocene environmental variability (Herzsuh et al. 2013) and climatic dynamics (e.g. Biskaborn et al. 2012; Biskaborn et al. 2013; Biskaborn et al. 2016) in previously "unexplored" areas of the Russian Arctic with only sparse insights into pre-Holocene climatic fluctuations. Given the high spatial variability of climate features over time and space, it is necessary to collect longer lake sediment cores from multiple representative glacial lake sites, especially in the vast Russian permafrost regions where only few data exist available to the community in earth science. This is particularly the case in the remote region of Chukotka, where currently only one long core of exceptional quality exists in a region of 737.700 km<sup>2</sup>. The expedition "Chukotka 2018" thus aimed to gain further insights into Quaternary Arctic environmental history. To this aim, a second expedition was planned to return to the two large glacial lake bodies of Ilirney and Rauchuagytgyn within the Chukotka Autonomous Okrug, located in the far Siberian northeast. The uppermost sediments of both lakes have already been investigated previously within a pilot study in 2016 (Keeperveem expedition, Kruse and Stoof-Leichsenring 2016) using principally a UWITEC gravity corer to obtain numerous short cores, as well as a hammer action modified UWITEC gravity corer to produce 2.9 m long cores. Initial sedimentological results in the form of XRF data along with several radiocarbon ages derived from cores from both lakes have been analyzed and published in bachelor thesis work (Hemmens 2017). The results from both cores show a high variability within geochemical proxies over the Holocene punctuated with numerous short term fluctuations in XRF data.

Obtaining longer sediment cores that allow greater temporal coverage into the Pleistocene was a primary aim of the 2018 expedition. Moreover two parallel cores per lake were planned in order to derive an inflow distal, undisturbed palaeoenvironmental record as well as an inflow proximal lake record for sedimentological investigations.

## Methods

### Modern vegetation surveys and samples

#### Plot selection

We visited 64 locations for vegetation surveys on the Russian-German Expedition "Chukotka 2018" in summer 2018. This expedition extends the tundra and forest structure analyses started in 2016 in Chukotka (Kruse et al. 2016). Prior the fieldwork, we placed locations into areas with different larch tree cover: from treeless tundra to open larch forests at slopes and in lowlands, covering different tree densities on various slopes and aspect based on satellite imagery (Figure 3.2.1).

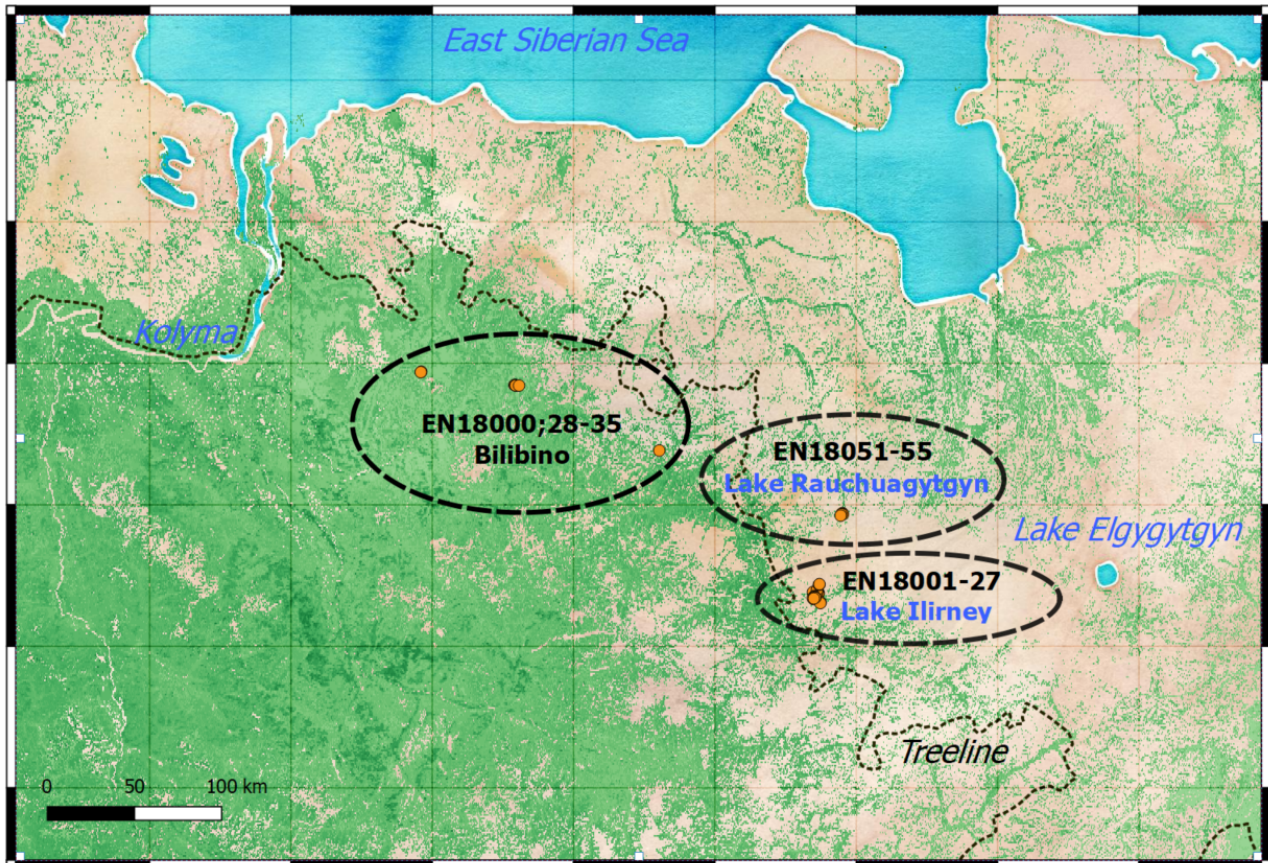


Figure 3.2.1: Overview map of the first expedition part to Chukotka, visiting different tundra and forested plots across the tundra-taiga transition zone. See Figure 3.1.1 for details.

#### Vegetation cover and biomass

Ground vegetation cover (shrubs, herb layer and moss layer) was recorded at all locations on three 2 x 2 m plots for each of 1-3 dominant vegetation types within the investigated plot of a radius of 15 m. On each of these plots, we recorded the projective cover (total and separated by taxa). All major vascular plant species, lichen, moss, deadwood, and open soil cover were considered. Above ground biomass (dominant plant species, moss and lichen, other remains) samples were taken on a subplot from each vegetation type within one location. The size of a sampling plot for all plant taxa excluding moss and lichen was 50 x 50 cm. Moss and lichen cover was sampled on 10 x 10 cm plots.

Additionally to the tree forming genera *Larix*, *Pinus*, *Picea*, *Abies*, *Alnus*, *Betula* and *Salix*, the four occurring shrubby plant groups *Betula*, *Alnus*, *Salix* and *Pinus pumila*, the latter only in Chukotka, were estimated in their cover and their maximum height as well (Table A.3.1 & A.3.3).



### *Soil pits and sampling*

At one plot, for each vegetation class, a soil profile was dug at the centre and samples from the surface layer, the organic rich layer below, and the mineral layer at the bottom from the topsoil were taken standardized with a hand sampling cylinder of 50 cm<sup>3</sup>, and further samples at the transition zones for radio carbon dating. Additionally, the thaw depth of the active layer above the permafrost table was probed with a metal rod device. With a hand-held temperature sensor, the temperature profile of each soil profile was measured. Similarly, the soil moisture content was measured as the volumetric water content in percent, in the litter, organic and mineral horizons. Furthermore, at the plot's centre we took a topsoil sample standardized with a hand sampling cylinder of 50 cm<sup>3</sup> for pollen analyses. In circles with a radii increased by 50 cm steps, the percentage coverage of families were recorded.

### *Tree survey and sampling (genetic and biomass)*

At forested plots we separately estimated the tree stem density for each species by counting trees < 40 cm and recording the heights for each tree within a radius of 15 m from the centre. At two plots, trees strongly recruited after a wildfire, we had to adjust our sampling protocol to smaller plot sizes. From each of these visited plots we surveyed 10 trees more intensively (see protocol below), or else the closest individuals to the plot, and we searched for larch seedlings (> 40 cm) at each vegetation cover survey area and recorded their individual properties and took genetic samples of up to ten individuals per 2 x 2 m area. At one plot in each region, we laid out a grid over at least 20 x 20 m of a tree stand with 2 m sub-grids for detailed forest structure analyses. We extended the area by 2 m steps if necessary to ensure we have at least 50 individuals > 2 m in each plot. Inside this grid we surveyed every tree > 40 cm (see protocol below) and additionally individuals < 40 cm were recorded only at the centre 12 x 12 m.

For each surveyed tree, we recorded the position (with a GPS device at the plots or the exact position in the 2 m grid plots) and individual properties of every tree exceeding 40 cm: height, basal diameter and diameter at breast height (i.e. at a height of 130 cm), crown diameter (in two directions), height of crown start, number of cones (binned to three categories: this years', old, and degraded ones) and we assessed the vitality state of each tree in 5 categories ('-' highly damaged, less than 10% living branches to '++' very dense crown structure and vital). For dendrochronological analyses, we took from each plot tree cores or discs at basal and breast height of a maximum of 10 trees > 2 m which were surveyed at radial plots and on 2 m-grid plots additionally 10 between 0.4 and 2 m, and further 10 < 0.4 m, where the latter individuals were taken as a whole. Cones of the same individuals and, if available, 10 for each separated cone class were sampled for biomass and a more detailed seed analysis in the lab. Finally, for genetic analyses we took 4-5 short shoots of needles of analysed trees and dried them in the field on silica gel.

### *3D-Forest stand reconstruction*

For upscaling and forest structure analyses, we took images for each plot from different platforms. First, UAV-based imagery (onboard DJI Phantom 4 RGB and Mapir Survey3W RGNIR) with a standardized flight plan (double-gridded in near-nadir position and circular facing the plot center at take-off elevation) on a 50 x 50 m area. And with the same RGNIR and additional Survey2W RGB cameras, we took images facing to the centre walking along on a circle with a radius of 15 m, from breast height and from approximately 7 m height.

In addition, for 360 x 180° panoramas we took images from the plot centre with a 10 to 18 mm ultra-wide focus lense Canon, mounted on a DSLR Canon EOS 7D. For optimized focal point positioning, a panorama head was used. The camera's ISO was fixed to a level of 100 and HDR images (-1/0/+1 brightness) were shot with the following protocol after adjusting the camera's shutter speed for each site to the optimum settings. (1) Two sets of images handheld downfacing with an 90° between the sets of images, (2) three circles 15° angles between the images resulting in an overlap of approximately 85%.

Furthermore, a Samsung Gear 360 camera was used to take single 360 x 180° panoramas from the centre of each plot. To test the potential of this double fisheye lense camera for 3D-reconstructions, we took at some sites time lapse videos by taking images (3840 x 1920 pixel) every half a second with automatic ISO level and shutter speed adjustment, and stored them as 10 frames per second MP4 video format.

### Weather stations and permafrost instrumentation

The two weather stations (Figure 3.2.2) collect temperature and humidity at two heights (110 cm and 250 cm), wind speed and direction at 320 cm, precipitation, solar radiation and snow depth. Underground, 2.5 m away from the station, soil sensors measure the temperature and moisture profile from the top to the bottom of the active layer and the soil heat flux in the topsoil layer.

iButtons, small, standalone temperature loggers were dispersed in a transect from the weather station to the treeline and in the topsoil layer of different vegetation types in taiga and tundra plots. In addition, HoboLoggers, higher-capacity soil temperature loggers, were set up in the soil pit close to the weather station and in larch dominated forests. Together, the instrumentation with a variety of different loggers will record the spatial and temporal variances across the vegetation and soil types that were found and sampled. In total, 2 weather stations, 6 HoboLoggers and 100 iButtons were set up. These sensors will be collected and read out in summer and fall 2019.

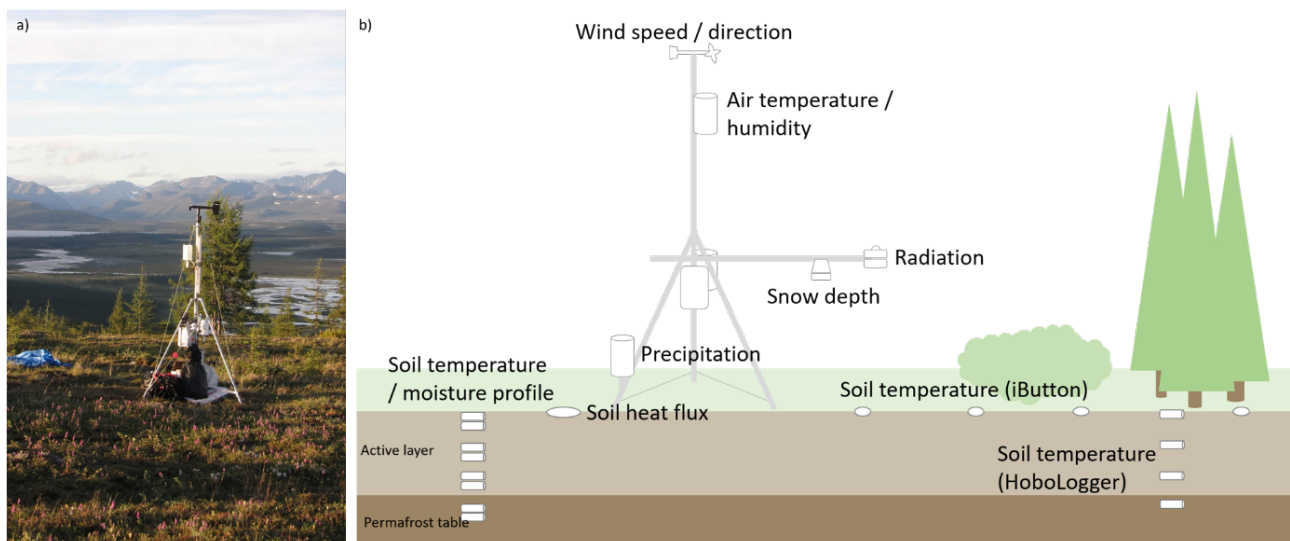


Figure 3.2.2: a) Picture of the weather station set up in Chukotka. The blue plane marks the position of the soil temperature/moisture profile at the station near Lake Ilirney, Chukotka. b) Sketch showing the setup of the two microclimate stations in Chukotka and Yakutia. Sensors with different applications are fixed at different heights and in different directions. The soil temperature and moisture profile is located a couple meters away from the station and provides the reference values for the comparison to the permafrost soil in vegetated areas. The iButton soil temperature sensors record the change in the temperature of the active layer from the station towards and into the vegetated areas. The HoboLoggers record a vertical temperature profile in both, larch and mixed-species forests.

### Core retrieval from Chukotkan glacial lake system

Russian MI-8 helicopters were utilized to reach the two lake sites from the town of Bilibino (Figure 3.2.1). Investigations of lake Ilirney were carried out over a longer time period and prior to fieldwork at lake Rauchuagytyn due to its greater surface area.

Our field work consisted of a comprehensive and holistic approach comprising geophysical, palaeolimnological and limnogeological methods that were conducted in a similar manner at each lake site. A parametrical sub-bottom profiling, echosounding approach was applied in order to derive high resolution bathymetric information as well as the stratigraphy of underlying sediments to enable the optimal location of drilling sites for coring. For this approach, the SES-2000 "compact" seismic device from INNOMAR was chosen and mounted to a steerable drilling platform on the water (UWITEC Niederreiter). The optimal settings for the device were determined during an initial test run at Lake Ilirney. The pulse frequencies were chosen as 8 and 10 kHz for low frequency pulses and 100 kHz for high frequency pulses. Pulse width was set at 2 seconds for low frequency and 253 microseconds for high frequency pulses respectively. A range of 45 m was chosen and was continuously altered

during profiling with changes in depth to the sediment surface. A total of 16 seismic transects were recorded at Lake Ilirney and 25 at Rauchuagytgyn (Figure 3.2.8). Seismic data were pre-processed within the Innomar ISE software environment and assessed immediately following geophysical surveys to determine the optimal drilling locations for long and undisturbed sediment records (Figure 3.2.7).

Upon site selection, short sediment cores were obtained from the UWITEC Niederreiter platform with the aid of a UWITEC gravity coring system. Subsequently, long cores were retrieved with an UWITEC piston coring system operated from the platform. Cores were subsequently collected within 3 m PVC plastic liners, cut into 1 meter sections and were stored in stable climate conditions in polystyrene thermoboxes to prevent thermal degradation.

Surface sediments as well as water samples from Lake Ilirney were collected at 16 locations across the lake and within the inflowing rivers for geochemistry, hydrochemistry and biology (bioindicators, aDNA and environmental DNA) (Figure 3.2.8). In addition, 6 locations were selected for sampling at Lake Rauchuagytgyn. Sampling of surface sediments was carried out using a HYDRO-BIOS sediment grabber with the top 1 centimeter being taken for the majority of samples. Water samples were collected in large (2040 mL) Whirl-Pak(R) bags for environmental DNA (eDNA) analysis and in 250 mL sample bottles for hydrochemistry. An UWITEC water sampler was deployed at the coring locations to retrieve water samples along a depth profile prior to any drilling or surface sediment retrieval. Collected eDNA samples were filtered using a vacuum pump in the field. Moreover, hydrochemistry samples were processed into: isotope, cation, anion, DOC and cDOM subsamples soon after collection. These subsamples will be later analyzed at the laboratories of AWI Potsdam.

Water chemistry parameters including pH, water temperature, oxygen content, conductivity and Secchi depth were measured *in situ* from the mobile drilling platform or from a rubber boat.

## Preliminary results

### Vegetation plots

The analysed tundra plots (N=17, Table A.3.1, Figure 3.2.3) near Lake Ilirney (N 67.40°, E 168.35°) were of a variety of tundra assemblages: mountain tundra grows in harsh environments on stony and rubbly screes with a poor vegetation cover by *Dryas spec.*, *Vaccinium uliginosum*, *V. vitis-idaea* or *Empetrum nigrum*, and in more favourable, wetter areas denser, tussocky *Eriophorum* communities prevail, and steep slopes were dominated by *Pinus pumila* with up to 60-80% coverage. Near the lake and westwards in the direction of the Kolyma River, larch forest stands (N=24) of the species *Larix cajanderi* reached up to 55% coverage. The moss and moss-lichen-rich forest floor is dominated with typical tundra dwarf-shrub species (*Betula exilis*, *Vaccinium uliginosum*, *V. vitis-idaea* or *Ledum palustre*) and larger shrubs > 20% *Salix spec.* and > 5% *Pinus pumila* occur.

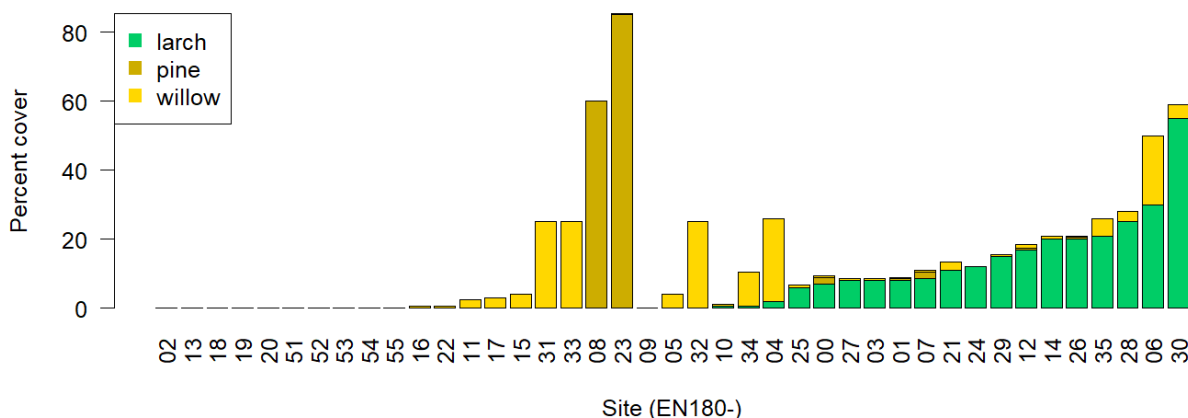
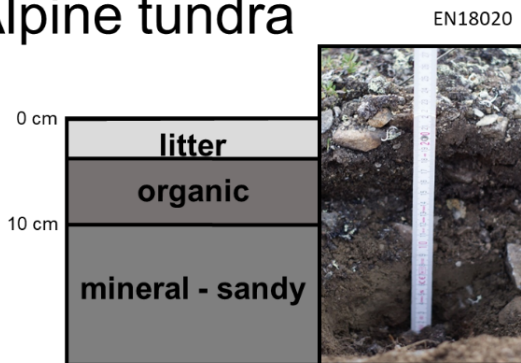


Figure 3.2.3: Vegetation projective cover of most dominant tree and larger shrub species

The soils below the tundra or open taiga were shallow and we observed active layer depths of approximately 18 to 84 cm (Figure 3.2.4). With the taken samples at the transition zones, especially from mineral to organic layers, we will determine the onset of soil formation in these areas and the interaction of soil carbon content with the standing biomass and vegetation type.

## Alpine tundra



## Tundra wet

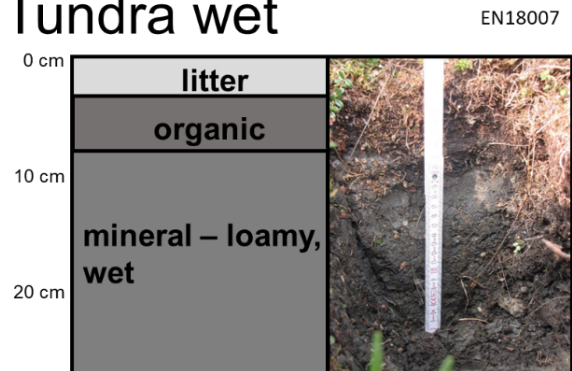


Figure 3.2.4: Permafrost soil profile examples below different vegetation cover. Photos by Luise Schulte)

At plot EN18014 we laid out a 40 x 40 m grid, subdivided by a 2 m-grid, for a detailed forest structure analysis. In addition, we sampled on the same site roots of *Larix* on a 6 x 6 m area with a 0.5 m resolution out of soil profiles below an area of 20 x 20 cm for biomass estimation and individual determination by genetic analysis. Further, one complete root system of one large tree was excavated and we estimated the biomass of all roots down to approximately 1 cm diameter. Additional images were taken for 3D-reconstruction of the root system.

The first results from 3D reconstructions using the UAV-based imagery show that our field sampling approach (forest plots of radius of 15 m) are representatively capturing the tree stands, or the field plot information could be upscaled using these 3D-forest reconstructions (e.g. Figure 3.2.5). In addition, from the recovered point clouds, single-tree information and forest metrics can be derived (Brieger et al. 2019).

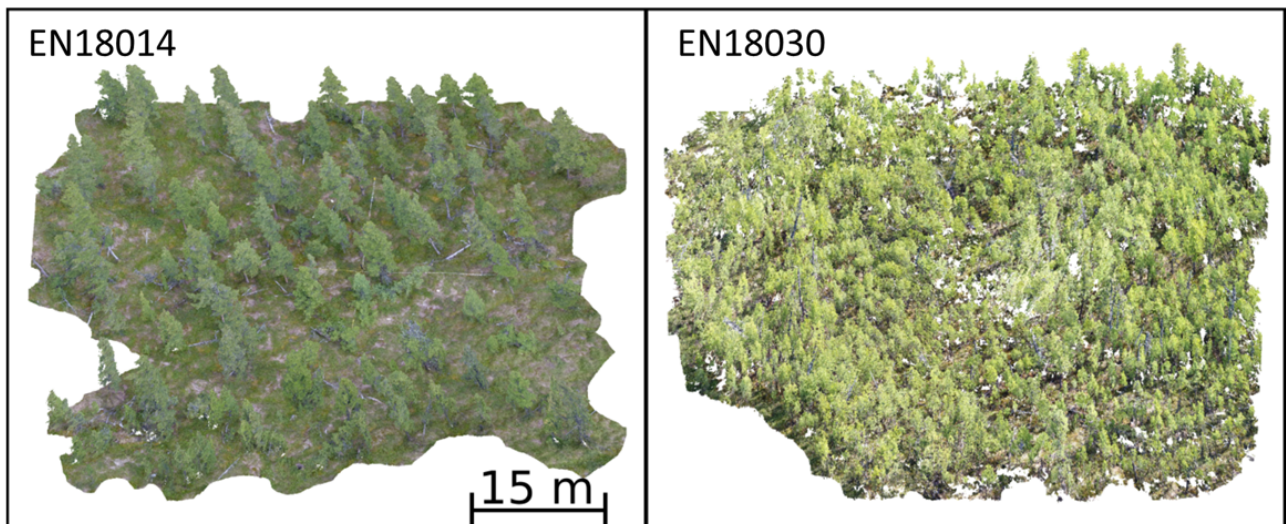


Figure 3.2.5: Two reconstructed three dimensional point clouds for an open larch forest (left) and a very dense stand (right) that blocks the view and thus leads to holes in the reconstructed forest floor

The weather stations started recording as soon as possible during the installation and were both read out shortly before leaving the locations. The data collected during the installation seems plausible, i.e. the air and soil temperature data over the course of four days at Lake Ilirney, Chukotka (Figure 3.2.6). We will retrieve the station and soil sensors in summer and fall 2019.

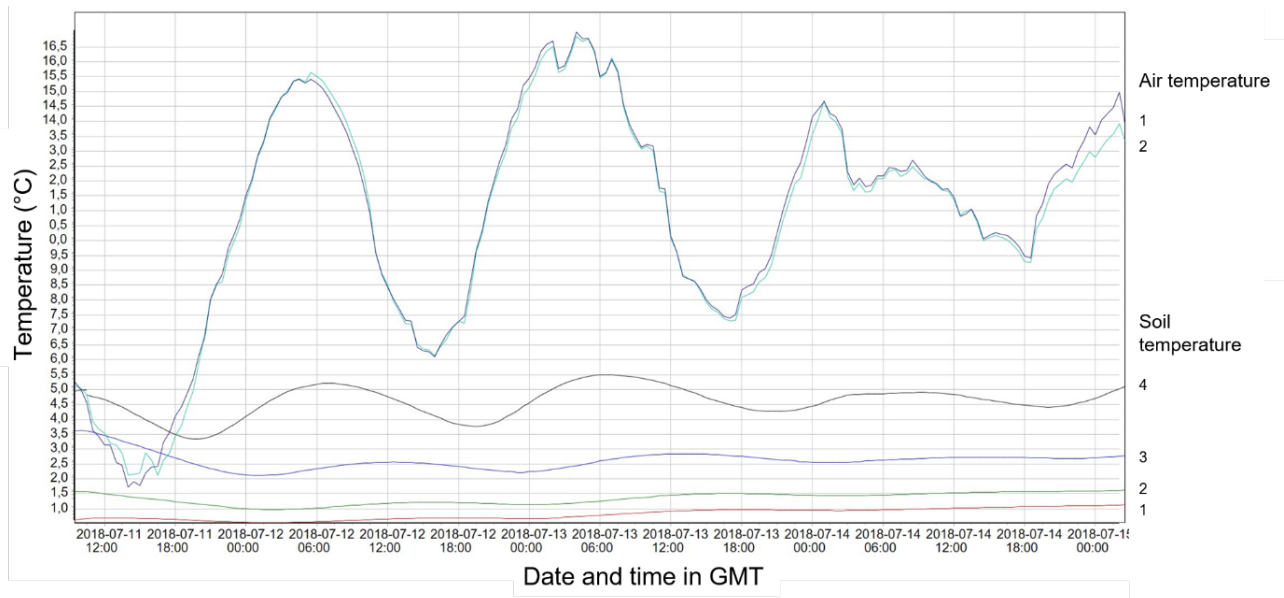


Figure 3.2.6: Recorded air and soil temperature data during and after the installation of the weather station at Lake Ilirney. Soil sensor 1 is located at the bottom of the soil pit at 45 cm depth, 2 at 35 cm, 3 at 25 cm and 4 at the top, 15 cm below the surface. Air temperature sensor 1 is mounted at a height of 110 cm and 2 at 250 cm.

### Lake sampling

An overview of limnological parameters determined during the Chukotka 2018 expedition are shown in Table A.3.1. Two long cores with penetration depths of 12.5 m (EN18208) and 14.3 m (EN18214) were obtained from Lake Ilirney at inflow distal and proximal sites respectively (Figure 3.2.8). The cores obtained at both sites were retrieved from raised plateaus of flat-lying strata away from sites of potential disturbance by density currents and terrestrial mass movement events. Drilling site EN18214 was located on a plateau between two small palaeochannel bodies close to the main fluvial inflows with the aim of capturing the effects of palaeoenvironmental catchment changes on the inflowing fluvial bodies and hence lake sedimentation. On the other hand, the site EN18208 was situated away from channel bodies on a plateau of presumably background sedimentation. These cores covered the majority of the bedded sedimentary lake infill reaching sand and eventually coarse gravel dominated material near to the maximum depth of penetration. In both cores, this corresponded closely to a change in sediment structure to unbedded, homogenous sediment seen within the echosound data that was taken to represent the oldest material at Lake Ilirney.

At Lake Rauchuagytygn, a 7.8 m (EN18218) and 5.7 m (EN18221) core were retrieved in the same manner to that at Lake Ilirney. Site EN18218 represented a central lake plateau of flat-lying beds sheltered from the steep lake margin, whereas site EN18221 occupied a shallower water position towards the lake outflow. The shorter length of these cores in comparison to those extracted from Lake Ilirney represents the reduced thickness of sedimentary infill present within the Lake Rauchuagytygn basin. This was observed both within echosound data and from the observance of gravelly material at a depth of approximately 7 m within core EN18218.

In addition to providing an efficient approach for the identification of drilling sites and respective sediment infill thicknesses at these selected sites, echosound data obtained during the 2018 expedition is already providing a highly effective method for the creation of high resolution water depth models at both lakes (Figure 3.2.8). Moreover, the abundance of gathered echosound data will allow an effective appraisal of basin development at both lakes that will significantly aid in palaeoenvironmental interpretations (Figure 3.2.7). A total of 51 sediment surface (0 to 1 cm) and water surface samples were collected at both lakes during the Chukotka 2018 expedition. These samples will be analyzed at AWI Potsdam and will contribute markedly to an understanding of present limnological conditions and spatial variability at the studied lake sites. The location and description of collected surface sediment and water samples are displayed in Table A.3.2.

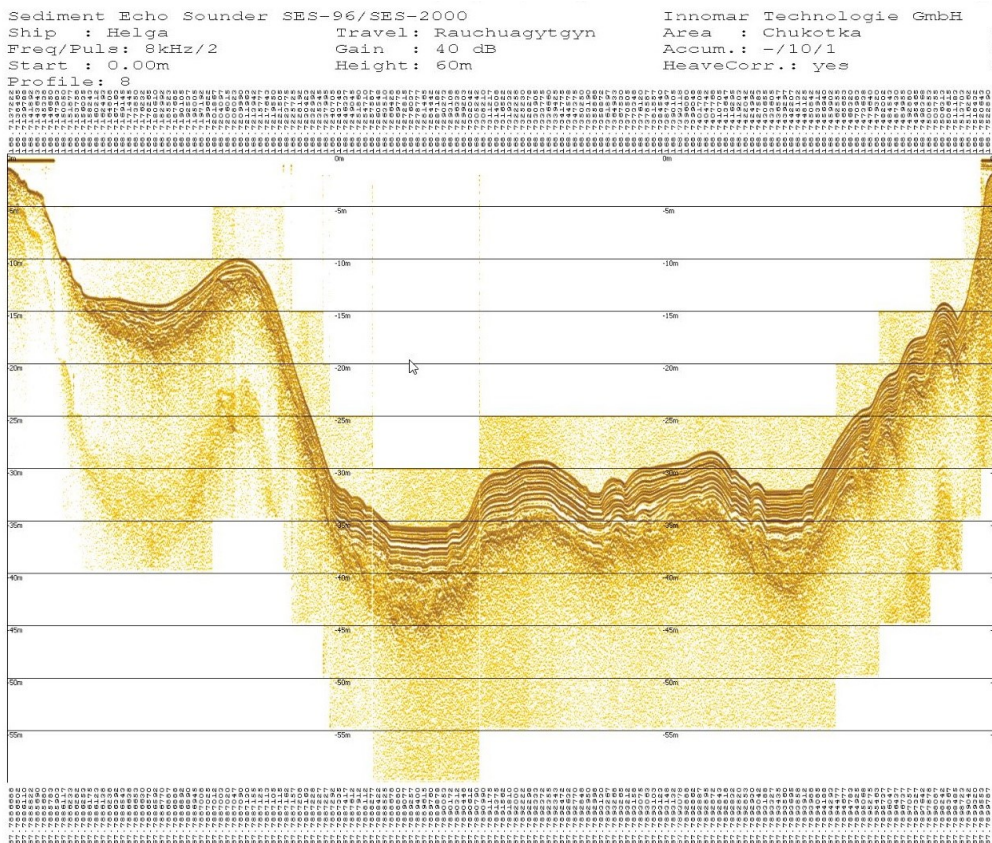


Figure 3.2.7: Oblique seismic profile across Lake Rauchuagytgyn. Both bathymetry and underlying sedimentological are visible

Table 3.2.1: Parameters of lakes studied during Expedition Chukotka 2018

Parameter/Lake	Ilirney	Rauchuagytgyn
Coordinates	N 67.3403°, E 168.29567°	N 64.4880°, E 122.7220°
Elevation [m]	306	619
Max Water Depth [m]	43.4	35.9
Mean Water Depth [m]	18.7	18.5
Length [km]	12	4.35
Lake area [km <sup>2</sup> ]	29.7	6.24
Catchment area [km <sup>2</sup> ]	1214	214.5
Catchment area / Lake area ratio	40.7	34.3
Origin	Glacial	Glacial
Summer Water temperature [°C] (Surface)	8.8	7.8
Summer Water temperature [°C] (Bottom)	4.6	7.9
Electrical conductivity [µS/cm]	69	85
Secchi depth [m]	3.85	3.9
Oxygen content (mg/L, %)	8.36/ 79	16.85/146.9
Max depth of bedded sediment fill [m]	19	8

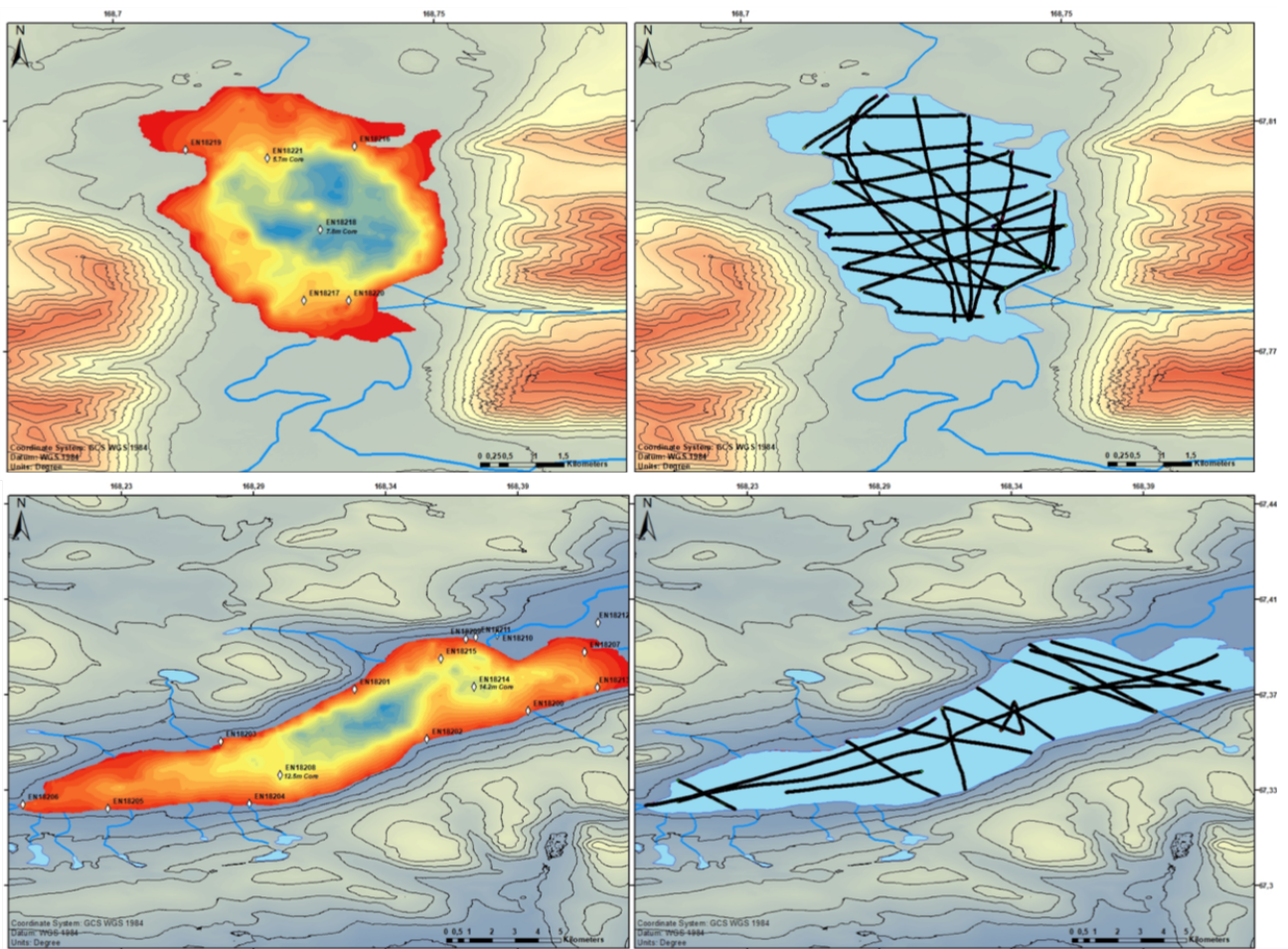


Figure 3.2.8: a) Water depth model and sampling locations at Lake Ilirney. b) Lake Ilirney seismic profiles. c) Water depth model and sampling locations at Lake Rauchuagytygn. d) Lake Rauchuagytygn seismic profiles

### 3.3 Sampling mixed-species boreal forests affected by disturbances and mountain lake mountain lake and alas lake coring in Central Yakutia

Stefan Kruse <sup>1</sup>, Ulrike Herzs Schuh <sup>1,2</sup>, Simone Stünzi <sup>1</sup>, Stuart Vyse <sup>1</sup>, Evgenii Zakharov <sup>3</sup>

<sup>1</sup> Alfred Wegener Institute Helmholtz Center for Polar and Marine Research, Potsdam, Germany

<sup>2</sup> University of Potsdam, Potsdam, Germany

<sup>3</sup> Federal State Autonomous Educational Institution of Higher Education "M.K. Ammosov North-Eastern Federal University", Yakutsk, Russian Federation

#### Fieldwork period and location

From July 24<sup>th</sup> to August 21<sup>st</sup>, 2018 (westwards of Yakutsk along the road towards Lensk via Nyrba and Mirny, and Lake Khamra, Yakutia)

#### Objectives

In mixed forest stands of the warmer Boreal Forests in Central Yakutia towards South Yakutia, light-demanding *Larix* trees are outcompeted by evergreen taxa. It is an open question as to how *Larix* forests, once established, hinder their replacement by evergreen forests and thus maintain a vegetation-climate disequilibrium. This self-stabilisation most likely results from the unique interactions between vegetation, fire, permafrost, and climate. However, rare modelling evidence suggests that feedbacks only provide weak protection for larch forests against evergreen taxa invasion. The inference of feedbacks is strongly dependent on the processes that are incorporated and their parameterisation, requiring a broader empirical base than is currently available for northern Asia. Therefore, we aim to quantify the feedbacks in the coupled forest-fire-permafrost-climate system along broad environmental gradients.

The bioclimatic gradient covered on the first part of the expedition in Chukotka, was extended in the warmer areas of Yakutia (Figure 3.3.1). Here we visited forest stands that capture the southwestwardly replacement of summergreen larch dominance in forests by evergreen taxa (*Picea*, *Pinus*, *Abies*), and sites having different disturbance histories (wildfire, wind throw, land-use).

#### Methods

##### Modern vegetation surveys and samples

We extended the bioclimatic gradient visited in northeastern Siberia during the first part of the CHUKOTKA 2018 expedition to the warmer south with evergreen/summergreen mixed species boreal forests. In central Yakutia, we selected additional sites that were disturbed by fires in the past and were selected beforehand by satellite imagery. Following a road for 1800 km, we sampled vegetation sites following the same protocols explained in detail in the methods section in section 3.2.



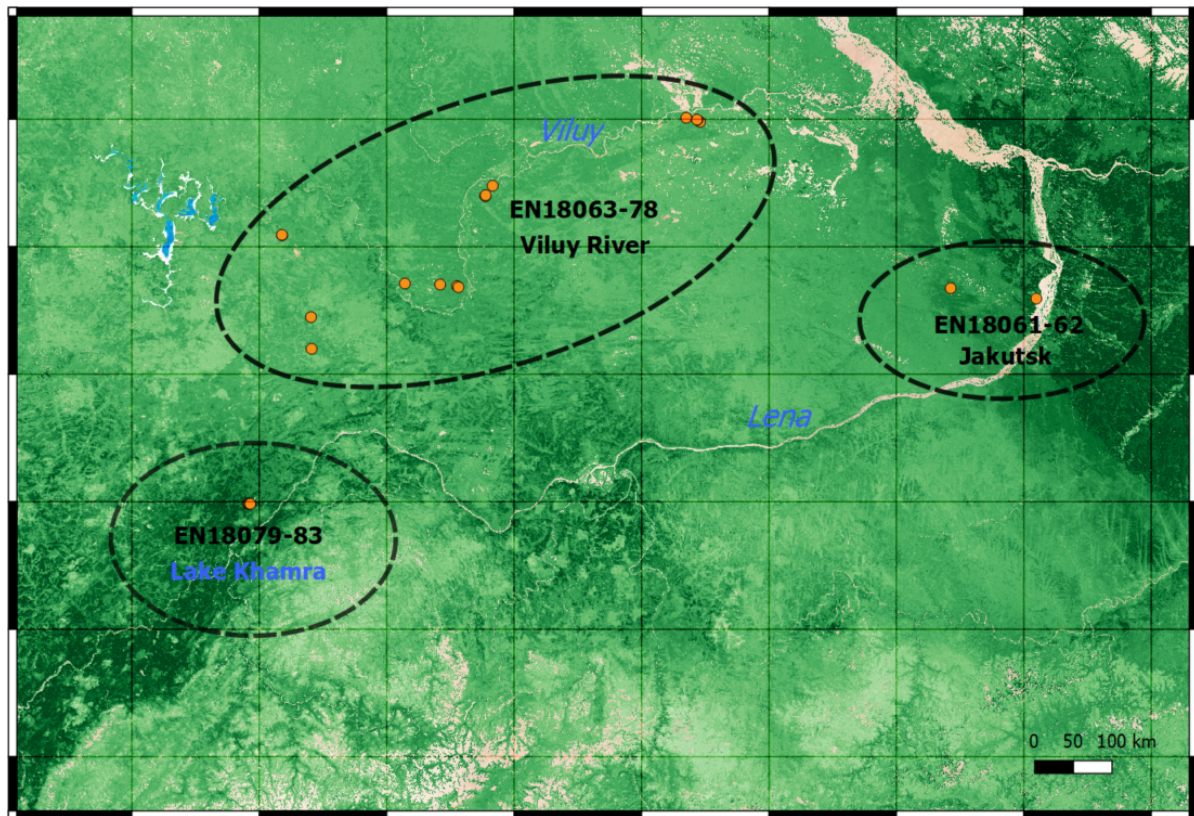


Figure 3.3.1: Overview map of the second expedition part to Yakutia, visiting forest stands along the summergreen-evergreen boreal forest transition along a NE-SW gradient. See caption of Figure 3.1.1 for details.

### Coring and sampling of Yakutian thermokarst lake systems and mountain lake Khamra

Within the summergreen-evergreen transition zone, 10 thermokarst lakes in the vicinity of studied vegetation plots were cored and sampled. In addition, basic physical and chemical water measurements (including water depth, Secchi depth, pH, conductivity, temperature) were performed at the lakes. Further, water samples were sub-sampled and prepared at the camp for subsequent laboratory analyses at AWI including for cations, anions, DOC, cDOM, stable isotopes and eDNA. Surface sediment samples were taken from thermokarst lakes from the position of maximum water depth. All surface samples were taken with a sediment grabber. Similarly, several short sediment cores and long cores were taken from the thermokarst lakes using the UWITEC gravity corer and hammer-action modification. Sediment cores to be utilized for chronology surveys were sub-sampled in the field in 0.5 cm slices and stored in Whirl-Pak(R) plastic bags. The other cores were stored within thermoboxes to maintain dark and cold conditions and will be sampled at AWI laboratories later on. In addition to the 10 thermokarst lakes, the mountain lake Khamra in Southern Yakutia was also cored and sampled using a modified peat corer within the inflow river region and a UWITEC modified hammer-action corer at the lake center. In total, over 32 m of cores from Yakutian thermokarst and mountain lakes were taken.

### Preliminary results

#### Vegetation analyses

We visited 23 forest plots on the transect between Yakutsk (N 62.08°, E 129.62°) to Lake Khamra (N 59.97°, E 112.96°; Table A.3.3, Figure 3.3.2). In contrast to the open forests of northeastern Chukotka, up to 70% of the areas were covered in southeastern, mixed-coniferous forests. These forests were dominated by *Larix gmelinii* with a cover of > 60%, growing together with other tree species: tree-forming *Salix spec.* (> 30%), *Picea obovata* (> 30%), *Betula pendula* (30%) and *Pinus sylvestris* (> 20%) that is replaced by *P. sibirica* at the southernmost areas near Lake Khamra (EN18079-83) at which also *Abies sibirica* was observed on one plot with a cover of 8%. Other stands were dominated by *Picea obovata* with 30-50% cover but also mixed with *Larix* > 10%, or by

*Pinus sylvestris* and *P. sibirica* with 15-30%. At some stands, we found clear signs of recent or recurrent fires events, either fire scars on tree trunks, burnt bark and/or cohort-like recruitment indicating a strong disturbance.

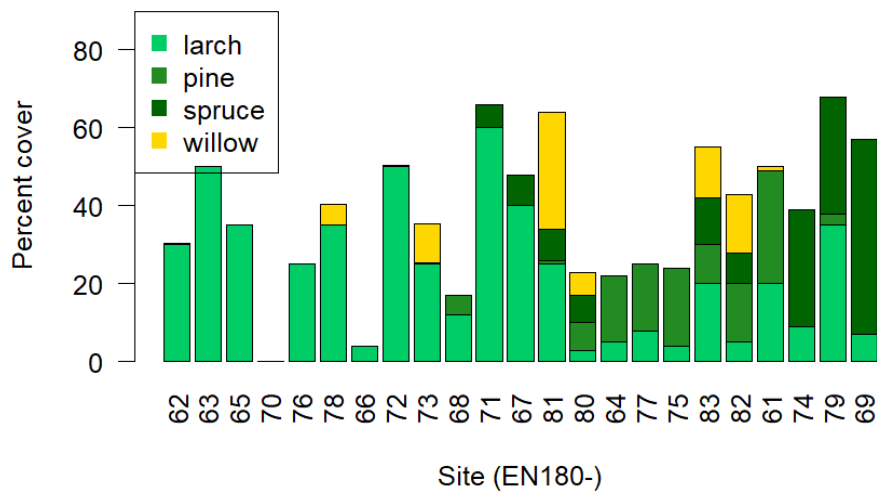


Figure 3.3.2: *Vegetation projective cover of most dominant tree and shrub species*

The 2 m-grid was laid out at EN18065 on 20 x 20 m for a detailed forest structure analysis. Furthermore, at the location of the weather station, we recorded all tree heights in 2 m steps along a 150 m-long line transect passing a forest edge (EN18070, Figure 3.3.3), and placed three vegetation plots outside, at the transition and within the forest.



Figure 3.3.3: *Reconstructed 3D-point cloud at site EN18070, which is a line transect starting at the weather station reaching to the centre of the forest patch*

The soils were in general developed deeper with approximately 48 to 226 cm in southeastern forests rather than in the tundra-taiga transition zone (Figure 3.3.4). Processed samples will help to understand the impact of disturbances on soil-vegetation interaction and carbon deposition.

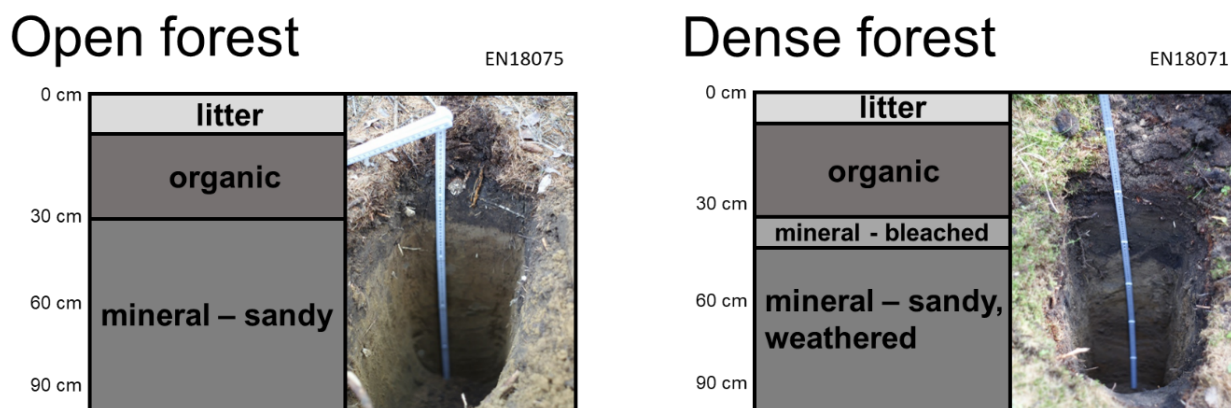


Figure 3.3.4: Permafrost soil profile examples below different vegetation cover. Photos by Luise Schulte

The weather stations recorded plausible data between July and November 2018 and will most probably provide a comprehensive view on the permafrost-vegetation interaction after the full year data is available.

### Lake sampling

Amongst the 32 meters of retrieved core (Table A.3.4), work has already begun on cores from mountain lake Khamra where XRF data already exist for cores EN18232-2, drilled from the lake center at 22.3 m water depth as well as from the russian peat core at 1.9 m depth near to the river inflow. We expect the results to display high resolution changes in catchment inflows (represented by Ti, Zr elemental profiles) at lake Khamra over the course of the Holocene related to palaeoclimatic developments in the region. Cores retrieved from thermokarst lakes will allow us to look at the processes controlling thermokarst development and the timing of thermokarst development in Southern Yakutia.

### Acknowledgements

We thank our Russian and German colleagues from the joint Russian–German expedition 2018 for support in the field. Special thanks to the staff of the BIOM-laboratory in Yakutsk for their great support in the logistics. We thank Julia Boike and Moritz Langer with whom we planned the setup of the weather stations and for their technical support. We like to thank Guido Grosse and Thomas Laepple who provided us with computational resources for the point cloud reconstruction from UAV-based data. A part of this research has received funding from the ERC consolidator grant Glacial Legacy of Ulrike Herzschuh (grant no. 772852).

## Bibliography

- ACIA (2005) Arctic Climate Impact Assessment. ACIA Overview report. Cambridge University Press, Cambridge, United Kingdom and New York, NY, USA:1020. ISBN: 0521865093.
- Biskaborn BK, Herzschuh U, Bolshiyarov D, Savelieva L, and Diekmann B (2012) Environmental variability in northeastern Siberia during the last similar to 13,300 yr inferred from lake diatoms and sediment-geochemical parameters. *Palaeogeography Palaeoclimatology Palaeoecology* 329:22–36. <https://doi.org/10.1016/j.palaeo.2012.02.003>.
- Biskaborn BK, Herzschuh U, Bolshiyarov D, Savelieva L, Zibulski R, and Diekmann B (2013) Late Holocene thermokarst variability inferred from diatoms in a lake sediment record from the Lena Delta, Siberian Arctic. *Journal of Paleolimnology* 49:155–170. <https://doi.org/10.1007/s10933-012-9650-1>.
- Biskaborn BK, Subetta DA, Savelieva LA, Vakhrameva PS, Hansche A, Herzschuh U, Klemm J, Heinecke L, Pestryakova LA, Meyer H, Kuhn G, and Diekmann B (2016) Late Quaternary vegetation and lake system dynamics in north-eastern Siberia: Implications for seasonal climate variability. *Quaternary Science Reviews* 147:406–421. <https://doi.org/10.1016/j.quascirev.2015.08.014>.
- Bonan GB (2008) Forests and Climate Change: Forcing Feedbacks, and the Climate Benefits of Forests. *Science* 320:1444–1449. <https://doi.org/10.1126/science.1155121>.
- Brieger F, Herzschuh U, Pestryakova LA, Bookhagen B, Zakharov ES, and Kruse S (2019) Advances in the Derivation of Northeast Siberian Forest Metrics Using High-Resolution UAV-Based Photogrammetric Point Clouds. *Remote Sensing* 11:1447. <https://doi.org/10.3390/rs11121447>.
- Epp LS, Kruse S, Kath NJ, Stoof-Leichsenring KR, Tiedemann R, Pestryakova LA, and Herzschuh U (2018) Temporal and spatial patterns of mitochondrial haplotype and species distributions in Siberian larches inferred from ancient environmental DNA and modeling. *Science Repository* 8:17436. <https://doi.org/10.1038/s41598-018-35550-w>.
- Hemmens E (2017) Late Quaternary sedimentary processes in Chukotkan lake systems. MA thesis. University of Potsdam.
- Herzschuh U, Pestryakova LA, Savelieva LA, Heinecke L, Böhmer T, Biskaborn B, Andreev A, Ramisch A, Shineman ALC, and Birks HJB (2013) Siberian larch forests and the ion content of thaw lakes form a geochemically functional entity. *Nature Communications* 4. <https://doi.org/10.1038/ncomms3408>.
- Kruse S, Gerdes A, Kath NJ, Epp LS, Stoof-Leichsenring KR, Pestryakova LA, and Herzschuh U (2019) Dispersal distances and migration rates at the arctic treeline in Siberia - a genetic and simulation-based study. *Biogeosciences* 16:1211–1224. <https://doi.org/10.5194/bg-16-1211-2019>.
- Kruse S and Stoof-Leichsenring KR (2016) Russian-German Cooperation: Expeditions to Siberia in 2016. Ed. by PP Overduin, F Blender, DY Bolshiyarov, MN Grigoriev, A Morgenstern, and H Meyer. Alfred-Wegener-Institut, Helmholtz-Zentrum für Polar- und Meeresforschung, Bremerhaven, Germany, Alfred-Wegener-Institut, Helmholtz-Zentrum für Polar- und Meeresforschung, Bremerhaven, Germany. Chap. Keperveem - Past and present vegetation dynamics at the most eastern extension of the Siberian boreal treeline:130–137. [https://doi.org/10.2312/BzPM\\_0709\\_2017](https://doi.org/10.2312/BzPM_0709_2017).
- Kruse S, Wiczorek M, Jeltsch F, and Herzschuh U (2016) Treeline dynamics in Siberia under changing climates as inferred from an individual based model for *Larix*. *Ecological Modelling* 338:101–121. <https://doi.org/10.1016/j.ecolmodel.2016.08.003>.
- Niemeyer B, Epp LS, Stoof-Leichsenring KR, Pestryakova LA, and Herzschuh U (2017) A comparison of sedimentary DNA and pollen from lake sediments in recording vegetation composition at the Siberian treeline. *Molecular Ecology Resources* 17:e46–e62. <https://doi.org/10.1111/1755-0998.12689>.

Wieczorek M, Kruse S, Epp LS, Kolmogorov A, Mikolaey AN, Heinrich I, Jeltsch F, Pestryakova LA, Zibulski R, and Herzsuh U (2017) Dissimilar responses of larch stands in northern Siberia to increasing temperatures - a field and simulation based study. *Ecology* 98:2343–2355. <https://doi.org/10.1002/ecy.1887>.

**Chapter 4**

**Appendix**

## A.1 List of participants

Table A.1.1: List of participants in Samoylov Island Campaigns

No.	Name	Institution	Duration
<i>Samoylov Island</i>			
1	Abramova, Katja	LDR	05.04.18-12.05.18 and 20.05.18-31.08.18
2	Assmann, Volkmar	AWI P	04.09.18-15.09.18
3	Avdeev, Denis	IPGG, NSU	22.07.18-15.08.18
4	Barsukov, Pavel	ISSA	01.07.18-31.07.18
5	Beckebanze, Lutz	UHH	17.04.18-27.04.18
6	Bornemann, Niko	AWI P	14.06.18-15.07.18
7	Buchwal, Agata	AMU	16.08.18-31.08.18
8	Buchwalder, Xavier	EPFL	22.08.18-15.09.18
9	Chappius, Flore	EPFL	22.08.18-15.09.18
10	Chernyshov, Gleb	IPGG, NSU	22.07.18-15.08.18
11	Eckhardt, Tim	UHH	04.07.18-29.07.18
12	Esin, Egor	IPGG, NSU	22.07.18-15.08.18
13	Evgrafova, Svetlana	SIF, SFU	31.07.18-31.08.18
14	Faguet, Alexey	IPGG, NSU	22.07.18-15.08.18
15	Fedorova, Irina	SPU	17.04.18-27.04.18
16	Frolova, Larisa	KFU	17.04.18-27.04.18
17	Fuchs, Matthias	AWI P	31.07.18-31.08.18
18	Gerber, Franziska	EPFL, WLS	22.08.18-15.09.18
19	Gonta, Taras	IPGG	15.08.18-29.08.18
20	Hainbach, Till	AWI P, UP	17.04.18-27.04.18
21	Heim, Birgit	AWI P	17.04.18-27.04.18 and 31.07.18-31.08.18
22	Holm, Stine	GFZ	17.07.18-14.08.18
23	Juhls, Bennet	ISS FU	04.07.18-15.07.18
24	Jullien, Nicolas	EPFL	22.08.18-15.09.18
25	Kadutskiy, Valeriy	NSU, SFU	31.07.18-31.08.18
26	Kahl, Annelen	EPFL, WLS	22.08.18-15.09.18
27	Kaufmann, Oliver	UHH	04.09.18-15.09.18
28	Khabibulina, Raliya	IPGG	15.08.18-29.08.18
29	Khazin, Leonid	IPGG	22.07.18-15.08.18
30	Khazina, Irina	IPGG	22.07.18-15.08.18
31	Knoblauch, Christian	UHH	04.07.18-29.07.18
32	Kuzmina, Olga	IPGG	22.07.18-15.08.18
33	Lashchinskiy, Nikolay	CSBG	22.07.18-15.08.18
34	Lebedeva, Liudmila	MPI	31.07.18-14.08.18
35	Makarieva, Olga	SPU, MPI	31.07.18-14.08.18
36	Melchert, Jan	UC	31.07.18-29.08.18
37	Meyer, Hanno	AWI P	17.04.18-13.05.18
38	Mikhailsov, Nikolai	IPGG, NSU	01.08.18-15.08.18
39	Morgenstern, Anne	AWI P	17.04.18-27.04.18
40	Novikov, Alexander	KFU	04.07.18-31.08.18

No.	Name	Institution	Duration
<i>Samoylov Island</i>			
41	Opel, Thomas	US, AWI P	17.04.18-13.05.18
42	Polyakov, Vyacheslav	SPU, AARI	04.07.18-29.07.18
43	Pravkin, Sergey	SPU, AARI	01.08.18-20.08.18 and 22.08.18-15.09.18
44	Rachelwicz, Grzegorz	JLU, AMU	16.08.18-31.08.18
45	Riedhauser, Annina	EPFL	22.08.18-15.09.18
46	Rüggen, Norman	UHH	04.09.18-15.09.18
47	Runge, Alexandra	AWI P	31.07.18-31.08.18
48	Schreiber, Peter	AWI P	14.06.18-04.07.18
49	Sennikov, Nikolay	IPGG	15.08.18-29.08.18
50	Shamov, Vladimir	MPI, PIG	31.07.18-14.08.18
51	Shevtsova, Iuliia	AWI P	31.07.18-29.08.18
52	Sidorov, Roman	GC	10.08.18-15.08.18
53	Skryabin, Artem	SPU	04.07.18-15.07.18
54	Tarbeeveva, Anna	LMSU	31.07.18-14.08.18
56	Tsibizov, Leonid	MPI, SIGM, NSU	22.07.18-21.08.18
57	Wille, Christian	GFZ	14.06.18-04.07.18
58	Wischhöfer, Philipp	UC	17.07.18-14.08.18
59	Zaplavnova, Anna	IPGG, NSU	22.07.18-15.08.18



Table A.1.2: List of Participants in Samoylov Deep Drilling Campaigns 2018

<b>No.</b>	<b>Name</b>	<b>Institution</b>	<b>Duration</b>
<i>Samoylov Deep Drilling Spring Campaign 2018</i>			
1	Bolshiyarov, Dmitri	AARI	05.04.18-27.04.18
2	Grigoriev, Boris	NEFU	01.04.18-30.04.18
3	Grigoriev, Mikhail	MPI, IPGG	05.04.18-27.04.18
4	Jongejans, Loeka	AWI P	05.04.18-27.04.18
5	Kartozia, Andrey	IPGG, SIGM, NSU	17.04.18-27.04.18
6	Kupriyanov, Aleksey	RS SI	05.04.18-27.04.18
7	Maksimov, Georgii	MPI, IPGG	05.04.18-27.04.18
8	Ostrelidin, Semen	NEFU	05.04.18-27.04.18
9	Ostrelidin, Stanislav	NEFU	05.04.18-27.04.18
10	Schneider, Waldemar	AWI P	05.04.18-27.04.18
11	Sellyakhov, Fedor	RS SI	05.04.18-27.04.18
12	Strauss, Jens	AWI P	05.04.18-27.04.18
<i>Samoylov Deep Drilling Summer Campaign 2018</i>			
1	Bolshiyarov, Dmitri	AARI	04.07.18-15.07.18
2	Kartozia, Andrey	IPGG	14.06.18-29.08.18
3	Schneider, Waldemar	AWI P	14.06.18-31.08.18

Table A.1.3: List of Participants in Lena Delta Land Expeditions

No.	Name	Institution	Duration
<i>Buor-Khaya Bay</i>			
1	Bolshiyanova, Olga	AARI	01.08.18-20.08.18
2	Danilov, Kencheeri	MPI	01.08.18-20.08.18
3	Khristoforov, Ivan	MPI	01.08.18-20.08.18
4	Michealis, Rune	AWI S	01.08.18-20.08.18
5	Papenmeier, Svenja	AWI S, IBSR	01.08.18-20.08.18
6	Pravkin, Sergey	AARI, SPU	01.08.18-20.08.18 and (22.08.18-15.09.18 on Samoylov)
7	Sander, Lasse	AWI S	01.08.18-20.08.18
<i>Sobo-Sise Island</i>			
1	Aksenov, Aleksey	AARI	11.07.18-25.07.18
2	Fritz, Michael	AWI P	05.07.18-27.07.18
3	Kizyakov, Alexandr	LMSU	11.07.18-25.07.18
4	Schirrmeister, Lutz	AWI P	11.07.18-25.07.18
5	Wetterich, Sebastian	AWI P	05.07.18-27.07.18
<i>SOILA - Buor-Khaya Bay, Tiksi, Lena Delta</i>			
1	Fromm, Tanja	AWI B	31.08.18-17.09.18
2	Gukov, Stepan	YB GC	31.08.18-15.09.18
3	Haberland, Christian	GFZ	04.09.18-17.09.18
4	Krueger, Frank	UP	31.08.18-17.09.18
5	Peresyarkin, Dimitri	YB GC	31.08.18-15.09.18
6	Petrinin, Sergey	YB GC	31.08.18-15.09.18
7	Ploetz, Aline	AWI B	04.09.18-17.09.18
8	Tuktarov, Rustam	YB GC	04.09.18-17.09.18
9	Vollmer, Daniel	UP	31.08.18-17.09.18
<i>Tit-Ary</i>			
1	Alfirov, Alexander	IPGG	22.07.18-15.08.18
2	Glinskikh, Larisa	IPGG	22.07.18-15.08.18
3	Metelkin, Egor	IPGG, NSU	22.07.18-15.08.18
4	Popov, Aleksey	IPGG	22.07.18-15.08.18

Table A.1.4: List of Participants in Chukotka 2018 Campaign

No.	Name	Institution	Duration
<i>Chukotka 2018</i>			
1	Bernhardt, Nadine	AWI P	25.07.18-21.08.18
2	Biskaborn, Boris	AWI P	29.06.18-24.07.18
3	Brieger, Frederic	AWI P	30.06.18-24.07.18 and 25.07.18-21.08.18
4	Gorodnichev, Ruslan	NEFU	30.06.18-24.06.18
5	Herzschuh, Ulrike	AWI P	30.06.18-24.07.18 and 25.07.18-21.08.18
6	Kirillin, Nikolai	NEFU	30.06.18-24.07.18 and 25.07.18-21.08.18
7	Kruse, Stefan	AWI P	29.06.18-24.07.18 and 25.07.18-21.08.18
8	Mariuiuv, German	NEFU	25.07.18-21.08.18
9	Nikitin, Evgenii	NEFU	30.06.18-24.07.18
10	Orlov, Aleksandr	SPU	10.08.18-21.08.18
11	Ossipova, Nadezhda	NEFU	25.07.18-21.08.18
12	Pestryakov, Aleksei	NEFU	25.07.18-21.08.18
13	Pestryakova, Luidmila	NEFU	30.06.18-24.07.18 and 25.07.18-21.08.18
14	Schulte, Luise	AWI P, UP	30.06.18-24.07.18 and 25.07.18-21.08.18
15	Shevtsova, Iuliia	AWI P	30.06.18-24.07.18
16	Sitnikov, Dmitrii	NEFU	30.06.18-24.07.18
17	Stünzi, Simone	AWI P	30.06.18-24.06.18 and 25.07.18-21.08.18
18	Ushnitskaia, Lena	NEFU	30.06.18-24.07.18 and 25.07.18-21.08.18
19	Vyse, Stuart	AWI P	30.06.18-24.07.18 and 25.07.18-21.08.18
20	Zakharov, Evgenii	NEFU	30.06.18-24.07.18 and 25.07.18-21.08.18

*1<sup>st</sup> Part: Expedition to Chukotka from 29.06.2018 to 24.07.2018*

*2<sup>nd</sup> Part: Expedition to Central-Yakutia from 25.07.2018 to 21.08.2018*

Table A.1.5: List of Participating Institutions

<b>Abbr.</b>	<b>Institution</b>
AARI	Arctic and Antarctic Research Institute, St. Petersburg, Russian Federation
AMU	Adam Mickiewicz University, Poznan, Poland
AWI B	Alfred Wegener Institut Helmholtz Centre for Polar and Marine Research, Bremerhaven, Germany
AWI P	Alfred Wegener Institut Helmholtz Centre for Polar and Marine Research, Potsdam, Germany
AWI S	Alfred Wegener Institut Helmholtz Centre for Polar and Marine Research, List/Sylt, Germany
CSBG	Central Siberian Botanical Garden, Siberian Branch, Russian Academy of Sciences, Novosibirsk, Russian Federation
EPFL	École Polytechnique Fédérale de Lausanne, Lausanne, Switzerland
GC	Geophysical Center of the Russian Academy of Sciences, Moscow, Russian Federation
GFZ	GFZ German Research Centre for Geoscience Helmholtz Centre Potsdam, Potsdam, Germany
IBSR	Leibnitz Institute for Baltic Sea Research, Warnemünde, Germany
IPGG	Trofimuk Institute of Petroleum-Gas Geology and Geophysics, Siberian Branch, Russian Academy of Sciences, Novosibirsk, Russian Federation
ISS FU	Institute of Space Sciences, Freie Universität Berlin, Berlin, Germany
ISSA	Institute of Soil Science and Agrochemistry, Siberian Branch, Russian Academy of Sciences, Novosibirsk, Russian Federation
JLU	Xi'an Jiaotong-Liverpool University, Suzhou, China
KFU	Kazan Federal University, Kazan, Russian Federation
LDR	Lena Delta Reserve, Tiksi, Yakutia, Russian Federation
LMSU	Lomonosov Moscow State University, Moscow, Russian Federation
MPI	Melnikov Permafrost Institute, Siberian Branch, Russian Academy of Sciences, Yakutsk, Russian Federation
NEFU	Federal State Autonomous Educational Institution of Higher Education "M.K. Ammosov North-Eastern Federal University", Yakutsk, Russian Federation
NSU	Novosibirsk State University, Novosibirsk, Russian Federation
PIG	Pacific Institute of Geography, Vladivostok, Russia
RS SI	Research Station Samoylov Island, Russian Federation
SFU	Siberian Federal University, Krasnoyarsk, Russian Federation
SIF	Sukachev Institute of Forest, Siberian Branch, Russian Academy of Sciences, Krasnoyarsk, Russian Federation
SIGM	V.S. Sobolev Institute of Geology and Mineralogy, Siberian Branch, Russian Academy of Sciences, Novosibirsk, Russian Federation
SPU	St. Petersburg University, St. Petersburg, Russian Federation
UC	Institute of Geology and Mineralogy, University of Cologne, Cologne, Germany
UHH	Universität Hamburg, Hamburg, Germany
UP	University of Potsdam, Germany
US	University of Sussex, Brighton, United Kingdom
WLS	WSL Institute for Snow and Avalance Research SLF, Davos, Switzerland
YB GC	Yakutsk Branch Federal Research Centre Geophysical Survey, Russian Academy of Science, Yakutia, Russian Federation

## A.2 Supplementary material to Lena 2018 Expedition

### Sediment core pictures - Deep Drilling Campaign Spring 2018



Figure A.2-1: *Wooden remains around 21.5 m (Drive XIX)*



Figure A.2-2: *Oxidized spots in sandy sediments around 42 m (Drive XXXI)*



Figure A.2-3: Pebbles around 48 m (Drive XXXV)



Figure A.2-4: Organic-rich layer around 35.5 m (Drive XXVIII)



Figure A.2-5: *Polosatic (vertical ice bands) cryostructure around 27 m (Drive XXIII)*



Figure A.2-6: *Pure ice around 22.6 m (Drive XX)*



Figure A.2-7: Cryoturbation, vertical contact of silty and sandy material around 30.3 m (Drive XXV)



Table A.2.1: Sediment core description - Samoylov Island sediment core

Sample-ID	Depth		Sub-sample		Packing type	Sediment type		State	Ground ice fabric cryostructure	Organic Matter	Core barrel diameter [mm]
	from	to	from	to		sediment	color				
SAM18-01											
SAM18-01-I	0	8									146
SAM18-01-I	0	3				vegetation, moss to sedge	greenish	frozen			146
SAM18-01-I	3	8				degraded recent vegetation, peaty	brownish	frozen			146
SAM18-01-I			1	0	WHIRLPAK						146
SAM18-01-II	8	82									146
SAM18-01-II	8	22				sandy	grey		in between lenticular layers, macro lenses to banded	at 21: wooden remain	146
SAM18-01-II	22	82	1	8	CORE FOIL	sand, oxidized brownish lenses at 22-27, 2cm wide, horizontal orientated	grey	frozen	non-visible, structureless		146
SAM18-01-III	82	215									146
core loss	202	215									146
SAM18-01-III	82	92				sandy, like above	grey	frozen	macro lenses	wooden remain up to 1 cm diameter	146
SAM18-01-III	92	202				sandy, like above	grey	frozen	non visible to lenticular		146
SAM18-01-III			1	82	CORE FOIL						146
SAM18-01-III			2	105	CORE FOIL						146
SAM18-01-IV	215	315									146
SAM18-01-IV	215	277				broken because wing of an ice wedge					146
SAM18-01-IV	277	300				sand	grey		lenticular to layered, macro lenses and bands, connected	sparse wooden remains	146
SAM18-01-IV	300	315				sand	grey		less ice than above		146

Sample-ID	Depth		Sub-sample			Packing type	Sediment type		State	Ground ice fabric cryostructure	Organic Matter	Core barrel diameter [mm]
	from	to		from	to		sediment	color				
SAM18-01-IV			1	215	245	WHIRLPAK						146
SAM18-01-IV			2	245	265	WHIRLPAK						146
SAM18-01-IV			3	265	277	WHIRLPAK						146
SAM18-01-IV			4	277	315	CORE FOIL						146
SAM18-01-V	315	405										146
SAM18-01-V	315	335					sand	grey		ice rich, layered, diagonal oriented bands due to ice wedge uplift	organic remains	146
SAM18-01-V	335	380					sand	grey		ice rich, macro lenses to ataxitic	organic remains	146
SAM18-01-V	380	405					sand	grey		bit less ice	lot of organic, also diagonal oriented, same direction as bands above	146
SAM18-01-V			1	315	405	CORE FOIL						146
SAM18-01-VI	405	515										146
SAM18-01-VI	405	515					sand, to cm thick sand layer at 430	brownish grey		structureless to lenticular, agglomerates of ice non connected	down to 429 more wood, below: more peat, in general organic rich	146
SAM18-01-VI			1	405	487	CORE FOIL						146
SAM18-01-VI			2	487	515	CORE FOIL						146

Sample-ID	Depth		Sub-sample		Packing type	Sediment type sediment	color	state	Ground ice fabric cryostructure	Organic Matter	core barrel diameter [mm]
	from	to		from to							
SAM18-01-VII	515	635									127
SAM18-01-VII	515	528				peat dominated sand	brownish grey		lenticular, very ice rich, macro lenses	peaty	
SAM18-01-VII	528	540				sandy silt	grey		lenticular to layered, macro lenses oriented to bands	organic remains	
SAM18-01-VII	540	635				peat dominated sand	brownish grey		in general: lenticular, ice rich, 580 to 598: close to vertical oriented lenses (vertical)	peaty	
SAM18-01-VII			1	515	CORE FOIL						
SAM18-01-VII			2	580	CORE FOIL						
SAM18-01-VIII	635	725									
SAM18-01-VIII	635	706				peat dominated sand	brownish grey		: lenticular, ice rich,		
SAM18-01-VIII	706	725				silty sand	grey				
SAM18-01-VIII			1	635	CORE FOIL						
SAM18-01-IX	725	875									
SAM18-01-IX	725	733				peaty sand	brownish grey		non visible, ice rich	peaty	
SAM18-01-IX	733	775				sandy, peat dominated	brownish grey		lenticular	peaty, at 760 wooden remain of 1.5 cm length	
SAM18-01-IX	775	782				sand interlayered	grey		non visible		
SAM18-01-IX	782	790				sandy, peat dominated	brownish grey		lenticular		
SAM18-01-IX	790	802				sandy	grey		lenticular	brown band at 794	
SAM18-01-IX	802	834				peat wit sandy layer of 3 cm thickness at 811, 819, 826	grey		very ice rich	peaty	

Sample-ID	Depth		Sub-sample		Packing type	Sediment type		State	Ground ice fabric cryostructure	Organic Matter	Core barrel diameter [mm]
	from	to				sediment	color				
SAM18-01-IX	834	837				sand interlayer	grey		non visible		
SAM18-01-IX	837	875				sand with peaty layers at 843, 857, 870					
SAM18-01-IX			1	725	CORE FOIL						
SAM18-01-IX			2	800	CORE FOIL						
SAM18-01-X	875	963									
SAM18-01-X	875	890				peaty	greyish brown		ice rich but structureless	peat	
SAM18-01-X	890	963				sand	grey		ice rich, macro lenses, 2 ice bands of 1 cm thickness at 918 and 920	organic remain at 913, piece of woo 7 cm long and 3 cm thick, horizontal, in general organic rich and macro remains	
SAM18-01-X			1	875	CORE FOIL						
SAM18-01-XI	963	1083									
SAM18-01-XI	963	980				sandy	dark grey		ice rich, lenticular to layered, 3 bands 0.5 cm thick at 968, 973, 978, in between lenticular		
SAM18-01-XI	980	995				sand	grey		structureless		
SAM18-01-XI	995	1006				sand	grey		micro lenticular, dense		
SAM18-01-XI	1006	1017				sand	grey		structureless		
SAM18-01-XI	1017	1083				sandy	grey		lenticular, ice rich layer 2cm	woody remains up to 2 cm diameter 1044	

Sample-ID	Depth		Sub-sample		Packing type	Sediment type		State	Ground ice fabric cryostructure	Organic Matter	Core barrel diameter [mm]
	from	to	from	to		sediment	color				
SAM18-01-XI			1	1024	CORE FOIL						
SAM18-01-XI			2	1083	CORE FOIL						
SAM18-01-XII	1083	1212									
SAM18-01-XII	1083	1212				sandy	grey		lenticular, macro lenses	wooden remains, 1090 1cm long, 0.5 thick, 1116, 4 cm long diagonal, 1124: 4 cm long diagonal	
SAM18-01-XII			1	1148	CORE FOIL						
SAM18-01-XII			2	1212	CORE FOIL						
SAM18-01-XIII	1212	1415									
core loss	1388	1415									
SAM18-01-XIII	1212	1225				sandy	dark grey		structureless	peat inclusions	
SAM18-01-XIII	1225	1235				sandy silt			lenticular, sparse macro lenses		
SAM18-01-XIII	1235	1388				sandy	grey		structureless	macro remain at 1288, 1383	
SAM18-01-XIII			1	1212	CORE FOIL						
SAM18-01-XIII			2	1299	CORE FOIL						
SAM18-01-XIV	1388	1452									
SAM18-01-XIV	1452	1452									
SAM18-01-XIV			1	1388	CORE FOIL	sandy	grey		non visible	woody remains	

Sample-ID	Depth		Sub-sample		Packing type	Sediment type		State	Ground ice fabric cryostructure	Organic Matter	Core barrel diameter [mm]
	from	to	from	to		sediment	color				
SAM18-01-XV	1452	1695							general_ non visible- ice layers at: 1483, micro lense, 1573-74, micro lenses, 1607: micro lenses, 1765 to 73: 2 diagonal macro lenses	woody remains all across the core, especially large at 1514 5 cm long, 1637: the very bottom is especially organic rich	
SAM18-01-XV	1695	1695				sandy					
SAM18-01-XV			1	1452	1547						
SAM18-01-XV			2	1547	1616	CORE FOIL					
SAM18-01-XV			3	1616	1695	CORE FOIL					
SAM18-01-XVI	1640	1830									
SAM18-01-XVI	1640	1744				sand	grey		ice rich interlayers, lenticular	woody remains across the core	
SAM18-01-XVI	1744	1815				sand	grey		structureless, macro lenses and ice band between 1794-98	woody remains across the core	
SAM18-01-XVI	1815	1827				coarser sand	grey		non visible	woody remains across the core	
SAM18-01-XVI	1827	1830				sand	gray		micro lenticular		
SAM18-01-XVI			1	1640	1742	CORE FOIL					
SAM18-01-XVI			2	1742	1830	CORE FOIL					
SAM18-01-XVII	1830	1870									

Sample-ID	Depth		Sub-sample		Packing type	Sediment type		State	Ground ice fabric cryostructure	Organic Matter	Core barrel diameter [mm]
	from	to	from	to		sediment	color				
SAM18-01-XVII	1830	1870				medium sand	grey		non visible	general: woody remains across the core, 1833, circle shaped object 2cm diameter, 1849-53: dense woody remain layer	
SAM18-01-XVII			1	1830 1870	CORE FOIL						
SAM18-01-XVIII	1870	2075									
SAM18-01-XVIII	1870	1950				silty sand, with coarse sand interlayers of , at 1888: 0.5 cm thick, 1934- 1938	grey, coarse sand is lighter		non visible	woody remains in silty interlayers	
SAM18-01-XVIII	1950	1987				coarser sand than above	grey		non visible	1 wooden remain at 1957	
SAM18-01-XVIII	1987	2017				silty sand with sand interlayers, 1997-2002	grey		non visible	wooden remains across, especially in sand interlayer	
SAM18-01-XVIII	2017	2053				medium sand	grey		non visible	sparse black dots up to 3 mm diameter	
SAM18-01-XVIII	2053	2075				sand with peat			non visible	lots of organic	
SAM18-01-XVIII			1	1870 1913	CORE FOIL						
SAM18-01-XVIII			2	1913 2011	CORE FOIL						
SAM18-01-XVIII			3	2011 2075	CORE FOIL						
SAM18-01-XIX	2075	2230									

Sample-ID	Depth		Sub-sample			Packing type	Sediment type		State	Ground ice fabric cryostructure	Organic Matter	Core barrel diameter [mm]
	from	to		from	to		sediment	color				
SAM18-01-XIX	2075	2127					sandy matrix with silty organic rich interlayers of 1 cm thickness at 2083, 93, 99, 2111			non visible	stem or twig at 2087, 2 cm diameter, ice lense on top, also 3 cm diameter wood a 2114, surrounded by an ice lense	
SAM18-01-XIX	2127	2157					silty sand like silt band above			non visible	2150: 5 cm organic remain	
SAM18-01-XIX	2157	2204					sandy matrix with silty organic rich interlayers of 1 cm thickness at 2163, 2170, 85, 93			non visible	2202: 4 cm remain	
SAM18-01-XIX	2204	2230					sandy with organic rich ice layer, especial 2213-2230, broken parts because ice rich			ice rich and micro lenticular		
SAM18-01-XIX			1	2075	2140	CORE FOIL						
SAM18-01-XIX			2	2140	2213	CORE FOIL						
SAM18-01-XIX			3	2213	2230	WHIRLPAK						
SAM18-01-XX	2230	2375										
SAM18-01-XX	2230	2284					ice sand mixture, drilling crashed ice/compacted snow			pure ice between 2247 and 60, freshwater ice	sparse wooden remains	
SAM18-01-XX	2284	2343					frozen peat			ice rich	peat	
SAM18-01-XX	2343	2375					silty sand			lenticular, vertical lenses, horizontal bands	brown spots close to ice lenses. Likely oxidized, not OM	



Sample-ID	Depth		Sub-sample		Packing type	Sediment type		State	Ground ice fabric cryostructure	Organic Matter	Core barrel diameter [mm]
	from	to	from	to		sediment	color				
SAM18-01-XX			1	2320	CORE FOIL						
SAM18-01-XX			2	2322	CORE FOIL						
SAM18-01-XXI	2375	2454									
Drilling mud, removed	2375	2370				sand	brown		not that ice rich and a bit softer, you can stick the knife a bit in it		
SAM18-01-XXI	2370	2429				sand	brown		ice rich, lenticular, lenses in all orientations		
SAM18-01-XXI	2429	2437				broken parts			ice rich, layers or banded		
SAM18-01-XXI	2437	2465				sand	brownish grey		lenticular, micro lenses, at 2483: ice band diagonal oriented, 1cm thick		
SAM18-01-XXI			1	2370	CORE FOIL						
SAM18-01-XXI			2	2429	CORE FOIL						
SAM18-01-XXII	2454	2615									
SAM18-01-XXII	2454	2527				silty sand getting coarser to the bottom			structureless	wooden remains at 2477, 2525	
SAM18-01-XXII	2527	2615				sad, getting coarser to bottom			structureless		
SAM18-01-XXII			1	2454	CORE FOIL						
SAM18-01-XXII			2	2527	CORE FOIL						

Sample-ID	Depth		Sub-sample		Packing type	Sediment type		State	Ground ice fabric	Organic Matter	Core barrel diameter [mm]
	from	to	from	to		sediment	color				
SAM18-01-XXIII	2615	2795									
SAM18-01-XXIII	2615	2662				medium to coarse sand			ice rich, non visible		
SAM18-01-XXIII	2662	2744				sand, coarse, rocks at 2685 (2cm) 2712 (2 thick, 4 long)			layered, vertical bandy, polosatic (Kunitzky)		
SAM18-01-XXIII	2744	2795				sand, coarse			lots of visible ice bands, up to 1 cm thick		
SAM18-01-XXIII			1	2615 2717	CORE FOIL						
SAM18-01-XXIII			2	2717 2795	CORE FOIL						
SAM18-01-XXIV	2795	2965									
SAM18-01-XXIV	2795	2965				coarse sand			ice rich, vertical bands, up to 1 cm thick		
SAM18-01-XXIV			1	2795 2884	CORE FOIL						
SAM18-01-XXIV			2	2884 2965	CORE FOIL						
SAM18-01-XXV	2965	3085									
SAM18-01-XXV	2965	3034				coarse sand			ice rich, vertical bands, up to 1 cm thick		
SAM18-01-XXV	3034	3085				vertical contact of silty material and coarse sand (Dima: cryoturbation), bottom cross section looks like breccia (picture)			in silty area slightly diagonal oriented micro lenses		

Sample-ID	Depth		Sub-sample			Packing type	Sediment type		State	Ground ice fabric cryostructure	Organic Matter	Core barrel diameter [mm]
	from	to		from	to		sediment	color				
SAM18-01-XXV			1	2965	3021	CORE FOIL						
SAM18-01-XXV			2	3021	3085	CORE FOIL						
SAM18-01-XXVI	3085	3225										
SAM18-01-XXVI		3097					coarse sand and silty contact, like the end of the previous drive					
SAM18-01-XXVI		3024					finer sand than above, dark sediment until 3103 (corr 3102) with interl. lamination (lake phase?), oxidation lenses/parts					
SAM18-01-XXVI		3096					sand, few layers, dark, but further apart than above, same oxidation spots than above			vertical ice band 0.5cm thick		
SAM18-01-XXVI		3225					fine sand, slightly diagonal oriented, dark layer from 3201 to 3217 (corrected 16 cm lower), oxidized parts					
SAM18-01-XXVI			1		3144	CORE FOIL						
SAM18-01-XXVI			2		3225	CORE FOIL						
SAM18-01-XXVII	3225	3415										
SAM18-01-XXVII	3225	3246					finer sand, dark and light laminated, oxidized layers					
SAM18-01-XXVII	3246	3375					coarse sand, 2 diagonal dark black layers of 2mm thickness at 3327 an 3344, oxidized part from 3350 to 3375					

Sample-ID	Depth		Sub-sample		Packing type	Sediment type		State	Ground ice fabric cryostructure	Organic Matter	Core barrel diameter [mm]
	from	to	from	to		sediment	color				
SAM18-01-XXVII	3375	3385				fine sand, darker than above					
SAM18-01-XXVII	3385	3415				coarse sand, oxidized, black dots at 3388					
SAM18-01-XXVII			1	3225 3322	CORE FOIL						
SAM18-01-XXVII			2	3322 3415	CORE FOIL						
SAM18-01-XXVIII	3415	3575									
SAM18-01-XXVIII	3415	3419				fine sand, darker than below					
SAM18-01-XXVIII	3419	3449				very coarse with pebbles up to 2cm diameter					
SAM18-01-XXVIII	3449	3488				coarse sand with oxidized parts					
SAM18-01-XXVIII	3488	3512				coarse sand with slightly diagonal coalish woody remains, black, in bands, pebble at 3509 (1 cm diameter)					
SAM18-01-XXVIII	3512	3517				pebble 6x4cm				slightly diagonal coalish black layers at 3548, 3555	
SAM18-01-XXVIII	3517	3575				coarse sand with oxidized parts, pebble at 3550					
SAM18-01-XXVIII			1	3415 3512	CORE FOIL						
SAM18-01-XXVIII			2	3512 3517	WHIRLPAK						
SAM18-01-XXVIII			3	3517 3575	CORE FOIL						

Sample-ID	Depth		Sub-sample		Packing type	Sediment type		State	Ground ice fabric cryostructure	Organic Matter	Core barrel diameter [mm]
	from	to	from	to		sediment	color				
SAM18-01-XXIX	3575	3760									
SAM18-01-XXIX	3575	3760					coarse sand, oxidized parts, coarser horizon at 3718 - 3760	grey	ice band, 0.5 cm thick at 3704	org rich layer at 3581 (3cm thick with large remain (2cm diameter), detail photo	
SAM18-01-XXIX			1	3575	3663	CORE FOIL					
OSL sample			2	3663	3686	CORE FOIL					
SAM18-01-XXIX			3	3686	3760	CORE FOIL					
SAM18-01-XXX	3760	4045									
SAM18-01-XXX	3760	3784					coarse sand, oxidized parts				
SAM18-01-XXX	3784	3787					organic layer like at 3581			org rich layer (3cm thick with large remain (2cm diameter)	
SAM18-01-XXX	3787	3807					silty lense in sand, 3802-3807 laminated silt (2mm thick organic dark and lighter bands, possibly cryoturbation				
SAM18-01-XXX	3807	4045					sandy, oxidized parts, special: 3890 - 3904, slightly diagonal dark (org) bands; 4027: org black dots	grey			
SAM18-01-XXX			1	3760	3846	CORE FOIL					
SAM18-01-XXX			2	3846	3920	CORE FOIL					
SAM18-01-XXX			3	3920	3989	CORE FOIL					
SAM18-01-XXX			4	3989	4045	CORE FOIL					

Sample-ID	Depth		Sub-sample		Packing type	Sediment type		State	Ground ice fabric cryostructure	Organic Matter	Core barrel diameter [mm]
	from	to		from to		sediment	color				
SAM18-01-XXXI	4045	4235									
SAM18-01-XXXI	4045	4055					coarse sand, oxidized parts, gravely up to 1 cm thick				
core loss	4055	4098									
SAM18-01-XXXI	4098	4235					coarse sand, oxidized parts, 4124: stone (4x4 cm), oxidized parts 4189-4200				
SAM18-01-XXXI			1	4045	4055	CORE FOIL					
SAM18-01-XXXI			2	4055	4098	WHIRLPAK					
SAM18-01-XXXI			3	4098	4175	CORE FOIL					
SAM18-01-XXXI			4	4175	4235	CORE FOIL					
SAM18-01-XXXII	4235	4445									
core loss											
SAM18-01-XXXII	4235	4400					coarse sand, oxidized parts				
SAM18-01-XXXII	4400	4445					coarse sand, oxid. parts, silty lenses: 4403-4430; black layers in sandy matrix: 4405-4409, single layers up to 0.5 cm thick			grey	
SAM18-01-XXXII			1	4235	4245	CORE FOIL					
SAM18-01-XXXII			2	4254	4350	CORE FOIL					
SAM18-01-XXXII			3	4360	4445	CORE FOIL					

Sample-ID	Depth		Sub-sample		Packing type	Sediment type		State	Ground ice fabric cryostructure	Organic Matter	Core barrel diameter [mm]
	from	to	from	to		sediment	color				
SAM18-01-XXXIII	4445	4570									
core loss	4545	4570									
SAM18-01-XXXIII	4445	4460					sand, bin finer than below				
SAM18-01-XXXIII	4460	4545					coarse sand, pebbles up to 2x1 cm, 4 times visible, more in the core	grey		4537-39: 2cm layer of coaly wooden remains	
SAM18-01-XXXIII			1	4445	CORE FOIL						
SAM18-01-XXXIV	4570	4690									
SAM18-01-XXXIV	4570	4670									
core loss											
SAM18-01-XXXIV			1	4570	WHIRLPAK		metamorphic rock, calcareous, large stones, bigger than the core diameter, up to 5 cm thick, smaller pebbles round shapes				
SAM18-01-XXXIV											
SAM18-01-XXXV	4690	4855									89
SAM18-01-XXXV	4690	4747					fluvial gravel, 0.5cm, partly rounded				89
SAM18-01-XXXV	4747	4813					finer material, coarse sand matrix with smaller pebbles than above				89
SAM18-01-XXXV	4813	4830					rounded pebbles up 6cm diameter				89
SAM18-01-XXXV	4830	4842					(core part ) coarse sand matrix with pebbles, oxidized parts	grey	vertical ice bands up to 3mm thick		89

Sample-ID	Depth		Sub-sample		Packing type	Sediment type		State	Ground ice fabric cryostructure	Organic Matter	Core barrel diameter [mm]
	from	to	from	to		sediment	color				
SAM18-01-XXXV	4842	4855				one clayish sand stone, aleurite, destroyed by manual hammering (Dima)					147
SAM18-01-XXXV			1	4690	4747	WHIRLPAK					
SAM18-01-XXXV			2	4747	4780	WHIRLPAK					
SAM18-01-XXXV			3	4780	4813	WHIRLPAK					
SAM18-01-XXXV			4	4813	4830	WHIRLPAK					
SAM18-01-XXXV			5	4830	4842	WHIRLPAK					
SAM18-01-XXXV			6	4842	4855	WHIRLPAK					
SAM18-01-XXXVI	4855	5010									108
core loss	4855	4910									108
SAM18-01-XXXVI	4910	4930					dark grey with brown grey interl of 0.5cm thick				108
SAM18-01-XXXVI	4930	4940					dark grey with brown grey interl of 0.5cm thick				108
SAM18-01-XXXVI	4940	4955					dark grey with brown grey interl of 0.5cm thick				108
SAM18-01-XXXVI	4955	4961					plate like (schuppenartig) organic parts, organic layer				108



Sample-ID	Depth		Sub-sample		Packing type	Sediment type		State	Ground ice fabric cryostructure	Organic Matter	Core barrel diameter [mm]
	from	to	from	to		sediment	color				
SAM18-01-XXXVI	4961	5010				coarse sand, darker band from 4064 to 69 (organic?)	grey				108
SAM18-01-XXXVI			1	4910 5010	CORE FOIL						108
SAM18-01-XXXVII	5010	5110									108
SAM18-01-XXXVII	5010	5035				coarse sand, oxidized parts					
SAM18-01-XXXVII	5035	5057				mix of sand an silt, partly rounded pebbles up to 1 cm		unfrozen due to drilling			
SAM18-01-XXXVII	5057	5077				mix of sand an silt, partly rounded pebbles up to 1 cm		unfrozen due to drilling			
SAM18-01-XXXVII	5077	5094									
SAM18-01-XXXVII	5094	5110									
SAM18-01-XXXVII			1	5010 5035	CORE FOIL						
SAM18-01-XXXVII			2	5035 5057							
SAM18-01-XXXVII			3	5057 5077							
SAM18-01-XXXVII			4	5077 5094							
SAM18-01-XXXVII			5	5094 5110							
SAM18-01-XXXVIII	5110	5195						unfrozen due to drilling heat			
SAM18-01-XXXVIII	5110	5195				sandy with many partly rounded pebbles, big pebble of 10 cm diameter at 5175-5185		unfrozen due to drilling heat			
SAM18-01-XXXVIII			1	5110 5140	CORE FOIL						

Sample-ID	Depth		Sub-sample			Packing type	Sediment type		State	Ground ice fabric cryostructure	Organic Matter	Core barrel diameter [mm]
	from	to		from	to		sediment	color				
SAM18-01-XXXVIII			2	5140	5165	CORE FOIL						
SAM18-01-XXXVIII			3	5165	5195	CORE FOIL						
SAM18-01-XXXIX	5195	5265						unfrozen due to drilling heat				
SAM18-01-XXXIX	5195	5265					silts matrix with pebbles, rounded, at 5202 to 08: pebble bigger than core diameter	unfrozen due to drilling heat				
SAM18-01-XXXIX			1	5195	5265	CORE FOIL		unfrozen due to drilling heat				
SAM18-01-XL	5265	5535						mainly unfrozen				
SAM18-01-XL	5535	5535					sandy sediments, pebbles up to 2 cm diameter, partly rounded, pebbles in part 5282, 5207, up to 8 cm, big stone at very bottom at 5330: 6cm; lower part from 5530 to b was bit coarser matrix	Parts retrieved frozen: 5317-5338, 5376-5380, 5513-5535, rest unfrozen				
SAM18-01-XL			1	5265	5280	WHIRLPAK						
SAM18-01-XL			2	5280	5307	WHIRLPAK						
SAM18-01-XL			3	5307	5338	WHIRLPAK						
SAM18-01-XL			4	5338	5395	WHIRLPAK						
SAM18-01-XL			5	5395	5407	WHIRLPAK						
SAM18-01-XL			6	5407	5440	WHIRLPAK						
SAM18-01-XL			7	5440	5485	WHIRLPAK						
SAM18-01-XL			8	5485	5510	WHIRLPAK						
SAM18-01-XL			9	5510	5535	WHIRLPAK						

Sample-ID	Depth		Sub-sample		Packing type	Sediment type		State	Ground ice fabric cryostructure	Organic Matter	Core barrel diameter [mm]
	from	to	from	to		sediment	color				
SAM18-01-XLI	5535	5620									
SAM18-01-XLII	5535	5620				medium sand, pebbles up to 5cm: 5549 to 5552, also 5559 to 5562, and 5588 to 5591	grey	frozen			
SAM18-01-XLIII			1	5535 5620	CORE FOIL						
SAM18-01-XLIV	5620	5660						unfrozen due to drilling			
SAM18-01-XLV	5620	5660	1	5620 5660	WHIRLPAK	sandy, no stones, very liquid					
SAM18-01-XLVI											
SAM18-01-XLVII	5660	5770									
SAM18-01-XLVIII	5660	5667				bi stone, bigger than core diameter		frozen after being thawed because drilled and retrieved yesterday			
SAM18-01-XLIX	5667	5738				sandy silt, mixed with rounded pebbles up to 3cm	grey	frozen			
SAM18-01-XLV	5738	5770				bit more silty than part above		frozen			
SAM18-01-XLVI			1	5660 5770	CORE FOIL						
SAM18-01-XLVII	5770	5800									
SAM18-01-XLVIII	5770	5800				gravel in sand with silty composed, one big rounded pebble, 4x3		unconsolidated, overheated, not wet			

Sample-ID	Depth		Sub-sample		Packing type	Sediment type		State	Ground ice fabric cryostructure	Organic Matter	Core barrel diameter [mm]
	from	to	from	to		sediment	color				
SAM18-01-XLV			1	5770	5788	CORE FOIL					
SAM18-01-XLV			2	5788	5800	CORE FOIL					
SAM18-01-XLVI	5800	5865									
SAM18-01-XLVI	5800	5865					sand, upper part up to 5814; bit wetter; 2 rocks at 5815, 5830 of 8x6 cm, pebbles up to 2 cm	unfrozen, overheated			
SAM18-01-XLVI			1	5800	5830	WHIRLPAK					
SAM18-01-XLVI			2	5830	5865	WHIRLPAK					
SAM18-01-XLVII	5865	5965									
SAM18-01-XLVII	5865	5965					sand, from 5910 to 5965: rounded pebbles up to 7x5cm, in the part between 5910 and 5930: a bit frozen	unfrozen due to drilling, wet			
SAM18-01-XLVII			1	5865	5910	WHIRLPAK					
SAM18-01-XLVII			2	5910	5930	WHIRLPAK					
SAM18-01-XLVII			3	5930	5965	WHIRLPAK					
SAM18-01-XLVIII	5965	6185									
SAM18-01-XLVIII	5965	6185					silty sand, rounded pebbles up to 10 cm diameter	unfrozen due to drilling, wet			
SAM18-01-XLVIII			1	5965	5992	WHIRLPAK					
SAM18-01-XLVIII			2	5992	6020	WHIRLPAK					

Sample-ID	Depth		Sub-sample			Packing type	Sediment type		State	Ground ice fabric cryostructure	Organic Matter	Core barrel diameter [mm]
	from	to		from	to		sediment	color				
SAM18-01-XLVIII			3	6020	6075	WHIRLPAK						
SAM18-01-XLVIII			4	6075	6105	WHIRLPAK						
SAM18-01-XLVIII			5	6105	6140	WHIRLPAK						
SAM18-01-XLVIII			6	6140	6185	WHIRLPAK						
SAM18-01-XLIX	6185	6245										
SAM18-01-XLIX	6185	6245					silty sand with rounded pebbles up to 10x5 cm,	unfrozen due to drilling				
SAM18-01-XLIX			1	6185	6215	WHIRLPAK						
SAM18-01-XLIX			2	6215	6245	WHIRLPAK						
SAM18-01-L	6245	6285										
SAM18-01-L	6245	6285					silty sand with rounded pebbles, up to 6cm	unfrozen due to drilling, very wet, material surplus, drilling mud incl?				
SAM18-01-L			1	6245	6260	WHIRLPAK						
SAM18-01-L			2	6260	6285	WHIRLPAK						
SAM18-01-LI	6285	6325										
core loss	6295	6325										
SAM18-01-LI	6285	6295					no sediment matrix, but metamorphic rock pebbles, up to 10x10cm, bottom part solid rock, filling the core diam.,					
SAM18-01-LI			1	6285	6295	WHIRLPAK						

Sample-ID	Depth		Sub-sample		Packing type	Sediment type		State	Ground ice fabric cryostructure	Organic Matter	Core barrel diameter [mm]
	from	to	from	to		sediment	color				
SAM18-01-LII	6295	6400									
SAM18-01-LII	6295	6400				no sediment matrix, but metamorphic rock pebbles, up to 8x8cm					
SAM18-01-LII			1	6325	6340	WHIRLPAK					
SAM18-01-LIII	6400	6440									
SAM18-01-LIII	6400	6440				silty sand with pebbles likely drilling mud from above or leftovers from the previous drive					
SAM18-01-LIII			1	6400	6425	WHIRLPAK					108
SAM18-01-LIV	6440	6530									127
SAM18-01-LIV	6440	6530				matrix sandy silty, unfrozen part coarser with larger pebbles up to 4 cm. Frozen part are finer		frozen at 6335-6345, 6370-83, 6432-80.			
SAM18-01-LIV			1	6335	6400	CORE FOIL					
SAM18-01-LIV			2	6400	6485	CORE FOIL					
OSL sample				6455	6470						
SAM18-01-LIV			2.2	6470	6485						
SAM18-01-LIV			3	6485	6535	CORE FOIL					

Table A.2.2: Lena sediment core

Sample-ID	Depth		Sub-sample		Packing type	Sediment type		State	Ground ice fabric cryostructure	Organic Matter	Core barrel diameter [mm]
	from	to	from	to		sediment	color				
SAM18-06, Lena River											
SAM18-06-D1	30	90						frozen			146
SAM18-06-D1	30	90				clear ice with a few horizontal cracks and small bubble from 30 to 47		frozen			146
SAM18-06-D1			1	30	90			frozen			146
SAM18-06-D2	90	210			CORE FOIL			frozen			146
core loss	180	210						frozen			146
SAM18-06-D2	90	93				ice, like above		frozen			146
SAM18-06-D2	93	100				silty band with sand interlayer		frozen	macro lenticular	macro remains, peaty in both layers	146
SAM18-06-D2	100	114				sand getting coarser to the bottom, fine to medium, change at 106 cm		frozen			146
SAM18-06-D2	114	126				peaty horizon		frozen	structureless, but ice rich	peaty horizon	146
SAM18-06-D2	126	132				sand and silt layers		frozen	micro lenses in silty part	organic layers and macro remains	146
SAM18-06-D2	132	144				sand getting finer to the bottom, fine to medium, change at 137 cm		frozen			146
SAM18-06-D2	144	150				peat silt sand layers, 1mm thick, laminated, thicker silt layer at the bottom (2cm)		frozen	in the lowest layer, lenticular to reticulate, lenses oriented in all direction		146
SAM18-06-D2	150	180				sand		frozen			146
SAM18-06-D2			1	90	180			frozen			146
					CORE FOIL						

Sample-ID	Depth		Sub-sample		Packing type	Sediment type		State	Ground ice fabric cryostructure	Organic Matter	Core barrel diameter [mm]
	from	to	from	to		sediment	color				
SAM18-06-D3	180	450						frozen			127
core loss	405	450						frozen			127
core loss	370	405						frozen			127
SAM18-06-D3	180	285					fine to medium sand, 205 to 225: coarse sand and fine sand interbedding, 245:silt band, 2 cm thick	frozen			
SAM18-06-D3	285	292					silt layer	frozen	lenticular at top		
SAM18-06-D3	292	324					fine to medium sand 308 to 325: coarse and fine sand interbedding.	frozen			
SAM18-06-D3	324	370					medium to coarse sand	frozen			
SAM18-06-D3			1	180	CORE FOIL	275		frozen			
SAM18-06-D3			2	275	CORE FOIL	370		frozen			
SAM18-06-D4	370	615						frozen			
core loss	545	615						frozen			
SAM18-06-D4	370	388					coarse sand	frozen			
SAM18-06-D4	388	420					silt and fine sand interbedding. From 409 to 412: coarse sand, from 388 to 393 and 414 to 419: silt layers	frozen		406, and 414 organic layer of 0.5 cm thickness	
SAM18-06-D4	420	505					medium to coarse sand	frozen		organic layers down to 460, brownish bands. No layers visible from 460 to 505	
SAM18-06-D4	505	515					silty layer				
SAM18-06-D4	515	535					fine to medium sand, getting coarser downwards				
SAM18-06-D4	535	545					silty, talik/drilling mud (packed separately)	unfrozen		528 to 31: 1 to 2 mm thick dark bands	



Sample-ID	Depth		Sub-sample		Packing type	Sediment type		State	Ground ice fabric cryostructure	Organic Matter	Core barrel diameter [mm]
	from	to	from	to		sediment	color				
SAM18-06-D4			1	370 467	CORE FOIL						
SAM18-06-D4			2	467 535	CORE FOIL						
SAM18-06-D4			3	535 545	CORE FOIL						
SAM18-06-D5+6	595	680						frozen			
SAM18-06-D5+6	595	605				silty			few macro lenses		
SAM18-06-D5+6	605	623				medium sand					
SAM18-06-D5+6	623	638				silty					
SAM18-06-D5+6	638	680				medium to coarse sand					
SAM18-06-D5+6			1	595 680	CORE FOIL						
SAM18-06-D7	680	930									
SAM18-06-D7	680	740				medium to coarse sand		frozen		731: organic band	
SAM18-06-D7	740	784				sand silt bedding, 1mm thick bands					
SAM18-06-D7	784	860				medium to coarse sand	grey			organic lenses up to 2mm, also wooden remain at 835 of 0.5 cm diameter	
SAM18-06-D7	860	875				matrix silty, frozen		frozen	3mm thick ice bands		
SAM18-06-D7	875	910				medium to coarse sand		frozen		organic layer sup to 1cm thick, also 888 to 894: peat layer	
SAM18-06-D7	910	930				silty		maybe unfrozen			

Sample-ID	Depth		Sub-sample			Packing type	Sediment type		State	Ground ice fabric cryostructure	Organic Matter	Core barrel diameter [mm]
	from	to		from	to		sediment	color				
SAM18-06-D7			1	680	783	CORE FOIL						
SAM18-06-D7			2	783	850	CORE FOIL						
SAM18-06-D7			3	850	930	CORE FOIL						
SAM18-06-D8	930	1160										
core loss	1145	1160										
SAM18-06-D8	930	946					medium to coarse sand					
SAM18-06-D8	946	960					silty			958 to 60: organic layers with silt interbedding of 0.5cm thick		
SAM18-06-D8	960	963					medium sand					
SAM18-06-D8	963	973					silt, maybe unfrozen	maybe unfrozen silty part				
SAM18-06-D8	973	980					medium sand	frozen				
SAM18-06-D8	980	989					silt	maybe unfrozen silty part				
SAM18-06-D8	989	1145					medium sand			down to 1000 dense organic layers, wavy, 0.5 cm thick; org. layer between 1027-1031, also from 1093-1095; down to 1037 there is sparse darker layers		
SAM18-06-D8			1	930	1025	CORE FOIL						
SAM18-06-D8			2	1025	1102	CORE FOIL						
SAM18-06-D8			3	1102	1145	CORE FOIL						

Sample-ID	Depth		Sub-sample		Packing type	Sediment type		State	Ground ice fabric cryostructure	Organic Matter	Core barrel diameter [mm]
	from	to	from	to		sediment	color				
SAM18-06-D9	1145	1355									
SAM18-06-D9	1145	1225				medium sand					
SAM18-06-D9	1225	1250				sand and organic bedding up to 1cm thick					
SAM18-06-D9	1250	1303				silt and organic bedding up to 0.5cm thick					
SAM18-06-D9	1303	1318				organics, silt and sand bedding, all wavy					
SAM18-06-D9	1318	1355				silty		ice band of 3mm at 1322			
SAM18-06-D9			1	1145							
SAM18-06-D9			2	1212							
SAM18-06-D9			3	1300							
SAM18-06-D10	1355	1650									
core loss	1420	1650									
SAM18-06-D10	1355	1380				silt					
SAM18-06-D10	1380	1388				sand organic bedding up to 0.5 cm					
SAM18-06-D10	1388	1395				fine to medium sand			2 organic bands in lower 5 cm		
SAM18-06-D10	1395	1405				silt layer		2 ice bands at 1396 and 1401 of 1 mm thickness			
SAM18-06-D10	1405	1420				sand silt interlayers, sand bands starting from 1417					
SAM18-06-D10			1	1355							
SAM18-06-D11	1420	1650									
SAM18-06-D11	1420	1428				silt		ice band of 2mm at 1424			
SAM18-06-D11	1428	1516				silty sand, browner than above			1455: organic layer of 0.5mm thickness		
SAM18-06-D11	1516	1530						organic layer with sand inclusions	low degraded roots and leaves visible		

Sample-ID	Depth		Sub-sample		Packing type	Sediment type		State	Ground ice fabric cryostructure	Organic Matter	Core barrel diameter [mm]
	from	to	from	to		sediment	color				
SAM18-06-D11	1530	1650				dryer sand, broken into parts down to 1597					
SAM18-06-D11			1	1420 1493	CORE FOIL						
SAM18-06-D11			2	1493 1530	CORE FOIL						
SAM18-06-D11			3	1530 1560	WHIRLPAK						
SAM18-06-D11			4	1560 1597	WHIRLPAK						
SAM18-06-D11			5	1597 1650	CORE FOIL						
SAM18-06-D12	1650	1905									
SAM18-06-D12	1650	1652				very low degraded peat				low degraded roots and leaves visible especially	
SAM18-06-D12	1652	1700				peat dominated, with lighter interlayers				peaty layers of 1 cm thick at 1675 and 1694	
SAM18-06-D12	1700	1714								fine sand layer with slightly diag. bands down to 1705: dense horiz. bands	
SAM18-06-D12	1714	1825								medium sand	
SAM18-06-D12	1825	1891								broken into parts, dryer sands	
SAM18-06-D12	1891	1905								dryer sediment, not broken	
SAM18-06-D12			1	1650 1741	CORE FOIL						
SAM18-06-D12			2	1741 1825	CORE FOIL						
SAM18-06-D12			3	1825 1891	WHIRLPAK						
SAM18-06-D12			4	1891 1905	WHIRLPAK						

Sample-ID	Depth		Sub-sample		Packing type	Sediment type		State	Ground ice fabric cryostructure	Organic Matter	Core barrel diameter [mm]
	from	to	from	to		sediment	color				
SAM18-06-D13	1905	2135								water came out of the hole while drilling, transition from frozen to unfrozen	
SAM18-06-D13	1905	1923				fine sand		frozen			
SAM18-06-D13	1923	1970				silty matrix dominating, fine interbedding of silt sand and organic layers		frozen		1966-70: organic horizon	
SAM18-06-D13	1970	2000				medium sand; 1970-78: core shape, down to 2000: hockey puck shaped core		frozen		organic remains	
SAM18-06-D13	2000	2013				medium sand like above, but wetter, transition to talk, half frozen		half frozen			
SAM18-06-D13	2013	2135				same sediments		unfrozen, but some frozen interlayers			
SAM18-06-D13			1	1905	2000	CORE FOIL					
SAM18-06-D13			2	2000	2013	WHIRLPAK					
SAM18-06-D13			3	2013	2055	WHIRLPAK					
SAM18-06-D13			4	2055	2095	WHIRLPAK					
SAM18-06-D13			5	2095	2135	WHIRLPAK					
SAM18-06-D14	2135	2380						unfrozen			
SAM18-06-D14	2135	2155				medium sand, broken into parts		frozen		getting more organic rich downwards, roots an twigs up to 5cm length	
SAM18-06-D14	2155	2180				sandy matrix, transition from sand to organic layer, broken into parts		frozen			

Sample-ID	Depth		Sub-sample		Packing type	Sediment type		State	Ground ice fabric cryostructure	Organic Matter	Core barrel diameter [mm]
	from	to	from	to		sediment	color				
SAM18-06-D14	2180	2243				sandy organic horizon, broken into parts				twigs up to 16 cm long, 1 cm diam.	
SAM18-06-D14	2243	2290				sandy, transition from organic to sandy at 2255, broken into parts					
SAM18-06-D14	2290	2380				sharp transition from sand to silt, silty parts are in core shape				2cm thick organic layers at 2320 and 2370, in the parts between organics up to 2cm long	
SAM18-06-D14			1	2135 2155	WHIRLPAK						
SAM18-06-D14			2	2155 2180	WHIRLPAK						
SAM18-06-D14			3	2180 2210	WHIRLPAK						
SAM18-06-D14			4	2210 2243	WHIRLPAK						
SAM18-06-D14			5	2243 2275	WHIRLPAK						
SAM18-06-D14			6	2275 2290	WHIRLPAK						
SAM18-06-D14			7	2290 2380	CORE FOIL						

Table A.2.3: Sample list of Lena Monitoring series from April 2018 to September 2018

Sample Name	Date & time (local time)	Lat [° N]	Lon [° E]
1	20.4.18 21:00	72.368133	126.469
2	24.4.18 20:30	72.367977	126.46355
3	26.4.18 18:00	72.367972	126.46955
4	30.4.18 12:00	72.367972	126.46955
5	4.5.18 19:00	72.367997	126.49955
6	8.5.18 14:00	72.367977	126.45955
7	12.5.18 10:30	72.367977	126.49955
8	16.5.18 10:00	72.367977	126.49955
9	20.5.18 10:00	72.367977	126.49955
10	24.5.18 12:00	72.367977	126.49955
11	28.5.18 14:00	72.367977	126.49955
12	1.6.18 12:00	72.367977	126.49955
13	5.6.18 13:00	72.367977	126.49955
14	9.6.18 14:00	72.967977	126.49955
15	13.6.18 12:00	72.967977	126.49955
18	17.6.18 12:00	72.967977	126.49955
19	21.6.18 14:00	72.967977	126.49955
20	25.6.18 15:00	72.967977	126.49955
21	29.6.18 11:00	72.967977	126.46955
22	3.7.18 20:00	72.368539	126.4718
23	8.7.18 11:30	72.36779	126.47155
24	12.7.18 8:30	72.36785	126.47227
25	16.7.18 19:00	72.36791	126.4723
26	20.7.18 20:00	72.36792	126.4723
27	26.7.18 19:00	72.36793	126.4725
28	30.7.18 20:05	72.36795	126.4743
29	3.8.18 20:00	72.368524	126.470758
30	7.8.18 21:00	72.368254	126.470458
31	11.8.18 19:00	72.368456	126.476868
32	15.8.18 19:00	72.368958	126.47687
33	19.8.18 19:00	72.36846	126.476868
34	23.8.18 19:00	72.368465	126.476868
35	27.8.18 19:00	72.368465	126.476865
36	1.9.18 19:00	72.368487	126.476879
37	5.9.18 19:00	72.36849	126.476868
38	9.9.18 19:00		
39	13.9.18 19:00		

Table A.2.4: Sample list additional studies in June 2018 by Bennet Juhls

Station	Date	Time	Lat [° N]	Lon [° E]	Site	CTD	Cond. meter	ACS 0.22	ACS 0.45	ACS 0.7	ACS 0.8	ACS unfiltered	COOM bottle	DOC 0.7	DOC 0.45	SPM	Chl a	POC	Isotopes	Cond [µS/cm], Temp [°C]	Radiometry	comments
LE18-01-B	04.07.2018	15:35:00	72.3692	126.4683	Beach Samoylov	1		1	1	1	1	1	1	1	1	1	1	1	1			n
LE18-02-C	05.07.2018	09:58:00	72.3665	126.4677	Center Samoylov Channel	1		1	1	1	1	1	1	1	1	1	1	1	1			n
LE18-03-B	05.07.2018	16:00:00	72.36843	126.47234	Beach Samoylov			1	1	1	1	1	1	1	1				1	CTD didnt work		n
LE18-04-C	06.07.2018	10:01:00	72.3672	126.46584	Center Samoylov Channel	1		1	1	1	1	1	1	1	1	1	1	1	1	CTD didnt properly		n
LE18-05-B	06.07.2018	15:30:00	72.36843	126.47234	Beach Samoylov		1	1	1	1	1	1	1	1	1	1	1	1	1	106,16.2		n
LE18-06-C	07.07.2018	10:30:00	72.36696	126.468	Center Samoylov Channel		1	1	1	1	1	1	1	1	1	1	1	1	1	107,15.7		n
LE18-07-B	07.07.2018	16:00:00	72.36843	126.47234	Beach Samoylov		1	1	1	1	1	1	1	1	1	1	1	1	1	107,15.4		n
LE18-08-B	07.07.2018	20:00:00	72.36843	126.47234	Beach Samoylov		1	1	1	1	1	1	1	1	1	1	1	1	1	108,15.2		n
LE18-09-B	07.07.2018	23:59:00	72.36843	126.47234	Beach Samoylov		1	1	1	1	1	1	1	1	1	1	1	1	1			a lot of sediment from waves
LE18-10-C	08.07.2018	11:15:00	72.36779	126.47155	Center Samoylov Channel		1	1	1	1	1	1	1	1	1	1	1	1	1	108,14.9		The same as 023 from Andrei
LE18-11-B	08.07.2018	16:00:00	72.36843	126.47234	Beach Samoylov		1	1	1	1	1	1	1	1	1	1	1	1	1	109,14.9		
LE18-12-B	08.07.2018	23:59:00	72.36843	126.47234	Beach Samoylov		1	1	1	1	1	1	1	1	1	1	1	1	1			
LE18-13-C	09.07.2018	10:06:00	72.36722	126.46836	Center Samoylov Channel		1	1	1	1	1	1	1	1	1	1	1	1	1	117,15.1		cant read cond. for sure
LE18-14-B	09.07.2018	17:04:00	72.36843	126.47234	Beach Samoylov		1	1	1	1	1	1	1	1	1	1	1	1	1	110,15.5		
LE18-15-C	10.07.2018	09:54:00	72.36741	126.46937	Center Samoylov Channel		1	1	1	1	1	1	1	1	1	1	1	1	1	112,15.9	Ram- ses; air & water	forgot conductivity meter
LE18-16-C	10.07.2018	16:00:00	72.37161	126.45112	Center Samoylov Channel		1	1	1	1	1	1	1	1	1	1	1	1	1			conductivity meter was uncalibrated 0.1
LE18-17-B	11.07.2018	10:00:00	72.36843	126.47234	Beach Samoylov		1	1	1	1	1	1	1	1	1	1	1	1	1	16.2		
LE18-18-B	11.07.2018	15:44:00	72.36843	126.47234	Beach Samoylov		1	1	1	1	1	1	1	1	1	1	1	1	1	113.3, 16.1		very windy, wavy conditions at beach
LE18-20-C	12.07.2018	08:38:00	72.36785	126.47227	Center Samoylov Channel		1	1	1	1	1	1	1	1	1	1	1	1	1	114.3, 16.3		The same as 024 from Andrei
LE18-21-B	12.07.2018	17:00:00	72.36843	126.47234	Beach Samoylov		1	1	1	1	1	1	1	1	1	1	1	1	1			forgot conductivity meter



Station	Date	Time	Lat [° N]	Lon [° E]	Site	CTD	Cond. meter	ACS 0.22	ACS 0.45	ACS 0.7	ACS 0.8	ACS unfiltered	CDOM bottle	DOC 0.7	DOC 0.45	SPM	Chl a	POC	Isotopes	Cond [µS/cm], Temp [°C]	Radio-metry	comments
LE18-22-C	13.07.2018	11:09:00	72.36702	126.47066	Center Samoylov Channel		1	1	1	1	1	1	1	1	1	1	1	1	1	111.7, 16.6		fluorometer logger didnt log
LE18-23-B	14.07.2018	09:00:00	72.36843	126.47234	Beach Samoylov		1	1	1	1	1	1	1	1	1				1	118.5, 16.2		on way back to Tiksi but close to Samoylov
LE18-24-C	15.07.2018	11:00:00	72.36893	126.5202	Center Samoylov Channel			1	1			1	1		1							on way back to Tiksi but close to Samoylov
LE18-24-C	15.07.2018	11:00:00	72.36893	126.5202	Center Samoylov Channel			1	1			1	1		1							on way back to Tiksi but close to Samoylov
LE18-01-T	15.07.2018	11:21:00	72.40237	126.74132				1	1			1	1		1				1			on way back to Tiksi but close to Samoylov
LE18-02-T	15.07.2018	11:50:00	72.39097	127.34133				1	1			1	1		1				1			on way back to Tiksi but close to Samoylov
LE18-03-T	15.07.2018	12:13:00	72.33135	127.77962				1	1			1	1		1				1			on way back to Tiksi but close to Samoylov
LE18-04-T	15.07.2018	12:50:00	72.14143	128.20393				1	1			1	1		1				1			on way back to Tiksi but close to Samoylov
LE18-05-T	15.07.2018	13:16:00	72.02946	128.51956				1	1			1	1		1				1			on way back to Tiksi but close to Samoylov
LE18-06-T	15.07.2018	13:38:00	71.91867	128.5559				1	1			1	1		1				1			on way back to Tiksi but close to Samoylov
LE18-19-L	11.07.2018	15:55:00			Banya Lakes		X			X	X	X	X	X					X	67.6, 10.9		Banya Lake at Ponton
LE18-22-L	12.07.2018	16:30:00	72.36901	126.486	Banya Lake																	Ram- ses Air & water
LE18-01-D	10.07.2018	10:50:00	72.40308	126.66856	Stoib			1	1	1	1	1	1	1	1			1	1			from Niko, 0.8CA is wrong at beginning
LE18-02-D	10.07.2018	11:50:00	72.55391	127.08383	Sardakh			1	1	1	1	1	1	1	1			1	1			from Niko
LE18-03-D	12.07.2018	13:45:00	72°30'22.7"	125°16'57.6"	Oleneskaya			1	1	1	1	1	1	1	1			1	1			

Station	Date	Time	Lat [° N]	Lon [° E]	Site	CTD	Cond. meter	ACS 0.22	ACS 0.45	ACS 0.7	ACS 0.8	ACS unfiltered	CDOM bottle	DOC 0.7	DOC 0.45	SPM	Chl a	POC	Isotopes	Cond [µS/cm], Temp [°C]	Radiometry	comments	
LE18-04-D	10.07.2018	19:30:00	72°17'54.7"	126°03'55.8"	Olenetskaya			1	1	1	1	1	1	1					1				
LE18-05-D	10.07.2018	12:50:00	72°21'44.5"	125°40'17.9"	Olenetskaya			1	1	1	1	1	1	1					1				
LE18-Cr-01	09.07.2018	12:39:00	72°35'32.9"	126°32'57.4"	Creek on Kurugnakh		1		1				1	1					1	30, 6.3			
LE18-Cr-02	09.07.2018	12:45:00	72°34'7.3"	126°31'35.3"	Creek on Kurugnakh		1		1				1	1					1	57, 0.4	photo		
LE18-Cr-03	09.07.2018	13:10:00	72°34'	126°29'12"	Creek on Kurugnakh		1		1				1	1					1	93, 1.0	photo		
LE18-Cr-04	09.07.2018	13:17:00	72°33'24.6"	126°28'66"	Creek on Kurugnakh		1		1				1	1					1	71, 1.6	photo		
LE18-Cr-05	13.07.2018	10:31:00	72°34'11.6"	126°29'38.5"	Creek on Kurugnakh		1		1				1	1					1	0, 0.2	On plateau, 10m inland of cliff	Strong rain 10 min before samplign	
LE18-Cr-06	13.07.2018	10:31:00	72°34'10.2"	126°29'41.7"	Creek on Kurugnakh				1				1	1					1		below cliff break (2m), maybe side channel	Strong rain 10 min before samplign	
LE18-Cr-07	13.07.2018	10:37:00	72°34'09"	126°29'48.3"	Creek on Kurugnakh				1				1	1					1		upper cliff half, maybe side channel	Strong rain 10 min before samplign	
LE18-Cr-08	13.07.2018	10:44:00	72°34'04.5"	126°29'54.7"	Creek on Kurugnakh				1				1	1					1		below steep ice cliff, below waterfall, photo, main channel	Strong rain 10 min before samplign	
LE18-Cr-09	13.07.2018	10:41:00							1				1	1					1				Strong rain 10 min before samplign
LE18-Cr-10	13.07.2018	10:49:00	72°34'00.5"	126°29'7.9"	Creek on Kurugnakh				1				1	1					1				Strong rain 10 min before samplign

Table A.2.5: Sampling stations on channels and ice condition

Date	Channel	Vertical	Latitude [° N]	Longitude [° E]	Max depth of a vertical [m]	Ice thickness [cm]	Snow thickness [cm]	water level on "+" / "-" under ice [cm]
20.04. 2018	Tumatskaya Channel	vertic 1	72.416444	126.458861	9	195	65	+10
21.04. 2018	Main Channel	vertic 1	72.377417	126.760056	15.9	200	55	+5
21.04. 2018	Main Channel	vertic 2	72.376639	126.752472	21.7	160	60	+3
21.04. 2018	Main Channel	vertic 3	72.374833	126.752472	28.5	170	60	+7
22.04. 2018	Main Channel	vertic 4	72.373194	126.746556	21.3	180	30	-5
22.04. 2018	Main Channel	vertic 5	72.371833	126.741361	18	210	15 - 20	-13
24.04. 2018	Bykovskaya Channel	vertic 1	72.412306	126.867306	15.4	215	0 - 12	-15
24.04. 2018	Bykovskaya Channel	vertic 2	72.413806	126.867778	10.4	205	0 - 10	-20
24.04. 2018	Bykovskaya Channel	vertic 3	72.415194	126.8675	5.4	195	0 - 5	-17
25.04. 2018	Olenekskaya Channel	vertic 1	72.297167	126.067278	3.1	200	25	-4

Table A.2.6: Water velocity under ice of channels

Channel	Number of vertical	Max depth [m]	Depth on vertical [m]	Velocity [m/s]
Main Channel	Vertical 1	15.9	0.15H = 3.2	0.043
			0.55H = 7	0.072
			0.85H = 12.5	0.080
			Bottom = 14	0.047
	Vertical 2	21.7	0.15H = 3.5	0.043
			0.55H = 12	0.113
			0.85H = 18	0.113
			Bottom = 21	0.102
	Vertical 3	28.5	0.15H = 5.5	0.113
			0.55H = 14	0.131
			0.85H = 23	0.089
	Vertical 4	21.3	0.15H = 3	0.072
			0.55H = 12	0.093
			0.85H = 18	0.089
			Bottom = 20	0.069
Vertical 5	18	0.15H = 2.7	0.085	
		0.55H = 9.3	0.091	
		0.85H = 15	0.087	
Bykovskaya Channel	Vertical 1	15.4	0.15H = 3	0.176
			0.55H = 7	0.176
			0.85H = 13	0.156
	Vertical 2	10.4	0.15H = 1.5	0.100
			0.55H = 6	0.103
			0.85H = 8.5	0.102
	Vertical 3	5.4	V average	>0.03
Olenekskaya Channel	Vertical 1	3.10	0.15H = 2.1	0.036
			0.55H = 2.5	0.036
			0.85H = 3.0	0.043

Table A.2.7: Hydrochemical samples of the channels. April 2018

Date	Channel	Vertical	Sample depth [m]	pH	Eh [mV]	conductivity [ $\mu$ S/cm]	O <sub>2</sub> under ice, on 2 m depth [mg/L]	O <sub>2</sub> under ice, on 2 m depth [%]	Samples for main ions, nutrient, DOC, CDOM, Isotopes, zooplankton
20.04. 2018	Tumatskaya Channel	vertic 1		7.13	-5	426			+
20.04. 2018	Tumatskaya Channel	vertic 1		7.2	-10	424			+
21.04. 2018	Main Channel	vertic 1	12.5	7.16	-8	463			+
21.04. 2018	Main Channel	vertic 1	3.2	7.31	-17	471			+
21.04. 2018	Main Channel	vertic 2	3.5	7.25	-13	462			
21.04. 2018	Main Channel	vertic 2	21.7	7.25	-13	467			
21.04. 2018	Main Channel	vertic 3	5	7.33	-19	469			Only methane sample
21.04. 2018	Main Channel	vertic 3	14	7.16	-7	464			+
21.04. 2018	Main Channel	vertic 3	24	7.3	-16	463			+
22.04. 2018	Main Channel	vertic 4	3	7.2	-11	460			
22.04. 2018	Main Channel	vertic 4	19	7.23	-12	461			
22.04. 2018	Main Channel	vertic 5	2.7	7.28	-15	459			+
22.04. 2018	Main Channel	vertic 5	15	7.28	-15	459			+
24.04. 2018	Bykovskaya Channel	vertic 1	3	7.4	-22	451	57.4	8.11	+ and methane sample
24.04. 2018	Bykovskaya Channel	vertic 1	7	7.25	-14	642			
24.04. 2018	Bykovskaya Channel	vertic 1	15	7.27	-15	467			Only methane sample
24.04. 2018	Bykovskaya Channel	vertic 2	6	7.25	-14	464			
24.04. 2018	Bykovskaya Channel	vertic 2	1.5	7.23	-13	467	57.7	8.16	+
24.04. 2018	Bykovskaya Channel	vertic 2	9	7.23	-12	464			
24.04. 2018	Bykovskaya Channel	vertic 3	3.5	7.27	-15	467	50.5	7.14	+
25.04. 2018	Oleneskaya Channel	vertic 1	2.1	7.27	-15	443	54.5	7.7	+ and methane sample
25.04. 2018	Oleneskaya Channel	vertic 1	2.1	7.16	-9	441			Only methane sample

+ - samples for all parameters had been taken

Table A.2.8: List of water samples of Samoylov Island lakes, ice condition. April 2018

<b>Date</b>	<b>Name of a lake</b>	<b>Latitude N [°]</b>	<b>Longitude E [°]</b>	<b>Type of a lake genesis</b>	<b>Ice thickness [cm]</b>	<b>Snow thickness on ice, [cm]</b>
19.04.2018	Banya lake 2	72°22 07.2	126°30 05.3	oxbow-thermocarst	193	12 - 20
19.04.2018	Banya lake 3	72°22 13.3	126°30 59.0	oxbow-thermocarst	206	20 - 25
20.04.2018	Northern lake	72°23 03.9	126°29 24.4	thermocarst	220	3 - 5
20.04.2018	Northern-eastern lake	72°23 03.5	126°30 00.4	thermocarst	190	50
20.04.2018	Fish lake	72°22 07.2	126°30 05.3	thermocarst	180	20
23.04.2018	Molo lake	72°22 41.0	126°29 50.2	thermocarst	140	45
23.04.2018	Southern lake	72°22 08.2	126°30 40.8	thermocarst	210	1 - 3
23.04.2018	Eastern lake	72°22 29.9	126°31 05.5	thermocarst	180	90
23.04.2018	Banya 1 lake	72°22 08.2	126°29 11.6	oxbow-thermocarst	200	10

Table A.2.9: Hydrochemical parameters of Samoylov Island lakes. April 2018

Date	Name	Sample depth	pH	Eh [mV]	water temperature [°C]	conductivity [µS/cm]	Dis-solved oxygen water [mg/L]	Dis-solved oxygen water [%]	Samples for main ions, nutrient, DOC, CDOM, Isotopes, zooplankton
19.04.2018	Banya lake 2	1.0	6.65	21	-0.1	162	13.43	91.5	+
19.04.2018	Banya lake 2	6.0	6.60	22	-	146	-	-	+
19.04.2018	Banya lake 2	11.0	6.65	21	1.3	138	10.88	78.5	+
19.04.2019	Banya lake 3	1.0	6.94	5	-0.1	200	10.65	73.2	+
19.04.2020	Banya lake 3	5	6.81	12	-	210	-	-	+
19.04.2021	Banya lake 3	7	6.84	10	1.2	220	8.42	60	+
20.04.2018	Northern lake	1	6.72	19	2.6	129	9.44	69.5	+
20.04.2018	Northern lake	5	6.58	25	-	129	-	-	+
20.04.2018	Northern-eastern lake	1	6.58	26	1.1	272	3.26	24.2	+
20.04.2018	Northern-eastern lake	2.5	6.56	26	-	279	-	-	+
20.04.2018	Fish lake	1	6.77	15	-	134	-	-	+
20.04.2018	Fish lake	6.5	6.7	18	-	134	-	-	+
23.04.2018	Molo lake	0.10	6.75	15	2	168	7.91	57.2	+
23.04.2018	Molo lake	6	6.91	6	-	126	-	-	+
23.04.2018	Southern lake	3.9	6.94	5	1.7	323	9.14	64.3	+
23.04.2018	Eastern lake	3	6.48	32	1.1	110	4.78	65.1	+
23.04.2018	Banya 1 lake	4,2	7.45	-25	1.8	466	3.87	29.7	+

+ - samples for all parameters had been taken

Table A.2.10: List of samples obtained during fieldwork.

Nr	Sample	Date	Type	Use	Depth/ Height from [cm]	Depth/ Height to [cm]	Remarks
1	LD18-SP-1-0	19.04.2018	snow	isotopes	0	19	
2	LD18-SP-1-1	19.04.2018	snow	isotopes	0	30	
3	LD18-SP-1-2	19.04.2018	snow	isotopes	0	20.5	
4	LD18-SP-1-3	19.04.2018	snow	isotopes	0	17	
5	LD18-SP-1-4	19.04.2018	snow	isotopes	0	29	
6	LD18-SP-1-5	19.04.2018	snow	isotopes	0	30	
7	LD18-SP-1-6	19.04.2018	snow	isotopes	0	28	
8	LD18-SP-1-7	19.04.2018	snow	isotopes	0	28,5	
9	LD18-SP-1-8	19.04.2018	snow	isotopes	0	31	
10	LD18-SP-1-9	19.04.2018	snow	isotopes	0	32	
11	LD18-SP-1-10	19.04.2018	snow	isotopes	0	29.5	
12	LD18-SP-1-11	19.04.2018	snow	isotopes	0	28	
13	LD18-SP-1-12	19.04.2018	snow	isotopes	0	26	
14	LD18-SP-1-13	19.04.2018	snow	isotopes	0	24	
15	LD18-SP-1-14	19.04.2018	snow	isotopes	0	23.5	
16	LD18-SP-1-15	19.04.2018	snow	isotopes	0	24.5	
17	LD18-SP-1-16	19.04.2018	snow	isotopes	0	27	
18	LD18-SP-1-17	19.04.2018	snow	isotopes	0	20	
19	LD18-SP-1-18	19.04.2018	snow	isotopes	0	17	
20	LD18-SP-1-19	19.04.2018	snow	isotopes	0	10	
21	LD18-SP-1-20	19.04.2018	snow	isotopes	0	9	
22	LD18-SP-1-21	19.04.2018	snow	isotopes	0	10	
23	LD18-SP-1-0-I1	20.04.2018	snow	isotopes	20	16	
24	LD18-SP-1-0-I2	20.04.2018	snow	isotopes	15	11	
25	LD18-SP-1-0-I3	20.04.2018	snow	isotopes	10	6	
26	LD18-SP-1-0-I4	20.04.2018	snow	isotopes	5	0	
27	LD18-SP-1-1-I1	20.04.2018	snow	isotopes	30	26	
28	LD18-SP-1-1-I2	20.04.2018	snow	isotopes	25	21	
29	LD18-SP-1-1-I3	20.04.2018	snow	isotopes	20	16	
30	LD18-SP-1-1-I4	20.04.2018	snow	isotopes	15	11	
31	LD18-SP-1-1-I5	20.04.2018	snow	isotopes	10	6	
32	LD18-SP-1-1-I6	20.04.2018	snow	isotopes	5	0	
33	LD18-SP-1-2-I1	20.04.2018	snow	isotopes	21	17	
34	LD18-SP-1-2-I2	20.04.2018	snow	isotopes	16	12	
35	LD18-SP-1-2-I3	20.04.2018	snow	isotopes	11	7	
36	LD18-SP-1-2-I4	20.04.2018	snow	isotopes	6	2	
37	LD18-SP-1-4-I1	20.04.2018	snow	isotopes	28	24	
38	LD18-SP-1-4-I2	20.04.2018	snow	isotopes	23	19	
39	LD18-SP-1-4-I3	20.04.2018	snow	isotopes	18	14	
40	LD18-SP-1-4-I4	20.04.2018	snow	isotopes	13	9	
41	LD18-SP-1-4-I5	20.04.2018	snow	isotopes	8	4	
42	LD18-SP-1-6-I1	20.04.2018	snow	isotopes	27	23	
43	LD18-SP-1-6-I2	20.04.2018	snow	isotopes	22	18	
44	LD18-SP-1-6-I3	20.04.2018	snow	isotopes	17	13	
45	LD18-SP-1-6-I4	20.04.2018	snow	isotopes	12	8	
46	LD18-SP-1-6-I5	20.04.2018	snow	isotopes	7	3	
47	LD18-SP-1-8-I1	20.04.2018	snow	isotopes	30	26	
48	LD18-SP-1-8-I2	20.04.2018	snow	isotopes	25	21	
49	LD18-SP-1-8-I3	20.04.2018	snow	isotopes	20	16	
50	LD18-SP-1-8-I4	20.04.2018	snow	isotopes	15	11	



Nr	Sample	Date	Type	Use	Depth/ Height from [cm]	Depth/ Height to [cm]	Remarks
51	LD18-SP-1-8-I5	20.04.2018	snow	isotopes	10	6	
52	LD18-SP-1-8-I6	20.04.2018	snow	isotopes	5	1	
53	LD18-SP-1-10-I1	20.04.2018	snow	isotopes	28	24	
54	LD18-SP-1-10-I2	20.04.2018	snow	isotopes	23	19	
55	LD18-SP-1-10-I3	20.04.2018	snow	isotopes	18	14	
56	LD18-SP-1-10-I4	20.04.2018	snow	isotopes	13	9	
57	LD18-SP-1-10-I5	20.04.2018	snow	isotopes	8	4	
58	LD18-SP-1-10-I6	20.04.2018	snow	isotopes	4	0	
59	LD18-SP-1-12-I1	20.04.2018	snow	isotopes	25	21	
60	LD18-SP-1-12-I2	20.04.2018	snow	isotopes	20	16	
61	LD18-SP-1-12-I3	20.04.2018	snow	isotopes	15.5	11.5	
62	LD18-SP-1-12-I4	20.04.2018	snow	isotopes	11.5	8	
63	LD18-SP-1-12-I5	20.04.2018	snow	isotopes	8	4	
64	LD18-SP-1-12-I6	20.04.2018	snow	isotopes	4	0	
65	LD18-SP-1-14-I1	20.04.2018	snow	isotopes	23	19	
66	LD18-SP-1-14-I2	20.04.2018	snow	isotopes	18	14	
67	LD18-SP-1-14-I3	20.04.2018	snow	isotopes	13	9	
68	LD18-SP-1-14-I4	20.04.2018	snow	isotopes	8	4	
69	LD18-SP-1-14-I5	20.04.2018	snow	isotopes	4	0	
70	LD18-SP-1-16-I1	20.04.2018	snow	isotopes	27	23	
71	LD18-SP-1-16-I2	20.04.2018	snow	isotopes	23	21.5	
72	LD18-SP-1-16-I3	20.04.2018	snow	isotopes	20	16	
73	LD18-SP-1-16-I4	20.04.2018	snow	isotopes	15	11	
74	LD18-SP-1-16-I5	20.04.2018	snow	isotopes	10	6	
75	LD18-SP-1-16-I6	20.04.2018	snow	isotopes	4	0	
76	LD18-SP-1-18-I1	20.04.2018	snow	isotopes	15	12	
77	LD18-SP-1-18-I2	20.04.2018	snow	isotopes	11	7	
78	LD18-SP-1-18-I3	20.04.2018	snow	isotopes	6	1	
79	LD18-SP-1-19-I1	20.04.2018	snow	isotopes	10	5	
80	LD18-SP-1-19-I2	20.04.2018	snow	isotopes	5	0	
81	LD18-SP-1-20-I1	20.04.2018	snow	isotopes	9.5	5	
82	LD18-SP-1-20-I2	20.04.2018	snow	isotopes	5	0	
83	LD18-SP-1-21-I1	20.04.2018	snow	isotopes	10	5	
84	LD18-SP-1-21-I2	20.04.2018	snow	isotopes	5	0	
85	LD18-SP-1-S1	20.04.2018	snow	isotopes			
86	LD18-SP-1-S2	20.04.2018	snow	isotopes			
87	LD18-SP-1-S3	20.04.2018	snow	isotopes			
88	LD18-SP-1-S4	20.04.2018	snow	isotopes			
89	LD18-SP-1-S5	20.04.2018	snow	isotopes			
90	LD18-FCI-1	21.04.2018	frost crack ice	isotopes	-20	-22	referred to wall surface
91	LD18-FCI-2	21.04.2018	frost crack ice	isotopes	-20	-21.5	referred to wall surface
92	LD18-FCS-1	21.04.2018	snow	isotopes	20	6	referred to wall surface
93	LD18-FCD-1	21.04.2018	depth hoar	isotopes	6	0	referred to wall surface
94	LD18-FCS-2	21.04.2018	snow	isotopes	34	18	referred to wall surface
95	LD18-FCD-2	21.04.2018	depth hoar	isotopes	18	0	referred to wall surface
96	LD18-FCS-3	21.04.2018	snow	isotopes	23	10	referred to wall surface
97	LD18-FCS-4	21.04.2018	snow	isotopes	10	7	ice layer, referred to wall surface
98	LD18-FCD-3	21.04.2018	depth hoar	isotopes	7	0	referred to wall surface
99	LD18-FCS-5	21.04.2018	snow	isotopes	21	12	referred to wall surface

Nr	Sample	Date	Type	Use	Depth/ Height from [cm]	Depth/ Height to [cm]	Remarks
100	LD18-FCS-6	21.04.2018	snow	isotopes	12	9	ice layer, referred to wall surface
101	LD18-FCD-4	21.04.2018	depth hoar	isotopes	9	0	referred to wall surface
102	LD18-FCD-5	21.04.2018	depth hoar	isotopes	0	-15	referred to wall surface
103	LD18-FCI-3	21.04.2018	frost crack ice	isotopes	-20	-25	referred to wall surface
104	LD18-FCI-4	21.04.2018	frost crack ice	isotopes	-20	-25	referred to wall surface
105	LD18-FCS-7	21.04.2018	snow	isotopes	28	18	referred to wall surface
106	LD18-FCS-8	21.04.2018	snow	isotopes	18	16	ice layer, referred to wall surface
107	LD18-FCD-6	21.04.2018	depth hoar	isotopes	16	0	referred to wall surface
108	LD18-FCD-7	21.04.2018	depth hoar	isotopes	0	-15	referred to wall surface
109	LD18-FCI-5	22.04.2018	frost crack ice	isotopes	-20	-25	referred to wall surface
110	LD18-FCS-9	22.04.2018	snow	isotopes	20	9	referred to wall surface
111	LD18-FCD-8	22.04.2018	depth hoar	isotopes	9	0	referred to wall surface
112	LD18-FCS-10	22.04.2018	snow	isotopes	15	0	referred to wall surface
113	LD18-FCS-11	22.04.2018	snow	isotopes	0	-3	ice layer, referred to wall surface
114	LD18-FCD-9	22.04.2018	depth hoar	isotopes	-3	-23	referred to wall surface
115	LD18-BH-1-1	23.04.2018	snow	isotopes	0	100	transferred to bottles, see below
116	LD18-BH-1-2	23.04.2018	snow	isotopes	100	105	transferred to bottles, see below
117	LD18-BH-2-1	23.04.2018	pond ice	isotopes	0	40	snow profile pond
118	LD18-BH-3-1	24.04.2018	lake ice	isotopes	0	97	Shallow Lake; transferred to bottles; see below
119	LD18-BH-3-2	24.04.2018	lake ice	isotopes	97	161	Shallow Lake; transferred to bottles; see below
120	LD18-BH-3-3	24.04.2018	lake ice	isotopes	161	201	Shallow Lake; transferred to bottles; see below
121	LD18-BH-3-4	24.04.2018	lake water	isotopes	under	201	
122	LD18-SP-2-0	25.04.2018	snow	isotopes	0	44	
123	LD18-SP-2-1	25.04.2018	snow	isotopes	0	48	
124	LD18-SP-2-2	25.04.2018	snow	isotopes	0	37.5	
125	LD18-SP-2-3	25.04.2018	snow	isotopes	0	28	
126	LD18-SP-2-4	25.04.2018	snow	isotopes	0	50	no density
127	LD18-SP-2-5	25.04.2018	snow	isotopes	0	58	
128	LD18-SP-2-6	25.04.2018	snow	isotopes	0	47	
129	LD18-SP-2-7	25.04.2018	snow	isotopes	0	46.5	
130	LD18-SP-2-8	25.04.2018	snow	isotopes	0	55	
131	LD18-SP-2-9	25.04.2018	snow	isotopes	0	50	
132	LD18-SP-2-10	25.04.2018	snow	isotopes	0	47	
133	LD18-SP-2-11	25.04.2018	snow	isotopes	0	50	
134	LD18-SP-2-12	25.04.2018	snow	isotopes	0	45.5	
135	LD18-SP-2-13	25.04.2018	snow	isotopes	0	43	
136	LD18-SP-2-14	25.04.2018	snow	isotopes	0	46	
137	LD18-SP-2-15	25.04.2018	snow	isotopes	0	47	

Nr	Sample	Date	Type	Use	Depth/ Height from [cm]	Depth/ Height to [cm]	Remarks
138	LD18-SP-2-16	25.04.2018	snow	isotopes	0	46	
139	LD18-SP-2-17	25.04.2018	snow	isotopes	0	29	
140	LD18-SP-2-18	25.04.2018	snow	isotopes	0	10	
141	LD18-SP-2-19	25.04.2018	snow	isotopes	0	10	
142	LD18-SP-2-20	25.04.2018	snow	isotopes	0	14.5	
143	LD18-SP-2-21	25.04.2018	snow	isotopes	0	13	
144	LD18-SP-2-0-11	26.04.2018	snow	isotopes	46	42	
145	LD18-SP-2-0-12	26.04.2018	snow	isotopes	41	37	
146	LD18-SP-2-0-13	26.04.2018	snow	isotopes	36	32	
147	LD18-SP-2-0-14	26.04.2018	snow	isotopes	31	27	
148	LD18-SP-2-0-15	26.04.2018	snow	isotopes	26	22	
149	LD18-SP-2-0-16	26.04.2018	snow	isotopes	21	17	
150	LD18-SP-2-0-17	26.04.2018	snow	isotopes	16	12	IL
151	LD18-SP-2-0-18	26.04.2018	snow	isotopes	10	6	DH
152	LD18-SP-2-0-19	26.04.2018	snow	isotopes	5	0	DH
153	LD18-SP-2-1-11	26.04.2018	snow	isotopes	48	44	
154	LD18-SP-2-1-12	26.04.2018	snow	isotopes	43	39	
155	LD18-SP-2-1-13	26.04.2018	snow	isotopes	35	31	IL
156	LD18-SP-2-1-14	26.04.2018	snow	isotopes	29	25	
157	LD18-SP-2-1-15	26.04.2018	snow	isotopes	24	20	
158	LD18-SP-2-1-16	26.04.2018	snow	isotopes	18	14	
159	LD18-SP-2-1-17	26.04.2018	snow	isotopes	8	4	DH
160	LD18-SP-2-1-18	26.04.2018	snow	isotopes	4	0	DH
161	LD18-SP-2-2-11	27.04.2018	snow	isotopes	34	30	loose snow
162	LD18-SP-2-2-12	27.04.2018	snow	isotopes	29	25	loose snow
163	LD18-SP-2-2-13	27.04.2018	snow	isotopes	24	20	compact snow
164	LD18-SP-2-2-14	27.04.2018	snow	isotopes	19	15	compact snow
165	LD18-SP-2-2-15	27.04.2018	snow	isotopes	12	8	
166	LD18-SP-2-2-16	27.04.2018	snow	isotopes	8	4	DH
167	LD18-SP-2-2-17	27.04.2018	snow	isotopes	4	0	DH
168	LD18-SP-2-2-18	27.04.2018	snow	isotopes	14.5	12.5	IL
169	LD18-SP-2-4-11	27.04.2018	snow	isotopes	50	46	loose snow
170	LD18-SP-2-4-12	27.04.2018	snow	isotopes	45	41	loose snow
171	LD18-SP-2-4-13	27.04.2018	snow	isotopes	40	36	loose snow
172	LD18-SP-2-4-14	27.04.2018	snow	isotopes	33	29	compact snow
173	LD18-SP-2-4-15	27.04.2018	snow	isotopes	29	25	compact snow
174	LD18-SP-2-4-16	27.04.2018	snow	isotopes	24	20	softer snow
175	LD18-SP-2-4-17	27.04.2018	snow	isotopes	18	14	compact snow
176	LD18-SP-2-4-18	27.04.2018	snow	isotopes	10	5	DH
177	LD18-SP-2-4-19	27.04.2018	snow	isotopes	5	0	DH
178	LD18-SP-2-6-11	27.04.2018	snow	isotopes	54	50	loose snow
179	LD18-SP-2-6-12	27.04.2018	snow	isotopes	49	45	loose snow
180	LD18-SP-2-6-13	27.04.2018	snow	isotopes	42	38	loose snow
181	LD18-SP-2-6-14	27.04.2018	snow	isotopes	38	34	loose snow
182	LD18-SP-2-6-15	27.04.2018	snow	isotopes	32	28	loose snow
183	LD18-SP-2-6-16	27.04.2018	snow	isotopes	27	23	loose snow
184	LD18-SP-2-6-17	27.04.2018	snow	isotopes	22	18	compact snow incl IL 22-21
185	LD18-SP-2-6-18	27.04.2018	snow	isotopes	17	14	
186	LD18-SP-2-6-19	27.04.2018	snow	isotopes	12	8	DH
187	LD18-SP-2-6-110	27.04.2018	snow	isotopes	8	0	DH
188	LD18-SP-2-8-11	27.04.2018	snow	isotopes	56	52	loose snow

Nr	Sample	Date	Type	Use	Depth/ Height from [cm]	Depth/ Height to [cm]	Remarks
189	LD18-SP-2-8-I2	27.04.2018	snow	isotopes	51	47	loose snow
190	LD18-SP-2-8-I3	27.04.2018	snow	isotopes	46	42	loose snow
191	LD18-SP-2-8-I4	27.04.2018	snow	isotopes	41	37	loose snow
192	LD18-SP-2-8-I5	27.04.2018	snow	isotopes	36	32	loose snow
193	LD18-SP-2-8-I6	27.04.2018	snow	isotopes	31	27	loose snow
194	LD18-SP-2-8-I7	27.04.2018	snow	isotopes	26	22	loose snow
195	LD18-SP-2-8-I8	27.04.2018	snow	isotopes	16	12	old snow
196	LD18-SP-2-8-I9	27.04.2018	snow	isotopes	11	7	compact snow
197	LD18-SP-2-8-I10	27.04.2018	snow	isotopes	5	1	DH
198	LD18-SP-2-8-I11	27.04.2018	snow	isotopes	18.5	17	IL
199	LD18-SP-2-10-I1	27.04.2018	snow	isotopes	52	48	loose snow
200	LD18-SP-2-10-I2	27.04.2018	snow	isotopes	47	43	loose snow
201	LD18-SP-2-10-I3	27.04.2018	snow	isotopes	42	38	loose snow
202	LD18-SP-2-10-I4	27.04.2018	snow	isotopes	37	33	loose snow
203	LD18-SP-2-10-I5	27.04.2018	snow	isotopes	31.5	27.5	loose snow
204	LD18-SP-2-10-I6	27.04.2018	snow	isotopes	27	23	old snow
205	LD18-SP-2-10-I7	27.04.2018	snow	isotopes	23	19	slightly compacted snow
206	LD18-SP-2-10-I8	27.04.2018	snow	isotopes	17	13	sugar snow
207	LD18-SP-2-10-I9	27.04.2018	snow	isotopes	12	8	DH with crust on top
208	LD18-SP-2-10-I10	27.04.2018	snow	isotopes	6	2	DH
209	LD18-SP-2-12-I1	27.04.2018	snow	isotopes	54	50	loose snow
210	LD18-SP-2-12-I2	27.04.2018	snow	isotopes	49	45	loose snow
211	LD18-SP-2-12-I3	27.04.2018	snow	isotopes	44	40	loose snow
212	LD18-SP-2-12-I4	27.04.2018	snow	isotopes	39	35	loose snow
213	LD18-SP-2-12-I5	27.04.2018	snow	isotopes	34	30	slightly compacted snow
214	LD18-SP-2-12-I6	27.04.2018	snow	isotopes	29	25	slightly compacted snow
215	LD18-SP-2-12-I7	27.04.2018	snow	isotopes	23	19	sugar snow
216	LD18-SP-2-12-I8	27.04.2018	snow	isotopes	18	14	sugar snow
217	LD18-SP-2-12-I9	27.04.2018	snow	isotopes	11	7	DH
218	LD18-SP-2-12-I10	27.04.2018	snow	isotopes	5	1	DH
219	LD18-SP-2-14-I1	27.04.2018	snow	isotopes	50	46	loose snow
220	LD18-SP-2-14-I2	27.04.2018	snow	isotopes	45	41	loose snow
221	LD18-SP-2-14-I3	27.04.2018	snow	isotopes	40	36	old snow
222	LD18-SP-2-14-I4	27.04.2018	snow	isotopes	35	31	old snow
223	LD18-SP-2-14-I5	27.04.2018	snow	isotopes	30	26	old snow
224	LD18-SP-2-14-I6	27.04.2018	snow	isotopes	25	21	old snow
225	LD18-SP-2-14-I7	27.04.2018	snow	isotopes	20	16	old snow including IL 17-16
226	LD18-SP-2-14-I8	27.04.2018	snow	isotopes	15	11	DH
227	LD18-SP-2-14-I9	27.04.2018	snow	isotopes	10	6	DH
228	LD18-SP-2-14-I10	27.04.2018	snow	isotopes	5	1	DH
229	LD18-SP-2-16-I1	27.04.2018	snow	isotopes	45	41	loose snow
230	LD18-SP-2-16-I2	27.04.2018	snow	isotopes	40	36	old snow
231	LD18-SP-2-16-I3	27.04.2018	snow	isotopes	35	31	old snow
232	LD18-SP-2-16-I4	27.04.2018	snow	isotopes	30	26	loose snow
233	LD18-SP-2-16-I5	27.04.2018	snow	isotopes	25	21	old snow including crust above DH
234	LD18-SP-2-16-I6	27.04.2018	snow	isotopes	20	16	DH
235	LD18-SP-2-16-I7	27.04.2018	snow	isotopes	15	11	DH
236	LD18-SP-2-16-I8	27.04.2018	snow	isotopes	10	6	DH
237	LD18-SP-2-16-I9	27.04.2018	snow	isotopes	5	1	DH
238	LD18-SP-2-18-I1	27.04.2018	snow	isotopes	19	15	

Nr	Sample	Date	Type	Use	Depth/ Height from [cm]	Depth/ Height to [cm]	Remarks
239	LD18-SP-2-18-I2	27.04.2018	snow	isotopes	13	9	DH
240	LD18-SP-2-18-I3	27.04.2018	snow	isotopes	6	1	DH
241	LD18-SP-2-19-I1	27.04.2018	snow	isotopes	9	6	
242	LD18-SP-2-19-I2	27.04.2018	snow	isotopes	5	1	DH
243	LD18-SP-2-20-I1	27.04.2018	snow	isotopes	15	10	compact snow
244	LD18-SP-2-20-I2	27.04.2018	snow	isotopes	10	5	DH
245	LD18-SP-2-20-I3	27.04.2018	snow	isotopes	5	1	DH
246	LD18-SP-2-21-I1	27.04.2018	snow	isotopes	15	10	compact snow
247	LD18-SP-2-21-I2	27.04.2018	snow	isotopes	10	5	compact snow
248	LD18-SP-2-21-I3	27.04.2018	snow	isotopes	5	0	sugar snow
249	LD18-SP-2-21-I4	27.04.2018	snow	isotopes	6.5	6	IL
250	LD18-FCS-12	28.04.2018	snow	isotopes	27	21	referred to wall surface
251	LD18-FCS-13	28.04.2018	snow	isotopes	21	19	ice layer, referred to wall surface
252	LD18-FCS-14	28.04.2018	snow	isotopes	19	16	referred to wall surface
253	LD18-FCS-15	28.04.2018	snow	isotopes	16	15	ice layer, referred to wall surface
254	LD18-FCD-10	28.04.2018	snow	isotopes	15	0	referred to wall surface
255	LD18-FCD-11	28.04.2018	snow	isotopes	0	-16	referred to wall surface
256	LD18-BH-4-1	29.04.2018	lake ice	isotopes	0	90	
257	LD18-BH-4-2	29.04.2018	lake ice	isotopes	90	181	
258	LD18-BH-5-1	29.04.2018	lake ice	aDNA, isotopes	130	156	
259	LD18-BH-5-2	29.04.2018	lake ice	aDNA, isotopes	156	181	
260	LD18-BH-6-1	29.04.2018	lake ice	isotopes	0	95	
261	LD18-BH-6-2	29.04.2018	lake ice	isotopes	95	150	
262	LD18-BH-6-3	29.04.2018	lake water	isotopes	under	150	
263	LD18-BH-7-1	29.04.2018	lake ice	isotopes	0	93	
264	LD18-BH-7-2	29.04.2018	lake ice	isotopes	93	123	
265	LD18-FCS-16	29.04.2018	snow	isotopes	48	41	referred to trough bottom
266	LD18-FCS-17	29.04.2018	snow	isotopes	41	32	referred to trough bottom
267	LD18-FCS-18	29.04.2018	snow	isotopes	32	30	ice layer, referred to trough bottom
268	LD18-FCD-12	29.04.2018	snow	isotopes	30	20	referred to trough bottom
269	LD18-FCD-13	29.04.2018	snow	isotopes	20	10	referred to trough bottom
270	LD18-FCD-14	29.04.2018	snow	isotopes	10	0	referred to trough bottom
271	LD18-FCS-19	30.04.2018	snow	isotopes	31	24	referred to trough bottom
272	LD18-FCD-15	30.04.2018	snow	isotopes	24	12	referred to trough bottom
273	LD18-FCD-16	30.04.2018	snow	isotopes	12	0	referred to trough bottom
274	LD18-FCS-20	30.04.2018	snow	isotopes	16	10	referred to trough bottom
275	LD18-FCD-17	30.04.2018	snow	isotopes	10	0	referred to trough bottom

Nr	Sample	Date	Type	Use	Depth/ Height from [cm]	Depth/ Height to [cm]	Remarks
276	LD18-FCS-21	30.04.2018	snow	isotopes	42	21	referred to trough bottom
277	LD18-FCS-22	30.04.2018	snow	isotopes	21	20	referred to trough bottom, IL
278	LD18-FCD-18	30.04.2018	snow	isotopes	20	0	referred to trough bottom
279	LD18-FCS-23	30.04.2018	snow	isotopes	32	23	referred to trough bottom
280	LD18-FCS-24	30.04.2018	snow	isotopes	23	22	referred to trough bottom, IL
281	LD18-FCS-25	30.04.2018	snow	isotopes	22	13.5	referred to trough bottom
282	LD18-FCS-26	30.04.2018	snow	isotopes	13.5	13	referred to trough bottom, IL
283	LD18-FCD-19	30.04.2018	snow	isotopes	13	0	referred to trough bottom
284	LD18-FCS-27	30.04.2018	snow	isotopes	12	8	referred to trough bottom
285	LD18-FCS-28	30.04.2018	snow	isotopes	8	6	referred to trough bottom, IL
286	LD18-FCS-29	30.04.2018	snow	isotopes	31	16	referred to trough bottom
287	LD18-FCS-30	30.04.2018	snow	isotopes	16	13	referred to trough bottom
288	LD18-FCS-31	30.04.2018	snow	isotopes	13	10	referred to trough bottom, IL
289	LD18-FCD-20	30.04.2018	snow	isotopes	10	0	referred to trough bottom
290	LD18-FCD-21	30.04.2018	snow	isotopes	12	0	referred to trough bottom
291	LD18-FCS-32	30.04.2018	snow	isotopes	37	12	referred to trough bottom
292	LD18-FCD-22	30.04.2018	snow	isotopes	10	0	referred to trough bottom
293	LD18-FCS-33	30.04.2018	snow	isotopes	10.5	10	referred to trough bottom, IL
294	LD18-FCS-34	30.04.2018	snow	isotopes	26	10.5	referred to trough bottom
295	LD18-FCS-35	30.04.2018	snow	isotopes	32	26.5	referred to trough bottom
296	LD18-FCS-36	30.04.2018	snow	isotopes	26.5	25	referred to trough bottom, IL
297	LD18-FCD-23	30.04.2018	snow	isotopes	25	15	referred to trough bottom
298	LD18-FCD-24	30.04.2018	snow	isotopes	15	0	referred to trough bottom
299	LD18-SP-3-0	02.05.2018	snow	isotopes	0	39	
300	LD18-SP-3-1	02.05.2018	snow	isotopes	0	44	
301	LD18-SP-3-2	02.05.2018	snow	isotopes	0	30	
302	LD18-SP-3-3	02.05.2018	snow	isotopes	0	26	
303	LD18-SP-3-4	02.05.2018	snow	isotopes	0	49,5	
304	LD18-SP-3-5	02.05.2018	snow	isotopes	0	62	
305	LD18-SP-3-6	02.05.2018	snow	isotopes	0	54	

Nr	Sample	Date	Type	Use	Depth/ Height from [cm]	Depth/ Height to [cm]	Remarks
306	LD18-SP-3-7	02.05.2018	snow	isotopes	0	54	
307	LD18-SP-3-8	02.05.2018	snow	isotopes	0	56,5	
308	LD18-SP-3-9	02.05.2018	snow	isotopes	0	51	
309	LD18-SP-3-10	02.05.2018	snow	isotopes	0	50	
310	LD18-SP-3-11	02.05.2018	snow	isotopes	0	51	
311	LD18-SP-3-12	02.05.2018	snow	isotopes	0	47.5	
312	LD18-SP-3-13	02.05.2018	snow	isotopes	0	46	
313	LD18-SP-3-14	02.05.2018	snow	isotopes	0	50	
314	LD18-SP-3-15	02.05.2018	snow	isotopes	0	55.5	
315	LD18-SP-3-16	02.05.2018	snow	isotopes	0	53	
316	LD18-SP-3-17	02.05.2018	snow	isotopes	0	26.5	
317	LD18-SP-3-18	02.05.2018	snow	isotopes	0	7	
318	LD18-SP-3-19	02.05.2018	snow	isotopes	0	9	
319	LD18-SP-3-20	02.05.2018	snow	isotopes	0	13	
320	LD18-SP-3-21	02.05.2018	snow	isotopes	0	15	
321	LD18-FCS-37	02.05.2018	snow	isotopes	25	16	referred to trough bottom
322	LD18-FCS-38	02.05.2018	snow	isotopes	16	14	referred to trough bottom, IL
323	LD18-FCD-25	02.05.2018	snow	isotopes	14	0	referred to trough bottom
324	LD18-FCI-6	02.05.2018	snow	isotopes	6	2	referred to trough bottom, ice plug
325	LD18-FCS-39	02.05.2018	snow	isotopes	-	-	referred to trough bottom
326	LD18-FCD-26	02.05.2018	snow	isotopes	-	-	referred to trough bottom
327	LD18-FCI-7	02.05.2018	snow	isotopes	-	-	referred to trough bottom, ice plug
328	LD18-FCS-40	02.05.2018	snow	isotopes	24	21	referred to trough bottom
329	LD18-FCD-27	02.05.2018	snow	isotopes	21	0	referred to trough bottom
330	LD18-FCI-8	02.05.2018	snow	isotopes	-	-	referred to trough bottom, ice plug
331	LD18-FCS-41	02.05.2018	snow	isotopes	24	13	referred to trough bottom
332	LD18-FCD-28	02.05.2018	snow	isotopes	13	0	referred to trough bottom
333	LD18-SP-3-0-I1	04.05.2018	snow	isotopes	38	36	crust
334	LD18-SP-3-0-I2	04.05.2018	snow	isotopes	35	31	loose snow
335	LD18-SP-3-0-I3	04.05.2018	snow	isotopes	30	26	loose snow
336	LD18-SP-3-0-I4	04.05.2018	snow	isotopes	25	21	compacted snow
337	LD18-SP-3-0-I5	04.05.2018	snow	isotopes	17	16	ice layer
338	LD18-SP-3-0-I6	04.05.2018	snow	isotopes	15	11	depth hoar
339	LD18-SP-3-0-I7	04.05.2018	snow	isotopes	10	6	depth hoar
340	LD18-SP-3-0-I8	04.05.2018	snow	isotopes	5	1	depth hoar
341	LD18-SP-3-1-I1	04.05.2018	snow	isotopes	41	40	crust
342	LD18-SP-3-1-I2	04.05.2018	snow	isotopes	36	31	loose snow
343	LD18-SP-3-1-I3	04.05.2018	snow	isotopes	30	26	loose snow
344	LD18-SP-3-1-I4	04.05.2018	snow	isotopes	26	22	compacted snow
345	LD18-SP-3-1-I5	04.05.2018	snow	isotopes	22	21	ice layer

Nr	Sample	Date	Type	Use	Depth/ Height from [cm]	Depth/ Height to [cm]	Remarks
346	LD18-SP-3-1-16	04.05.2018	snow	isotopes	16	12	loose snow
347	LD18-SP-3-1-17	04.05.2018	snow	isotopes	11	7	sugar snow
348	LD18-SP-3-1-18	04.05.2018	snow	isotopes	6	0	depth hoar
349	LD18-SP-3-2-11	04.05.2018	snow	isotopes	36	32	loose snow
350	LD18-SP-3-2-12	04.05.2018	snow	isotopes	31	27	compacted snow
351	LD18-SP-3-2-13	04.05.2018	snow	isotopes	25	24	ice layer
352	LD18-SP-3-2-14	04.05.2018	snow	isotopes	23	19	compacted snow
353	LD18-SP-3-2-15	04.05.2018	snow	isotopes	18	14	compacted snow
354	LD18-SP-3-2-16	04.05.2018	snow	isotopes	14	13	ice layer
355	LD18-SP-3-2-17	04.05.2018	snow	isotopes	13	9	sugar snow
356	LD18-SP-3-2-18	04.05.2018	snow	isotopes	6	2	depth hoar
357	LD18-SP-3-4-11	04.05.2018	snow	isotopes	43	42.5	crust
358	LD18-SP-3-4-12	04.05.2018	snow	isotopes	41	37	loose snow
359	LD18-SP-3-4-13	04.05.2018	snow	isotopes	36	32	loose snow
360	LD18-SP-3-4-14	04.05.2018	snow	isotopes	31	27	loose snow
361	LD18-SP-3-4-15	04.05.2018	snow	isotopes	25	21	compacted snow
362	LD18-SP-3-4-16	04.05.2018	snow	isotopes	18	16.5	ice layer
363	LD18-SP-3-4-17	04.05.2018	snow	isotopes	15	11	compacted snow and depth hoar
364	LD18-SP-3-4-18	04.05.2018	snow	isotopes	9	0	depth hoar
365	LD18-SP-3-6-11	04.05.2018	snow	isotopes	55	54	loose snow
366	LD18-SP-3-6-12	04.05.2018	snow	isotopes	54	52	crust
367	LD18-SP-3-6-13	04.05.2018	snow	isotopes	50	46	loose snow
368	LD18-SP-3-6-14	04.05.2018	snow	isotopes	45	41	loose snow
369	LD18-SP-3-6-15	04.05.2018	snow	isotopes	39	35	loose snow
370	LD18-SP-3-6-16	04.05.2018	snow	isotopes	33	29	loose snow
371	LD18-SP-3-6-17	04.05.2018	snow	isotopes	27	23	loose snow
372	LD18-SP-3-6-18	04.05.2018	snow	isotopes	23	19	compacted snow
373	LD18-SP-3-6-19	04.05.2018	snow	isotopes	18	14	sugar snow
374	LD18-SP-3-6-110	04.05.2018	snow	isotopes	13	9	depth hoar
375	LD18-SP-3-6-111	04.05.2018	snow	isotopes	6	2	depth hoar
376	LD18-SP-3-8-11	04.05.2018	snow	isotopes	58	55	crust
377	LD18-SP-3-8-12	04.05.2018	snow	isotopes	54	50	loose snow
378	LD18-SP-3-8-13	04.05.2018	snow	isotopes	49	48	ice layer
379	LD18-SP-3-8-14	04.05.2018	snow	isotopes	45	41	loose snow
380	LD18-SP-3-8-15	04.05.2018	snow	isotopes	40	36	loose snow
381	LD18-SP-3-8-16	04.05.2018	snow	isotopes	33	32	ice layer
382	LD18-SP-3-8-17	04.05.2018	snow	isotopes	30	26	loose snow
383	LD18-SP-3-8-18	04.05.2018	snow	isotopes	23.5	19.5	loose snow
384	LD18-SP-3-8-19	04.05.2018	snow	isotopes	17	13	ice layer
385	LD18-SP-3-8-110	04.05.2018	snow	isotopes	13	9	sugar snow
386	LD18-SP-3-8-111	04.05.2018	snow	isotopes	5	1	depth hoar
387	LD18-SP-3-10-11	04.05.2018	snow	isotopes	48.5	48	loose snow
388	LD18-SP-3-10-12	04.05.2018	snow	isotopes	48	42	compacted snow with ice layers
389	LD18-SP-3-10-13	04.05.2018	snow	isotopes	40	36	loose snow
390	LD18-SP-3-10-14	04.05.2018	snow	isotopes	34	30	loose snow
391	LD18-SP-3-10-15	04.05.2018	snow	isotopes	29	26.5	ice layer
392	LD18-SP-3-10-16	04.05.2018	snow	isotopes	23	19	sugar snow
393	LD18-SP-3-10-17	04.05.2018	snow	isotopes	18	14	sugar snow
394	LD18-SP-3-10-18	04.05.2018	snow	isotopes	14	11	ice layer
395	LD18-SP-3-10-19	04.05.2018	snow	isotopes	8	4	depth hoar



Nr	Sample	Date	Type	Use	Depth/ Height from [cm]	Depth/ Height to [cm]	Remarks
396	LD18-SP-3-10-I10	04.05.2018	snow	isotopes	3	0	ice layer on pond ice
397	LD18-SP-3-14-I1	04.05.2018	snow	isotopes	49.5	48.5	crust
398	LD18-SP-3-14-I2	04.05.2018	snow	isotopes	46	42	loose snow
399	LD18-SP-3-14-I3	04.05.2018	snow	isotopes	41	37	loose snow
400	LD18-SP-3-14-I4	04.05.2018	snow	isotopes	35	31	loose snow
401	LD18-SP-3-14-I5	04.05.2018	snow	isotopes	29	25	loose snow
402	LD18-SP-3-14-I6	04.05.2018	snow	isotopes	24	20	loose snow
403	LD18-SP-3-14-I7	04.05.2018	snow	isotopes	19	16	ice layer
404	LD18-SP-3-14-I8	04.05.2018	snow	isotopes	12	8	depth hoar
405	LD18-SP-3-14-I9	04.05.2018	snow	isotopes	5	1	depth hoar
406	LD18-SP-3-16-I1	04.05.2018	snow	isotopes	53.5	52.5	crust
407	LD18-SP-3-16-I2	04.05.2018	snow	isotopes	52	48	loose snow
408	LD18-SP-3-16-I3	04.05.2018	snow	isotopes	47	43	loose snow
409	LD18-SP-3-16-I4	04.05.2018	snow	isotopes	42	38	loose snow with ice layer
410	LD18-SP-3-16-I5	04.05.2018	snow	isotopes	37	33	loose snow
411	LD18-SP-3-16-I6	04.05.2018	snow	isotopes	33	29	loose snow
412	LD18-SP-3-16-I7	04.05.2018	snow	isotopes	29	24	ice layer
413	LD18-SP-3-16-I8	04.05.2018	snow	isotopes	24	20	depth hoar
414	LD18-SP-3-16-I9	04.05.2018	snow	isotopes	12	8	depth hoar
415	LD18-SP-3-16-I10	04.05.2018	snow	isotopes	5	1	depth hoar
416	LD18-SP-3-18-I1	04.05.2018	snow	isotopes	7.5	4	crust
417	LD18-SP-3-18-I2	04.05.2018	snow	isotopes	4	0	depth hoar
418	LD18-SP-3-19-I1	04.05.2018	snow	isotopes	5	0	crust and depth hoar
419	LD18-SP-3-20-I1	04.05.2018	snow	isotopes	12	7	compacted snow and depth hoar
420	LD18-SP-3-20-I2	04.05.2018	snow	isotopes	7	0	compacted snow and depth hoar
421	LD18-SP-3-21-I1	04.05.2018	snow	isotopes	18	12	compacted snow
422	LD18-SP-3-21-I2	04.05.2018	snow	isotopes	12	1	sugar snow
423	LD18-SP-3-21-I3	04.05.2018	snow	isotopes	1	0	ice layer on vegetation
424	LD18-BH-8-1	04.05.2018	river ice	isotopes	0	80	Lena River
425	LD18-BH-8-2	04.05.2018	river ice	isotopes	80	144	Lena River
426	LD18-BH-8-3	04.05.2018	river water	isotopes			Lena River; cond. 453µS
427	LD18-BH-9-1	06.05.2018	lake ice	isotopes	0	91	Shallow/Dry Lake
428	LD18-BH-9-2	06.05.2018	lake ice	isotopes	91	163	Shallow/Dry Lake
429	LD18-BH-9-3	06.05.2018	lake water	isotopes			Shallow/Dry Lake
430	LD18-BH-10-1	06.05.2018	pond ice	isotopes	0	101	pond near snow profile
431	LD18-FCS-42	06.05.2018	snow	isotopes			
432	LD18-FCS-43	06.05.2018	snow	isotopes			ice layer
433	LD18-FCD-29	06.05.2018	depth hoar	isotopes			
434	LD18-FCD-30	06.05.2018	depth hoar	isotopes			
435	LD18-FCI-9	06.05.2018	ice layer	isotopes			
436	LD18-FCI-10	06.05.2018	ice layer	isotopes			
437	LD18-BH-11-1	07.05.2018	lake ice	isotopes	0	92	Larisa Lake II
438	LD18-BH-11-2	07.05.2018	lake ice	isotopes	92	149	Larisa Lake II
439	LD18-BH-11-3	07.05.2018	lake ice	aDNA, isotopes	149	183	Larisa Lake II
440	LD18-BH-11-4	07.05.2018	lake water	isotopes			Larisa Lake II
441	LD18-BH-12-1	07.05.2018	lake ice	isotopes	0	85	Larisa Lake I
442	LD18-BH-12-2	07.05.2018	lake ice	isotopes	85	154	Larisa Lake I

Nr	Sample	Date	Type	Use	Depth/Height from [cm]	Depth/Height to [cm]	Remarks
443	LD18-BH-12-3	07.05.2018	lake ice	aDNA, isotopes	154	176	Larisa Lake I
444	LD18-BH-12-4	07.05.2018	lake ice	aDNA, isotopes	176	200	Larisa Lake I
445	LD18-BH-12-5	07.05.2018	lake ice	isotopes	200	201	Larisa Lake I
446	LD18-BH-12-6	07.05.2018	lake water	isotopes			Larisa Lake I
447	LD18-SP-4-0	09.05.2018	snow	isotopes	0	41	
448	LD18-SP-4-1	09.05.2018	snow	isotopes	0	41	
449	LD18-SP-4-2	09.05.2018	snow	isotopes	0	33	
450	LD18-SP-4-3	09.05.2018	snow	isotopes	0	24	
451	LD18-SP-4-4	09.05.2018	snow	isotopes	0	46	
452	LD18-SP-4-5	09.05.2018	snow	isotopes	0	59	
453	LD18-SP-4-6	09.05.2018	snow	isotopes	0	52	
454	LD18-SP-4-7	09.05.2018	snow	isotopes	0	52	
455	LD18-SP-4-8	09.05.2018	snow	isotopes	0	54	
456	LD18-SP-4-9	09.05.2018	snow	isotopes	0	50	
457	LD18-SP-4-10	09.05.2018	snow	isotopes	0	46	
458	LD18-SP-4-11	09.05.2018	snow	isotopes	0	53	
459	LD18-SP-4-12	09.05.2018	snow	isotopes	0	47	
460	LD18-SP-4-13	09.05.2018	snow	isotopes	0	44	
461	LD18-SP-4-14	09.05.2018	snow	isotopes	0	48	
462	LD18-SP-4-15	09.05.2018	snow	isotopes	0	56	
463	LD18-SP-4-16	09.05.2018	snow	isotopes	0	49	
464	LD18-SP-4-17	09.05.2018	snow	isotopes	0	26	
465	LD18-SP-4-18	09.05.2018	snow	isotopes	0	9	
466	LD18-SP-4-19	09.05.2018	snow	isotopes	0	4.5	
467	LD18-SP-4-20	09.05.2018	snow	isotopes	0	7	
468	LD18-SP-4-21	09.05.2018	snow	isotopes	0	16	
469	LD18-SP-4-0-11	10.05.2018	snow	isotopes	35.5	31.5	compacted and wind drifted snow
470	LD18-SP-4-0-12	10.05.2018	snow	isotopes	31	27	wind drifted snow
471	LD18-SP-4-0-13	10.05.2018	snow	isotopes	26	22	wind drifted snow
472	LD18-SP-4-0-14	10.05.2018	snow	isotopes	21	16	ice layer and snow
473	LD18-SP-4-0-15	10.05.2018	snow	isotopes	15	11	compacted snow
474	LD18-SP-4-0-16	10.05.2018	snow	isotopes	10	6	depth hoar
475	LD18-SP-4-0-17	10.05.2018	snow	isotopes	5	0	depth hoar
476	LD18-SP-4-0-18	10.05.2018	snow	isotopes	37.5	37	loose snow
477	LD18-SP-4-1-11	10.05.2018	snow	isotopes	39	35	loose snow
478	LD18-SP-4-1-12	10.05.2018	snow	isotopes	34	30	loose snow
479	LD18-SP-4-1-13	10.05.2018	snow	isotopes	29	25	compacted snow
480	LD18-SP-4-1-14	10.05.2018	snow	isotopes	24	20	loose snow with ice layer
481	LD18-SP-4-1-15	10.05.2018	snow	isotopes	19	15	loose snow
482	LD18-SP-4-1-16	10.05.2018	snow	isotopes	13	9	loose snow with ice layer
483	LD18-SP-4-1-17	10.05.2018	snow	isotopes	8	4	depth hoar
484	LD18-SP-4-2-11	10.05.2018	snow	isotopes	33	29	compacted and loose snow
485	LD18-SP-4-2-12	10.05.2018	snow	isotopes	28	24	compacted and loose snow
486	LD18-SP-4-2-13	10.05.2018	snow	isotopes	23	19	loose snow
487	LD18-SP-4-2-14	10.05.2018	snow	isotopes	18.5	16	ice layer
488	LD18-SP-4-2-15	10.05.2018	snow	isotopes	15	11	loose snow

Nr	Sample	Date	Type	Use	Depth/ Height from [cm]	Depth/ Height to [cm]	Remarks
489	LD18-SP-4-2-16	10.05.2018	snow	isotopes	8	0	depth hoar
490	LD18-SP-4-4-11	10.05.2018	snow	isotopes	42	40	loose snow and crust
491	LD18-SP-4-4-12	10.05.2018	snow	isotopes	38	34	loose snow
492	LD18-SP-4-4-13	10.05.2018	snow	isotopes	34	30	loose snow
493	LD18-SP-4-4-14	10.05.2018	snow	isotopes	30	26	loose snow
494	LD18-SP-4-4-15	10.05.2018	snow	isotopes	24	20	compacted snow
495	LD18-SP-4-4-16	10.05.2018	snow	isotopes	18	14	compacted snow with ice layer
496	LD18-SP-4-4-17	10.05.2018	snow	isotopes	13	9	depth hoar
497	LD18-SP-4-4-18	10.05.2018	snow	isotopes	8	0	depth hoar
498	LD18-SP-4-4-19	10.05.2018	snow	isotopes	26	25	ice layer
499	LD18-SP-4-6-11	10.05.2018	snow	isotopes	51	49	crust
500	LD18-SP-4-6-12	10.05.2018	snow	isotopes	48	44	loose snow
501	LD18-SP-4-6-13	10.05.2018	snow	isotopes	42.5	38.5	loose snow
502	LD18-SP-4-6-14	10.05.2018	snow	isotopes	37	33	loose snow
503	LD18-SP-4-6-15	10.05.2018	snow	isotopes	31	27	loose snow
504	LD18-SP-4-6-16	10.05.2018	snow	isotopes	26	22	loose and compacted snow
505	LD18-SP-4-6-17	10.05.2018	snow	isotopes	21	17	loose snow
506	LD18-SP-4-6-18	10.05.2018	snow	isotopes	16	12	compacted snow
507	LD18-SP-4-6-19	10.05.2018	snow	isotopes	11	7	depth hoar
508	LD18-SP-4-6-110	10.05.2018	snow	isotopes	6	2	depth hoar
509	LD18-SP-4-8-11	10.05.2018	snow	isotopes	52	47	compacted snow
510	LD18-SP-4-8-12	10.05.2018	snow	isotopes	47	42	compacted and loose snow
511	LD18-SP-4-8-13	10.05.2018	snow	isotopes	42	37	loose snow with ice layer
512	LD18-SP-4-8-14	10.05.2018	snow	isotopes	37	32	loose snow with ice layer
513	LD18-SP-4-8-15	10.05.2018	snow	isotopes	32	27	loose snow
514	LD18-SP-4-8-16	10.05.2018	snow	isotopes	27	22	loose snow with ice layer
515	LD18-SP-4-8-17	10.05.2018	snow	isotopes	22	17	loose and compacted snow
516	LD18-SP-4-8-18	10.05.2018	snow	isotopes	17	12	compacted snow
517	LD18-SP-4-8-19	10.05.2018	snow	isotopes	12	7	loose snow and depth hoar
518	LD18-SP-4-8-110	10.05.2018	snow	isotopes	7	0	depth hoar
519	LD18-SP-4-10-11	10.05.2018	snow	isotopes	46.5	42	compacted snow
520	LD18-SP-4-10-12	10.05.2018	snow	isotopes	42	37	loose snow with ice layer
521	LD18-SP-4-10-13	10.05.2018	snow	isotopes	37	32	loose snow with ice layer
522	LD18-SP-4-10-14	10.05.2018	snow	isotopes	32	27	ice layer
523	LD18-SP-4-10-15	10.05.2018	snow	isotopes	27	22	loose snow
524	LD18-SP-4-10-16	10.05.2018	snow	isotopes	22	17	loose snow with ice layer
525	LD18-SP-4-10-17	10.05.2018	snow	isotopes	17	10	loose and compacted snow
526	LD18-SP-4-10-18	10.05.2018	snow	isotopes	10	5	depth hoar
527	LD18-SP-4-10-19	10.05.2018	snow	isotopes	5	0	depth hoar
528	LD18-SP-4-14-11	10.05.2018	snow	isotopes	48	46	crust

Nr	Sample	Date	Type	Use	Depth/ Height from [cm]	Depth/ Height to [cm]	Remarks
529	LD18-SP-4-14-I2	10.05.2018	snow	isotopes	44	40	loose snow with ice layer
530	LD18-SP-4-14-I3	10.05.2018	snow	isotopes	38	34	loose snow
531	LD18-SP-4-14-I4	10.05.2018	snow	isotopes	33	29	loose snow
532	LD18-SP-4-14-I5	10.05.2018	snow	isotopes	28	24	loose snow
533	LD18-SP-4-14-I6	10.05.2018	snow	isotopes	22	19	ice layer
534	LD18-SP-4-14-I7	10.05.2018	snow	isotopes	19	15	loose snow
535	LD18-SP-4-14-I8	10.05.2018	snow	isotopes	13	9	depth hoar
536	LD18-SP-4-14-I9	10.05.2018	snow	isotopes	8	0	depth hoar
537	LD18-SP-4-16-I1	10.05.2018	snow	isotopes	50	47	crust and loose snow
538	LD18-SP-4-16-I2	10.05.2018	snow	isotopes	47	43	loose and compacted snow
539	LD18-SP-4-16-I3	10.05.2018	snow	isotopes	42	37	loose and compacted snow
540	LD18-SP-4-16-I4	10.05.2018	snow	isotopes	36	32	loose snow
541	LD18-SP-4-16-I5	10.05.2018	snow	isotopes	31	27	loose snow
542	LD18-SP-4-16-I6	10.05.2018	snow	isotopes	26	22	ice layer and depth hoar
543	LD18-SP-4-16-I7	10.05.2018	snow	isotopes	21	13	depth hoar
544	LD18-SP-4-16-I8	10.05.2018	snow	isotopes	13	7	depth hoar
545	LD18-SP-4-16-I9	10.05.2018	snow	isotopes	7	0	depth hoar
546	LD18-SP-4-16-I10	10.05.2018	snow	isotopes	50.2	50	fresh snow
547	LD18-SP-4-18-I1	10.05.2018	snow	isotopes	6.5	5	crust
548	LD18-SP-4-18-I2	10.05.2018	snow	isotopes	5	0	depth hoar
549	LD18-SP-4-19-I1	10.05.2018	snow	isotopes	4.5	0	crust with depth hoar and ice layer
550	LD18-SP-4-20-I1	10.05.2018	snow	isotopes	6	0	crust with depth hoar and ice layer
551	LD18-SP-4-21-I1	10.05.2018	snow	isotopes	17	12	compacted snow with ice layer
552	LD18-SP-4-21-I2	10.05.2018	snow	isotopes	12	1	loose snow
553	LD18-SP-4-21-I3	10.05.2018	snow	isotopes	1	0	depth hoar
554	LD18-FCC-1	05.05.2018	core from frost crack	isotopes			
555	LD18-FCC-2	05.05.2018	core from frost crack	isotopes			
556	LD18-BH-1-I1	08.05.2018	snow	isotopes	0	4	
557	LD18-BH-1-I2	08.05.2018	snow	isotopes	4	8	
558	LD18-BH-1-I3	08.05.2018	snow	isotopes	8	12	
559	LD18-BH-1-I4	08.05.2018	snow	isotopes	12	16	
560	LD18-BH-1-I5	08.05.2018	snow	isotopes	16	20	
561	LD18-BH-1-I6	08.05.2018	snow	isotopes	20	24	
562	LD18-BH-1-I7	08.05.2018	snow	isotopes	24	28	
563	LD18-BH-1-I8	08.05.2018	snow	isotopes	28	32	
564	LD18-BH-1-I9	08.05.2018	snow	isotopes	32	36	
565	LD18-BH-1-I10	08.05.2018	snow	isotopes	36	40	
566	LD18-BH-1-I11	08.05.2018	snow	isotopes	40	44	
567	LD18-BH-1-I12	08.05.2018	snow	isotopes	44	48	
568	LD18-BH-1-I13	08.05.2018	snow	isotopes	48	52	
569	LD18-BH-1-I14	08.05.2018	snow	isotopes	52	56	
570	LD18-BH-1-I15	08.05.2018	snow	isotopes	56	60	
571	LD18-BH-1-I16	08.05.2018	snow	isotopes	60	64	
572	LD18-BH-1-I17	08.05.2018	snow	isotopes	64	68	

Nr	Sample	Date	Type	Use	Depth/ Height from [cm]	Depth/ Height to [cm]	Remarks
573	LD18-BH-1-I18	08.05.2018	snow	isotopes	68	72	
574	LD18-BH-1-I19	08.05.2018	snow	isotopes	72	76	
575	LD18-BH-1-I20	08.05.2018	snow	isotopes	76	80	
576	LD18-BH-1-I21	08.05.2018	snow	isotopes	80	84	
577	LD18-BH-1-I22	08.05.2018	snow	isotopes	84	88	
578	LD18-BH-1-I23	08.05.2018	snow	isotopes	88	93	
579	LD18-BH-3-I1	08.05.2018	lake ice	isotopes	0	4	
580	LD18-BH-3-I2	08.05.2018	lake ice	isotopes	4	8	
581	LD18-BH-3-I3	08.05.2018	lake ice	isotopes	8	13	
582	LD18-BH-3-I4	08.05.2018	lake ice	isotopes	13	15	
583	LD18-BH-3-I5	08.05.2018	lake ice	isotopes	15	19	
584	LD18-BH-3-I6	08.05.2018	lake ice	isotopes	19	23	
585	LD18-BH-3-I7	08.05.2018	lake ice	isotopes	23	28	
586	LD18-BH-3-I8	08.05.2018	lake ice	isotopes	28	33	
587	LD18-BH-3-I9	08.05.2018	lake ice	isotopes	33	38	
588	LD18-BH-3-I10	08.05.2018	lake ice	isotopes	38	42	
589	LD18-BH-3-I11	08.05.2018	lake ice	isotopes	42	44	
590	LD18-BH-3-I12	08.05.2018	lake ice	isotopes	44	48	
591	LD18-BH-3-I13	08.05.2018	lake ice	isotopes	48	53	
592	LD18-BH-3-I14	08.05.2018	lake ice	isotopes	53	56	
593	LD18-BH-3-I15	08.05.2018	lake ice	isotopes	56	58	
594	LD18-BH-3-I16	08.05.2018	lake ice	isotopes	58	62	
595	LD18-BH-3-I17	08.05.2018	lake ice	isotopes	62	64	
596	LD18-BH-3-I18	08.05.2018	lake ice	isotopes	64	69	
597	LD18-BH-3-I19	08.05.2018	lake ice	isotopes	69	72	
598	LD18-BH-3-I20	08.05.2018	lake ice	isotopes	72	75	
599	LD18-BH-3-I21	08.05.2018	lake ice	isotopes	75	79	
600	LD18-BH-3-I22	08.05.2018	lake ice	isotopes	79	84	
601	LD18-BH-3-I23	08.05.2018	lake ice	isotopes	84	88	correct order of pieces?
602	LD18-BH-3-I24	08.05.2018	lake ice	isotopes	88	91	correct order of pieces?
603	LD18-BH-3-I25	08.05.2018	lake ice	isotopes	91	94	correct order of pieces?
604	LD18-BH-3-I26	08.05.2018	lake ice	isotopes	94	97	
605	LD18-BH-3-I27	08.05.2018	lake ice	isotopes	97	100	
606	LD18-BH-3-I28	08.05.2018	lake ice	isotopes	100	104	
607	LD18-BH-3-I29	08.05.2018	lake ice	isotopes	104	107	
608	LD18-BH-3-I30	08.05.2018	lake ice	isotopes	107	111	
609	LD18-BH-3-I31	08.05.2018	lake ice	isotopes	111	114	
610	LD18-BH-3-I32	08.05.2018	lake ice	isotopes	114	118	
611	LD18-BH-3-I33	08.05.2018	lake ice	isotopes	118	122	
612	LD18-BH-3-I34	08.05.2018	lake ice	isotopes	122	126	
613	LD18-BH-3-I35	08.05.2018	lake ice	isotopes	126	131	
614	LD18-BH-3-I36	08.05.2018	lake ice	isotopes	131	137	
615	LD18-BH-3-I37	08.05.2018	lake ice	isotopes	137	141	
616	LD18-BH-3-I38	08.05.2018	lake ice	isotopes	141	145	
617	LD18-BH-3-I39	08.05.2018	lake ice	isotopes	145	148	
618	LD18-BH-3-I40	08.05.2018	lake ice	isotopes	148	152	
619	LD18-BH-3-I41	08.05.2018	lake ice	isotopes	152	155	
620	LD18-BH-3-I42	08.05.2018	lake ice	isotopes	155	158	
621	LD18-BH-3-I43	08.05.2018	lake ice	isotopes	158	161	
622	LD18-BH-3-I44	08.05.2018	lake ice	isotopes	161	165	
623	LD18-BH-3-I45	08.05.2018	lake ice	isotopes	165	169	

Nr	Sample	Date	Type	Use	Depth/ Height from [cm]	Depth/ Height to [cm]	Remarks
624	LD18-BH-3-I46	08.05.2018	lake ice	isotopes	169	174	
625	LD18-BH-3-I47	08.05.2018	lake ice	isotopes	174	178	
626	LD18-BH-3-I48	08.05.2018	lake ice	isotopes	178	182	
627	LD18-BH-3-I49	08.05.2018	lake ice	isotopes	182	185	
628	LD18-BH-3-I50	08.05.2018	lake ice	isotopes	185	189	
629	LD18-BH-3-I51	08.05.2018	lake ice	isotopes	189	193	
630	LD18-BH-3-I52	08.05.2018	lake ice	isotopes	193	197	
631	LD18-BH-3-I53	08.05.2018	lake ice	isotopes	197	201	
632	LD18-FCI-11	11.05.2018	frost crack ice	isotopes			
633	LD18-FCI-12	11.05.2018	frost crack ice	isotopes			
634	LD18-FCS-44	11.05.2018	snow	isotopes			
635	LD18-FCS-45	11.05.2018	snow	isotopes			IL
636	LD18-FCD-31	11.05.2018	depth hoar	isotopes			
637	LD18-FCI-13	11.05.2018	frost crack ice	isotopes			
638	LD18-FCS-46	11.05.2018	snow	isotopes			
639	LD18-FCS-47	11.05.2018	snow	isotopes			IL
640	LD18-FCD-32	11.05.2018	depth hoar	isotopes			
641	LD18-FCD-33	11.05.2018	depth hoar	isotopes			
642	LD18-FCI-14	11.05.2018	frost crack ice	isotopes			
643	LD18-FCI-15	11.05.2018	frost crack ice	isotopes			

Table A.2.11: Sampling protocol. The samples were taken at four sites: 1) Floodplain labelled (FL-L); 2) Floodplain control (FL-C); 3) Polygon center labelled (PC-L); 4) Polygon center control (PC-C)

Date	Sample	Type	Latitude [° N]	Longitude [° E]	Notes
11/07/2018	FL-L D0	Gas, Plant, Soil, Water	N 72.37692	E 126.48230	Labelling FL
	FL-C D0				
12/07/2018	PC-L D0	Gas, Plant, Soil, Water	72.37494	126.48230	Labelling PC
	PC-C D0				
	FL-L D1		72.37692	126.47775	
13/07/2018	FL-L D2	Gas, Plant, Soil, Water	72.37692	126.47775	
	PC-L D1		72.37494	126.48230	
14/07/2018	FL-L D3	Gas, Plant, Soil, Water	72.37692	126.47775	
	FL-C D3				
	PC-L D2		72.37494	126.48230	
	PC-C D2				
16/07/2018	FL-L D5	Gas, Plant, Soil, Water	72.37692	126.47775	
	PC-L D4		72.37494	126.48230	
18/07/2018	FL-L D7	Gas, Plant, Soil, Water	72.37692	126.47775	
	FL-C D7				
	PC-L D6		72.37494	126.48230	
	PC-C D6				
26/07/2018	FL-L D15	Gas, Plant, Soil, Water	72.37692	126.47775	
	FL-C D15				
	PC-L D14		72.37494	126.48230	
	PC-C D14				
03/08/2018	FL-L D23	Gas, Plant, Soil, Water	72.37692	126.47775	
	PC-L D22		72.37494	126.48230	
12/08/2018	FL-L D32	Gas, Plant, Soil, Water	72.37692	126.47775	
	FL-C D32				
	PC-L D31		72.37494	126.48230	
	PC-C D31				
25/08/2018	FL-L D45	Gas, Plant, Soil, Water	72.37692	126.47775	
	PC-L D44		72.37494	126.48230	
12/09/2018	FL-L D63	Gas, Plant, Soil, Water	72.37692	126.47775	
	FL-C D63				
	PC-L D62		72.37494	126.48230	
	PC-C D62				

Table A.2.12: Overview on landscapes, temporal coverage and snow melt and vegetation dynamics events captured by the time-lapse cameras

Time-Lapse Camera (TLC) Code	Event snowmelt	Event vegetation	Temporal Coverage
KUR-TLC-0A thermo-erosional valley	(i) May 25-27 snow melt water ponding starts on valley floor and on Yedoma upland (ii) May 29 snow melting starts on slopes, Yedoma upland becomes snow-free (iii) start of June: Yedoma upland largely snow free, June 9-10 Yedoma upland snow-free (iv) mid of June: steep slopes largely snow free, end of June, snow-free	(i) June 12-13 first leafing out of woody plants (Salix) (ii) June 18 canopy of wooden plants becomes dense (iii) end of June, first week of July: shooting of woody plants and further densification of woody canopy (iv) first week of July shooting of grasses on valley floor	TLC data April 21 to August 16 - no technical problems
KUR-TLC-1A zonal tussock tundra on drained slopes >5°	(i) May 23 snow melt starts on south-west facing slope, snow free within one day (ii) May 25 snow melt starts on north facing slope, snow free within 3 to 5 days at end of May (iii) end of May lower slopes and valley bottom still snow covered 1st week of June. East-facing slope still snow covered. (iv) June 13 melting of last snow patches on east-facing slopes	(i) June 12-13 first leafing out of woody plants (Salix) (ii) June 20 canopy of wooden plants becomes dense, flowering	TLC data April 20 to June 26 stopped in June due to power run out
KUR-TLC-2B moss and wet sedge tundra on Yedoma upland	(i) May 25-27 snow melt water ponding starts on Yedoma upland (ii) end of May, 1 <sup>st</sup> week of June: Yedoma upland ponded. (iii) after June 10 Yedoma upland snow-free and dry (iv) mid of June: steep slopes largely snow free, end of June, snow-free	(i) June 12-13 first leafing out of woody plants (Salix) and flowering (ii) June 20 canopy of wooden plants becomes dense, flowering (iii) end of June, first week of July: shooting of woody plants and further densification of woody canopy (iv) end of July start of autumn coloring (v) mid August autumn color	TLC data April 22 to August 26 - no technical problems



Time-Lapse Camera (TLC) Code	Event snowmelt	Event vegetation	Temporal Coverage
KUR-TLC-3A upper part of thermo-erosional valley, start of drainage system	(i) May 23 snow melt starts on south-facing slope, snow free within one day (ii) May 25 to first week of June slow melting of valley bottom and north-facing slope. (iii) June 10 slopes snow free, valley bottom still snow coverage (iv) June 20-23 snow melt on valley bottom	(i) June 12-13 first leafing out of woody plants (Salix) (ii) June 18 canopy of wooden plants becomes dense (iii) end of June, first week of July: shooting of woody and grassy plants and further densification of woody canopy	TLC data April 19 to June 23 stopped in June due to power run out
KUR-TLC-3IIA first breakpoint of thermo-erosional valley, snow barrier	(i) May 25 to first week of June slow melting of valley bottom and north-facing slope. (ii) mid of June melting of last snow patches on north-facing slopes, still dense snow coverage on valley floor (iii) June 21 to 24 thaw slumping	(i) June 18 canopy of grasses and wooden plants becomes dense	TLC data April 25 to June 24 stopped in June due to power run out
KUR-TLC-4A thermo-erosional valley, view on of steep east facing slope	(i) May 25 to first week of June fast melting of west-facing slope, slow melting of east-facing slope. (ii) mid July melt out of last snow patches on east facing slope	(i) June 12-13 first leafing out of woody plants (Salix) (ii) June 20 canopy of wooden plants becomes dense (iii) end of June, first week of July: shooting of woody plants and further densification of woody canopy (iv) July 20 larger-scale flowering	TLC data April 25 to August 8
KUR-TLC-4B thermo-erosional valley nadir-looking on plot	i) April 27 snow on off on plot, 1-6 snow on off on plot, then snow coverage, May 22 snow melt on plot ii) last snow on/off on June 1	(i) June 10-12 first leafing out of woody plants (Salix) (ii) June 18-20 canopy of wooden plants becomes dense (iii) end of June, first week of July: shooting of woody plants and further densification of woody canopy	TLC data April 25 to August 2 some corrupt data and missing date information

Time-Lapse Camera (TLC) Code	Event snowmelt	Event vegetation	Temporal Coverage
KUR-TLC-5B main drainage valley	<p>(i) May 23 snow melt starts on west-facing slope, May 25 snow melt starts on plateau, May 27 snow melt water in valley</p> <p>(ii) first week of June melting of last snow patches on east-facing slopes</p> <p>(iii) End of May Lena River spring flood intrudes in valley. May 30-31 first flooding, June 2-3 first sediment-loaden river ice, June 5-6 2<sup>nd</sup> flood level high up as the valley shoulders, June 7 sediment-loaden river ice, June 10 to 24 flooded river level goes down, end of June normal drainage and summer water level</p>	<p>(i) June 12-13 first leafing out of woody plants (Salix)</p> <p>(ii) June 20 canopy of wooden plants becomes dense</p> <p>(iii) end of June, first week of July: shooting of woody plants and further densification of woody canopy</p> <p>(iv) 2nd week in July larger-scale flowering of several plant species</p> <p>(v) end of July start of autumn coloring</p> <p>(vi) mid August autumn color</p>	TLC data April 23 to August 22 Block of TLC site tilted on June 10, TLC camera view changed to nearly nadir plot view
KUR-TLC-6B drainage valley	<p>(i) May 23 to first week of June fast melting of west-facing slope, slow melting of east facing slope.</p> <p>(ii) May 30 snow melt water stream on valley bottom, June 6 last snow patches melt on valley floor</p> <p>(iii) June 10-12 high water level</p>	<p>(i) June 13 first leafing out of woody plants (Salix) and flowering</p> <p>(ii) June 18-20 canopy of wooden plants becomes dense, flowering</p> <p>(iii) end of June, first week of July: shooting of woody plants and further densification of woody canopy</p> <p>(iv) end of July start of autumn colouring</p> <p>(v) mid August autumn colour</p>	TLC data April 23 to August 28
SAM-TLC-1B	<p>(i) May 23 start of snow melting</p> <p>(ii) end of May last snow patches in polygonal ridges melting</p> <p>(iii) end of May last pond ice is melting</p>	<p>(i) end of June, canopy development and shooting of few woody plants</p> <p>(ii) first week of July, shooting and canopy development of grasses in polygonal ridges and depressions</p>	TLC data April 22 to August 12

Table A.2.13: Permafrost samples and site characteristics in the central Lena Delta, mainly on Kurungnakh (KUR) Island and Samoylov (SAM) Island. Active layer depth (ALD) was measured during sampling and may not be at its full depth in the beginning of August. Principal Investigator (PI): Matthias Fuchs MF, Alexandra Runge AR, Birgit Heim BH, Stine Holm SH, Leonid Tsibizov LT

Sample Site Code	Latitude [° N]	Longitude [° E]	Date	ALD [cm]	Core Depth [cm]	N (subs.)	Landscape	PI
KUR18-P1-DRY	72.2922	126.1608	01.08.2018	19	107	8	Yedoma upland, dry	MF, AR
KUR18-P2-WET	72.2921	126.1605	01.08.2018	35	50	4	Yedoma upland, wet	MF, AR
KUR18-P3-WET	72.2910	126.1654	01.08.2018	22	111	9	Yedoma upland, shrub tundra, wet	MF, AR
KUR18-P4-SLO	72.2840	126.1955	02.08.2018	52	141	11	tundra slope south-facing	MF, AR
KUR18-P5-SHR	72.2818	126.1941	02.08.2018	59	126.5	11	terrace with shrub communities (<30 cm height)	MF, AR
KUR18-P6-BAY	72.3230	126.2553	03.08.2018	56	99	9	young drained lake, center, Baydzherakhs	MF, AR
KUR18-P7-DTLB	72.3230	126.2555	03.08.2018	35	107	8	young drained lake, center, wet basin floor	MF, AR
KUR18-P8-WET	72.3243	126.2637	04.08.2018	35	102	14	Yedoma upland, wet	MF, AR
KUR18-P9-DRY	72.3244	126.2630	04.08.2018	26	126.5	12	Yedoma upland, dry	MF, AR
KUR18-P10-PIN	72.3020	126.2348	07.08.2018	50	187	15	Pingo in Drained Lake Basin	MF, LT
KUR18-P11-DTLB	72.3044	126.2512	07.08.2018	23	70	5	Drained Lake Basin floor, tussock, dry	MF, AR
KUR18-P12-DTLB	72.3045	126.2510	07.08.2018	18	92	8	Drained Lake Basin floor, tussock, wet	MF, AR
KUR18-P13-YED	72.3292	126.2327	11.08.2018	21	122	17	Yedoma upland	MF, AR, SH
KUR18-P14-SLU	72.3286	126.2305	11.08.2018	67	105	11	Thaw Slump	MF, AR, SH
KUR18-P15-YED	72.3555	126.3124	13.08.2018	45	125	14	degraded Yedoma upland	MF, AR
KUR18-P16-SLO	72.3560	126.3146	13.08.2018	70	125	13	Yedoma slope, northeast facing	MF, AR
KUR18-P17-FLO	72.3566	126.3170	15.08.2018	36	113	15	floodplain, Salix and moss	MF, AR
KUR18-P18-SAN	72.3578	126.3212	15.08.2018	105	80	6	floodplain, sand	MF, AR
KUR18-P19-GRA	72.35 72	126.3192	15.08.2018	82	112	9	floodplain, grass / sedges	MF, AR

Sample Site Code	Latitude [° N]	Longitude [° E]	Date	ALD [cm]	Core Depth [cm]	N (subs.)	Landscape	PI
SAM18-P20-LSH	72.3827	126.4697	16.08.2018	82	120	12	floodplain, low shrubs	MF, AR
SAM18-P21-HST	72.3874	126.4791	17.08.2018	57	105	11	floodplain, moist, with shrub individuals	MF, AR
SAM18-P22-SAN	72.3782	126.4557	17.08.2018	>100	60	5	floodplain, sand	MF, AR
SAM18-P23-STA	72.3729	126.4699	17.08.2018	95	77	8	floodplain, dry ridge with shrub shrub communities	MF, AR
SAM18-P24-NEI	72.3550	126.4800	20.08.2018	54	95	10	floodplain, low shrub communities	MF, AR
SAM18-P25-ABC	72.3565	126.4754	20.08.2018	59	103	11	floodplain, dry, low shrubs	MF, AR
SAM18-P26-ORA	72.3700	126.5165	21.08.2018	>100	97	8	drained lake, grass	MF, AR
SAM18-P27-DBN	72.3818	126.4830	21.08.2018	33	93.5	14	drained thermokarst lake basin	MF, AR
KUR18-P28-MVA	72.3270	126.0481	22.08.2018	34	111	12	drained old Yedoma, slope >5°, dry	MF, AR
KUR18-P29-MVW	72.3269	126.0477	22.08.2018	46	95	15	drained old Yedoma, slope >5°, wet	MF, AR
KUR18-P30-ALA	72.3250	126.0606	22.08.2018	43	119	15	Drained Lake Basin	MF, AR
KUR18-P31-FFA	72.3512	126.1765	25.08.2018	26	26	4	Yedoma upland	MF, AR
KUR18-P32-QFA	72.3506	126.1859	25.08.2018	34	34	3	Yedoma upland	MF, AR
KUR18-P33-R66	72.3505	126.2081	25.08.2018	36	36	4	Drained Lake Basin	MF, AR
SAM18-P34	72.3750	126.4987	29.08.2018	30	30	4	polygonal tundra, Holocene terrace, dry	MF, BH
SAM18-P35	72.3752	126.4986	29.08.2018	52	25	3	polygonal tundra, Holocene terrace, wet	MF, BH

Table A.2.14: Vegetation Plots in the central Lena Delta, mainly on Kurungnakh (KUR) Island and Samoylov (SAM) Island. Coding Region/Topography: Kurungnakh Island KUR, Samoylov Island SAM, Holocene Terrace HOL, Titari Island TIT; Terrace T, Slope S, Alas A, Valley V. Principal Investigators (PI): Iuliia Shevtsova IS, Birgit Heim BH, Matthias Fuchs MF, Alexandra Runge AR, Jan Melchert JM

Sample Site Code	Latitude [° N]	Longitude [° E]	Date	Region Code	Topo Code	Landscape	PI
LD18-VP001	72.292097	126.160662	01.08.2018	KUR	T	Yedoma upland, wet sedge and moss-dominated tundra	IS, AR, MF, BH
LD18-VP002	72.291128	126.165117	01.08.2018	KUR	T	Yedoma upland, wet sedge and moss-dominated tundra	IS AR, MF
LD18-VP003	72.283945	126.195583	02.08.2018	KUR	S	tundra slope south facing	IS, BH
LD18-VP004	72.28179	126.194205	02.08.2018	KUR	T	terrace with shrub communities (<30 cm height)	IS, BH
LD18-VP005	72.32295	126.255394	03.08.2018	KUR	A	young drained lake, center, Baydzherakhs and wet basin floor	IS, BH
LD18-VP006	72.322883	126.258328	03.08.2018	KUR	A	young drained lake, rim with shrub communities(>50 cm height)	IS, BH
LD18-VP007	72.324343	126.263307	04.08.2018	KUR	T	Yedoma upland, wet sedge and moss-dominated tundra	IS, BH
LD18-VP008	72.326548	126.263804	04.08.2018	KUR	T	Yedoma upland, wet sedges and moss-dominated tundra	IS, BH
LD18-VP009	72.305718	126.250636	07.08.2018	KUR	A	Drained Lake Basin floor, tussock	IS, BH
LD18-VP010	72.304288	126.251116	07.08.2018	KUR	A	Drained Lake Basin floor, tussock	IS, BH
LD18-VP011	72.333029	126.281536	08.08.2018	KUR	V	thermoerosion val. southern slope	IS, BH
LD18-VP012	71.967274	127.092825	09.08.2018	TIT	T	Titari Larch forest	IS, JM
LD18-VP013	72.367942	126.257317	10.08.2018	KUR	S	tussock on slope, southwest-facing	IS, BH
LD18-VP014	72.365782	126.273124	10.08.2018	KUR	T	Yedoma upland, wet sedge and moss-dominated tundra	IS, BH

Sample Site Code	Latitude [° N]	Longitude [° E]	Date	Region Code	Topo Code	Landscape	PI
LD18-VP015	72.379485	126.389209	11.08.2018	HOL1	T	polygonal tundra, Holocene terrace	IS, BH
LD18-VP016	72.372855	126.470228	14.08.2018	SAM	F	floodplain, dry ridge with shrub communities	IS, JM, BH
LD18-VP017	72.387377	126.479113	15.08.2018	SAM	F	floodplain, moist Salix, Alder	IS, JM, BH
LD18-VP018	72.366995	126.255062	16.08.2018	KUR	V	grass wetland in drainage valley	IS, JM, BH
LD18-VP019	72.36234	126.26669	16.08.2018	KUR	S	disturbed slope, grasses and shrubs	IS, JM
LD18-VP020	72.324496	126.27312	18.08.2016	KUR	V	thermoerosion val. southern slope	IS, BH
LD18-VP021	72.375011	126.498771	19.08.2018	SAM	T	polygonal tundra, Holocene terrace	IS, BH
LD18-VP022	72.326926	126.047974	22.08.2018	KUR	S	degraded Yedoma on slope, transition to tussock	IS, BH
LD18-VP023	72.326044	126.054439	22.08.2018	KUR	S	degraded Yedoma on slope, transition to tussock	IS, BH
LD18-VP024	72.329226	126.043938	22.08.2018	KUR	V	steep valley slope with high shrub communities (<100 cm)	IS, BH
LD18-VP025	72.328319	126.039712	22.08.2018	KUR	T	terrace with shrub communities (<50 cm)	IS, BH
LD18-VP026	72.376726	126.503866	24.08.2018	SAM	T	polygonal tundra, Holocene terrace	IS, BH
LD18-VP027	72.344306	126.190795	25.08.2018	KUR	T	Yedoma upland wet sedge and moss-dominated tundra	IS, BH

Table A.2.15: Field-spectrometry plots in the central Lena Delta, mainly on Kurungnakh (KUR) Island and Samoylov (SAM) Island. Principal investigators (PI): Alexandra Runge AR, Matthias Fuchs MF, Birgit Heim BH

Sample Site Code	Latitude [° N]	Longitude [° E]	Date	Start (local time)	Stop (local time)	N (measurements)	Landscape	PI
SAM18-SP-001	72.37820	126.45566	06.08.2018	11:17	11:51	194	floodplain, sand	AR, MF
SAM18-SP-002	72.38271	126.46969	06.08.2018	13:13	14:08	206	floodplain, low shrubs	AR, MF
KUR18-SP-003	72.305718	126.250636	07.08.2018	15:00	15:30	89	Drained Lake Basin floor, tussock	AR, BH
KUR18-SP-004	72.304288	126.251116	07.08.2018	15:30	16:00	56	Drained Lake Basin floor, tussock	AR, BH
KUR18-SP-005	72.32301	126.25546	08.08.2018	11:25	11:45	106	young drained lake, Baydzherakhs and wet basin floor	AR, MF
KUR18-SP-006	72.32288	126.25827	08.08.2018	12:00	12:20	106	young drained lake, rim with shrub communities (<50 cm height)	AR, MF
KUR18-SP-007	72.32436	126.26338	08.08.2018	13:53	14:19	106	Yedoma upland, wet sedge and moss-dominated tundra	AR, MF
KUR18-SP-008	72.29214	126.16062	09.08.2018	11:16	11:37	107	Yedoma upland, wet sedge and moss-dominated tundra	AR, MF
KUR18-SP-009	72.29108	126.16534	09.08.2018	12:20	12:45	109	Yedoma upland, wet sedge and moss-dominated tundra	AR, MF
KUR18-SP-010	72.28394	126.1956	09.08.2018	14:18	14:45	111	tundra slope, south-facing	AR, MF
KUR18-SP-011	72.28178	126.19417	09.08.2018	15:05	15:30	108	terrace with shrub field (<30 cm height)	AR, MF F
KUR18-SP-012	72.28242	126.19426	09.08.2018	16:17	16:47	73	terrace, wet patch	AR, MF

Sample Site Code	Latitude [° N]	Longitude [° E]	Date	Start (local time)	Stop (local time)	N (measurements)	Landscape	PI
KUR18-SP-013	72.36581	126.27317	10.08.2018	12:16	12:38	106	Yedoma upland wet sedge and moss-dominated tundra	AR, MF
KUR18-SP-014	72.36234	126.26669	10.08.2018	13:41	14:08	120	disturbed slope grasses and shrubs	AR, MF
KUR18-SP-015	72.36797	126.25732	10.08.2018	15:03	15:25	106	tussock slope, southwest-facing	AR, MF
KUR18-SP-016	72.35656	126.31743	15.08.2018	12:30	12:45	116	floodplain, Salix and moss	AR, MF
KUR18-SP-017	72.35835	126.3217	15.08.2018	13:52	14:02	50	floodplain, sand	AR, MF
SAM18-SP-018	72.38738	126.47912	26.08.2018	09:35	09:55	106	floodplain, moist with shrub individuals	AR, MF
SAM18-SP-019	72.37284	126.47029	26.08.2018	10:57	11:25	106	floodplain, dry ridge with shrub communities	AR, MF
SAM18-SP-020	72.37368	126.47911	26.08.2018	12:18	12:53	106	drained thermokarst lake basin	AR, MF
SAM18-SP-021	72.37093	126.47875	26.08.2018	14:26	14:50	113	drained thermokarst lake basin	AR, MF
KUR18-SP-022	72.28178	126.19417	27.08.2018	10:55	11:17	110	terrace with shrub communities (<30 cm height)	AR, MF
KUR18-SP-023	72.28355	126.19807	27.08.2018	11:50	12:25	118	in between slopes, wet depression	AR, MF
KUR18-SP-024	72.28543	126.19228	27.08.2018	13:46	14:10	108	tundra slope, south-facing	AR, MF
KUR18-SP-025	72.28538	126.18834	27.08.2018	15:05	15:37	106	terrace, wet	AR, MF
KUR18-SP-026	72.32657	126.26369	28.08.2018	11:27	11:50	108	Yedoma upland wet sedge and moss-dominated tundra	AR, MF, BH
KUR18-SP-027	72.32301	126.25546	28.08.2018	12:33	13:10	126	young drained lake, Baydzherakhs and wet basin floor	AR, MF, BH
KUR18-SP-028	72.3234	126.27844	28.08.2018	14:53 228	15:30	109	floodplain, sand	AR, MF, BH



Table A.2.16: KoP1 'assessing above-ground and below-ground carbon': Cross Reference table for field survey plots for permafrost, vegetation and field spectrometry in the central Lena Delta. Coding: Kurungnakh Island KUR, Samoylov Island SAM, Terrace T, Slope S, Alas A, Valley V

Landscape	Region Code	Topo Code	Vegetation Plot Code	Permafrost Sample Code	Spectrometry Plot Code
Yedoma upland	KUR	Y	VP001 [01.08.2018]	P1 dry, P2 wet [01.08.2018]	SP008 [09.08.2018]
Yedoma upland	KUR	Y	VP002 [01.08.2018]	P3 dry [01.08.2018]	SP009 [09.08.2018]
Yedoma upland	KUR	Y	VP007 [04.08.2018]	P8 wet, P9 dry [04.08.2018]	SP007 [08.08.2018]
Yedoma upland	KUR	T	VP027 [25.08.2018]	P31 equivalent [500 m distance, closer to camera] [25.08.2018]	NaN
tundra slope, south facing	KUR	S	VP003 [02.08.2018]	P4 [02.08.2018]	SP024 [27.08.2018]
tussock, southwest-facing	KUR	S	VP013 [10.08.2018]	NaN	SP015 [10.08.2018]
degraded Yedoma on slope, transition to tussock	KUR	S	VP022 [22.08.2018]	P28, P29 [22.08.2018]	NaN
Drained Lake Basin, tussock	KUR	A	VP009	NaN	SP003 [07.08.2018]
Drained Lake Basin, tussock	KUR	A	VP010	/P11, dry; P12, wet [07.08.2018]	SP004 [07.08.2018]
young drained lake, Baydzherakhs, wet basin floor	KUR	L	VP005 [03.08.2018]	P6 Baydzherakh, P7 wet basin floor [03.08.2018]	SP005 [08.08.2018]; SP027 [28.08.2018]
young drained lake, rim with shrub communities (>50 cm height)	KUR	L	VP006 [03.08.2018]	NaN	SP006 [08.08.2019]
terrace with shrub communities (<30 cm height)	KUR	T	VP004 [02.08.2018]	P5 [02.08.2018]	SP011 [09.08.2018]
disturbed slope, grasses and shrubs	KUR	V	VP019 [16.08.2018]	NaN	SP014 [10.08.2018]
floodplain, Salix and moss	KUR	F	NaN	P17 [15.08.2018]	SP016 [15.08.2018]
floodplain, sand	KUR	F	NaN	P18 [15.08.2018]	SP017 [15.08.2018]
floodplain, dry ridge with shrub communities	SAM	F	VP016 [14.08.2018]	P23 [17.08.2018]	SP019 [26.08.2018]
floodplain, moist Salix, Alder	SAM	F	VP017 [15.08.2018]	P21 [17.08.2018]	SP018 [26.08.2018]
floodplain, low shrub communities	SAM	F	NaN	P20 [16.08.2018]	SP002 [06.08.2018]
floodplain, sand	SAM	F	NaN	P22 [17.08.2018]	SP001 [06.08.2018]
polygonal tundra, Holocene terrace	SAM	T	VP021 [19.08.2018]	P34 dry, P35 wet [29.08.2018]	NaN

Table A.2.17: Shrub sampling dates with sites GPS locations. Shrub species marked with colors: *Betula* (green); *Salix* (white); *Rhododendron* (blue); *Larix* (yellow); *Alnus* (grey). Note that at a single location in some cases more than one shrub was sampled.

Sampling Date	Shrub ID	Lat [° N]	Lon [° E]
17.08.18	SB01	72.36809	126.25860
17.08.18	SB16	72.37342	126.26624
18.08.18	1S01	72.32388	126.25084
18.08.18	2S01	72.32455	126.25343
18.08.18	3S01	72.32479	126.25345
18.08.18	3S10	72.32475	126.25394
18.08.18	SB19	72.32489	126.25342
18.08.18	SB23	72.32495	126.25384
21.08.18	SA01	72.38530	126.46684
21.08.18	SA02	72.38797	126.47208
21.08.18	SA03	72.38874	126.47492
21.08.18	SA04	72.38885	126.47789
21.08.18	SA05	72.38927	126.48039
22.08.18	SB27	72.47942	126.26033
22.08.18	SB37	72.48285	126.23113
23.08.18	RODO	72.25195	126.95241
24.08.18	SA06	72.37031	126.47401
24.08.18	SA07	72.37559	126.45789
24.08.18	SA08	72.37675	126.45736
24.08.18	SA11	72.37743	126.45993
24.08.18	SA12	72.37815	126.45966
24.08.18	SA13	72.37798	126.45951
24.08.18	SA14	72.37638	126.46064
25.08.18	SA09	72.37245	126.46205
25.08.18	SA10	72.37383	126.45968
25.08.18	SA15	72.37751	126.46102
25.08.18	Sa30	72.37758	126.46345
25.08.18	SA30A	72.37748	126.46343
25.08.18	SG60	72.37722	126.47918
25.08.18	SG70	72.37959	126.48033
27.08.18	LARIX	72.29198	126.13757
27.08.18	SB42	72.29204	126.16779
28.08.18	SB47	72.36234	126.29316
29.08.18	A011	72.37978	126.47274
29.08.18	A021	72.37995	126.47434
29.08.18	A031	72.37815	126.47301
29.08.18	A041	72.37719	126.47041
29.08.18	A051	72.37690	126.47054
29.08.18	A061	72.37622	126.46941
29.08.18	A071	72.37595	126.46977
29.08.18	A081	72.37489	126.46924
29.08.18	A091	72.37515	126.47347
29.08.18	A101	72.37355	126.47138

Table A.2.18: Station list Lena Delta

Name	Locality	Latitude [°N]	Longitude [°E]	Elevation [m]	s/n seismometer	s/n recorder	Date of Maintenance/ Deployment*/ Recovery <sup>o</sup>	Days of recording
LD010	Tchai-Tumus	72.32605	125.76013	34	1877	DC-766	08.09.2018*	-
LD011	Amerika-Khaya	72.47622	126.27493	73	1170	DC-772	06.09.2018	273
LD015 (B)	GeoCamp	72.11728	126.98167	54	1331a	DC-765	09.09.2018	273
LD016 (C)	By Stolb	72.40001	127.14722	71	1335	DC-767	07.09.2018	282
LD018	White Mountains	71.92932	127.31263	23	1348a	DC-768	09.09.2018*	-
LD019 (D)	Norden-shield	72.07499	128.32480	35	1342a	DC-764	12.09.2018	283
LD031	Stolb - Red Hut	72.40492	126.82227	15	-	-	07.09.2018 <sup>o</sup>	273
LD032	Stolb - Hill	72.39762	126.80732	71	-	-	07.09.2018 <sup>o</sup>	273
LD033	Stolb - Cliff	72.40308	126.79687	57	1178	DC-773	07.09.2018	282

Table A.2.19: Station list Buor-Khaya Bay

Name	Locality	Latitude [°N]	Longitude [°E]	Elevation [m]	s/n seismometer	s/n recorder	Date of Deployment*
BK001	Buor-Khaya Bay 1	-	-	-	-	-	-
BK002	Buor-Khaya Bay 2	-	-	-	-	-	-
BK003	Buor-Khaya Bay 3	70.85862	130.86668	24	1876	DC-770	07.09.2018*
BK004	Buor-Khaya Bay 4	71.06300	130.16185	16	1888	DC-771	07.09.2018*
BK005	Buor-Khaya Bay 5	71.40152	129.40797	13	1887	DC-775	11.09.2018*
BK006	Buor-Khaya Bay 6	71.81162	129.33142	33	1336	DC-774	09.09.2018*
BK007	Buor-Khaya Bay 7	71.57902	130.01262	1	1190	DC-769	06.09.2018*

Table A.2.20: Station list Tiksi array

Name	Locality	Latitude [°N]	Longitude [°E]	Elevation [m]	s/n seis- mometer	s/n recorder	Date of Maintenance	Days of recording
TIK01	central station	71.57404	129.07278	135	1831	DC-613	06.09.18	273
TIK02	inner circle	71.57619	129.06778	139	1889	DC-611	06.09.18	157
TIK03	inner circle	71.57623	129.07838	131	1895	DC-861	07.09.18	282
TIK04	inner circle	71.57397	129.08076	136	2828	DC-860	07.09.18	282
TIK05	inner circle	71.57166	129.07796	140	2829	DC-617	07.09.18	282
TIK06	inner circle	71.57156	129.06871	121	2860	DC-616	09.09.18	282
TIK07	inner circle	71.57433	129.06503	119	4191	DC-863	13.09.18	282
TIK08	outer circle	71.58415	129.06926	85	4192	DC-862	12.09.18	273
TIK09	outer circle	71.57856	129.09906	98	2830	DC-614	12.09.18	224
TIK10	outer circle	71.56872	129.09734	120	1015	DC-610	12.09.18	283
TIK11	outer circle	71.56288	129.07483	146	2895	DC-868	13.09.18	230
TIK12	outer circle	71.57182	129.04309	50	1007	DC-866	13.09.18	82
TIK13	outer circle	71.58188	129.04929	109	3052	DC-867	13.09.18	282

Table A.2.21: Sample list of sediment samples and pore ice field data from Sobo-Sise Island 2018 (m bs – meter below surface, m arl – meter above river level, wt% – weight percentage).

Sample ID	Date	depth [m bs]	height [m arl]	Ice content, absolute [wt%]	Bio- marker	Iso- topes	DOC	cDOM	Hydro- chemistry	EC [µS/cm]	pH
Profile SOB18-01 (N 72.53877°, E 128.27983°)											
Yedoma IC deposits, Yedoma top, cliff height of 24.2 m arl											
SOB18-01-01	14.07.18	0.1	24.1	na							
SOB18-01-02	14.07.18	0.5	23.7	80	x	x	x	x	x		
SOB18-01-03	14.07.18	1	23.2	41		x					
SOB18-01-04	14.07.18	1.5	22.7	47	x	x					
SOB18-01-05	14.07.18	2	22.2	61	x	x					
SOB18-01-06	14.07.18	2.5	21.7	51	x	x	x	x	x		
SOB18-01-07	14.07.18	3	21.2	47		x					
SOB18-01-08	14.07.18	3.5	20.7	52	x	x	x	x	x		
SOB18-01-09	14.07.18	4	20.2	33							
SOB18-01-10	14.07.18	4.5	19.7	40	x	x	x				
SOB18-01-11	14.07.18	5	19.2	40		x					
SOB18-01-12	14.07.18	5.5	18.7	45	x	x	x	x	x		
SOB18-01-13	14.07.18	6	18.2	54		x					
SOB18-01-14	14.07.18	6.5	17.7	40	x	x	x				
SOB18-01-15	14.07.18	7	17.2	42		x					
SOB18-01-16	14.07.18	7.5	16.7	42	x	x	x	x	x		
SOB18-01-17	14.07.18	8	16.2	51		x					
SOB18-01-18	14.07.18	8.5	15.7	20	x	x	x				
Profile SOB18-03 (N 72.53877°, E 128.28012°)											
Yedoma IC deposits, Yedoma top, cliff height of 24.2 m arl											
SOB18-03-01	16.07.18	6	18.2	35		x					
SOB18-03-02	16.07.18	6.5	17.7	44		x	x				
SOB18-03-03	16.07.18	7	17.2	52	x	x					
SOB18-03-04	16.07.18	7.5	16.7	24		x	x	x	x		
SOB18-03-05	16.07.18	8	16.2	73	x						
SOB18-03-06	16.07.18	8.5	15.7	55		x	x				
SOB18-03-07	16.07.18	9	15.2	49	x	x					
SOB18-03-08	16.07.18	9.5	14.7	74		x	x	x	x		
SOB18-03-09	16.07.18	10	14.2	54	x	x					
SOB18-03-10	16.07.18	10.5	13.7	45		x	x				
SOB18-03-11	16.07.18	11	13.2	51	x						
SOB18-03-12	16.07.18	11.5	12.7	65		x	x	x	x		
SOB18-03-13	16.07.18	12	12.2	39	x	x					
SOB18-03-14	16.07.18	12.5	11.7	51		x	x				
SOB18-03-15	16.07.18	13	11.2	48	x	x					
SOB18-03-16	16.07.18	13.5	10.7	51		x	x	x	x		
SOB18-03-17	16.07.18	14	10.2	51	x	x					
Profile SOB18-06 (N 72.53812°, E 128.28267°)											
Yedoma IC deposits, Yedoma top, cliff height of 24.2 m arl											
SOB18-06-01	18.07.18		13.4	37	x	x	x				
SOB18-06-02	18.07.18		13	50		x					
SOB18-06-03	18.07.18		12.5	36	x	x					
SOB18-06-04	18.07.18		12	44	x	x	x	x	x	2050	
SOB18-06-05	18.07.18		11.5	42	x	x					
SOB18-06-06	18.07.18		11	58		x	x			3230	
SOB18-06-07	18.07.18		10.5	51	x	x	x	x	x	5790	7.39
SOB18-06-08	18.07.18		10	48							
SOB18-06-09	18.07.18		9.5	56	x	x					
SOB18-06-10	18.07.18		9	60		x	x	x	x	4600	
SOB18-06-11	18.07.18		8.5	52	x	x					
SOB18-06-12	18.07.18		8	64							
SOB18-06-13	18.07.18		7.5	54	x	x	x			953	
SOB18-06-14	18.07.18		7	50	x	x	x	x	x	726	7.41
SOB18-06-15	18.07.18		6.5	42	x	x					
SOB18-06-16	18.07.18		6	43		x					
SOB18-06-17	18.07.18		5.5	52	x	x	x	x	x	3090	
SOB18-06-18	18.07.18		5	40		x					
SOB18-06-19	18.07.18		4.5	39	x						
SOB18-06-20	18.07.18		4	36							
SOB18-06-30	18.07.18		3.2	43	x	x	x			2260	
SOB18-06-31	18.07.18		2.7	43		x	x	x	x	1893	
SOB18-06-32	18.07.18		2.2	43	x	x	x			1421	
SOB18-06-33	18.07.18		1.9	55		x	x	x	x	1183	
SOB18-06-34	18.07.18		1.4	47	x	x	x	x	x	1855	7.73
SOB18-06-35	18.07.18		0.9	53		x					
SOB18-06-40 to SOB18-06-58	21.07.19		0.9								
Profile SOB18-08 (N 72.54211°, E 128.26817°)											
Yedoma IC wedge ice, Yedoma slope, cliff height of 10.2 m arl											
SOB-18-08-130	20.07.18		9.4								
Profile SOB18-09 (N 72.54134°, E 128.27118°)											
Yedoma IC wedge ice, Yedoma beach											
SOB18-09-100	21.07.18		1.8								

Sample ID	Date	depth [m bs]	height [m arl]	Ice content, absolute [wt%]	Bio- marker	Iso- topes	DOC	cDOM	Hydro- chemistry	EC [µS/cm]	pH
Profile SOB18-07 (N 72.53877°, E 128.27983°)											
Yedoma IC deposits, Yedoma top, cliff height of 24.2 m arl, SIPRE core											
SOB18-07-01	20.07.18	0.00 to 0.20	na	x	x						
SOB18-07-02	20.07.18	0.23 to 0.38	na	x	x						
SOB18-07-03	20.07.18	0.38 to 0.53	na	x	x						
SOB18-07-04	20.07.18	0.53 to 0.99	na	x	x						
SOB18-07-05	20.07.18	1.02 to 1.10	na	x	x						
SOB18-07-06	20.07.18	1.10 to 1.13	na	x	x						
SOB18-07-07	20.07.18	1.30 to 1.49	na	x	x						
SOB18-07-08	20.07.18	1.49 to 1.72	na	x	x						
Profile SOB18-04 (N 72.53503°, E 128.30771°)											
thermokarst deposits, eastern alas, cliff height of 3.6 m arl											
SOB18-04-11	16.07.18	0	3.6	na							
SOB18-04-10	16.07.18	0.6	3	48		x					
SOB18-04-09	16.07.18	0.4	3.2	na							
SOB18-04-08	16.07.18	0.7	2.9	44		x					
SOB18-04-07	16.07.18	0.8	2.8	na							
SOB18-04-06	16.07.18	0.9	2.7	na							
SOB18-04-05	16.07.18	1	2.6	43		x					
SOB18-04-04	16.07.18	1.5	2.1	27		x					
SOB18-04-03	16.07.18	1.5	2.1	na							
SOB18-04-02	16.07.18	2	1.6	18		x					
SOB18-04-01	16.07.18	2.5	1.1	19		x					
Profile SOB18-05 (N 72.53877°, E 128.27983°)											
thermokarst deposits, eastern alas, cliff height 4.0 m arl											
SOB18-05-02	17.07.18	0.65	3.35	na							
SOB18-05-01	17.07.18	2.15	1.85	na							
Profile SOB18-10 (N 72.543260°, E 128.26579°)											
thermokarst deposits, western alas, cliff height 1.3 m arl											
SOB18-10-03	22.07.18	0.7	0.6	na							
SOB18-10-02	22.07.18	1.1	0.2	na							
SOB18-10-01	22.07.18	1.35	0	na							
Profile SOB18-A (N 72.53516°, E 128.30931°)											
thermokarst deposits, eastern alas, cliff height 4.0 m arl											
SOB18-A-01	17.07.18	0.75		na							
SOB18-A-02	17.07.18	1.85		na							
SOB18-A-03	17.07.18	2.00		na							

Table A.2.22: Cryolithological description of the sediment profiles from Sobo-Sise Island 2018 (CS – cryostructures, al – active layer, pl – protective layer)

Vertical position	Samples	Description
Profile SOB18-01 (N 72.53877°, E 128.27983°)		
Yedoma IC deposits, Yedoma top, cliff height of 24.2 m arl		
24.2-24.0 m arl	SOB18-01-01	al depth on 14 <sup>th</sup> July: 0.2, modern vegetation, roots, peat
24.0-23.7 m arl	SOB18-01-02	pl, grey fine sand, high ice content, irregular reticulate CS (2-4 mm thick ice lenses, enclosed sediments 4x10 mm large)
23.7-23.6 m arl		light brown-grey fine sand, peaty, structureless CS
23.6-23.1 m arl	SOB18-01-03	grey fine sand, peat lenses (diam. 5-10 to 15-25 cm), layered CS (up to 10 mm thick ice layers in 2-8 cm distance), between ice layers irregular reticulate CS (2-4 mm thick ice lenses)
23.1-22.6 m arl	SOB18-01-04	grey fine sand, peat lenses (2x5 to 5x8 cm large), reticulate CS (1-3 mm thick ice lenses, enclosed sediments 6x12 mm large)
22.6-21.6 m arl	SOB18-01-05 SOB18-06	grey fine sand, peat lenses (diam. 8-12 cm), layered CS (1-2 mm thick ice lenses in 10-20 mm distance) and rare sub-horizontal layered CS (up to 8 mm thick ice lenses in 60 mm distance)
21.6-21.0 m arl	SOB18-01-07	grey fine sand, peat lens at 19.5 m arl (diam. 20 cm), layered CS (1-2 cm thick ice layers in 10-20 mm distance) between ice layers reticulate CS (1-2 mm thick ice lenses, enclosed sediments 6x12 mm)
21.0-20.6 m arl	SOB18-01-08	grey fine sand, disperse fine organic remains, wavy non-parallel CS (0.5 to 2 mm thick ice lenses 3-5 mm long, enclosed sediments 3x5 mm large)
20.6-19.8 m arl	SOB18-01-09	grey fine sand, peat at 20 m arl, disperse fine organic remains, wavy parallel and sub-horizontal layered CS (0.5-1 mm thick ice lenses up to 10 mm long)
19.8-19.0 m arl	SOB18-01-10 SOB18-01-11	grey fine sand, disperse fine organic remains, layered and sub-horizontal layered CS (2-3 to 6-8 mm thick ice layers at 3-20 cm distance), between ice layers unclear expressed reticulate and wavy parallel CSs (ice lenses 0.5-1 mm thick, enclosed sediments 4x6 mm)
19.0-17.5 m arl	SOB18-01-12 SOB18-01-13 SOB18-01-14	grey fine sand, layered CS (10-12 mm thick ice lenses at 3-10 cm distance), between ice layers reticulate CS (2-3 mm thick ice lenses, enclosed sediments 4x8 mm large); at 17.7 m arl (sample SOB18-04): sand lens (diam. 60 cm) with disperse fine organic remains and structureless CS
17.5-17.0 m arl	SOB18-01-15	grey sand, twigs (diam. 2-4 mm), wavy parallel CS (up to 10 mm thick ice lenses, 20-30 cm long at 8-10 cm distance), between ice lenses structureless CS
17.0-16.5 m arl	SOB18-01-16	grey fine sand, peat lenses (diam. 20-25 cm), twigs (diam. 4-6 mm), layered CS (10-20 mm thick ice lenses at 5-10 cm distance), between ice lenses wavy parallel CS (0.5-1.5 mm thick ice lenses, 4-8 mm long)

Vertical position	Samples	Description
16.6-16.0 m arl	SOB18-01-17	grey fine sand, peaty dark grey sand lenses (diam. 25 cm) with twigs, wavy parallel CS (10-15 mm thick ice lenses at 3-5 cm distance), between ice lenses reticulate CS
16.0-15.5 m arl	SOB18-01-18	light grey sand, single dark organic spots, structureless CS
Profile SOB18-03 (N 72.5387°, E 128.28012°) Yedoma IC deposits, Yedoma top, cliff height of 24.2 m arl		
24.2-21.8 m arl	Not sampled	wedge ice, elongated bubbles (diam. 0.5 mm) in vertical chains
21.8-21.7 m arl	Not sampled	dark grey fine sand and sand, dark brown organic spots, twig fragments, structureless CS, lower border of the unit parallel to the upper ground to wedge-ice border
21.7-21.2 m arl	Not sampled	beige grey sand, structureless CS
21.2-20.6 m arl	Not sampled	grey fine sand, layered CS (2-5 cm thick ice layers in 1.5-3 up to 15 cm distance), between ice layers reticulate CS (1-3 mm thick ice lenses, enclosed sediments 5x8 mm)
20.6-18.8 m arl	Not sampled	light brown grey fine sand and sand, dark brown organic spots, twig fragments, fine sand with non-regular reticulate CS and single sub-horizontal ice lenses (up to 10 mm thick and up to 20 cm long), sand with structureless CS
18.8-17.9 m arl	SOB18-03-01	grey fine sand, dark brown black organic spots, twig remains, layered CS (10-50 mm thick ice layers at 1-20 cm distance), between ice layers reticulate CS (1-2 mm thick ice lenses, enclosed sediments 3x6 mm large)
17.9-17.0 m arl	SOB18-03-02 SOB18-03-03	brown fine sand, peaty interlayers, honeycombed CS (0.5-1 mm thick ice lenses, enclosed sediments 2x4 to 5x6 mm large)
17.0-15.7 m arl	SOB18-03-04 SOB18-03-05	dark brown peat, grey fine sand matrix, lenticular CS (1-2 mm thick, 5-10 mm long ice lenses) and sub-horizontal ice lenses (10-50 mm thick)
15.7-10.2 m arl (8.5-14 m bs)	SOB18-03-06 SOB18-03-07 SOB18-03-08 SOB18-03-09 SOB18-03-10 SOB18-03-11 SOB18-03-12 SOB18-03-13 SOB18-03-14 SOB18-03-15 SOB18-03-16 SOB18-03-17	layered light grey and dark brown fine sand, peat lenses, single twig remains (diam. 2-4 mm), layered CS (5-50 mm thick ice layers), between ice layers unclear expressed reticulate and wavy parallel CSs (ice lenses 1-2 mm thick, enclosed sediments 2x3 to 5x15 mm)



Vertical position	Samples	Description
Profile SOB18-06 (N 72.53812°, E 128.28267°)		
Yedoma IC deposits, Yedoma top, cliff height of 24.2 m arl		
13.4-13.3 m arl	SOB18-06-01	grey fine sand, brown spots, twig fragments, structureless CS
13.3-13.2 m arl		grey fine sand, reticulate CS (0.5-3 mm thick ice lenses, enclosed sediments 3x5 to 5x7 mm large)
13.2-12.9 m arl	SOB18-06-02	grey fine sand, twig and grass remains, layered CS (0.5 mm thick ice layers in 2-8 cm distance), between ice layers reticulate CS (1 mm thick ice lenses, enclosed sediments 2x3 to 4x5 mm large)
12.9-12.2 m arl	SOB18-06-03	grey fine sand, twig and grass remains, structureless CS except for organic inclusions, there irregular reticulate CS (1-2 mm thick ice lenses, enclosed sediments 3x4 to 8x8 mm large), subvertical ice lenses (3 mm thick)
12.2-11.9 m arl	SOB18-06-04	grey fine sand, single brown organic spots (diam. 1-3 mm), wavy parallel CS (ice lenses 1-2 mm long in 2-5 mm distance)
11.9-8.3 m arl	SOB18-06-05 SOB18-06-06 SOB18-06-07 SOB18-06-08 SOB18-06-09 SOB18-06-10 SOB18-06-11	grey fine sand, twig and grass remains, peat lens (diam. 15-20 cm) at 11.7-11.5 m arl, organic spots (diam. 3 mm) at 11 m arl, layered CS (10-15 mm thick ice layers in 7-15 cm distance), between ice layers reticulate CS (1-2 mm thick ice lenses, enclosed sediments 3x5 to 5x8 mm large)
8.3-6.1 m arl	SOB18-06-12 SOB18-06-13 SOB18-06-14 SOB18-06-15	grey fine sand, peat horizon (15 cm thick) at 6 m arl, layered CS (4-20 mm thick ice layers in 1-4 cm distance), between ice layers irregular reticulate CS (>1 mm thick ice lenses, enclosed sediments 2x2 to 4x6 mm large)
6.1-4.2 m arl	SOB18-06-16 SOB18-06-17 SOB18-06-18 SOB18-06-19	grey fine sand, twig remains, peat horizon at 6.2 m arl (10 cm thick), brown spots (diam. 2-5 mm) at 6 m arl, black spots (diam. 2 mm) at 4.5 m arl, layered CS (5-15 mm thick ice layers in 1-4 cm distance), between ice layers reticulate CS (1-1.5 mm thick ice lenses, enclosed sediments 5x10 mm large)
4.2-3.5 m arl	SOB18-06-20	grey fine sand, peat lens at 4 m arl, honeycombed CS (0.5-1 mm thick ice lenses, enclosed sediments 2x2 mm large)

Vertical position	Samples	Description
3.5-0.8 m arl	SOB18-06-30	grey fine sand, peat lenses (diam. 5-10 cm) and twig remains (diam. 5 mm) between 3.5 and 2.0 m arl, peat horizon at 0.9 m arl (10 cm thick), <i>in situ</i> grass roots of the peat horizon at 0.8-0.9 m arl subsampled for radiocarbon dating in samples SOB18-06-40 ->SOB18-06-58, layered CS (10-50 mm thick ice layers in 5-10 cm distance), between ice layers wavy parallel CS (1-2 mm thick, 5-20 mm long ice lenses in 2-5 mm distance)
	SOB18-06-31	
	SOB18-06-32	
	SOB18-06-33	
	SOB18-06-34	
	SOB18-06-35	
	SOB18-06-40	
	SOB18-06-41	
	SOB18-06-42	
	SOB18-06-43	
	SOB18-06-44	
	SOB18-06-45	
	SOB18-06-46	
	SOB18-06-47	
	SOB18-06-48	
	SOB18-06-49	
	SOB18-06-50	
	SOB18-06-51	
	SOB18-06-52	
	SOB18-06-53	
SOB18-06-54		
SOB18-06-56		
SOB18-06-57		
SOB18-06-58		
Profile SOB18-08 (N 72.54211°, E 128.26817°)		
Yedoma IC wedge ice, Yedoma slope, cliff height of 10.2 m arl		
9.4 m arl	SOB18-08-130	grey fine sand, peat inclusions, layered CS (2-5 mm thick ice layers in 10 cm distance), between ice layers wavy non-parallel CS (1 mm thick ice lenses)
Profile SOB18-09 (N 72.54134°, E 128.27118°)		
Yedoma IC wedge ice, Yedoma beach		
1.8 m arl	SOB18-09-100	grey-brown silt, layered CS (1-2 cm thick ice layers in 10 cm distance), between ice layers wavy non-parallel and irregular reticulate CS (ice lenses 1-2 mm thick and 2-4 cm long)
Profile SOB18-07 (N 72.53877°, E 128.27983°)		
Yedoma IC deposits, Yedoma top, cliff height of 24.2 m arl, SIPRE core		
0.00-0.20 m bs	SOB18-07-01	al
0.23-0.38 m bs	SOB18-07-02	frozen, not yet described
0.38-0.53 m bs	SOB18-07-03	frozen, not yet described
0.53-0.99 m bs	SOB18-07-04	frozen, not yet described
1.02-1.10 m bs	SOB18-07-05	frozen, not yet described
1.10-1.13 m bs	SOB18-07-06	frozen, not yet described
1.30-1.49 m bs	SOB18-07-07	frozen, not yet described
1.49-1.72 m bs	SOB18-07-08	frozen, not yet described

Vertical position	Samples	Description
Profile SOB18-04 (N 72.53503 °, E 128.30771 °) thermokarst deposits, eastern alas, cliff height of 3.6 m arl		
0.0-0.05 m bs	SOB18-04-11	al, surface vegetation
0.6 m bs	SOB18-04-10	right of the IW, 40 cm darker silty fine sand with thin roots, horizontal lenticular CS (2-3 mm thick ice lenses, 20-30 mm long); this layer surrounds the wood horizon
0.4 m bs	SOB18-04-09	al, left of the IW, 40 cm active layer, sand layer, roots remains, in between darker silty layers irregular bedded below a lighter 3-4 cm thick sand layer
0.4-0.7 m bs	SOB18-04-08	left of the IW, sandy silt with single wood fragments (diam. 2-3 cm in diameter) and fine-distributed plant remains, horizontal and diagonal lenticular CS (1-2 mm thick ice lenses, 20-30 mm long) above an ice layer
0.7-0.8 m bs	SOB18-04-07	left of the IW, 10 cm thick (drift?) wood layer
0.8-0.9 m bs	SOB18-04-06	left of the IW, 4 cm thick light fine sand, structureless CS
0.9-1.1 m bs	SOB18-04-05	left of the IW, 20 cm thick greyish-brown silty fine sand, layered CS (5-10 mm thick ice layers), between ice layers horizontal, diagonal or non-regular lenticular CS (1 mm thick, 20-30 mm long)
1.1-1.5 m bs	SOB18-04-04	left of the IW, 30 cm thick alternate bedding of light sand and darker silty fine sand layers with numerous small roots (each 1-2 cm thick), structureless CS in sand layers, horizontal lenticular and reticulated CS (1 mm thick ice lenses, 10-20 mm long) in silty fine sand layers
1.5 m bs	SOB18-04-03	right of the IW, 10-15 cm thick wood layer with relative large twigs (diam. 5-10 cm)
1.5-2.0 m bs	SOB18-04-02	left of the IW, alternate bedding of 4-6 cm thick fine sand beds with numerous small roots and 1 cm thick silty fine sand beds, layered CS (1-2 mm thick ice layers in 10-20 mm distance) in sand layers, horizontal layered CS (0.5-1 mm thick ice layers, 10-30 mm long) in silty fine sand layers
2.5 m bs	SOB18-04-01	right of the IW, 20 cm thick alternate bedding of sand and silty fine sand, each bed 2-3 cm thick, structureless CS in sand bed, horizontal lenticular CS (1 mm thick ice lenses, 20 mm long) in silty fine sand beds

Vertical position	Samples	Description
Profile SOB18-05 (N 72.53877°, E 128.27983°) thermokarst deposits, eastern alas, cliff height 4.0 m arl		
0.0-0.23 m bs		al, 23 cm thick horizon of silty grey sands, roots
0.23-0.55 m bs		32 cm thick alternate bedding of 6 cm pale grey fine sand layers and 9-11 cm dark grey silt, roots, unfrozen, active layer
0.55-0.75 m bs	SOB18-05-02	20 cm thick grey silt, organic material, with non-regular lenticular CS, at the bottom sandy lens, more organic consisted
0.75-0.95 m bs		20 cm thick greyish brown silt, organic material, structureless and diagonal lenticular CS
0.95-1.28 m bs		33 cm thick dark grey silt, sandy lenses, organic lenses, large lenticular CS
1.28-1.5 m bs		32 cm thick pale grey silt, grain size is increasing to the bottom at the top organic lenses, reticulated CS
1.5-1.6 m bs		10 cm thick layer of wood and other organic material
1.6-1.8/2.3 m bs		20-50 cm thick pale grey sand with grey silt lenses, structureless CS, layer's thickness is increasing to the left part of the section, bottom is cryoturbated
1.8-2.3 m bs	SOB18-05-01	20 cm thick grey silt, organic material is also at the bottom, at the top diagonal layered CS, in the middle horizontal layered CS, at the bottom wavy lenticular CS
Profile SOB18-10 (N 72.543260°, E 128.26579°) thermokarst deposits, western alas, cliff height 1.3 m arl		
0.0-0.27 m bs		al, 27 cm thick dark brown and pale grey silt with sandy lenses, roots and organic material, contact with bedding layer is gradual
0.27-0.5 m bs		al, 23 cm thick alternate bedding of fine-sized pale grey sand and brownish grey silt with organic; contact with bedding layer is sharp
0.5-0.56 m bs		left hand side, 6 cm grey silt, ironed strip is on the contact with upper layer, structureless CS
0.56-0.86 m bs	SOB18-10-03	left hand side, 30 cm grey sandy silt, pit material and pale grey sandy lenses, ironed strips are closer to right part of the section, reticulated CS
0.86-1.31 m bs		left hand side, 45 cm thick grey silt, organic lenses, layered CS (30-40 mm thick ice layers in 10-15 cm distance), some silt lenses with non-regular reticulated CS
0.5-1.2 m bs	SOB18-10-02	right hand side, 70 cm thick alternate bedding of pale, pale grey fine sand (grain size is increasing to the bottom) with 7 cm thickness and grey silt with organic lenses and 6 cm thickness, closer to left part bedding is destroying, contact with bedding layer is rough, deformed
1.2/1.31-1.4 m bs	SOB18-10-01	20 cm thick grey silt, wood layer at the top, with parallel wavy CS (30 mm thick ice lenses in 30-50 mm distance)

Vertical position	Samples	Description
Profile SOB18-A (N 72.53516°, E 128.30931 °) thermokarst deposits, eastern alas, cliff height 4.0 m arl		
0-0.3 m bs		al, grey sandy silt, roots, unfrozen
0.3-0.6 m bs		al, interchanging layers of silty sand and sand lenses up to 6 cm thick (5-6 and layers, unfrozen
0.6-1.8 m bs	SOB18-A-01	drak grey sandy silt, organic material interspersed, some organoc matter layers, thick ice lens at bottom
1.8-1.85 m bs	SOB18-A-02	drift wood layer with relative large twigs (up to 5 cm) in sandy matrix
1.85-1.95 m bs		yellowish browns sand, indulating wavy bedding
beyond 1.95 m bs	SOB18-A-03	grey fine sand, some silt, some organic rich layers (looks like detrital)

Table A.2.23: Sample list of ice wedge samples from Sobo-Sise Island 2018 (m bs – meter below surface, m arl – meter above river level)

Sample ID	Date	sampling depth [m bs]	sampling height [m arl]	Comment / Description
Profile SOB18-02 (N 72.53873°, E 128.28002 °)				
Yedoma IC wedge ice, Yedoma top, cliff height of 24.2 m arl				
SOB18-02-01	15.07.18	4.5	19.7	drilled by ice screw
SOB18-02-02	15.07.18	4.5	19.7	drilled by ice screw
SOB18-02-03	15.07.18	4.5	19.7	drilled by ice screw
SOB18-02-04	15.07.18	4.5	19.7	drilled by ice screw
SOB18-02-05	15.07.18	4.5	19.7	drilled by ice screw
SOB18-02-06	15.07.18	4.5	19.7	drilled by ice screw
SOB18-02-07	15.07.18	4.5	19.7	drilled by ice screw
SOB18-02-08	15.07.18	4.5	19.7	drilled by ice screw
SOB18-02-09	15.07.18	4.5	19.7	drilled by ice screw
SOB18-02-10	15.07.18	4.5	19.7	drilled by ice screw
SOB18-02-11	15.07.18	4.5	19.7	drilled by ice screw
SOB18-02-12	15.07.18	4.5	19.7	drilled by ice screw
SOB18-02-13	15.07.18	4.5	19.7	drilled by ice screw
SOB18-02-14	15.07.18	4.5	19.7	drilled by ice screw
SOB18-02-15	15.07.18	4.5	19.7	drilled by ice screw
SOB18-02-16	15.07.18	4.5	19.7	drilled by ice screw
SOB18-02-17	15.07.18	4.5	19.7	drilled by ice screw
SOB18-02-18	15.07.18	4.5	19.7	drilled by ice screw
SOB18-02-19	15.07.18	4.5	19.7	drilled by ice screw
SOB18-02-20	15.07.18	4.5	19.7	drilled by ice screw
SOB18-02-21	15.07.18	4.5	19.7	drilled by ice screw
SOB18-02-22	15.07.18	4.5	19.7	drilled by ice screw
SOB18-02-23	15.07.18	4.5	19.7	drilled by ice screw
SOB18-02-24	15.07.18	4.5	19.7	drilled by ice screw
SOB18-02-25	15.07.18	4.5	19.7	drilled by ice screw
SOB18-02-26	15.07.18	4.5	19.7	drilled by ice screw
SOB18-02-27	15.07.18	4.5	19.7	drilled by ice screw
SOB18-02-28	15.07.18	4.5	19.7	drilled by ice screw
SOB18-02-29	15.07.18	4.5	19.7	drilled by ice screw
SOB18-02-30	15.07.18	4.5	19.7	drilled by ice screw
SOB18-02-A	15.07.18	4.5	19.7	drilled by ice screw
SOB18-02-B	15.07.18	4.5	19.7	drilled by ice screw
SOB18-02-C	15.07.18	4.5	19.7	drilled by ice screw
Profile SOB18-08 (N 72.54211°, E 128.26817°)				
Yedoma IC wedge ice, Yedoma slope, cliff height of 10.2 m arl				
SOB18-08-01	20.07.18		9.4	frozen, cut by chain saw
SOB18-08-02	20.07.18		9.4	frozen, cut by chain saw
SOB18-08-03	20.07.18		9.4	frozen, cut by chain saw
SOB18-08-04	20.07.18		9.4	frozen, cut by chain saw
SOB18-08-05	20.07.18		9.4	frozen, cut by chain saw
SOB18-08-06	20.07.18		9.4	frozen, cut by chain saw
SOB18-08-07	20.07.18		9.4	frozen, cut by chain saw
SOB18-08-08	20.07.18		9.4	frozen, cut by chain saw
SOB18-08-09	20.07.18		9.4	frozen, cut by chain saw
SOB18-08-10	20.07.18		9.4	frozen, cut by chain saw
SOB18-08-11	20.07.18		9.4	frozen, cut by chain saw
SOB18-08-12	20.07.18		9.4	frozen, cut by chain saw
SOB18-08-13	20.07.18		9.4	frozen, cut by chain saw
SOB18-08-14	20.07.18		9.4	frozen, cut by chain saw
SOB18-08-15	20.07.18		9.4	frozen, cut by chain saw
SOB18-08-16	20.07.18		9.4	frozen, cut by chain saw
SOB18-08-17	20.07.18		9.4	frozen, cut by chain saw
SOB18-08-18	20.07.18		9.4	frozen, cut by chain saw
SOB18-08-19	20.07.18		9.4	frozen, cut by chain saw
SOB18-08-20	20.07.18		9.4	frozen, cut by chain saw



Sample ID	Date	sampling depth	sampling height	Comment / Description
SOB18-08-81	20.07.18		9.4	frozen, cut by chain saw
SOB18-08-82	20.07.18		9.4	frozen, cut by chain saw
SOB18-08-83	20.07.18		9.4	frozen, cut by chain saw
SOB18-08-84	20.07.18		9.4	frozen, cut by chain saw
SOB18-08-85	20.07.18		9.4	frozen, cut by chain saw
SOB18-08-86	20.07.18		9.4	frozen, cut by chain saw
SOB18-08-87	20.07.18		9.4	frozen, cut by chain saw
SOB18-08-88	20.07.18		9.4	frozen, cut by chain saw
SOB18-08-89	20.07.18		9.4	frozen, cut by chain saw
SOB18-08-90	20.07.18		9.4	frozen, cut by chain saw
SOB18-08-91	20.07.18		9.4	frozen, cut by chain saw
SOB18-08-92	20.07.18		9.4	frozen, cut by chain saw
SOB18-08-93	20.07.18		9.4	frozen, cut by chain saw
SOB18-08-94	20.07.18		9.4	frozen, cut by chain saw
SOB18-08-95	20.07.18		9.4	frozen, cut by chain saw
SOB18-08-96	20.07.18		9.4	frozen, cut by chain saw
SOB18-08-97	20.07.18		9.4	frozen, cut by chain saw
SOB18-08-98	20.07.18		9.4	frozen, cut by chain saw
SOB18-08-99	20.07.18		9.4	frozen, cut by chain saw
SOB18-08-100	20.07.18		9.4	frozen, cut by chain saw
SOB18-08-101	20.07.18		9.4	frozen, cut by chain saw
SOB18-08-102	20.07.18		9.4	frozen, cut by chain saw
SOB18-08-103	20.07.18		9.4	frozen, cut by chain saw
SOB18-08-104	20.07.18		9.4	frozen, cut by chain saw
SOB18-08-105	20.07.18		9.4	frozen, cut by chain saw
SOB18-08-106	20.07.18		9.4	frozen, cut by chain saw
SOB18-08-107	20.07.18		9.4	frozen, cut by chain saw
SOB18-08-108	20.07.18		9.4	frozen, cut by chain saw
SOB18-08-109	20.07.18		9.4	frozen, cut by chain saw
SOB18-08-110	20.07.18		9.4	frozen, cut by chain saw
SOB18-08-111	20.07.18		9.4	frozen, cut by chain saw
SOB18-08-112	20.07.18		9.4	frozen, cut by chain saw
SOB18-08-113	20.07.18		9.4	frozen, cut by chain saw
SOB18-08-114	20.07.18		9.4	frozen, cut by chain saw
SOB18-08-115	20.07.18		9.4	frozen, cut by chain saw
SOB18-08-116	20.07.18		9.4	frozen, cut by chain saw
SOB18-08-117	20.07.18		9.4	frozen, cut by chain saw
SOB18-08-118	20.07.18		9.4	frozen, cut by chain saw
SOB18-08-119	20.07.18		9.4	frozen, cut by chain saw
SOB18-08-120	20.07.18		9.4	frozen, cut by chain saw
SOB18-08-121	20.07.18		9.4	frozen, cut by chain saw
SOB18-08-122	20.07.18		9.4	frozen, cut by chain saw
SOB18-08-123	20.07.18		9.4	frozen, cut by chain saw
SOB18-08-124	20.07.18		9.4	frozen, cut by chain saw
SOB18-08-125	20.07.18		9.4	frozen, cut by chain saw
SOB18-08-126	20.07.18		9.4	frozen, cut by chain saw
SOB18-08-127	20.07.18		9.4	frozen, cut by chain saw
SOB18-08-A	20.07.18		9.4	2 blocks, 1 small - 1 large, frozen
SOB18-08-B	20.07.18		9.4	2 blocks, 1 small - 1 large, frozen
SOB18-08-C	20.07.18		9.4	2 blocks, 1 small - 1 large, frozen
Profile SOB18-09 (N 72.54134°, E 128.27118°)				
Yedoma IC wedge ice, Yedoma beach				
SOB18-09-01	21.07.18		2	cut by chain saw
SOB18-09-02	21.07.18		2	cut by chain saw
SOB18-09-03	21.07.18		2	cut by chain saw
SOB18-09-04	21.07.18		2	cut by chain saw
SOB18-09-05	21.07.18		2	cut by chain saw
SOB18-09-06	21.07.18		2	cut by chain saw
SOB18-09-07	21.07.18		2	cut by chain saw
SOB18-09-08	21.07.18		2	cut by chain saw
SOB18-09-09	21.07.18		2	cut by chain saw



Sample ID	Date	sampling depth	sampling height	Comment / Description
SOB18-09-10	21.07.18		2	cut by chain saw
SOB18-09-11	21.07.18		2	cut by chain saw
SOB18-09-12	21.07.18		2	cut by chain saw
SOB18-09-13	21.07.18		2	cut by chain saw
SOB18-09-15	21.07.18		2	cut by chain saw
SOB18-09-16	21.07.18		2	cut by chain saw
SOB18-09-17	21.07.18		2	cut by chain saw
SOB18-09-18	21.07.18		2	cut by chain saw
SOB18-09-19	21.07.18		2	cut by chain saw
SOB18-09-20	21.07.18		2	cut by chain saw
SOB18-09-21	21.07.18		2	cut by chain saw
SOB18-09-22	21.07.18		2	cut by chain saw
SOB18-09-23	21.07.18		2	cut by chain saw
SOB18-09-24	21.07.18		2	cut by chain saw
SOB18-09-25	21.07.18		2	cut by chain saw
SOB18-09-26	21.07.18		2	cut by chain saw
SOB18-09-27	21.07.18		2	cut by chain saw
SOB18-09-28	21.07.18		2	cut by chain saw
SOB18-09-29	21.07.18		2	cut by chain saw
SOB18-09-30	21.07.18		2	cut by chain saw
SOB18-09-31	21.07.18		2	cut by chain saw
SOB18-09-32	21.07.18		2	cut by chain saw
SOB18-09-33	21.07.18		2	cut by chain saw
SOB18-09-34	21.07.18		2	cut by chain saw
SOB18-09-35	21.07.18		2	cut by chain saw
SOB18-09-36	21.07.18		2	cut by chain saw
SOB18-09-37	21.07.18		2	cut by chain saw
SOB18-09-38	21.07.18		2	cut by chain saw
SOB18-09-39	21.07.18		2	cut by chain saw
SOB18-09-40	21.07.18		2	cut by chain saw
SOB18-09-41	21.07.18		2	cut by chain saw
SOB18-09-42	21.07.18		2	cut by chain saw
SOB18-09-43	21.07.18		2	cut by chain saw
SOB18-09-44	21.07.18		2	cut by chain saw
SOB18-09-45	21.07.18		2	cut by chain saw
SOB18-09-46	21.07.18		2	cut by chain saw
SOB18-09-47	21.07.18		2	cut by chain saw
SOB18-09-48	21.07.18		2	cut by chain saw
SOB18-09-49	21.07.18		2	cut by chain saw
SOB18-09-50	21.07.18		2	cut by chain saw
SOB18-09-51	21.07.18		2	cut by chain saw
SOB18-09-52	21.07.18		2	cut by chain saw
SOB18-09-53	21.07.18		2	cut by chain saw
SOB18-09-54	21.07.18		2	cut by chain saw
SOB18-09-55	21.07.18		2	cut by chain saw
SOB18-09-56	21.07.18		2	cut by chain saw
SOB18-09-57	21.07.18		2	cut by chain saw
SOB18-09-58	21.07.18		2	cut by chain saw
SOB18-09-59	21.07.18		2	cut by chain saw
SOB18-09-60	21.07.18		2	cut by chain saw
SOB18-09-61	21.07.18		2	cut by chain saw
SOB18-09-62	21.07.18		2	cut by chain saw
SOB18-09-63	21.07.18		2	cut by chain saw
SOB18-09-64	21.07.18		2	cut by chain saw
SOB18-09-65	21.07.18		2	cut by chain saw
SOB18-09-66	21.07.18		2	cut by chain saw
SOB18-09-67	21.07.18		2	cut by chain saw
SOB18-09-68	21.07.18		2	cut by chain saw
SOB18-09-69	21.07.18		2	cut by chain saw
SOB18-09-70	21.07.18		2	cut by chain saw

Sample ID	Date	sampling depth	sampling height	Comment / Description
SOB18-09-71	21.07.18		2	cut by chain saw
SOB18-09-72	21.07.18		2	cut by chain saw
SOB18-09-73	21.07.18		2	cut by chain saw
SOB18-09-74	21.07.18		2	cut by chain saw
SOB18-09-75	21.07.18		2	cut by chain saw
SOB18-09-76	21.07.18		2	cut by chain saw
SOB18-09-77	21.07.18		2	cut by chain saw
SOB18-09-78	21.07.18		2	cut by chain saw
SOB18-09-79	21.07.18		2	cut by chain saw
SOB18-09-80	21.07.18		2	cut by chain saw
SOB18-09-81	21.07.18		2	cut by chain saw
SOB18-09-82	21.07.18		2	cut by chain saw
SOB18-09-83	21.07.18		2	cut by chain saw
SOB18-09-84	21.07.18		2	cut by chain saw
SOB18-09-85	21.07.18		2	cut by chain saw
SOB18-09-A	21.07.18		2	block, frozen, cut by chain saw
SOB18-09-B	21.07.18		2	block, frozen, cut by chain saw
SOB18-09-C	21.07.18		2	block, frozen, cut by chain saw
Profile SOB18-04 (N 72.53503°, E 128.30771°)				
eastern alas, cliff height of 3.6 m arl, 10 cm distance				
SOB18-04-12	16.07.18	1.7	1.9	drilled by ice screw
SOB18-04-13	16.07.18	1.7	1.9	drilled by ice screw
SOB18-04-14	16.07.18	1.7	1.9	drilled by ice screw
SOB18-04-15	16.07.18	1.7	1.9	drilled by ice screw
SOB18-04-16	16.07.18	1.7	1.9	drilled by ice screw
SOB18-04-17	16.07.18	1.7	1.9	drilled by ice screw
SOB18-04-18	16.07.18	1.7	1.9	drilled by ice screw
SOB18-04-19	16.07.18	1.7	1.9	drilled by ice screw
SOB18-04-20	16.07.18	1.7	1.9	drilled by ice screw
SOB18-04-21	16.07.18	1.8	1.8	large sample from the IW centre taken by axe

Table A.2.24: Sample list of surface water samples and hydrochemical field data from Sobo-Sise Island 2018

Sample ID	Date	Lat [°N]	Lon [°N]	Iso- topes	DOC	cDOM	Hydro- chemistry	EC [µS/cm]	pH	Comment / Description
SOB18_rain_01	13.07.18	72.53883	128.26669	x						rain
SOB18_rain_02	15.07.18	72.53883	128.26669	x						rain
SOB18_rain_03	19.07.18	72.53883	128.26669	x						heavy rain during the night; sampling in the morning
SOB18_rain_04	21.07.18	72.53883	128.26669	x						multiple rain events
SOB18-SW-01	14.07.18	72.5402	128.27359	x	x	x	x	28	6.1	Thermoerosional valley btw. camp and pf sampling site
SOB18-SW-02	14.07.18	72.54336	128.26367	x	x	x	x	44	6.22	Thermoerosional valley of alas west of camp; central outflow right at the edge of alas into Lena River
SOB18-SW-03	14.07.18	72.53893	128.28003	x	x	x	x	132	6.94	Lena River water at shore directly below outcrop of window 1 (SOB18-01)
SOB18-SW-04	14.07.18	72.53503	128.30196	x	x	x	x	21	6.28	Thermoerosional valley; creek water ca. 50 m before it flows over the cliff; valley at east end of Yedomia island
SOB18-SW-05	15.07.18	72.54504	128.25861	x	x	x	x	118	na	Lena River water in front of western alas close to camp
SOB18-SW-06	15.07.18	72.53893	128.28003	x	x	x	x	685	na	Permafrost outflow; pf meltwater directly below outcrop of window no.1 (SOB18-01) and adjacent ice wedge; 2 samples 10 m apart from each other
SOB18-SW-07	15.07.18	72.53893	128.28003	x	x	x	x	896	na	Permafrost outflow; pf meltwater directly below outcrop of window no.1 (SOB18-01) and adjacent ice wedge; 2 samples 10 m apart from each other

Sample ID	Date	Lat [°N]	Lon [°N]	Iso- topes	DOC	cDOM	Hydro- chemistry	EC [µS/cm]	pH	Comment / Description
SOB18-SW-08	15.07.18	72.53893	128.28003	x	x	x	x	124	na	Lena River water at shore directly below outcrop of window 1 (SOB18-01)
SOB18-SW-09	15.07.18	72.53767	128.28339	x	x	x	x	27	6.87	Thermoerosional valley; creek water ca. 150m east of pf sediment sampling site
SOB18-SW-10	17.07.18	72.53516	128.30931	x	x	x	x	80	6.81	Thermoerosional valley draining western edge of eastern alas; little creek ca. 100 m east of Yedomia cliff
SOB18-SW-11	17.07.18	72.53516	128.30931	x	x	x	x	123	7.24	Lena River water at shore directly next to alas exposure sampling site in eastern alas; ca. 100 m east of Yedomia; storm from west, high waves; white caps, very turbid water
SOB18-SW-12	19.07.18	72.53812	128.28267	x	x	x	x	142	7.99	Lena River water at shore directly below noutcrop of window 3 (SOB18-06), 14:30
SOB18-SW-13	19.07.18	72.53812	128.28267	x	x	x	x	955	7.46	permafrost outflow; pf meltwater directly below outcrop of window no.3 (SOB18-06), ca. 10%, 14:30
SOB18-SW-14	22.07.18	72.54316	128.26598	x	x	x	x	132	7.35	Lena river water directly at outcrop of Alexey in western alas
SOB18-SW-15	22.07.18	72.54324	128.26105	x	x	x	x	343	6.7	very little pond in western alas, almost no open water
SOB18-SW-16	23.07.18	72.53883	128.26669	x	x	x	x	24	6.48	interpolygonal pond at camp
SOB18-02-A	15.07.18	72.53873	128.28002	x			x	44	6.79	wedge ice
SOB18-02-B	15.07.18	72.53873	128.28002	x			x	111	8.31	wedge ice
SOB18-02-C	15.07.18	72.53873	128.28002	x			x	108	8.88	wedge ice

### **A.3 Supplementary material to Chukotka 2018 Expedition**

Table A.3.1: Visited vegetation plots in Chukotka

Site ID	General information				Altitude [m asl]	Date	Plot type [m]	Slope [°/m]	Aspect	Tree species cover	Soil pits (# samples; # samples dating)	Image surveys				Handheld (Sam-sung360 time lapse)
	Region	Latitude [° N]	Longitude [° E]	Handheld (RGB / NIR)								Flight (RGB / NIR)	Panorama (# Canon / # Sam-sung360)	6 m (RGB / NIR)	Handheld (RGB / NIR)	
EN18000	Billbino	68.097147	166.375447	435	03.07.2018	Circle r=15 m	1.50/15	SSW	7% Larix	1-1	1/0	x/x	x/x	x/x	-	
EN18001	Ilirney	67.39273	168.34662	492	04.07.2018	Circle r=15 m	1.10/20	SSO	8% Larix	5-3	1/0	x/x	x/x	x/x	x (circle)	
EN18002	Ilirney	67.386775	168.336731	416	05.07.2018	Circle r=15 m	0.40/20	OSO	8% Larix	2-3	1/4	x/x	x/x	x/x	x (circle)	
EN18003	Ilirney	67.39691	168.34702	492	05.07.2018	Circle r=15 m	5.00/20	SSO	8% Larix	2-2	1/4	x/x	x/x	x/x	x (circle)	
EN18004	Ilirney	67.397489	168.351225	473	05.07.2018	Circle r=15 m	5.00/20	S	2% Larix	2-2	2/2	x/x	x/x	x/x	-	
EN18005	Ilirney	67.4196515	168.387511	597	06.07.2018	Circle r=15 m	0.75/20	SSW	0.1% Larix	3-3	1/5	x/x	x/x	x/x	-	
EN18006	Ilirney	67.414969	168.402874	438	06.07.2018	Circle r=15 m	2.00/20	SO	30% Larix	5-3	1/4	x/x	x/x	x/x	-	
EN18007	Ilirney	67.403274	168.371965	563	07.07.2018	Circle r=15 m	1.75/20	SSO	8.5% Larix	3-3	1/4	x/x	x/x	x/x	-	
EN18008	Ilirney	67.402135	168.375284	511	07.07.2018	Circle r=15 m	3.75/20	SO		2-3	1/4	x/x	x/x	x/x	-	
EN18009	Ilirney	67.400725	168.379683	511	07.07.2018	Circle r=15 m	5.25/20	SSW	0.1% Larix	5-2	1/3	x/x	x/x	x/x	-	
EN18010	Ilirney	67.402371	168.3662	611	08.07.2018	Circle r=15 m	1.50/20	SO	0.5% Larix	0-0	0 (partly)/1	x/x (90%)	x/x	x/x	-	
EN18011	Ilirney	67.404042	168.364252	611	08.07.2018	Circle r=15 m	1.25/20	NO		0-1	0/6	x/x (90%)	x/x	x/x	-	
EN18012	Ilirney	67.402142	168.378078	511	09.07.2018	Circle r=15 m	2.00/20	OOS	17% Larix	1-2	1/4	x/x	x/x	x/x	-	
EN18013	Ilirney	67.405174	168.355304	650	09.07.2018	Circle r=15 m	1.25/20	SOOO		1-1	1/4	x/x	x/x	x/x	-	
EN18014	Ilirney	67.395309	168.349106	492	11.07.2018	Grid 40x40 m	1.75/20	SO	20% Larix	1-2	1/5	x/x	x/x	x/x	-	
EN18015	Ilirney	67.420379	168.33061	663	12.07.2018	Circle r=15 m	1.75/20	NWW		1-2	1/4	x/x	x/x	x/x	-	
EN18016	Ilirney	67.426726	168.390047	690	12.07.2018	Circle r=15 m	1.50/20	NO		1-2	1/4	x/x	x/x	x/x	-	
EN18017	Ilirney	67.43229	168.383376	690	12.07.2018	Circle r=15 m	1.00/20	NOO		1-2	1/3	x/x	x/x	x/x	-	
EN18018	Ilirney	67.456295	168.405961	730	13.07.2018	Circle r=15 m	5.15/20	SW		1-3	1/2	x/x	x/x	x/x	-	
EN18019	Ilirney	67.457073	168.408963	717	13.07.2018	Circle r=15 m	6.65/15	S		0-3	1/3	x/x	x/x	x/x	-	
EN18020	Ilirney	67.459159	168.411934	887	13.07.2018	Circle r=15 m	4.95/15	SW		1-2	1/3	x/x	x/x	x/x	-	
EN18021	Ilirney	67.392129	168.328815	504	14.07.2018	Circle r=15 m	2.25/20	SSO	11% Larix	3-3	1/3	x/x	x/x	x/x	-	
EN18022	Ilirney	67.401024	168.348006	672	14.07.2018	Circle r=15 m	2.00/20	SSW		2-2	1/4	x/x	x/x	x/x	-	
EN18023	Ilirney	67.399236	168.351285	473	14.07.2018	Circle r=15 m	7.00/15	S		3-3	1/3	x/x	x/x	x/x	-	
EN18024	Ilirney	67.370964	168.426362	476	15.07.2018	Circle r=15 m	2.50/15	NNW	12% Larix	2-2	1/4	x/x	x/x	x/x	-	
EN18025	Ilirney	67.367027	168.42381	437	15.07.2018	Circle r=15 m	6.75/15	NNW	6% Larix	2-2	1/4	x/x	x/x	x/x	-	
EN18026	Ilirney	67.396089	168.354297	473	16.07.2018	Circle r=15 m	3.20/15	SSO	20% Larix	2-2	1/4	x/x	x/x	x/x	-	
EN18027	Ilirney	67.393408	168.35905	455	16.07.2018	Circle r=15 m	1.60/15	SSO	8% Larix	3-3	1/3	x/x	x/x	x/x	-	
EN18028	Billbino	68.46781	163.357622	305	20.07.2018	Circle r=15 m	0.50/15	O	25% Larix	3-3	1/3	x/x	x/x	x/x	-	
EN18029	Ilirney	68.465606	163.352262	353	20.07.2018	Circle r=15 m	1.00/15	NO	15% Larix	3-3	1/5	x/x	x/x	x/x	-	
EN18030	Billbino	68.405539	164.532731	283	21.07.2018	Circle r=15 m	0.50/15	NO	55% Larix	2-2	1/3	x/x	x/x	x/x	-	
EN18031	Billbino	68.404918	164.545351	235	21.07.2018	Circle r=15 m	0.40/15	O		3-3	1/3	x/x	x/x	x/x	-	
EN18032	Billbino	68.404868	164.551181	220	21.07.2018	Circle r=15 m	0.75/15	OSO	0.1% Larix	1-1	1/3	x/x	x/x	x/x	-	
EN18033	Billbino	68.403212	164.551805	220	21.07.2018	Circle r=15 m	0.60/15	O		1-1	1/3	0/0	x/x	(intensive grid as no flight)	-	
EN18034	Billbino	68.403486	164.548043	235	22.07.2018	Circle r=15 m	0.50/15	O	0.5% Larix	3-3	1/3	x/x	x/x	x/x	-	
EN18035	Billbino	68.403166	164.590932	246	22.07.2018	Circle r=15 m	0.60/15	OSO	21% Larix	2-2	1/3	0/0	0/0	0/0	x (grid)	
EN18051	Rauchuagygn	67.80261	168.7047	631	18.07.2018	Circle r=15 m	-	-	-	2-2	0/0	0/0	0/0	0/0	-	
EN18052	Rauchuagygn	67.79941	168.7083	641	18.07.2018	Circle r=15 m	-	-	-	2-2	0/0	0/0	0/0	0/0	-	
EN18053	Rauchuagygn	67.79729	168.7107	629	19.07.2018	Circle r=15 m	-	-	-	2-2	0/0	0/0	0/0	0/0	-	
EN18054	Rauchuagygn	67.79766	168.6904	681	20.07.2018	Circle r=15 m	-	-	-	2-1	0/0	0/0	0/0	0/0	-	
EN18055	Rauchuagygn	67.79103	168.6825	843	21.07.2018	Circle r=15 m	-	-	-	2-3	0/0	0/0	0/0	0/0	-	

Table A.3.2: Lake sediment and water samples retrieved during Expedition Chukotka 2018

Lake	Site/ Core ID	Core length	Sample date	Longitude (° E)	Latitude (° N)	Gear	Water depth [m]
Illirney	EN18200-1	0-1	06.07.2018	168.392912	67.364706	water sampler	3.1
Illirney	EN18200-2	0-1	06.07.2018	168.392912	67.364706	sediment grabber	3.1
Illirney	EN18200-3	0-1	06.07.2018	168.392912	67.364706	water sampler	3.1
Illirney	EN18201-1	0-1	06.07.2018	168.32483	67.37295	water sampler	3.4
Illirney	EN18201-2	0-1	06.07.2018	168.32483	67.37295	sediment grabber	3.4
Illirney	EN18201-3	0-1	06.07.2018	168.32483	67.37295	water sampler	3.4
Illirney	EN18202-1	0-1	06.07.2018	168.35318	67.35393	water sampler	2.3
Illirney	EN18202-2	0-1	06.07.2018	168.35318	67.35393	sediment grabber	2.3
Illirney	EN18202-3	0-1	06.07.2018	168.35318	67.35393	water sampler	2.3
Illirney	EN18203-1	0-1	06.07.2018	168.27235	67.353	water sampler	0.9
Illirney	EN18203-2	0-1	06.07.2018	168.27235	67.353	sediment grabber	0.9
Illirney	EN18203-3	0-1	06.07.2018	168.27235	67.353	water sampler	0.9
Illirney	EN18204-1	0-1	06.07.2018	168.28351	67.32931	water sampler	5.3
Illirney	EN18204-2	0-1	06.07.2018	168.28351	67.32931	sediment grabber	5.3
Illirney	EN18204-3	0-1	06.07.2018	168.28351	67.32931	water sampler	5.3
Illirney	EN18205-1	0-1	06.07.2018	168.22804	67.32745	water sampler	3
Illirney	EN18205-2	0-1	06.07.2018	168.22804	67.32745	sediment grabber	3
Illirney	EN18205-3	0-1	06.07.2018	168.22804	67.32745	water sampler	3
Illirney	EN18206-1	0-1	06.07.2018	168.19453	67.32898	water sampler	5.1
Illirney	EN18206-2	0-1	06.07.2018	168.19453	67.32898	sediment grabber	5.1
Illirney	EN18206-3	0-1	06.07.2018	168.19453	67.32898	water sampler	5.1

Lake	Site/ Core ID	Core length	Sample date	Longitude (° E)	Latitude (° N)	Gear	Water depth [m]
Illirney	EN18207-1	0-1	07.07.2018	168.41524	67.38697	water sampler	0.8
Illirney	EN18207-2	0-1	07.07.2018	168.41524	67.38697	sediment grabber	0.8
Illirney	EN18207-3	0-1	07.07.2018	168.41524	67.38697	water sampler	0.8
Illirney	EN18208 (-1, -2, -3, -4, -5,-6,-7)	0-1256	07-10.07.2018	168.29567	67.3403	UWITEC Piston corer, gravity corer	19
Illirney	EN18209-2	0-1	10.07.2018	168.3685	67.392056	sediment grabber	4.8
Illirney	EN18210-1	0-1	11.07.2018	168.38096	67.3937	water sampler	1.4
Illirney	EN18210-2	0-1	11.07.2018	168.38096	67.3937	sediment grabber	1.4
Illirney	EN18210-3	0-1	11.07.2018	168.38096	67.3937	water sampler	1.4
Illirney	EN18211-1	0-1	11.07.2018	168.372483	67.3927	water sampler	7.5
Illirney	EN18211-2	0-1	11.07.2018	168.372483	67.3927	sediment grabber	7.5
Illirney	EN18211-3	0-1	11.07.2018	168.372483	67.3927	water sampler	7.5
Illirney	EN18212-1	0-1	11.07.2018	168.42045	67.39823	water sampler	8.2
Illirney	EN18212-2	0-1	11.07.2018	168.42045	67.39823	sediment grabber	8.2
Illirney	EN18212-3	0-1	11.07.2018	168.42045	67.39823	water sampler	8.2
Illirney	EN18213 (Land)	0-5	12.07.2018	168.42401	67.37243	sediment grabber	NA
Illirney	EN18213-1	0-1	12.07.2018	168.42029	67.3735	water sampler	7.7
Illirney	EN18213-2	0-1	12.07.2018	168.42029	67.3735	sediment grabber	7.7
Illirney	EN18213-3	0-1	12.07.2018	168.42029	67.3735	water sampler	7.7
Illirney	EN18214 (-1, -2, -3, -4, -5, -6, -7)	0-1428	12.07.2018	168.37175	67.37381	UWITEC piston corer, gravity corer	23.9



Lake	Site/ Core ID	Core length	Sample date	Longitude (° E)	Latitude (° N)	Gear	Water depth [m]
Illirney	EN18215-1	0-1	12.07.2018	168.358722	67.384611	water sampler	14.9
Illirney	EN18215-2	0-1	12.07.2018	168.358722	67.384611	sediment grabber	14.9
Illirney	EN18215-3	0-1	12.07.2018	168.358722	67.384611	water sampler	14.9
Rauchua-gyngyn	EN18216-1	0-1	19.07.2018	168.739	67.80259	water sampler	6.7
Rauchua-gyngyn	EN18216-2	0-1	19.07.2018	168.739	67.80259	sediment grabber	6.7
Rauchua-gyngyn	EN18217-1	0-1	19.07.2018	168.7308	67.77825	water sampler	11.5
Rauchua-gyngyn	EN18217-2	0-1	19.07.2018	168.7308	67.77825	sediment grabber	11.5
Rauchua-gyngyn	EN18218 (-1,-2,-3,-4)	0-780	20.07.2018	168.73352	67.78938	UWITEC piston corer, gravity corer	29.5
Rauchua-gyngyn	EN18219	0-1	21.07.2018	168.71165	67.80202	sediment grabber	3
Rauchua-gyngyn	EN18220-1	0-1	19.07.2018	168.73811	67.77824	water sampler	1
Rauchua-gyngyn	EN18220-2	0-1	19.07.2018	168.73811	67.77824	sediment grabber	1
Rauchua-gyngyn	EN18221	0-1	21.07.2018	168.72585	67.80135	water sampler	14.1
Rauchua-gyngyn	EN18221 (-1,-2,-3)	0-570	21.07.2018	168.72495	67.80069	UWITEC piston corer, gravity corer	14.1

Table A.3.3: Visited vegetation plots in Yakutia

Site ID	General Information					Soil pits (# samples; # samples dating)					Image surveys				
	Region	Latitude [° N]	Longitude [° E]	Altitude [m asl]	Date	Plot type [m]	Slope [m/m]	Aspect	Tree species cover	Soil pits (# samples; # samples dating)	Panorama (# Canon / # Sam-sung360)	Flight (RGB / NIR)	Handheld (RGB / NIR)	6 m (RGB / NIR)	Handheld (Sam-sung360 time lapse)
EN18061	Yakutsk	62.076376	129.618586	217	28.07.2018	Circle r=15	0,00/15	-	20% Larix / 29% Pinus	2 - 2	1 / 4	x / x	x / x	x / x	x (circle)
EN18062	Lena-Viluy	62.179065	127.805796	337	30.07.2018	Circle r=15	-	-	30% Larix	0 - 0	0 / 5	x / x	x / x	0 / 0	x (circle)
EN18063	Lena-Viluy	63.776636	122.501003	116	31.07.2018	Circle r=15	0,50/15	W	50% Larix	2 - 2	1 / 3	x / x	x / 0	0 / 0	x (grid)
EN18064	Lena-Viluy	63.814594	122.209683	94	01.08.2018	Circle r=15	0,05/15	O	5% Larix / 17% Pinus	2 - 2	1 / 3	x / x	x / x	0 / 0	-
EN18065	Lena-Viluy	63.795223	122.443715	111	01.08.2018	Grid 20x20	0,25/15	S	35% Larix	1 - 1	1 / 4	x / x	x / x	0 / 0	-
EN18066	Lena-Viluy	63.7971189	122.438071	112	02.08.2018	Circle r=15	0,25/15	N	4% Larix / 0,1% Picea	1 - 1	1 / 3	x / x	x / x	0 / 0	-
EN18067	Lena-Viluy	63.076368	117.975342	125	04.08.2018	Circle r=15	0,25/15	NW	40% Larix / 8% Picea	2 - 2	1 / 4	x / x	x / x	0 / 0	x (circle)
EN18068	Lena-Viluy	63.074232	117.98207	147	04.08.2018	Circle r=15	0,50/15	NNW	12% Larix / 5% Pinus	1 - 1	1 / 3	x / x	x / x	x / x	-
EN18069	Lena-Viluy	63.173288	118.132507	132	05.08.2018	Circle r=15	0,50/15	S	7% Larix / 50% Picea	2 - 2	1 / 3	x / x	x / x	0 / 0	-
EN18070	Lena-Viluy	63.082914	117.984905	121	06.08.2018	Transect	-	-	div	4 - 4	0 / 0	x / x	0 / 0	0 / 0	-
EN18071	Lena-Viluy	62.225093	116.275603	199	07.08.2018	Circle r=15	0,75/15	NO	60% Larix / 6% Picea	2 - 2	1 / 3	x / x	x / x	0 / 0	-
EN18072	Lena-Viluy	62.199571	117.379125	171	08.08.2018	Circle r=15	-	-	50% Larix / 0,5% Picea	2 - 2	1 / 3	x / x	x / x	0 / 0	-
EN18073	Lena-Viluy	62.188712	117.409917	169	08.08.2018	Circle r=15	-	-	25% Larix / 0,5% Pinus	1 - 1	1 / 3	x / x (manually operated)	x / x	0 / 0	-
EN18074	Lena-Viluy	62.215192	117.021599	203	09.08.2018	Circle r=15	0,50/15	NO	9% Larix / 30% Picea	2 - 2	1 / 3	x / x (manually operated)	x / x	0 / 0	x (grid)
EN18075	Lena-Viluy	62.696991	113.676535	337	10.08.2018	Circle r=15	0,75/15	W	4% Larix / 20% Pinus	2 - 2	1 / 3	x / x	x / x (extra video on grid)	0 / 0	-
EN18076	Lena-Viluy	62.70089	113.67341	341	11.08.2018	Circle r=15	-	-	25% Larix	1 - 1	0 / 4	0 / 0	0 / 0	0 / 0	-
EN18077	Lena-Viluy	61.892568	114.288623	349	12.08.2018	Circle r=15	0,75/15	NW	8% Larix / 17% Pinus	2 - 2	1 / 3	x / x	x / x	x / x	-
EN18078	Lena-Viluy	61.575058	114.29995	395	12.08.2018	Circle r=15	0,25/15	O	35% Larix	1 - 1	1 / 4	x / x	x / x	0 / 0	-
EN18079	Khamra	59.974919	112.958985	414	14.08.2018	Circle r=15	0,50/15	N	35% Larix / 3% Pinus / 30% Picea	2 - 2	1 / 3	x / x	x / x	0 / 0	-
EN18080	Khamra	59.977106	112.961379	377	14.08.2018	Circle r=15	0,75/15	NO	3% Larix / 7% Pinus / 7% Picea	2 - 2	1 / 4	x / x	x / x	0 / 0	-
EN18081	Khamra	59.970563	112.987096	439	15.08.2018	Circle r=15	1,38/15	N	25% Larix / 1% Pinus / 8% Picea	2 - 2	1 / 3	x / 0	x / 0	0 / 0	-
EN18082	Khamra	59.97764	112.98218	379	15.08.2018	Circle r=15	-	-	5% Larix / 15% Pinus / 8% Picea	0 - 0	1 / 3	x / 0	x / 0	0 / 0	-
EN18083	Khamra	59.974714	113.002874	467	16.08.2018	Circle r=15	1,75/15	N	20% Larix / 10% Pinus / 12% Picea / 8% Abies	1 - 1	0 / 3	x / x	x / x	0 / 0	x (grid)

Table A.3.4: Lacustrine sediment cores retrieved from in Yakutia

Lake ID	Site/Core ID	Core length	Sample date	Longitude (° E)	Latitude (° N)	Gear	Water depth [m]
EN18232	EN18232-1	42	14.08.2018	112.98373	59.99091	UWITEC gravity corer	22.3
EN18232	EN18232-2	39	14.08.2018	112.98373	59.99091	UWITEC gravity corer	22.3
EN18232	EN18232-4	43	14.08.2018	112.98373	59.99091	UWITEC gravity corer	22.3
EN18232	EN18232-5	190	14.08.2018	112.98373	59.99091	UWITEC gravity corer with hammer action	22.3
EN18232	EN18232-6	177	14.08.2018	112.98373	59.99091	UWITEC gravity corer with hammer action	22.3
EN18232	EN18232-3	242	14.08.2018	112.98373	59.99091	UWITEC gravity corer with hammer action	22.3
EN18233	EN18233-1 (11 parts: 2.0-2.5, 2.0-3.0, 2.5-3.5, 3.0-4.0, 3.5-4.5, 4.0-5.0, 4.5-5.5, 4.92-5.95, 5.51-6.51, 6.0-7.0, 6.32-7.32 m)	532	15.08.2018	112.96513	59.98505	Russian Corer	1.9
EN18233	EN18233-2	134	15.08.2018	112.96513	59.98505	UWITEC gravity corer with hammer action	1.9
EN18231	EN18231-1	32	12.08.2018	114.53098	61.62811	UWITEC gravity corer	1.5
EN18231	EN18231-3	50	12.08.2018	114.53098	61.62811	Russian corer	1.5
EN18231	EN18231-3	50	12.08.2018	114.53098	61.62811	Russian corer	1.5

Lake ID	Site/Core ID	Core length	Sample date	Longitude (° E)	Latitude (° N)	Gear	Water depth [m]
EN18230	EN18230-1	18	12.08.2018	113.67583	62.74326	UWITEC gravity corer	1.1
EN18230	EN18230-2	59	12.08.2018	113.67583	62.74326	UWITEC gravity corer	1.1
EN18225	EN18225-1	38	07.08.2018	117.15831	62.22748	UWITEC gravity corer	2.1
EN18225	EN18225-3	62	07.08.2018	117.15831	62.22748	UWITEC gravity corer	2.1
EN18225	EN18225-2	36	07.08.2018	117.15831	62.22748	UWITEC gravity corer	2.1
EN18225	EN18225-4	63	07.08.2018	117.15831	62.22748	UWITEC gravity corer with hammer action	2.1
EN18226	EN18226-1	36	07.08.2018	117.12644	62.23262	UWITEC gravity corer	1.1
EN18227	EN18227-1	56	08.08.2018	116.88097	62.29211	UWITEC gravity corer	1.3
EN18227	EN18227-2	57	08.08.2018	116.88097	62.29211	UWITEC gravity corer	1.3
EN18227	EN18227-3	68	08.08.2018	116.88097	62.29211	UWITEC gravity corer with hammer action	1.3
EN18228	EN18228-1	52	08.08.2018	116.93067	62.2941	UWITEC gravity corer	1.6
EN18228	EN18228-2	56	08.08.2018	116.93067	62.2941	UWITEC gravity corer	1.6
EN18228	EN18228-3	71	08.08.2018	116.93067	62.2941	UWITEC gravity corer with hammer action	1.6

Lake ID	Site/Core ID	Core length	Sample date	Longitude (° E)	Latitude (° N)	Gear	Water depth [m]
EN18224	EN18224-1	45	03.08.2018	117.99806	63.07816	UWITEC gravity corer	1.8
EN18224	EN18224-2	60	03.08.2018	117.99806	63.07816	UWITEC gravity corer	1.8
EN18224	EN18224-3	60	03.08.2018	117.99806	63.07816	UWITEC gravity corer	1.8
EN18224	EN18224-4	121	03.08.2018	117.99806	63.07816	UWITEC gravity corer with hammer action	1.8
EN18224	EN18224-5	45	03.08.2018	117.99806	63.07816	UWITEC gravity corer	1.8
EN18222	EN18222-1	10	01.08.2018	122.50538	63.78056	UWITEC gravity corer	1.1
EN18223	EN18223-1	25	01.08.2018	122.34398	63.79819	UWITEC gravity corer	1
EN18223	EN18223-2	50	01.08.2018	122.34398	63.79819	UWITEC gravity corer	2
EN18229	EN18229-1	55.5	09.08.2018	116.93469	62.19975	UWITEC gravity corer	1.7
EN18229	EN18229-2	100	09.08.2018	116.93469	62.19975	UWITEC gravity corer with hammer action	1.7

Die **Berichte zur Polar- und Meeresforschung** (ISSN 1866-3192) werden beginnend mit dem Band 569 (2008) als Open-Access-Publikation herausgegeben. Ein Verzeichnis aller Bände einschließlich der Druckausgaben (ISSN 1618-3193, Band 377-568, von 2000 bis 2008) sowie der früheren **Berichte zur Polarforschung** (ISSN 0176-5027, Band 1-376, von 1981 bis 2000) befindet sich im electronic Publication Information Center (**ePIC**) des Alfred-Wegener-Instituts, Helmholtz-Zentrum für Polar- und Meeresforschung (AWI); see <https://epic.awi.de>. Durch Auswahl "Reports on Polar- and Marine Research" (via "browse"/"type") wird eine Liste der Publikationen, sortiert nach Bandnummer, innerhalb der absteigenden chronologischen Reihenfolge der Jahrgänge mit Verweis auf das jeweilige pdf-Symbol zum Herunterladen angezeigt.

The **Reports on Polar and Marine Research** (ISSN 1866-3192) are available as open access publications since 2008. A table of all volumes including the printed issues (ISSN 1618-3193, Vol. 377-568, from 2000 until 2008), as well as the earlier **Reports on Polar Research** (ISSN 0176-5027, Vol. 1-376, from 1981 until 2000) is provided by the electronic Publication Information Center (**ePIC**) of the Alfred Wegener Institute, Helmholtz Centre for Polar and Marine Research (AWI); see URL <https://epic.awi.de>. To generate a list of all Reports, use the URL <http://epic.awi.de> and select "browse"/"type" to browse "Reports on Polar and Marine Research". A chronological list in declining order will be presented, and pdf-icons displayed for downloading.

#### **Zuletzt erschienene Ausgaben:**

**734 (2019)** Russian-German Cooperation: Expeditions to Siberia in 2018. Edited by Stefan Kruse, Dmitry Bolshiyarov, Mikhail Grigoriev, Anne Morgenstern, Luidmila Pestryakova, Leonid Tsibizov, Annegret Udke

**733 (2019)** Expeditions to Antarctica: ANT-Land 2018/19 Neumayer Station III, Kohnen Station, Flight Operations and Field Campaigns, edited by Tanja Fromm, Constance Oberdieck, Tim Heitland, Peter Köhler

**732 (2019)** The Expedition PS117 of the Research Vessel POLARSTERN to the Weddell Sea in 2018/2019, edited by Olaf Boebel

**731 (2019)** The Expedition PS116 of the Research Vessel POLARSTERN to the Atlantic Ocean in 2018, edited by Claudia Hanfland and Bjela König

**730 (2019)** The Expedition PS110 of the Research Vessel POLARSTERN to the Atlantic Ocean in 2017/2018, edited by Frank Niessen

**729 (2019)** The Expedition SO261 of the Research Vessel SONNE to the Atacama Trench in the Pacific Ocean in 2018, edited by Frank Wenzhöfer

**728 (2019)** The Expedition PS115/2 of the Research Vessel POLARSTERN to the Arctic Ocean in 2018, edited by Ruediger Stein

**727 (2019)** The Expedition PS115/1 of the Research Vessel POLARSTERN to the Greenland Sea and Wandel Sea in 2018, edited by Volkmar Damm

**726 (2019)** The Expedition PS108 of the Research Vessel POLARSTERN to the Fram Strait and the AWI-HAUSGARTEN in 2017, edited by Frank Wenzhöfer

**725 (2018)** Russian-German Cooperation: Expeditions to Siberia in 2017, edited by Jens Strauss, Julia Boike, Dmitry Yu. Bolshiyarov, Mikhail N. Grigoriev, Hassan El-Hajj, Anne Morgenstern, Pier Paul Overduin, Annegret Udke

#### **Recently published issues:**



**ALFRED-WEGENER-INSTITUT**  
HELMHOLTZ-ZENTRUM FÜR POLAR-  
UND MEERESFORSCHUNG

**BREMERHAVEN**

Am Handelshafen 12  
27570 Bremerhaven  
Telefon 0471 4831-0  
Telefax 0471 4831-1149  
[www.awi.de](http://www.awi.de)

**HELMHOLTZ**